TUNING THE ELECTRONIC PROPERTIES OF CYCLAM DERIVATIVES: ENHANCED INTERMETALLIC COUPLING AND CATALYSIS

by

Brandon Lee Mash

A Dissertation

Submitted to the Faculty of Purdue University

In Partial Fulfillment of the Requirements for the degree of

Doctor of Philosophy

Department of Chemistry

West Lafayette, Indiana

December 2020

THE PURDUE UNIVERSITY GRADUATE SCHOOL

STATEMENT OF COMMITTEE APPROVAL

Dr. Tong Ren, Chair

Department of Chemistry

Dr. Corey Thompson

Department of Chemistry

Dr. Adam Wasserman

Department of Chemistry

Dr. Jon Wilker

Department of Chemistry

Approved by:

Dr. Christine Hrycyna

Dedicated to Patricia Mash. You were such a monumental part of my life and I have no doubt I owe much of who I am and what I have achieved today to you. I will be eternally grateful for the joy you brought to my life and could not have asked for a better nan. I miss you dearly.

ACKNOWLEDGMENTS

It would have been impossible to achieve this moment without the help of others throughout the course of my life. I have my parents to thank for instilling the work ethic and providing the help I needed to get here. Thank you both for always being there for me. I sincerely thank my undergraduate advisors, Steve Haefner and Irina Seceleanu, as well as all the other professors, who supported me and saw potential for success even through my notorious absences and troubles throughout my Bachelor's studies. Upon reaching graduate school, Matthias Zeller introduced me to crystallography and I discovered my passion for the subject. He has put an extraordinary effort into properly teaching the craft and providing countless opportunities to learn and become involved in the field. From funding for conferences to opportunities to work and publish as a crystallographer he has done so much for me. Thank you so much for introducing me to the field and really allowing me to fully explore it. Finally, without Dr. Ren, my PhD would not have been possible. From taking me on as a zero-year until now, there has always been support. I joined this lab with the desire to develop molecular electronic devices, and I was given mostly free reign to pursue this goal while also realizing how important working towards the reduction of carbon dioxide is. Thank you Dr. Ren for providing an incredible research experience.

TABLE OF CONTENTS

LIST OF TABLES

LIST OF FIGURES

LIST OF SCHEMES

ABSTRACT

My thesis work revolves around the ability to modify the 1,4,8,11-tetraazacyclotetradecane (cyclam) framework in order tune the electronic properties of resulting metal complexes towards real life applications. A huge direction for science and engineering is the pursuit of Moore's Law, to constantly miniaturize electronic processes while improving their performance. With the physical limits of copper wiring being reached on nanoscale levels, alternative resources must be utilized. Naturally, the absolute limit of wiring would be on the single molecular scale. It is this idea that Chapters 1-3 are founded upon. Moving forward, I deemed three key concepts are important for success of this project: (1) the ability for modification of the molecule to be incorporated into existing technologies, (2) redox stability of the molecular complexes to allow multiple charges to pass through without losing integrity, and (3) the ability to function as a wire and allow current to pass through. Requirement (1) has been proven possible in previous work on cyclam, however (2) and (3) were yet to be shown for any cobalt tetraazamacrocyclic complex until this work.

Chapter 1 covers my first successful exploration into modification of the cylcam ligand in order to obtain favorable electronic properties. Cobalt complexes utilizing the MPC ligand (5,12-dimethyl-7,14-diphenyl-1,4,8,11-tetraazacyclotetradecane) show stability upon reduction, whereas the cyclam analogues did not. In fact, $[Co(MPC)(C_2Ph)_2]^+$ was the first cobalt based tetraazamacrocyclic alkynyl complex to show such redox stability without the use of heavily electron withdrawing axial ligands. It was found that this improvement of redox stability is a result of the weakened equatorial ligand field caused by the steric bulk of the phenyl substituents of the cyclam framework. This in turn led to improved axial ligand bonding and hence greater stability. This work shows the Co^{III}(MPC) framework can satisfy requirement (2).

Based on the results of Chapter 1, Chapter 2 realizes the idea that with improved axial ligand bond strengths in Co^{III}(MPC) complexes, the possibility for electronic delocalization between cobalt and the axial ligand performing as the wire is opened. A series of dinuclear Co^{III}(MPC) complexes, with cobalt centers linked through a butadiyndiyl bridge, were prepared. With each cobalt being identical, theoretically each should behave electrochemically similar and reduction of the complex should be a single two electron event. It is however shown that this two electron event was, in fact, split into two single electron events. The source of this result is the

delocalization of the first added electron between both cobalt centers, effectively making two half-reduced metals. Therefore, the ability for Co^{III}(MPC) complexes to satisfy requirement (3) has been proven.

Chapter 3 expands on the results shown in Chapters 1 and 2. Where Chapter 2 showed delocalization of an electron between cobalt centers, Chapter 3 shows delocalization of a hole through cobalt between ethynylferrocene ligands. With this, all three requirements are met and the ability as Co(MPC) to function as a wire has been proven for both oxidation and reduction, both between cobalt and through cobalt.

Chapter 4 takes a new direction, however applies the same basic principle as the previous three in modifying the cyclam ligand to achieve desired properties. Where application in electronic devices are made stable by use of the bulky MPC ligand, application towards catalysis requires an open catalytic site and weak enough axial coordination to allow the substrate to leave once reduced. Through the alkyl substitution of the cyclam ligand in Ni^{II}(CTMC) (5,7,12,14-tetramethyl-1,4,8,11-tetraazacyclotetradecane) in place of the MPC ligand, electronically donating properties of the macrocycle were maintained while opening the axial catalytic site. In this work, it was shown that reduction in steric bulk of the ligand from phenyl to ethyl to methyl, while maintaining electron donating properties, improved catalytic efficiency and all complexes were superior to Ni^{II}(cyclam).

CHAPTER 1. COBALT(III) PHENYLACETYLIDE COMPLEXES SUPPORTED BY TETRAAZAMACROCYCLIC LIGANDS

*"Reprinted with permission from: B. L. Mash, T. Ren, J. Organomet. Chem. **2018**, 880, 143–149. Copyright 2018 Elsevier B.V."*

1.1 Abstract

Reported herein are the syntheses and characterization of mono- and bis- Co(III) phenylacetylide complexes *trans*-$[Co(L)(C_2Ph)Cl]^+$ (**2a/b**) and *trans*-$[Co(L)(C_2Ph)_2]^+$ (**3a/b**), where L is MPD (**a**) or MPC (**b**) (MPD = 5,12-dimethyl-7,14-diphenyl-1,4,8,11-tetraazacyclotetradeca-4,11-diene, MPC = 5,12-dimethyl-9,14-diphenyl-1,4,8,11-tetraazacyclotetradecane). All the new complexes were characterized by UV-Vis, FT-IR spectroscopic and voltammetric techniques. Single crystal X-ray diffraction studies revealed that the MPD ligand is a stronger donor to the Co(III) center than the MPC ligand, and the enhanced Co-N interactions manifest some subtle contrast in terms of spectroscopic and voltammetric properties between Co(MPD) and Co(MPC) complexes. These experimental observations were further corroborated by DFT calculations.

1.2 Introduction

The chemistry of metal alkynyl compounds has been studied for decades since the pioneering work of Nast,[1–4] and both the structural rigidity and conjugated $M–(C\equiv C)_nR$ backbone render these compounds ideal candidates for molecular wires.[5–9] Earlier successful examples include the work of Lapinte with C_4-bridged diiron compounds[10] and that of Gladysz with C_4-bridged dirhenium compounds.[11] Similar compounds developed in the following years include Mn,[12] Ru,[13] Pt,[14] and Au.[15] The potential of diruthenium/triruthenium termini bridged by oligoyn-diyls as prototypical molecular wires were explored by our group,[16–18] and the laboratories of Lehn[19] and Peng,[20–22] where both wire characteristics[23,24] and functional devices[25,26] have been demonstrated.

With the exception of Fe[10] and Mn,[12] the majority of the aforementioned examples are based on 4*d* and 5*d* metals. Our group is interested in expanding this class of compounds to include 3*d* metal based systems supported by tetra-azamacrocyclic ligands.[27–33] In addition to our efforts, alkynyl

complexes supported by cyclam (1,4,8,11-tetraazacyclotetradecane) have been explored by other laboratories including Wagenknecht,[34–36] Shores[37,38] and Nishijo,[39–43] and provide a promising framework for low cost replacement for precious metal based materials. Although metal complexes of *C*- and *N*-substituted tetra-azamacrocyclic ligands have received significant attention as catalysts for oxygen activation and carbon dioxide reduction,[44,45] the exploration of alkynyl complexes remains limited.[32,46–49]

While the synthesis of M(cyclam) is fairly expedient with M as 3*d* metals, the cyclam ligand is costly to procure and nontrivial to synthesize. With *C*-substituted cyclam derivatives prepared from a simple route,[50] the cost is significantly reduced. The synthesis of these ligands and their complexes have been discussed in depth by the laboratories of Curtis,[50–52] Lloyd,[53–55] and Hay.[56,57] Notable among these are MPD (MPD = 5,12-dimethyl-7,14-diphenyl-1,4,8,11-tetraazacyclotetradeca-4,11-diene) and MPC (MPC = 5,12-dimethyl-9,14-diphenyl-1,4,8,11-tetraazacyclotetradecane).[51,54,57,58] While most of the macrocycles in diene form were produced via Schiff base condensation reaction of a singly protonated ethylenediamine and a vinyl ketone,[50] MPD can be formed simply by stirring ethylenediamine and benzylideneacetone in ether over several days. Subsequent reduction of MPD using sodium borohydride yields MPC. Due to the wide availability of the reagents, both MPD and MPC can be produced on any desired scale at low cost. Herein, we report the first examples of alkynyl complexes based on the tetraazacyclotetradeca-4,11-diene framework, complexes **2a** and **3a** (Scheme 1.1), and provide additional examples of alkynyl complexes of *C*-substituted cyclam with complexes **2b** and **3b**.

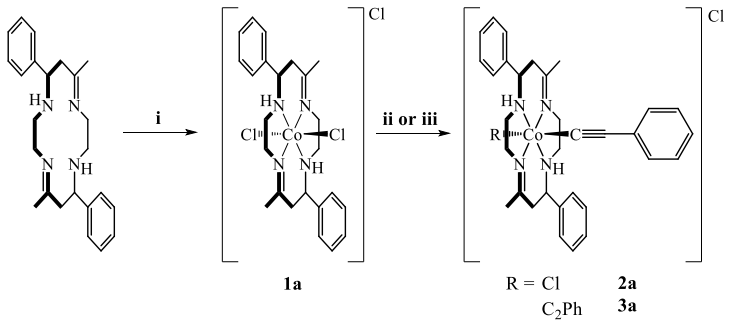

Scheme 1.1. Synthesis of Co(MPD) complexes **1a**-**3a**. (i) 1 equiv $CoCl_2$•$6H_2O$, MeOH, O_2, excess HCl; (ii) 7 equiv. HC_2Ph, Et_3N, MeOH, reflux, 24 h; (iii) excess LiC_2Ph, dry THF, 24 h. Co(MPC)-based complexes **1b**-**3b** were similarly prepared.

1.3 Results and Discussion

1.3.1 Synthesis

The complexes *trans*-[Co(MPD)Cl_2]Cl (**1a)** and *trans*-[Co(MPC)Cl_2]Cl (**1b)** were synthesized using a procedure modified from the preparation of [Co(cyclam)Cl_2]Cl.[59] Specifically, a methanolic solution of the desired macrocyclic ligand with $CoCl_2$•$6H_2O$ was sparged with oxygen followed by the addition of HCl to yield the desired cobalt(III) complex. Complex **1b** is insoluble in water, allowing for the removal of residual cobalt chloride with a water rinse to provide **1b** in 89% yield. Due to its solubility in water, complex **1a** was extracted using dichloromethane from the crude reaction mixture, and then recrystallized with ether for a yield of *ca.* 70%.

From complexes **1a** and **1b** were prepared the mono-phenylacetylide complexes, *trans*-[Co(MPD)(C_2Ph)Cl]Cl (**2a**) and *trans*-[Co(MPC)(C_2Ph)Cl]Cl (**2b**) under weak base conditions in ambient atmosphere, similar to the method developed by Shores.[37,38] Specifically, complex **1a** was reacted with 10-fold excess phenylacetylene in the presence of triethylamine under reflux for 24 h. The crude reaction mixture was purified on silica to afford **2a** in a yield of *ca.* 20%. It was noted in the synthesis of **2a** that the use of 5 equiv or more of phenylacetylene led to the formation of the bis-phenylacetylide complex as a minor product, and the yield of the *bis*-byproduct increases with equivalency of phenylacetylide. The extra phenylacetylene was used to fully consume starting material and simplify purification. Complex **2b** was similarly prepared from 1b with 5 equivalents of phenylacetylene and purified in a yield of 54%. The low yield of **2a** is likely due to the hydrolysis of the imino bonds of MPD under basic conditions,[60] as well as the lability of the chloro ligand. The bis-phenylacetylide complexes, *trans*-[Co(MPD)(C_2Ph)$_2$]Cl (**3a**) and *trans*-[Co(MPC)(C_2Ph)$_2$]Cl (**3b**), were prepared from the reaction between a large excess of LiC_2Ph and complexes **1a** or **1b**, and purified over silica with a gradient of dichloromethane and methanol in yields of 64% and 56%, respectively. All complexes are diamagnetic, which is consistent with a low spin Co(III) center.

1.3.2 Molecular Structures

Single crystals of X-ray quality were grown by slow diffusion of diethyl ether into either a 1:1 mixture of acetonitrile and water (**2a**, **2b**) or methanol (**3a**, **3b**). The ORTEP plots for the

complex cations are shown in Figures 1.1 and 1.2, and the selected geometric parameters are listed in Table 1.1. Each unit cell contains one crystallographically independent formula unit. All cations display a nearly linear Cl—Co—C or C—Co—C linkage, which lies normal to the plane of the coordinated nitrogen atoms, conforming to a pseudo-octahedral geometry. The bis-alkynyl cations, [**3a**]$^+$ and [**3b**]$^+$, are centrosymmetric at the cobalt center, while the mono-alkynyl cations, [**2a**]$^+$ and [**2b**]$^+$, possess no crystallographic symmetry. Both cyclam-based complexes, **2b** and **3b**, hold the *trans*-III conformation that is ubiquitous in this class of compounds with no apparent chiral variation at the methyl or phenyl sites (Figures 1.1 and 1.2).[59] Depending on the orientation of phenyl groups, the Co(III)(MPD) complexes **1a**, **2a** and **3a** may exist as one of three possible stereo-isomers, namely (*R*,*R*), (*S*,*S*) and (*R*,*S*) forms, as shown in Scheme 1.2. The ring conformation differs among stereo-isomers, with both (*R*,*R*) and (*S*,*S*) adopting a boat conformation (Figure 1.1) and (*R*,*S*) a chair conformation (Figure 1.2). It is possible that the (*R*,*R*), (*S*,*S*) isomers were lost in the purification of the reduced form, MPC, or they did not crystallize out of solution, hence those isomers are not seen in the Co(III)(MPC) complexes. A further source of isomerism is introduced in mono-acetylide complexes, depending on which chloride is displaced. Since the stereo-isomerism has minimal impact on the electronic structures of the resultant cobalt(III) complexes, isolation of each of possible isomers was not pursued in this work.

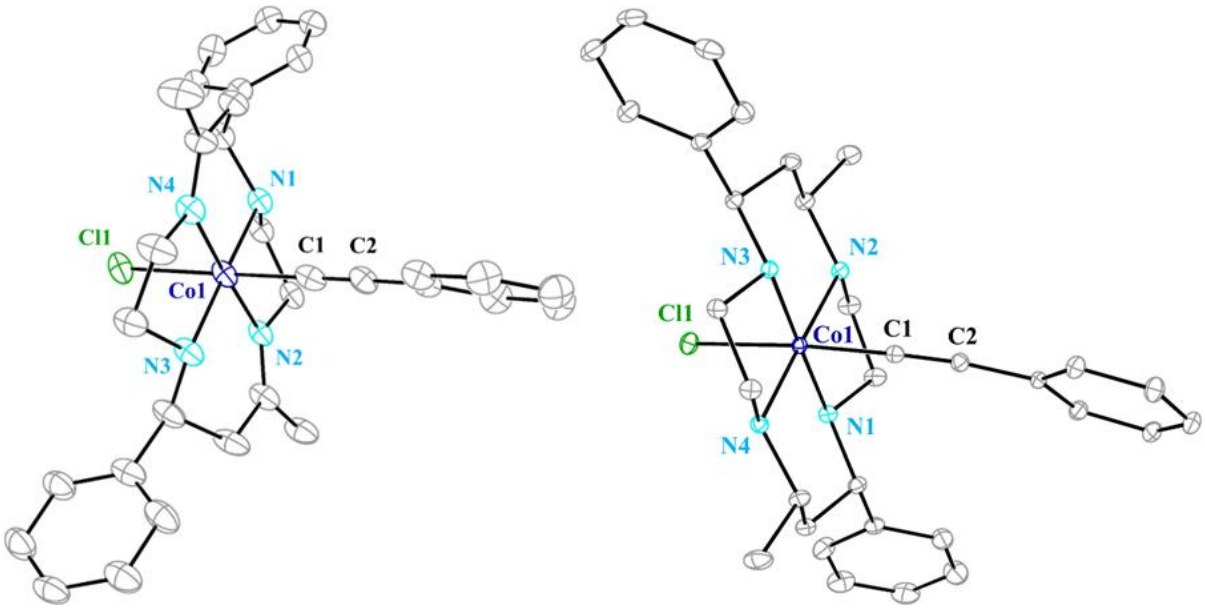

Figure 1.1. ORTEP plots of [**2a**]$^+$ (left) and [**2b**]$^+$ (right) at the 30% probability level. Hydrogen atoms, solvent molecules, and counter ions were omitted for clarity.

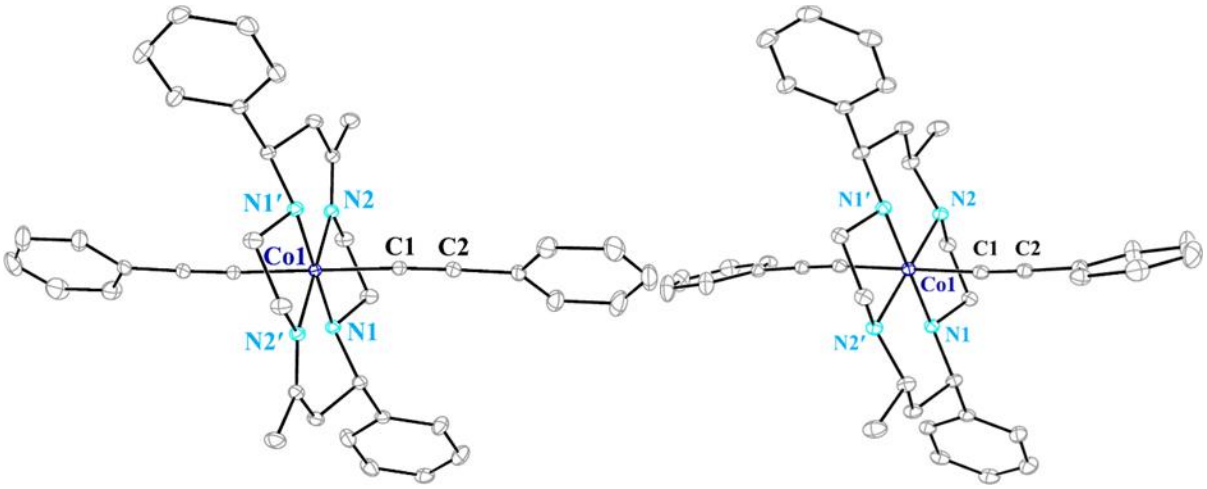

Figure 1.2. ORTEP plots of [**3a**]$^+$ (left) and [**3b**]$^+$ (right)at the 30% probability level. Hydrogen atoms, solvent molecules, and counter ions were omitted for clarity.

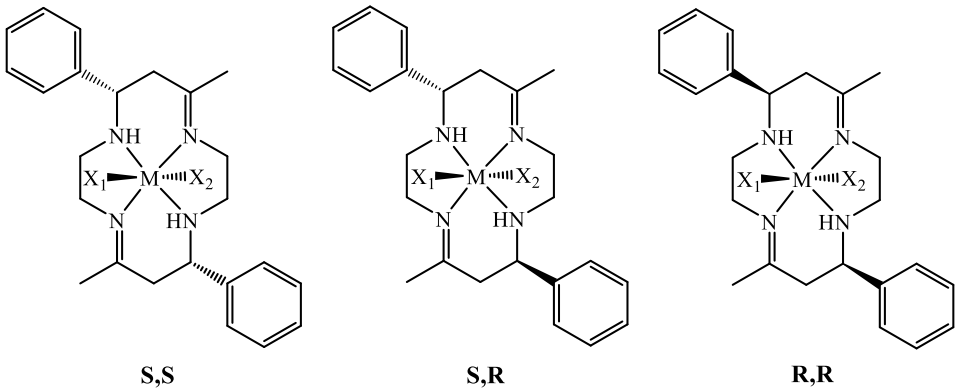

Scheme 1.2. Stereo-isomers of M(MPD). X_1, X_2 = axial ligands. (*R*,*S*) and (*S*,*R*) are meso when $X_1 = X_2$.

Table 1.1. Selected bond lengths and angles for [**2a**]$^+$, [**2b**]$^+$, [**3a**]$^+$ and [**3b**]$^+$.

	[**2a**]$^+$	[**2b**]$^+$	[**3a**]$^+$	[**3b**]$^+$
Co—N1	1.978(4)	2.005(2)	1.980(1)	2.019(2)
Co—N2	1.945(3)	2.012(2)	1.947(1)	1.990(2)
Co—N3	1.971(4)	2.007(2)	-	-
Co—N4	1.932(3)	2.002(2)	-	-
Co—Cl	2.329(1)	2.3115(6)	-	-
Co—C	1.876(5)	1.870(2)	1.943(1)	1.924(3)
C1—C2	1.202(7)	1.200(4)	1.212(2)	1.201(4)
Cl-Co-C1	177.3(1)	175.19(7)	-	-
Co-C1-C2	172.5(4)	171.8(2)	176.6(1)	172.0(2)
C1-C2-C3	176.7(5)	174.6(3)	178.6(1)	178.8(3)

X-ray structures of both the mono- and bis-phenyacetylide complexes of Co(III)(cyclam), $[Co(cyclam)(C_2Ph)Cl]^+$ and $[Co(cyclam)(C_2Ph)_2]^+$, were reported by Shores.[37] Compared with these structures, the addition of methyl and phenyl groups in compound **2b** causes an increase in averaged Co—N bond length to 2.006 [2] Å from the 1.975 [2] Å in $[Co(cyclam)(C_2Ph)Cl]^+$.[37] Intuitively, the σ-donation of the nitrogen atoms should be increased with the addition of electron rich substituents. Clearly, the lengthening of the Co—N bonds in **2b** is attributed to the steric effects of the added *C*-substitutents. The Co—C bond (1.870 (2) Å) is shortened while the Co—Cl bond (2.3115 (6) Å) is lengthened compared to those of Co(III)(cyclam) (Co—C 1.898 [2] Å, Co—Cl 23089 [5] Å). Similar lengthening of Co—N (2.004 [2] Å) and shortening of Co—C (1.924(3) Å) bond are observed for **3b** from $[Co(cyclam)(C_2Ph)_2]^+$ (Co—N 1.983 [2] Å, Co—C 2.001 [3] Å).[37] The strengthening of Co—C bond has a pronounced effect on the electrochemical properties as discussed later. Structures of the diene-based complexes, namely **2a** and **3a**, display substantial differences in bond lengths from those of cyclam-based complexes, **2b** and **3b**. As shown in Table 1.1, the π-accepting capability and structurally smaller ring of MPD shortens the Co—N bonds significantly, which also results in the lengthening of the Co—C and Co—Cl bonds. The C1—C2 alkynyl bond lengths exhibit little variation among the complexes studied, ranging from 1.200 (4) Å for **2b** to 1.212 (2) Å for **3a**. These bonds are longer than those reported for the unsubstituted cyclam variant,[37] however they are consistent with other Co(III)(cyclam) complexes reported from our laboratory.[28,30,61,62]

1.3.3 Voltammetric Studies

Cyclic voltammograms of complexes **2a**, **2b**, **3a** and **3b** are shown in Figure 1.3, and the electrode potentials are listed in Table 2. The overall characteristics are similar to those observed for related Co(III)(cyclam) based complexes.[37,61] Irreversible $Co^{3+/2+}$ (**A**) and $Co^{2+/1+}$ (**B**) couples were observed for both mono complexes. The cathodic shifts in potential from Co(III)(MPC) to Co(III)(MPD) complexes are likely due to a stronger σ-donation from MPD, consistent with the trend noted from structural studies. The presence of a second phenylacetylide in the bis complexes further shifts the reductions cathodically, so that only the $Co^{3+/2+}$ couple can be observed within the solvent window. An irreversible reduction for **3a** is present at -1.83 V, as noted previously for $[Co(cyclam)(C_2Ph)_2]^+$.[37] Interestingly, **3b** undergoes a quasi-reversible reduction at -1.81 V (ΔE_p = 63 mV, $i_{p,a}/i_{p,c}$ = 0.70). Though not observed in the cyclam analogue reported by Shores,[37] a

reversible couple was detected for Co(III)(cyclam) bearing both trifluoropropynyl[35] and pentafluorophenylacetylide ligands.[30] The irreversibility in Co(III)(cyclam) complexes is generally associated with the dissociation of labile axial ligands from the reduced Co(II) center.[30,35,61] Sun and coworkers attributed the reversibility of complexes with electron withdrawing ligands to the π-accepting nature of the alkyne rather than the electron density on the metal.[36] These results indicate it is in fact the electron density on the metal, or at least a combination of the two factors, which leads to the reversible couple. Notably, the Co—C bond length of **3b** is comparable to the aforementioned complexes ($[Co(cyclam)(C_2C_6F_5)_2]^+$ (1.926(3) Å); $[Co(cyclam)(C_2CF_3)_2]^+$ (1.917(4) Å)) without the use of electron withdrawing alkynyls. It is apparent that the reduced σ-donation from the macrocycle to the metal allows for a stronger axial ligand bond in both the Co(III) and Co(II) states. This improved stability is promising for the possible future application of Co(III)(MPC) to molecular wire type devices and opens the possibility of stable Co(II) complexes with sufficiently electron withdrawing cyclam derivatives.

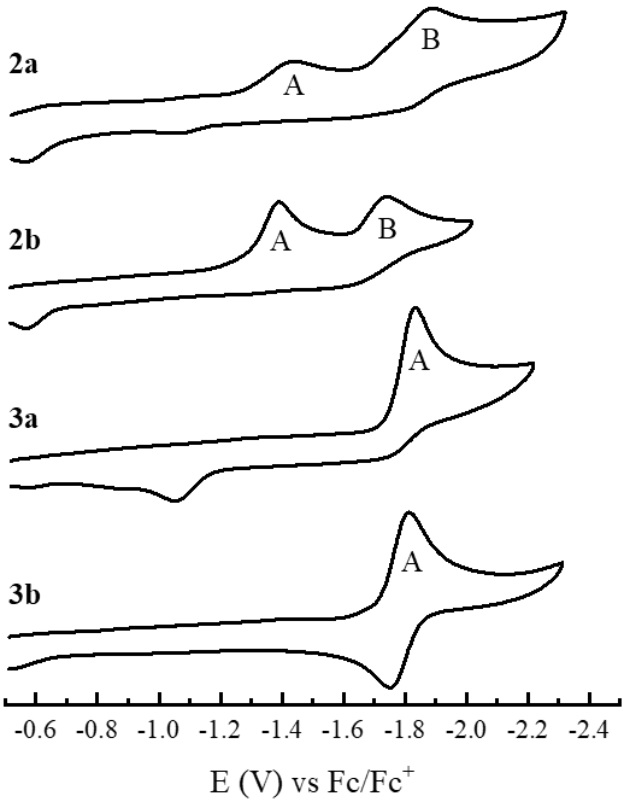

Figure 1.3. Cyclic voltammograms of 1.0 mM **2a**, **2b**, **3a**, and **3b** recorded in 0.1 M solution of Bu_4NPF_6 in MeCN at a scan rate of 0.10 V/s.

Table 1.2. Reduction potentials for **2a**, **2b**, **3a**, and **3b**.

	2a	**2b**	**3a**	**3b**
E_{pc} $Co^{3+/2+}$	-1.44	-1.39	-1.83	-1.81
E_{pc} $Co^{2+/1+}$	-1.89	-1.74	-	-

1.3.4 Electronic Absorption Spectra

Studies of electronic absorption spectra corroborate the findings in previous sections. As shown in Figures 1.5 and 1.6, the tighter binding of MPD results in a greater HOMO-LUMO energy gap and a hypsochromic shift in the absorption spectra. Consequently, the *d-d* transition located at 463 nm for **2a** is shifted to 499 nm for **2b**. For comparison, the *d-d* transition for $[Co(cyclam)(C_2Ph)Cl]^+$ lies between these compounds with its absorption band located at 486 nm (in THF).[37] The bis-phenylacetylide complexes show similar results with a bathochromic shift from MPD to cyclam and then MPC (453 nm in **3a**, 475 nm in **3b** and 463 nm in $[Co(cyclam)(C_2Ph)_2]^+$; spectra in Figure A.1).

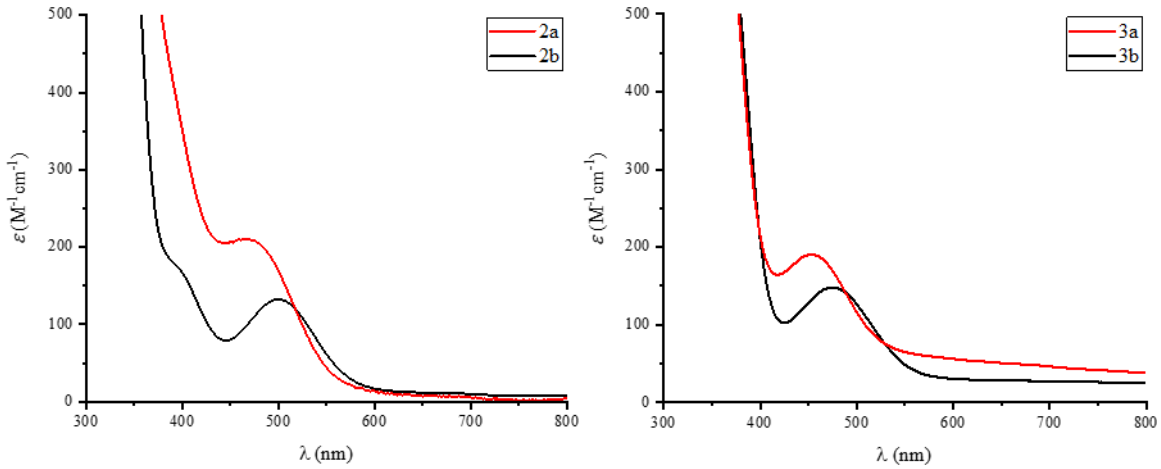

Figure 1.4. (left) Electronic absorption spectra for **2a** and **2b** in MeCN. (right) Electronic absorption spectra for **2b** and **3b** in MeCN.

1.3.5 Electronic Structures via DFT

In order to understand the electronic structures of Co(III)(MPD) alkynyl species and rationalize the geometric differences between Co(III)(MPD) and Co(III)(MPC) species, density functional theory (DFT) calculations were performed at the B3LYP/LANL2DZ level (for all atoms)

using the Gaussian16 suite.[63] All calculations were performed on gas phase cations without solvent interactions. Calculated bond lengths and angles are in agreement with the crystallographically determined parameters (Table A.2). The computed contour plots and energy levels for the frontier molecular orbitals are given in Figures 1.5 and 1.6. Expanded plots are given in Figures A.2-A.5.

In complexes **2a** and **3a**, the X and Y axes approximately coincide with the Co—N bonds. In such a setting, interactions between the d_{xz} orbitals and the π orbitals of the imino groups are clearly displayed (Figures A.2, A.4). For **2a** the d_{yz}, d_{z2}, and d_{xy} orbitals reside in the HOMO, LUMO, and LUMO+1, respectively (Figure A.2). For **3a** the d_{z2} lies in the LUMO+3, while the d_{yz} and d_{xy} lie in the HOMO and LUMO, respectively (Figure A.4). Both complexes **2b** and **3b** have the d_{yz}, d_{x2-y2}, and d_{z2} orbitals as the HOMO, LUMO, and LUMO+1, respectively (Figures A.3, A.5). It can be seen that the d_{xz} and d_{yz} orbitals form planes bisecting Co—N bonds, which conforms to the computational analysis in previous studies of related Co(III)(cyclam) species.[28–30,61,62,64] The axial phenylacetylide groups are major contributors to the frontier molecular orbitals, with antibonding interactions to the d_{yz} orbital in the HOMO of each compound (Figures A.2-A.5). The orbitals for the MPD compounds are also higher in energy than MPC, as noted in voltammetric studies.

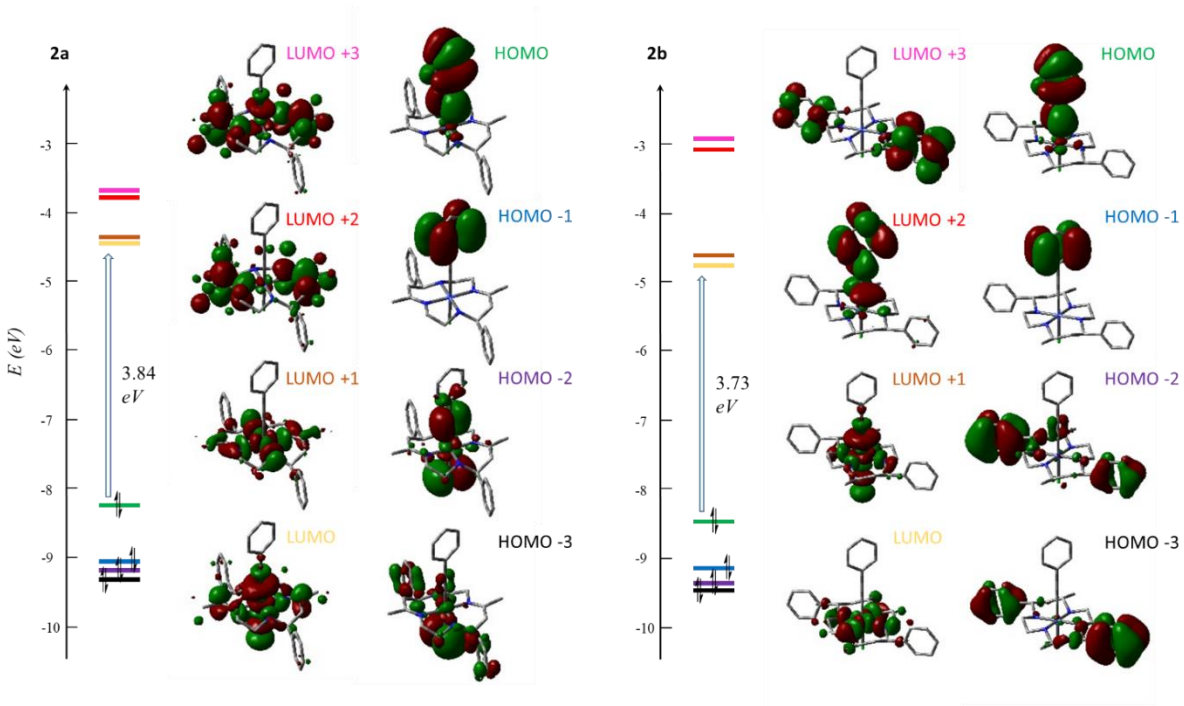

Figure 1.5. Molecular orbital diagrams and energy levels for **2a** and **2b**.

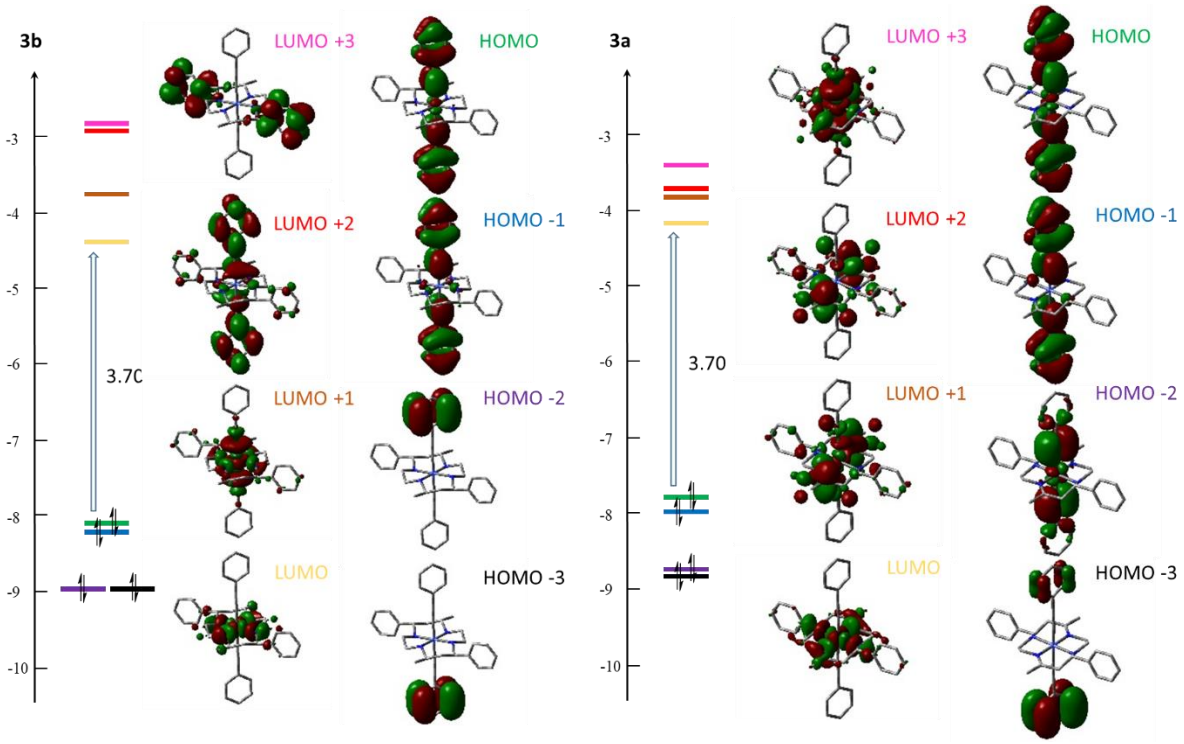

Figure 1.6. Molecular orbital diagrams and energy levels for **3a** and **3b**.

1.4 Conclusions

Cobalt(III) complexes supported by a diene-macrocycle (MPD, **1a-3a)** and its cyclam derivative (MPC, **1b**-**3b**) have been prepared in yields ranging from 20 to 90%. Complexes **2a** and **3a** are the first examples of metal acetylide complexes based on a 1,4,7,11-tetra-azacyclotetradeca-4,11-diene type ligand. In comparison with cobalt(III) cyclam complexes, complexes **2a** and **3a** display enhanced Co(III)-N bonding, which increases the HOMO-LUMO energy gap and decreases axial ligand bond strength. On the other hand, complexes **2b** and **3b** exhibit weaker Co—N bonding, resulting in enhanced axial ligand strength. With stronger axial ligand binding, pseudo-reversibility of the $Co^{3+/2+}$ couple was observed for **3b**. The pseudo-reversible reduction observed in **3b** and Co(III)(cyclam) complexes bearing electron-deficient axial ligands highlights the profound effect of changes in the macrocycle on axial ligation. The ability of the *C*-substituted macrocycles to support cobalt acetylide complexes encourages further exploration of similar chemistry based on other 3*d* metals, such as Cr, Fe and Ni, an ongoing effort in our laboratory.

1.5 Experimental

1.5.1 Materials

Phenylacetylene was purchased from GFS chemicals. $CoCl_2 \cdot 6H_2O$ and *n*-BuLi were purchased from Aldrich. MPD[52] and MPC[54] were prepared according to literature procedures. Tetrahydrofuran was freshly distilled over sodium/benzophenone. All lithiation reactions were carried out under N_2 using standard Schlenk techniques.

1.5.2 Physical Measurements

UV-vis spectra were obtained with a JASCO V-670 spectrophotometer. FT-IR spectra were measured as neat samples using a JASCO FT/IR-6300 spectrometer equipped with an ATR accessory. ESI-MS were analyzed on an Advion Expression Compact Mass Spectrometer. Elemental Analysis was carried out by Atlantic Micro Labs in Norcross, GA. Electrochemical analysis was done on a CHI620A voltammetric analyzer with a glassy carbon working electrode (diameter = 2 mm), a Pt-wire auxiliary electrode, and a Ag/AgCl reference electrode. The analyte concentration is 1.0 mM in 4 mL dry acetonitrile with a 0.1 M Bu_4NPF_6 electrolyte concentration.

1.5.3 Synthesis of [Co(MPD)Cl_2]Cl (1a)

A methanolic solution of $CoCl_2 \cdot 6H_2O$ (2.20 g, 9.24 mmol) with MPD (3.00 g, 7.97 mmol) was sparged with O_2 for 1h before addition of 7 mL of 12 M HCl. Upon addition of HCl, the solution changed from brown to green. The solution was allowed to sparge for 1 hour before being transferred to a petri dish and heated at 45° C until dry. The residue was taken up in CH_2Cl_2 and filtered to give an emerald green solution, which was recrystallized with ether. Yield: 3.03 g (70%, based on MPD).

1.5.4 Synthesis of [Co(MPC)Cl_2]Cl (1b)

A methanolic solution of $CoCl_2 \cdot 6H_2O$ (0.640 g, 2.69 mmol) with MPC (1.00 g, 2.63 mmol) was sparged with O_2 for 1 hour before addition of 4 mL of 12 M HCl. Upon addition of HCl, the solution changed from red to green with precipitate forming. The solution was allowed to sparge for 1h before the solvent was removed *in vacuo*. The crude solid was sonicated in H_2O before being filtered and washed with H_2O, THF, and ether. The collected green powder was dried under vacuum for 1.00 g. The combined filtrate was boiled down and allowed to cool producing an additional 0.28 g green crystals. Yield: 1.28 g (89% based on MPC).

1.5.5 Synthesis of [Co(MPD)(C_2Ph)Cl]Cl (2a)

To a methanolic solution of **1a** (0.500 g, 0.923 mmol) was added triethylamine (2.0 mL, 14 mmol), followed by phenylacetylene (1.01 mL, 9.23 mmol). The solution was allowed to reflux 24h. The solvent was removed via rotary evaporation and the residue was purified on silica gel with a gradient of CH_2Cl_2-MeOH. The collected orange product was recrystallized in CH_2Cl_2-Et_2O. Yield: 0.107 g, (20% based on Co). Data for **2a**: ESI-MS: (MeCN) 571 $[Co(MPD)(C_2Ph)Cl]^+$. Elem. Anal. Found (Calcd) for $C_{32.5}H_{40}N_4CoCl_3O_1$ ([**2a**]$\cdot H_2O \cdot 0.5CH_2Cl_2$) C, 58.47 (58.44); H, 6.05 (6.04); N, 8.58 (8.39). IR (cm^{-1}) 2124 (C≡C). UV-vis absorption spectrum (MeCN) λ_{max} nm (ε_{max}, L mol^{-1} cm^{-1}): 257 (38100), 463 (210).

1.5.6 Synthesis of [Co(MPC)(C_2Ph)Cl]Cl (2b)

To a methanolic solution of **1b** (0.200 g, 0.366 mmol) was added triethylamine (1.5 mL, 11 mmol), followed by phenylacetylene (0.20 mL, 1.8 mmol). The solution was allowed to reflux

4 hours. The solvent was removed via rotary evaporation and the residue was purified on silica gel with a gradient of CH_2Cl_2-MeOH. The collected red product was recrystallized in CH_2Cl_2-Et_2O. Yield: 0.120 g, (54% based on Co). Data for **2b**: ESI-MS (MeCN): 575 $[Co(MPC)(C_2Ph)Cl]^+$. Elem. Anal. Found (Calcd) for $C_{33}H_{46}N_4CoCl_4O_{1.5}$ ([**2b**]·$1.5H_2O$·CH_2Cl_2) C, 54.62 (54.79); H, 6.37 (6.41); N, 7.85 (7.74). IR (cm^{-1}) 2124 (C≡C). UV-vis absorption spectrum (MeCN) λ_{max} nm (ε_{max}, L mol^{-1} cm^{-1}): 256 (32900), 499 (132).

1.5.7 Synthesis of [Co(MPD)(C_2Ph)$_2$]Cl (3a)

A suspension of **1a** (0.250 g, 0.461 mmol) in THF was combined with a solution of LiC_2Ph (prepared from 4.6 mmol PhC_2H and 4.8 mmol *n*-BuLi) in THF and allowed to stir 24 h. The flask was opened to air and solvent was removed via rotary evaporation. The residue was purified on silica gel with a CH_2Cl_2-MeOH gradient. The solvent was removed and the remaining orange residue was recrystallized with CH_2Cl_2-Et_2O. Yield: 0.200 g (64% based on Co). Data for **3a**: ESI-MS (MeCN): 637 $[Co(MPD)(C_2Ph)_2]^+$. Elem. Anal. Found (Calcd) for $C_{41}H_{48}N_4CoCl_3O_2$ ([**3a**]·$2H_2O$·CH_2Cl_2) C, 61.83 (62.01); H, 6.19 (6.09); N, 7.31 (7.06). IR (cm^{-1}) 2100 (C≡C). UV-vis absorption spectrum (MeCN) λ_{max} nm (ε_{max}, L mol^{-1} cm^{-1}): 263 (39700), 453 (191).

1.5.8 Synthesis of [Co(MPC)(C_2Ph)$_2$]Cl (3b)

A suspension of **1b** (130 mg, 0.238 mmol) in THF was combined with a solution of LiC_2Ph (prepared from 4.6 mmol PhC_2H and 4.8 mmol *n*-BuLi) in THF and allowed to stir 24h. The flask was opened to air and solvent was removed via rotary evaporation. The residue was purified on silica gel with a CH_2Cl_2-MeOH gradient. The solvent was removed and the remaining orange residue was recrystallized with CH_2Cl_2-Et_2O. Yield: 0.090 g (56% based on Co). Data for **3b**: ESI-MS (MeCN): 641 $[Co(MPC)(C_2Ph)_2]^+$. Elem. Anal. Found (Calcd) for $C_{40.5}H_{48}N_4CoCl_2O_{0.5}$ ([**3b**]·$0.5H_2O$·$0.5CH_2Cl_2$) C, 66.24 (66.76); H, 6.70 (6.64); N, 7.74 (7.69). IR (cm^{-1}) 2111 (C≡C). UV-vis absorption spectrum (MeCN) λ_{max} nm (ε_{max}, L mol^{-1} cm^{-1}): 269 (50500), 475 (148).

1.5.9 Computational Details

The geometries of **2a**, **2b**, **3a**, and **3b** in the ground state were fully optimized from the crystal structures reported in this work using the density functional method B3LYP (Beck's three-

parameter hybrid functional using the Lee−Yang−Parr correlation functional) and employing the LanL2DZ basis sets. The calculation was accomplished by using the Gaussian03 program package.[63]

1.5.10 X-ray Crystallographic Analysis

Single crystal X-ray data was collected on a Bruker AXS D8 Quest CMOS diffractometer using MoKα ($\lambda = 0.71073$ Å) radiation with Apex3 software.[65] Data was reduced using SAINT[65] and structures were solved with SHELXTL.[66] Refinement was performed with SHELXL.[67] ORTEP plots were produced using SHELXTL.[66]

1.6 Acknowledgements

I thank the National Science Foundation for generously supporting this work (CHE 1764347 for research and CHE 1625543 for X-ray diffractometers).

1.7 Appendix A: Chapter 1

Crystal data for **2a**, **2b**, **3a** and **3b**; Relevant density functional theory calculation bond length/angle data; ^{1}HNMR spectra for **2a**, **2b**, **3a** and **3b** are provided in Appendix A: Chapter 1. Crystallographic data for the structural analysis have been deposited with the Cambridge Crystallographic Data Center, CCDC 1872102, 1872101, 1872103, and 1872100 for compounds **2a**, **2b**, **3a** and **3b**, respectively. Copies of this information may be obtained free of charge from, The Director, CCDC, 12 Union Road, Cambridge CB2 1EZ, UK, (Fax: þ44-1233-336033; email: deposit@ccdc.cam.ac.uk or www: http://ccdc.cam.ac.uk).
Supplementary data related to this article can be found at http://dx.doi.org/10.1016/j.jorganchem.xxxxxxxx.

1.8 References

[1] R. Nast, *Zeitschrift fur Naturforsch. - Sect. B J. Chem. Sci.* **1953**, *8*, 381-382b.

[2] R. Nast, *Coord. Chem. Rev.* **1982**, *47*, 89–124.

[3] J. Manna, K. D. John, M. D. Hopkins, **1995**, pp. 79–154.

[4] M. I. Bruce, *Coord. Chem. Rev.* **1997**, *166*, 91–119.

[5] F. Paul, C. Lapinte, *Coord. Chem. Rev.* **1998**, *178–180*, 431–509.

[6] T. Ren, *Organometallics* **2005**, *24*, 4854–4870.

[7] K. Costuas, S. Rigaut, *Dalt. Trans.* **2011**, *40*, 5643–5658.

[8] D. Xiang, X. Wang, C. Jia, T. Lee, X. Guo, *Chem. Rev.* **2016**, *116*, 4318–4440.

[9] A. Haque, R. A. Al-Balushi, I. J. Al-Busaidi, M. S. Khan, P. R. Raithby, I. J. Al-Busaidi, R. A. Al-Balushi, P. R. Raithby, A. Haque, *Chem. Rev.* **2018**, *118*, 8474–8597.

[10] N. Le Narvor, C. Lapinte, *J. Chem. Soc., Chem. Commun.* **1993**, *8*, 357–359.

[11] Y. Zhou, J. W. Seyler, W. Weng, A. M. Arif, J. A. Gladysz, *J. Am. Chem. Soc.* **1993**, *115*, 8509–8510.

[12] S. Kheradmandan, K. Heinze, H. W. Schmalle, H. Berke, *Angew. Chem., Int. Ed. Engl.* **1999**, *38*, 2270–2273.

[13] J.-F. F. Halet, M. I. Bruce, G. A. Heath, K. Costuas, S. P. Best, P. J. Low, K. Costuas, J.-F. F. Halet, S. P. Best, G. A. Heath, *J. Am. Chem. Soc.* **2000**, *122*, 1949–1962.

[14] Q. Zheng, J. A. Gladysz, *J. Am. Chem. Soc.* **2005**, *127*, 10508–10509.

[15] C. M. Che, H. Y. Chao, V. M. Miskowski, Y. Li, K. K. Cheung, *J. Am. Chem. Soc.* **2001**, *123*, 4985–4991.

[16] T. Ren, G. Zou, J. C. Alvarez, *Chem. Commun.* **2000**, *2*, 1197–1198.

[17] R. J. Crutchley, T. Ren, G. Zou, Y.-H. H. Ni, G.-L. L. Xu, M. C. DeRosa, G. Zou, Y.-H. H. Ni, M. C. DeRosa, R. J. Crutchley, et al., *J. Am. Chem. Soc.* **2003**, *125*, 10057–10065.

[18] Z. Cao, B. Xi, D. S. Jodoin, L. Zhang, S. P. Cummings, Y. Gao, S. F. Tyler, P. E. Fanwick, R. J. Crutchley, T. Ren, *J. Am. Chem. Soc.* **2014**, *136*, 12174–12183.

[19] K. T. Wong, J. M. Lehn, S. M. Peng, G. H. Lee, *Chem. Commun.* **2000**, *2*, 2259–2260.

[20] J.-C. Chang, C.-Y. Yeh, G.-H. Lee, C.-K. Kuo, S.-M. Peng, C.-C. Wang, *Dalt. Trans.* **2005**, 3696.

[21] T.-B. Tsao, G.-H. Lee, C.-K. Kuo, C.-Y. Yeh, C.-H. Chou, S.-M. Peng, I. P.-C. Liu, *Chem. - A Eur. J.* **2006**, *13*, 1442–1451.

[22] M. C. Cheng, S. A. Hua, Q. Lv, M. Sigrist, G. H. Lee, Y. C. Liu, M. H. Chiang, S. M. Peng, *Dalt. Trans.* **2018**, *47*, 1422–1434.

[23] A. S. Blum, T. Ren, D. A. Parish, S. A. Trammell, M. H. Moore, J. G. Kushmerick, G. L. Xu, J. R. Deschamps, S. K. Pollack, R. Shashidhar, *J. Am. Chem. Soc.* **2005**, *127*, 10010–10011.

[24] A. K. Mahapatro, J. Ying, T. Ren, D. B. Janes, *Nano Lett.* **2008**, *8*, 2131.

[25] S. Pookpanratana, H. Zhu, E. G. Bittle, S. N. Natoli, T. Ren, C. A. Richter, Q. Li, C. A. Hacker, *J. Phys. Condens. Matter* **2016**, *28*, 094009.

[26] H. Zhu, S. J. Pookpanratana, J. E. Bonevich, S. N. Natoli, C. A. Hacker, T. Ren, J. S. Suehle, C. A. Richter, Q. Li, *ACS Appl. Mater. Interfaces* **2015**, *7*, 27306–27313.

[27] T. Ren, *Chem. Commun.* **2016**, *52*, 3271–3279.

[28] S. N. Natoli, M. Zeller, T. Ren, *Inorg. Chem.* **2016**, *55*, 5756–5758.

[29] S. N. Natoli, T. J. Azbell, P. E. Fanwick, M. Zeller, T. Ren, *Organometallics* **2016**, *35*, 3594–3603.

[30] S. N. Natoli, M. Zeller, T. Ren, *Inorg. Chem.* **2017**, *56*, 10021–10031.

[31] Z. Cao, W. P. Forrest, Y. Gao, P. E. Fanwick, T. Ren, *Organometallics* **2012**, *31*, 6199–6206.

[32] E. C. Judkins, M. Zeller, T. Ren, *Inorg. Chem.* **2018**, *57*, 2249–2259.

[33] S. D. Banziger, T. D. Cook, S. N. Natoli, P. E. Fanwick, T. Ren, *J. Organomet. Chem.* **2015**, *799–800*, 1–6.

[34] C. Sun, C. R. Turlington, W. W. Thomas, J. H. Wade, W. M. Stout, D. L. Grisenti, W. P. Forrest, D. G. Vanderveer, P. S. Wagenknecht, *Inorg. Chem.* **2011**, *50*, 9354–9364.

[35] C. Sun, P. U. Thakker, L. Khulordava, D. J. Tobben, S. M. Greenstein, D. L. Grisenti, A. G. Kantor, P. S. Wagenknecht, *Inorg. Chem.* **2012**, *51*, 10477–10479.

[36] P. U. Thakker, R. G. Aru, C. Sun, W. T. Pennington, A. M. Siegfried, E. C. Marder, P. S. Wagenknecht, *Inorganica Chim. Acta* **2014**, *411*, 158–164.

[37] W. A. Hoffert, M. K. Kabir, E. A. Hill, S. M. Mueller, M. P. Shores, *Inorganica Chim. Acta* **2012**, *380*, 174–180.

[38] W. A. Hoffert, M. P. Shores, *Acta Crystallogr. Sect. E Struct. Reports Online* **2011**, *67*, DOI 10.1107/S1600536811019969.

[39] J. Nishijo, K. Judai, S. Numao, N. Nishi, *Inorg. Chem.* **2009**, *48*, 9402–9408.

[40] J. Nishijo, K. Judai, N. Nishi, *Inorg. Chem.* **2011**, *50*, 3464–3470.

[41] J. Nishijo, M. Enomoto, *Inorg. Chem.* **2013**, *52*, 13263–13268.

[42] J. Nishijo, *Polyhedron* **2013**, *66*, 43–47.

[43] J. Nishijo, M. Enomoto, *Inorganica Chim. Acta* **2015**, *437*, 59–63.

[44] J. Schneider, H. Jia, J. T. Muckerman, E. Fujita, *Chem. Soc. Rev.* **2012**, *41*, 2036–2051.

[45] W. Nam, Y.-M. Lee, S. Fukuzumi, *Acc. Chem. Res.* **2014**, *47*, 1146–1154.

[46] S. F. Tyler, S. N. Natoli, B. Vlaisavljevich, P. E. Fanwick, T. Ren, *Inorg. Chem.* **2015**, *54*, 10058–10064.

[47] S. F. Tyler, E. C. Judkins, Y. Song, F. Cao, D. R. McMillin, P. E. Fanwick, T. Ren, *Inorg. Chem.* **2016**, *55*, 8736–8743.

[48] E. C. Judkins, S. F. Tyler, M. Zeller, P. E. Fanwick, T. Ren, *Eur. J. Inorg. Chem.* **2017**, *2017*, 4068–4076.

[49] B. M. Oxley, B. Mash, M. Zeller, S. Banziger, T. Ren, *Acta Crystallogr. Sect. E Crystallogr. Commun.* **2018**, *74*, DOI 10.1107/S2056989018003997.

[50] N. F. Curtis, R. W. Hay, *Chem. Commun.* **1966**, 524.

[51] D. F. Cook, N. F. Curtis, R. W. Hay, *J. Chem. Soc. Dalt. Trans.* **1973**, 1160.

[52] N. F. Curtis, *Inorganica Chim. Acta* **2001**, *317*, 27–32.

[53] K. Hideg~, D. Lloyd, *Chem. Commun.* **1970**, 929–930.

[54] K. Hideg, D. Lloyd, *J. Chem. Soc. C* **1971**, 3441–3445.

[55] O. H. Hankovszky, K. Hideg, D. Lloyd, H. McNab, *J. Chem. Soc., Chem. Commun.* **1974**, 378–379.

[56] R. W. Hay, G. A. Lawrence, *J. Chem. Soc. Dalt. Trans.* **1975**, *3*, 1466.

[57] R. W. Hay, P. M. Gidney, *J. Chem. Soc. Dalt. Trans.* **1976**, 974–978.

[58] N. F. Curtis, *J. Chem. Soc. Dalt. Trans.* **1973**, 1212.

[59] B. Bosnich, C. K. Poon, M. L. Tobe, *Inorg. Chem.* **1965**, *4*, 1102–1108.

[60] R. W. Hay, G. A. Lawrance, *J. Chem. Soc. Dalt. Trans.* **1975**, 1556.

[61] T. D. Cook, S. N. Natoli, P. E. Fanwick, T. Ren, *Organometallics* **2015**, *34*, 686–689.

[62] T. D. Cook, S. N. Natoli, P. E. Fanwick, T. Ren, *Organometallics* **2016**, *35*, 1329–1338.

[63] M. J. Frisch, G. W. Trucks, H. B. Schlegel, G. E. Scuseria, M. A. Robb, J. R. Cheeseman, G. Scalmani, V. Barone, G. A. Petersson, H. Nakatsuji, et al., **2016**.

[64] S. N. Natoli, T. D. Cook, T. R. Abraham, J. J. Kiernicki, P. E. Fanwick, T. Ren, *Organometallics* **2015**, *34*, 5207–5209.

[65] S. V. 37. Apex3 v2016.9-0, Saint V8.34A, **2016**.

[66] 2000− 2003. SHELXTL, version 6.14; Bruker AXS Inc.: Madison, WI, **n.d.**

[67] 2016. Sheldrick, G. M. SHELXL 2016; University of Göttingen, Göttingen, Germany, **n.d.**

CHAPTER 2. IMPROVING REDOX STABILITY AND INTERMETALLIC COUPLING OF CO(III) ALKYNYLS THROUGH TUNING OF FRONTIER ORBITALS

*"Reprinted with permission from: Organometallics **2020**, 39, 10, 2019–2025. Copyright 2020, American Chemical Society "*

2.1 Abstract

Reported herein are the syntheses and characterizations for a series of butadiyndiyl-bridged Co^{III}(MPC) (MPC = 5,12-methyl-7.14-phenyl-1,4,8,11-tetraazacyclotetradecane) complexes, capped with chloride ([**1**]$^{2+}$), phenylacetylide ([**2**]$^{2+}$), or 3,5-dichlorophenylacetylide ([**3**]$^{2+}$). The MPC ligand is chosen to weaken the ligand field around the equatorial plane, allowing stronger axial coordination. Characterization by cyclic voltammetry reveals the first examples of delocalized single-electron reduction events in bridged M(cyclam′) complexes (M = any metal, cyclam′ = any ligand bearing the 1,4,8,11-tetraazacyclotetradecane framework), with single electron reductions separated by 100 mV in [**2**]$^{n+}$, as well as quasi-stable reduced states. Further analysis using NBu_4BArF (NBu_4BArF = tetrabutylammoniumtetrakis[3,5-bis(trifluoromethyl)phenyl]borate) as electrolyte further separates reduction events, revealing 150 mV separation and stable reduced states for [3]$^{n+}$. These features provide the possibility of application of earth-abundant metal complexes to function as molecular wires. Each complex was further characterized by infrared spectroscopy, UV-vis spectroscopy, density functional theory calculation, spectroelectrochemistry, and single crystal X-ray diffraction studies where possible.

2.2 Introduction

With rapidly increasing demands on performance and portability, there is incredible interest in miniaturization of electronic components. Nearing the limits of current technologies, with a goal to reach the ultimate limit of molecular scale, scientists have made great efforts to develop molecular electronic devices. Following Nast's seminal works with organometallic σ-alkynyl complexes,[1,2] considerable attention has since been given to the application of such materials as molecular wires due to their structural rigidity and high degree of conjugation. These investigations were largely carried out by the laboratories of Hagihara,[3] Lapinte,[4,5] and

Gladysz,[6,7] who refined the properties σ-alkynyl complexes functioning as wires. To this point several compounds developed for their ability to delocalize charge have been composed of metals such as Fe,[4] Mn,[8] Ru,[9] Ru_2,[10] W,[11] and Re.[6,7] Linear conjugated molecules began to represent a majority of molecular electronic devices, alongside carbon nanotubes and metallic nanowires.[12]

Since the 1990's our lab has worked to develop molecular wires based on a diruthenium paddlewheel motif, inspired by the works of Cotton[13] and Bear and Kadish.[14,15] Several of these compounds display excellent electronic properties and are easily modifiable,[16–18] which eventually led to use in effective flash memory devices.[19–21] The key properties of these compounds are: (i) their propensity for electron delocalization, allowing mixed valency and hence, flow of electric current; (ii) easy post-synthetic modification of the axial sites, allowing incorporation into existing technologies for electronic devices, and (iii) their ability to withstand nearly indefinite redox cycles while maintaining integrity. With the desire to use more earth-abundant and cost-efficient resources, recent efforts have focused on third row transition metals based on the M(cyclam) unit (cyclam = 1,4,8,11-tetraazacyclotetradecane). Our work,[22] alongside the works of Shores,[23] Nishijo,[24] and Wagenknecht[25] has expanded the knowledge in this previously underexplored field. Our previous work on oligoyndiyl-bridged Co^{III}(cyclam) units maintains the structural features which allowed the success of previous Ru_2 complexes, however their electronic properties are not ideal.[26–28] Each alkynyl-linked cobalt complex displays irreversible two-electron reductions which indicates localized charges on each cobalt center and instability of the reduced states. The instability of these complexes is generally attributed to lability of the axial ligands on a more electron rich reduced state of the metal.

Thus far, redox reversibility of Co(cyclam) complexes has been achieved only through the use of significantly electron-withdrawing axial ligands which are less labile on the reduced complex.[25,29–31] Recently, we reported a substituted cylam-based complex, $[Co(MPC)(C_2Ph)_2]Cl$ (MPC = 5,12-methyl-7.14-phenyl-1,4,8,11-tetraazacyclotetradecane), which displays a quasi-reversible reduction using non-electronically withdrawing axial ligands.[32] The corresponding reduction event for the cyclam analogue $[Co(cyclam)(C_2Ph)_2]^+$ is irreversible.[23] This change in electronic properties was achieved through strengthening of the axial bonds, similar in effect to the use of electronically withdrawing ligands, by weakening the equatorial ligand field. Addition of bulky phenyl groups to the cyclam skeleton results in enlargement of the cavity holding the

metal. This results in longer, weaker Co–N bonds and a net increase in positive charge density on the metal, allowing axial σ-alkynyl ligands to form stronger bonds to cobalt and stabilize reduced states. This strengthening of axial bonds not only increases stability, but results in lengthening of the alkynyl C-C bond, hinting at the possibility for delocalization of electrons across such fragments. The combination of these factors would allow for cobalt macrocycle based molecular frameworks to be applied as molecular wires and redox devices similar to previous ruthenium examples.[19–21]

It is the goal of the present work to determine if the increased electrochemical stability and axial ligand bond strength of Co^{III}(MPC) complexes translates into stable electronically delocalized reduced states of bridged complexes. To determine this, a series of butadiyndiyl-bridged complexes, [{Co(MPC)Cl}$_2$(μ-C$_4$)]Cl$_2$ ([**1**]Cl$_2$), [{Co(MPC)(C$_2$Ph)}$_2$(μ-C$_4$)]Cl$_2$ ([**2**]Cl$_2$), and [{Co(MPC)(C$_2$-3,5-Cl-C$_6$H$_3$}$_2$(μ-C$_4$)]Cl$_2$ ([**3**]Cl$_2$) have been prepared (Scheme 2.1). A pair of complexes, [Co(MPC)(C$_2$-3,5,-ClC$_6$H$_3$)Cl]Cl ([**4**]Cl) and [Co(MPC)(C$_2$-3,5,-ClC$_6$H$_3$)(C$_2$H)]Cl ([**5**]Cl), have also been prepared for comparison of properties with the bridged species [**3**]Cl$_2$. The syntheses and characterizations of [**1**]$^{2+}$-[**3**]$^{2+}$ will be discussed henceforth.

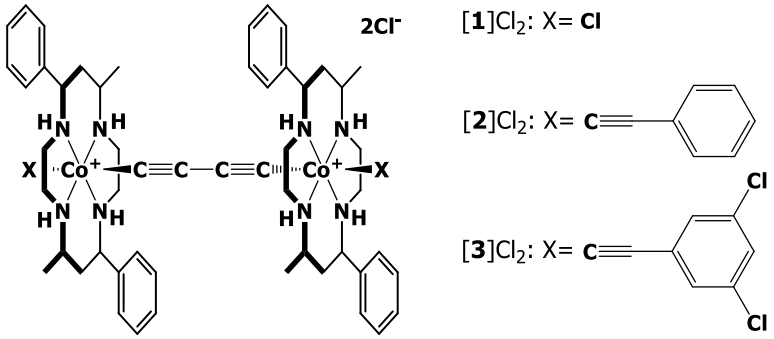

Scheme 2.1. Structures of compounds [**1**]Cl$_2$-[**3**]Cl$_2$ are shown.

2.3 Results and Discussion

2.3.1 Synthesis

To prepare [{Co(MPC)Cl}$_2$(μ-C$_4$)]Cl$_2$ ([**1**]Cl$_2$), Co(MPC)Cl$_3$ was dissolved in MeOH with 0.5 equivalents 1,4-bis(trimethylsilyl)butadiyne and excess triethylamine, then refluxed for 24 h under N$_2$. The resulting product was purified on silica gel and recrystallized for a yield of 44%. Under the given conditions, unreacted starting material and the mononuclear, mono-alkynyl

intermediate are the majority byproducts, as determined by mass spectrometry. Increased reaction time does not significantly increase the ratio of product to starting material. The reaction does proceed under ambient atmospheric conditions, albeit with slightly diminished yields and the appearance of degradation products.

The reaction of the chloride-capped complex ([**1**]Cl_2) with excess capping ligand and lithium diisopropylamide (LDA) at -78°C results in near quantitative conversion to product with minimal scrambling of acetylides or undesired products (Scheme 2.1). Other synthetic routes are available, such as attachment of the butadiyndiyl linker after coordination of the capping ligand, however they result in more difficult purification and lower yields. Compound [**2**]Cl_2 was prepared by adding ca. 6 equivalents LDA to ca. 4 equivalents HC_2Ph in THF at -78°C. While still cold, this solution was transferred to a cold THF solution of 1 equivalent [**1**]Cl_2. After warming to room temperature and stirring for 12 hours, complete conversion to product was apparent from mass spectrometry. The reaction was quenched, and purification on silica gave [**2**]Cl_2 in 68% yield. The synthesis of [**3**]Cl_2 followed a similar procedure, with HC_2-3,5-Cl-C_6H_3 in place of HC_2Ph. In this case, some scrambling of alkynyl ligands occurred, slightly diminishing yields. [**3**]Cl_2 was collected in 52% yield.

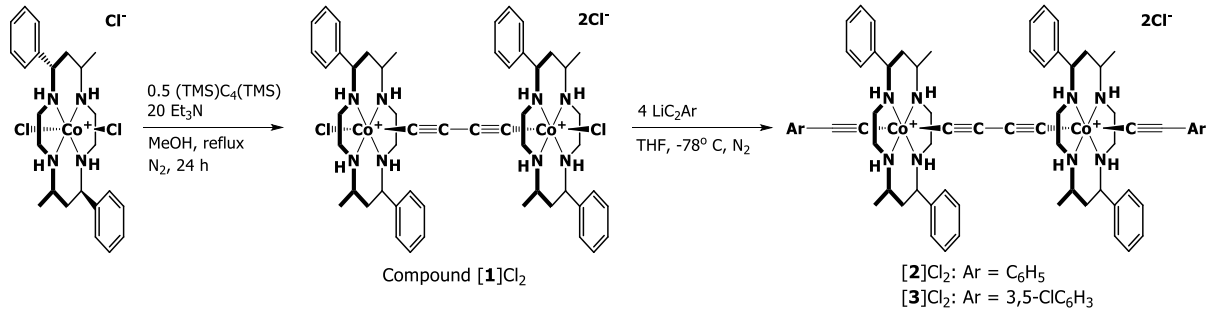

Scheme 2.2. The synthetic route to prepare [**1**]Cl_2, [**2**]Cl_2, and [**3**]Cl_2. Ar = C_6H_5 or 3,5-Cl-C_6H_3.

Compound [**4**]Cl was prepared following the same synthetic strategy as previous work.[32] [Co(MPC)Cl_2]Cl was refluxed for 16 hours in methanol with excess triethylamine and 5 equivalents 3,5-dichlorophenylacetylene. The resulting crude product was purified on silica gel with a mixture of CH_2Cl_2 and methanol for 49% yield. [**5**]Cl was prepared by adding 1 equivalent NaC_2H to [**4**]Cl at -78°C in THF under inert conditions and warming gradually to room

temperature. After purification on silica with a mixture of CH_2Cl_2 and methanol, 35% yield was obtained.

2.3.2 Molecular Structures

Quality single crystals of [**1**]Cl_2 were unable to be obtained. The tetraphenylborate salt, [**1**]$(BPh_4)_2$, was instead prepared for the purpose of a suitable crystal structure. Suitable crystals for $[\mathbf{2}]^{2+}$ and $[\mathbf{3}]^{2+}$ could not be obtained. The ORTEP plot for [**1**]$(BPh_4)_2$ and selected geometric parameters are given in Figure 2.1. Additional experimental and refinement details are given in Table B.1. [**1**]$(BPh_4)_2$ crystallized with one independent cationic unit and two tetraphenylborate anions. The phenyl groups of the BPh_4^- anions are wedged between the macrocyclic units around the alkyne (Figure B.1), allowing a stable solid state structure. The chloro ligands are connected to the amines of neighboring macrocyclic units through hydrogen bonding interactions (Figure B.1). As with previous Co^{III}(MPC) compounds, [**1**]Cl_2 maintains the *trans*-III conformation of the macrocyclic ring with equatorial methyl and phenyl substituents. The Co centers exhibit pseudo-octahedral geometries with the four nitrogen members of the macrocyclic ring forming the equatorial plane and alkynyl/chloro ligands in the axial sites.

It was presumed that the long Co-N bonds and shorter Co-axial bonds resulting from the MPC ligand compared to cyclam, as discussed in previous work,[32] may result in greater electronic communication between cobalt centers across an alkynyl bridge and stabilize a mixed valence state. As shown in Table 2.1, the structure of $[\mathbf{1}]^{2+}$ follows this trend of bond lengths, with longer Co-N bonds and shorter Co-axial bonds than its cyclam counterpart. This results in the alkynyl C≡C bonds being lengthened and the C-C single bond being shortened, indicating a more cumulenic structure and supporting the above hypothesis.

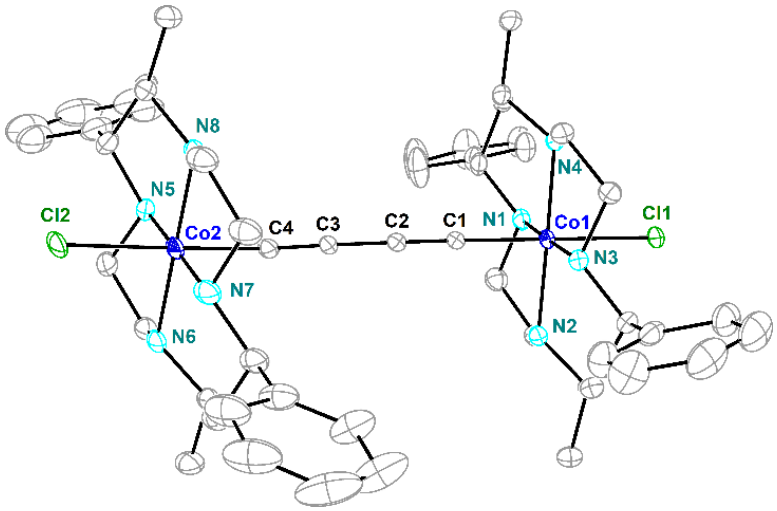

Figure 2.1. Molecular structure of $[\mathbf{1}]^{2+}$ at 30% probability level. Hydrogen atoms and tetraphenylborate anions have been removed for clarity. Selected bond lengths (Å) and angles (deg): Co1-N1, 1.975(2); Co1-N2, 2.014(1); Co1-N3, 1.992(1); Co1-N4, 1.992(1); Co2-N5, 1.991(2); Co2-N6, 1.994(2); Co2-N7, 1.998(2); Co2-N8, 2.001(2); Co1-Cl1, 2.2965(4); Co2-Cl2, 2.2990(5); Co1-C1, 1.874(2), Co2-C4, 1.875(2); C1-C2, 1.211(2); C2-C3, 1.376(2): C3-C4, 1.209(2); Cl1-Co1-C1, 178.92(5); Cl2-Co2-C4, 177.57(6); Co1-C1-C2, 177.5(2); Co2-C4-C3, 174.27(2).

Table 2.1. Bond length comparison for $[\mathbf{1}]^{2+}$ and the cyclam analogue[26] ([{Co(cyclam)Cl}$_2$(μ-C$_4$)]Cl$_2$, labelled as cyclam).

	[**1**]Cl$_2$	cyclam
Co-N$_{avg}$	1.996[1]	1.977[3]
Co-Cl$_{avg}$	2.2978[5]	2.3137[11]
Co1-C1	1.874(2)	1.878(4)
Co2-C4	1.875(2)	1.890(5)
C1-C2	1.211(2)	1.208(6)
C2-C3	1.376(2)	1.388(5)
C3-C4	1.209(2)	1.201(5)

2.3.3 Voltammetric Studies

The $Co^{III/II}$ couple of previously studied [Co(MPC)(C$_2$Ph)$_2$]Cl is quasi-reversible[32] whereas that of the cyclam analogue is irreversible.[23] This is a result of weaker Co-N bonding in the MPC analogue, which leads to increased axial bond strength. We hypothesized that this increased axial bond strength could not only improve reversibility of the redox couple, but also

allow for stabilization of a mixed-valent species through electronic delocalization across an alkynyl bridge. In order to determine these properties, the complexes in the present work were characterized by cyclic voltammetry (CV) and differential pulse voltammetry (DPV) which are shown in Figures 2.2 and 2.3, respectively. Further electrochemical characterization using NBu_4BArF_{24} ($BArF_{24}$ = tetrakis[3,5-bis(trifluoromethyl)phenyl]borate) electrolyte is shown in Figure 4. Redox potentials for each complex are given in Table 2.2.

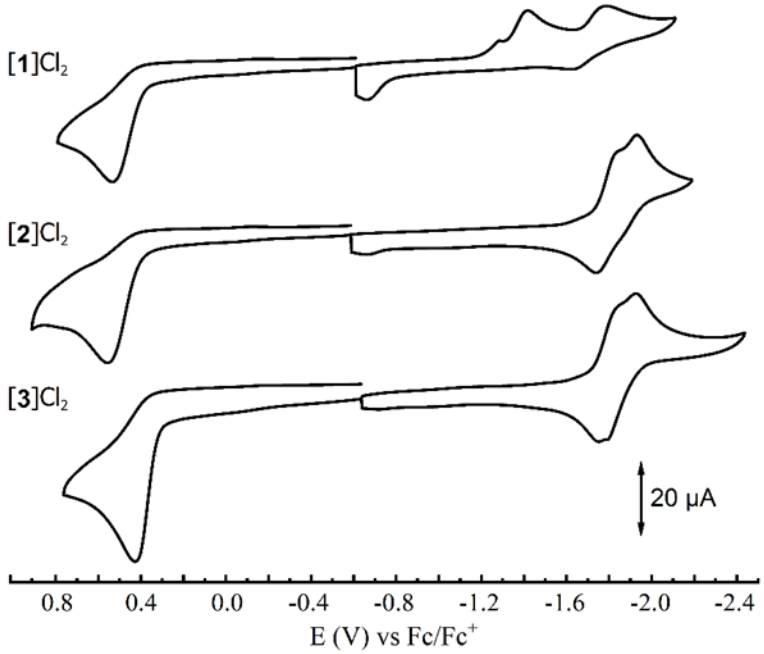

Figure 2.2. Cyclic voltammograms of 1.0 mM [**1**]Cl_2, [**2**]Cl_2, and [**3**]Cl_2 recorded in 0.1 M Bu_4NPF_6 MeCN solution at a scan rate of 0.10 V/s.

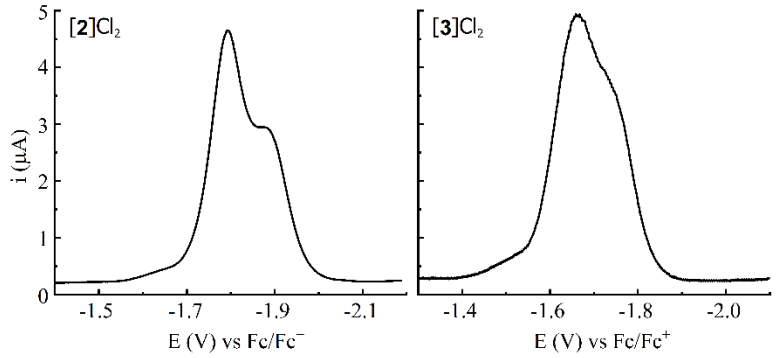

Figure 2.3. Differential pulse voltammograms of [**2**]Cl_2 (left) and [**3**]Cl_2 (right) recorded in 0.1 M Bu_4NPF_6 MeCN solution.

Table 2.2. Reduction potentials for [**1**]Cl_2, [**2**]Cl_2, [**3**]Cl_2, and [**5**]Cl.

E	[1]Cl_2	[2]Cl_2	[3]Cl_2	[5]Cl
4+/2+	0.52	0.56	0.64	-
2+/1+	-1.39[a]	-1.79[b]	-1.65[b]	0.61
1+/0	-	-1.89[b]	-1.74[b]	-1.71
0/2-	-1.76	-	-	-
2+/1+ ($BArF_{24}$)	-	-1.75	-1.66	-
1+/0 ($BArF_{24}$)	-	-1.91	-1.81	-

[a]Potential for 2 electron 2+/0 process. [b]Potential from deconvoluted DPV.

In Co^{III}(cyclam) derived complexes, the coordinated chloride is known to dissociate from cobalt upon reduction, resulting in irreversibility of the $Co^{III/II}$ redox couple.[29] [**1**]Cl_2 shares this feature, as expected, with two irreversible reductions at -1.39 V ($Co^{III/II}$) and -1.76 V ($Co^{II/I}$). An irreversible oxidation also appears at 0.52 V ($Co^{IV/III}$). [**2**]Cl_2 displays substantially different properties from previous Co^{III}(cyclam) based complexes.[28] As with the cyclam analogue, only the $Co^{III/II}$ reduction is visible within the solvent window. Uniquely, however, the $Co^{III/II}$ reduction is both quasi-reversible and split into two single electron events. Due to the overlap of each reduction peak, $i_{p,a}/i_{p,c}$ could not be accurately determined. As shown in Figure 2.3, the second reduction peak is smaller than the first, resulting from chemical degradation on the time scale of the experiment. By deconvolution of the DPV peaks (Figure B.4), each reduction peak was found to be centered at -1.79 and -1.89 V, with the second reduction being 69% the size of the first reduction. Oxidation of the cobalt occurred as a two-electron process at 0.56 V.

[**3**]Cl_2 was prepared with the goal of increasing stability of the reduced state by combining the effects seen from electron-withdrawing ligands with the effect of the MPC ligand. In this regard, [**3**]Cl_2 is more stable than [**2**]Cl_2, with a larger return wave and lack of the degradation peak around -0.55 V seen in the other two compounds (Figure 2.2). The reduction peaks were found to be separated by 0.09 V, located at -1.65 V and -1.74 V, with the second reduction being 90% the size of the first reduction (Figure B.5). The increased electron withdrawing effect of the 3,5-dichloro substituents shifts the reduction of [**3**]Cl_2 to a more anodic value than that of [**2**]Cl_2, indicating the increased affinity for an extra electron. While the enhanced coordination of the 3,5-dichlorophenylacetylide ligand improves stability of the reduced state, it also decreases the peak

separation of each reduction when compared to [**2**]Cl_2 (0.10 V for [**2**]Cl_2, 0.09 V for [**3**]Cl_2), as was hypothesized in previous works.[26]

The use of anions with low affinities for ion pairing as the electrolyte has been proven to improve separation of single electron reductions in mixed valence compounds by thermodynamically stabilizing the singly reduced state.[33,34] In order to increase the separation of the reduction processes for $[\mathbf{2}]^{2+}$ and $[\mathbf{3}]^{2+}$ further, NBu_4BArF was employed as the electrolyte, using dichloromethane as a non-coordinating solvent. As shown in Figure 2.4, the separation of one electron redox events is significantly increased, with separations of 160 mV between $E([\mathbf{2}]^{2+/+})/E([\mathbf{2}]^{+/0})$, and 150 mV between $E([\mathbf{3}]^{2+/+})/E([\mathbf{3}]^{+/0})$. Each redox event is also now resolved enough to see clear features of each individual process. For $[\mathbf{2}]^{2+}$, the first and second redox events occur at -1.69 V and -1.85 V, respectively. The stability of the reduced states of $[\mathbf{2}]^{2+}$ is no longer an issue, with the second reduction maintaining the same current as the first reduction in the DPV. This is attributed to the combination of non-coordinating solvent and low ion pairing electrolyte. Incredibly, each redox process appears quasi-reversible, although $i_{p,a}/i_{p,c}$ is still unable to be accurately determined due to overlap of the redox peaks. Each redox event in $[\mathbf{3}]^{2+}$ is more reversible than $[\mathbf{2}]^{2+}$, although there is still too much overlap of peaks to accurately determine $i_{p,a}/i_{p,c}$ and find whether the processes are fully reversible. The first and second redox events occur at -1.62 V and -1.77 V, respectively. In future work, use of an electronically withdrawing macrocyclic ligand which maintains the steric effects of MPC may allow an even further stabilized reduced state for incorporation of an electron donating axial ligand. This would increase both stability of the reduced state through macrocycle effects and splitting of the reduction peaks through axial ligand effects.

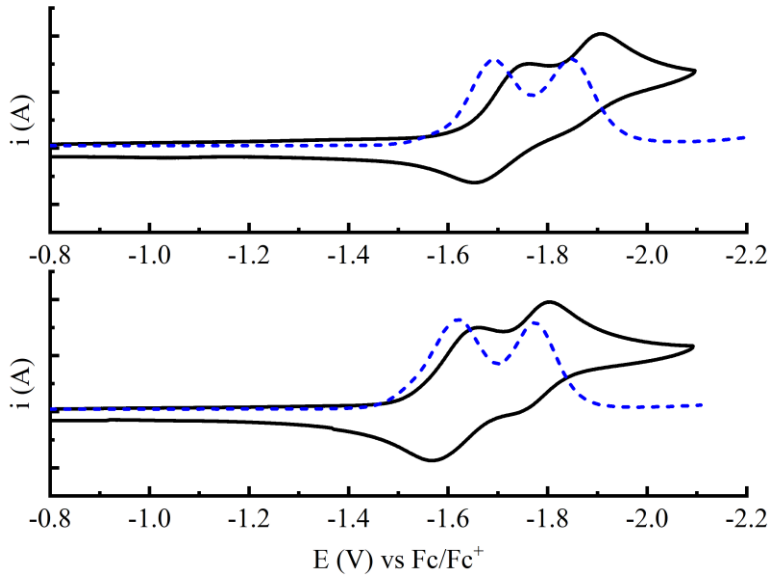

Figure 2.4. Cyclic voltammograms (black, solid) and differential pulse voltammograms (blue, dashed) for 1 mM [**2**]Cl_2 (top) or [**3**]Cl_2 (bottom) recorded in 0.1 M Bu_4BArF CH_2Cl_2 solutions.

The complex [**5**]Cl was prepared to compare electrochemical and spectroelectrochemical properties with [**3**]Cl_2. The CV and DPV for [**3**]Cl are shown in Figure 2.5. The reduction is clearly one defined peak, as expected for a mononuclear complex, and distinguishable from the voltammogram of the dinuclear analogue [**3**]Cl_2. The reduction is located at -1.71 V with an $i_{p,a}/i_{p,c}$ ratio of 71%. Given the similar environment of each cobalt atom in [**3**]Cl and [**5**]Cl_2, it is expected that this ratio would be similar for [**5**]Cl_2. The reduction potential for [3]Cl is also located in between each reduction process for [**5**]Cl_2, indicating the stabilization of the first reduction through delocalization and destabilization of the second reduction. The DPV current for the reduction of [**3**]Cl is identical to the current for each reduction of [**5**]Cl_2, indicating every reduction is in fact a one electron process.

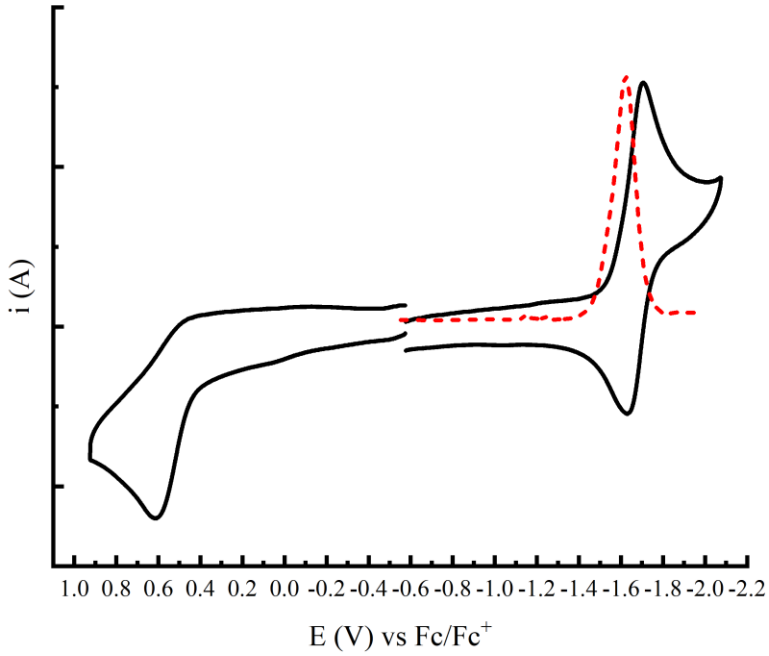

Figure 2.5. Cyclic voltammogram (black, solid) and differential pulse voltammogram (blue, dashed) for 1 mM [**5**]Cl_2 recorded in 0.1 M Bu_4PF_6 CH_2Cl_2 solutions.

2.3.4 Spectroelectrochemical Studies

In an attempt to learn more about the singly reduced [**3**]$^+$ species, spectroelectrochemical experiments were performed. For Robin-Day class II systems in which a mixed valent species exhibits delocalization of valency across a bridge, yet metal centers are distinguishable by at least one spectroscopic method, a charge transfer band should be present in the visible/near-IR region. To test whether this band is present, [**3**]Cl_2 and [**5**]Cl were electrochemically reduced at various potentials and characterized by electronic absorption spectroscopy and infrared spectroscopy in the reduced state. The electronic absorption and IR spectra for [**3**]Cl_2 and [**5**]Cl are presented in Figures 2.6 through 2.10. Unfortunately, the charge transfer band could not be found in the NIR region using the available instrumentation. Absence of this peak, however, is not evidence that [**3**]Cl_2 is incapable of mixed valency. There are several factors which could result in the absence of this peak such as the charge transfer band lying outside the instrumentation window (1600 nm maximum) or the molar absorptivity of the band being too weak to see (0.2 cm path length and other factors reduce absorption). In several literature examples, the charge transfer band can lie well over 2000 nm with weak molar absorptivity.[4,33] The reduction of [**3**]Cl_2 does result in the growth of a new peak at 378 nm, a shoulder at about 405 nm, a peak at 445 nm and a very broad

weak peak around 550 nm. [**5**]Cl shows nearly identical changes. The EA spectra for each complex returns partially to its base state, indicating at least slight stability when reduced.

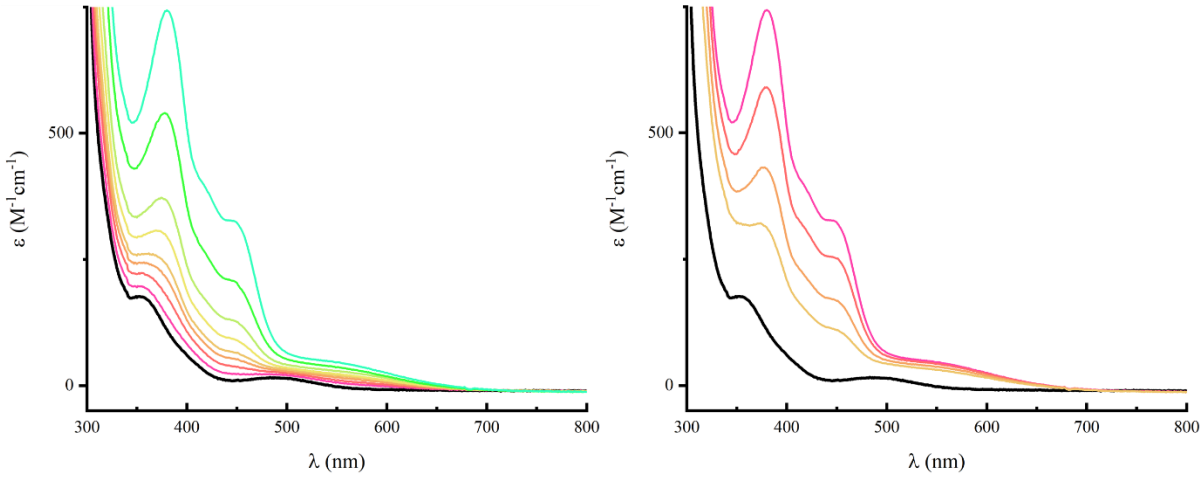

Figure 2.6. Electronic absorption spectra for reduction (left) and return to 0 V (right) for [**3**]Cl_2, with the neutral state in black.

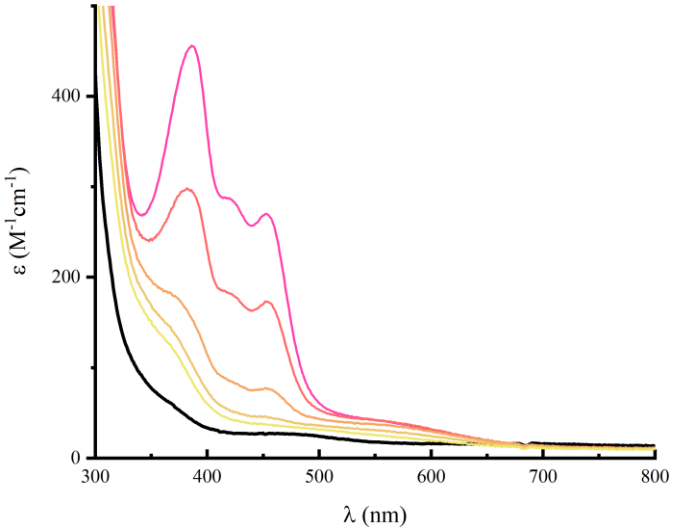

Figure 2.7. Electronic absorption spectra fully reduced to 0 V for [**5**]Cl, with the neutral state in black.

Although the electronic absorption spectra provide no evidence for mixed valency, the IR spectra offer some unique features. For $[\mathbf{3}]^{2+}$, there are three apparent alkyne stretches at 2090, 2120, and 2151 cm^{-1}. The stronger stretch at 2090 cm^{-1} can be attributed to the capping ligand, while the two weaker stretches appear to result from the butadiynyl bridge. Upon applying a weak

range of potentials around the first reduction, several drastic changes occur in the spectra. The stretches at 2151 and 2120 cm^{-1} decline in intensity. In their stead, at least 7 other peaks grow in. Two peaks appear then fade at 2149 and 2133 cm^{-1}, disappearing entirely when the most negative potentials are applied. A very strong peak grows in at 2110 cm^{-1}, continuing to increase as potential increases. A weaker peak grows at 2172 cm^{-1}, also continuing to increase in intensity with current. Two more very strong peaks grow in at 2048 and 2042 cm^{-1}. Initially the peak at 2048 cm^{-1} appears, and the peak at 2042 cm^{-1} is weaker, however as the potential increases the peak at 2042 cm^{-1} becomes more intense. Finally, a weak peak grows in at 1962 cm^{-1}. When the applied potential is removed, all of the peaks resulting from the higher potential fade, the two peaks which grew in and faded return again, and the peak at 2090 cm^{-1}, which had been gradually fading with potential, returns the same. All of this together indicates the complex is going through a two-step process in which one electron is added as new peaks rise. As the second electron is added, the properties of the singly reduced species fades. Both of these processes overlap, as do the reductions in the cyclic voltammogram. The reduction in intensity of the peak at 2090 cm^{-1} is a result of degradation of material, and remains unchanged by oxidation state. The mononuclear analogue, [**5**]Cl, does not hold any of these features. There is a shift in the baseline below 2200 cm^{-1} and the peak at 2124 cm^{-1} shifts to 2114 cm^{-1}. The lack of change in [**5**]Cl further supports the idea that the changes seen in [**3**]Cl_2 are the result of single electron reductions and delocalization across the butadiyndiyl bridge.

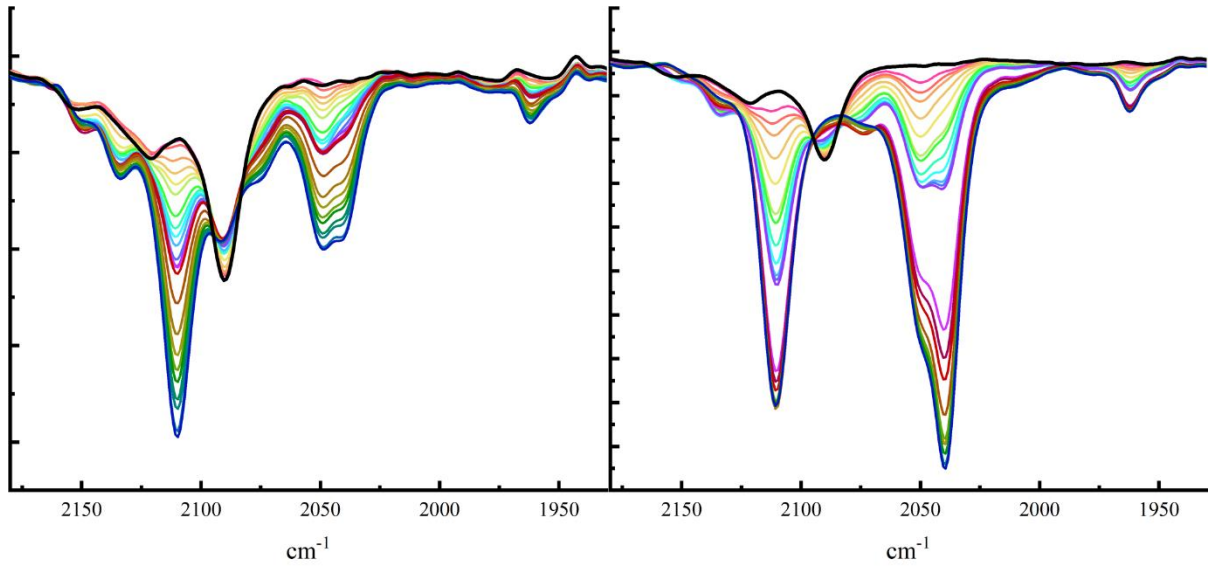

Figure 2.8. IR spectra with a less (left) and more (right) negative range of potentials applied for [**3**]Cl_2. The

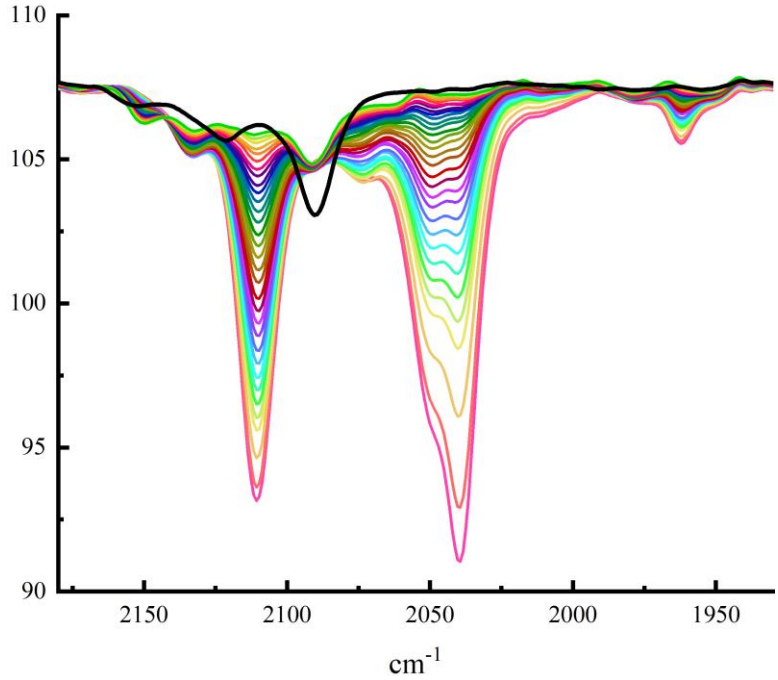

Figure 2.9. IR spectra during the removal of applied potential for [**3**]Cl_2.

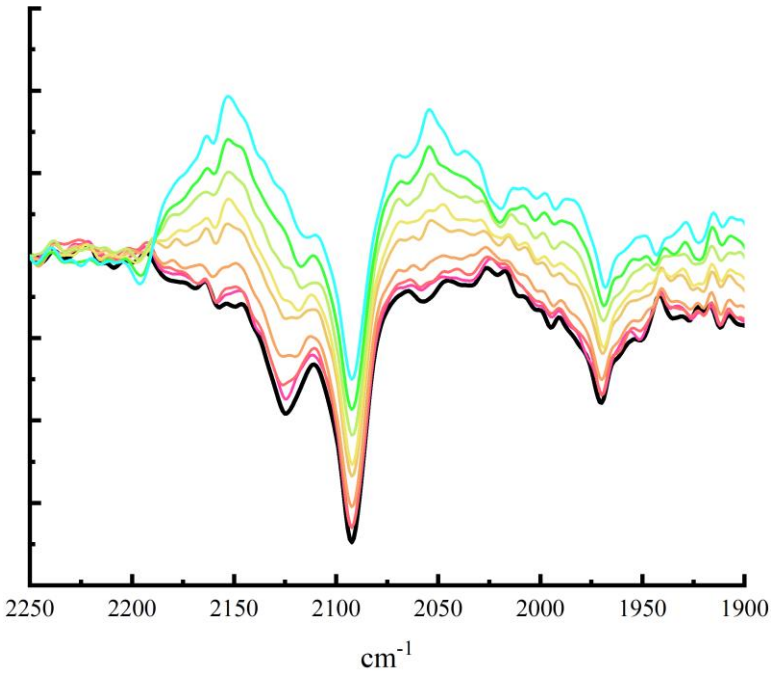

Figure 2.10. IR spectra during the gradual reduction of [**5**]Cl.

2.3.5 Density Functional Theory (DFT) Calculations

To gain more insight into the electronic properties of each compound, the molecular orbitals were calculated *via* DFT. In the absence of suitable crystal structures for $[\mathbf{2}]^{2+}$ and $[\mathbf{3}]^{2+}$, all DFT calculations used the molecular structure of $[\mathbf{1}]^{2+}$ (modified accordingly) as a starting point. The frontier orbitals and energy levels for $[\mathbf{1}]^{2+}$ and $[\mathbf{2}]^{2+}$ are displayed in Figure 2.6. The frontier orbitals and energy levels for $[\mathbf{3}]^{2+}$ are given in Figure S6 and relevant bonds lengths are given in Table B.2.

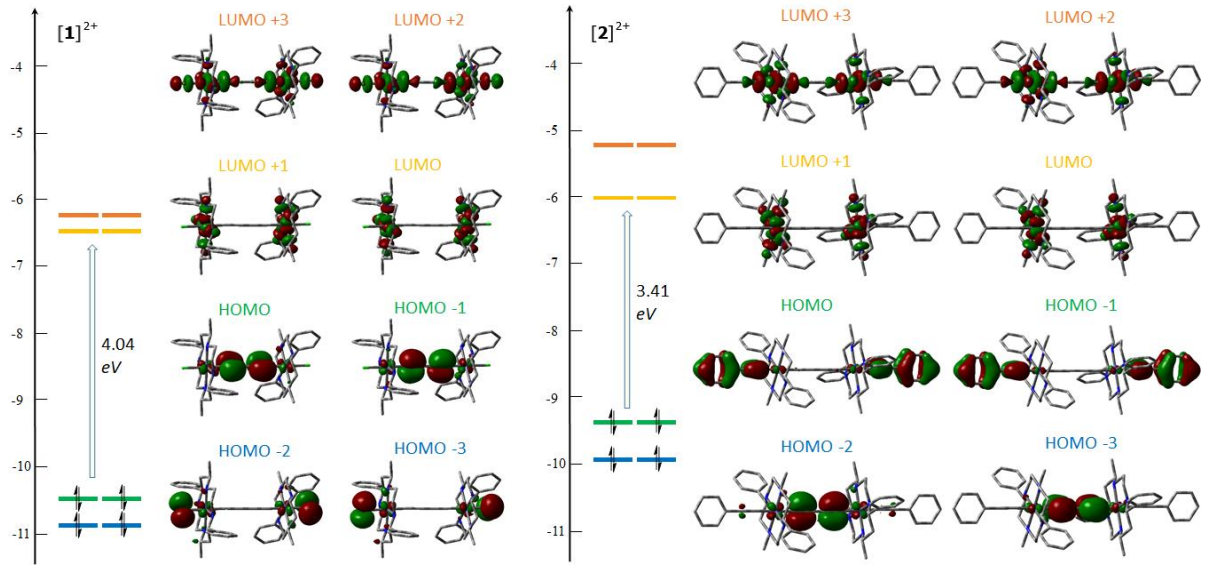

Figure 2.11. Molecular orbital diagrams for [**1**]$^{2+}$ and [**2**]$^{2+}$ from DFT calculations. The isovalue of the contour plots was set at 0.03.

[**1**]$^{2+}$, [**2**]$^{2+}$, and [**3**]$^{2+}$ all share similar features in their LUMO–LUMO+3, with the LUMO and LUMO+1 consisting of the d_{x2-y2} orbitals and LUMO+2 and LUMO+3 consisting of the d_{z2} orbitals. This is consistent with the e_g set of orbitals for low spin, pseudo-octahedral, d^6 Co(III). When compared to the cyclam analogues, it is clear the d_{x2-y2} orbitals are relatively lower in energy and the d_{z2} orbitals are higher for each compound.[26,27] This is a result of weaker ligand field in the xy plane resulting from the MPC ligand. In fact, for the cyclam analogue of [**1**]$^{2+}$, the d_{z2} orbital dominates the LUMO and LUMO+1.[26] The stabilization of the d_{x2-y2} orbitals means the electron added upon reduction will be relatively inert to the stability of the complex, whereas if it were to be directed towards the d_{z2} orbital, it would result in an antibonding interaction with the σ-donating axial ligands. The electronic coupling seen for [**2**]$^{2+}$ and [**3**]$^{2+}$ is not fully explained by DFT, however distortion of the octahedral geometry which would be present in reality but not in a single ion in the gas phase may allow for mixing of the d_{x2-y2} with the higher energy π* orbitals of the alkynyl bridge. This would give rise to the observed properties of each complex. The highest occupied orbitals of each MPC-based complex share similar features to their cyclam counterparts. For [**1**]$^{2+}$, the HOMO and HOMO+1 consist of d_{xz} and d_{yz} interactions with the butadiyndiyl bridge. For [**2**]$^{2+}$ and [**3**]$^{2+}$, the stronger interactions of the d_{xz} and d_{yz} orbitals with the alkynyl capping ligands dominate the HOMO and HOMO+1 while the interactions with the bridge shift to lower

energy levels. These orbitals are not generally attributed to have any major contribution to delocalization, as the electron added upon reduction would be placed in the LUMO.

2.4 Conclusions

A series of Co^{III}(MPC) alkynyl complexes have been prepared in modest to high yields from earth-abundant and commercially available materials. The alkynyl capped compounds [**2**]Cl_2 and [**3**]Cl_2 are the first examples of cyclam derived complexes which display electronic delocalization across a conjugated bridge. Furthermore, [**2**]Cl_2 is the first such cobalt cyclam derived complex to have a quasi-stable reduced state without the use of electron-withdrawing axial ligands. These properties are the result of weaker coordination of the MPC ligand when compared to cyclam, which allows for enhanced axial ligand binding. The use of electron-withdrawing axial ligands compounds with the effect of the MPC ligand for [**3**]Cl_2, giving almost entirely reversible single electron redox events. Based on the knowledge these complexes provide, future compounds bearing more electronically deficient macrocyclic ligands which maintain the steric bulk of MPC can be prepared to further weaken the ligand field in the xy plane and strengthen axial ligand bonding, improving the properties seen here.

2.5 Experimental

2.5.1 Materials

The synthesis for [Co(MPC)Cl_2]Cl was described previously.[32] 3,5-dichlorophenylacetylene was prepared according to a literature procedure.[35] Bis(trimethylsilyl)butadiyne was purchased from GFS Chemicals. *n*-BuLi was purchased from Aldrich. LDA was prepared in situ by addition of *n*-BuLi to diisopropylamine. All reagents were used as received. Tetrahydrofuran was freshly distilled over sodium/benzophenone. All lithiation reactions were carried out under N_2 using standard Schlenk techniques.

2.5.2 Physical Measurements

^{1}H NMR spectra were obtained with a Varian Mercury300 NMR instrument, with chemical shifts (δ) referenced to the residual solvent signal ($CHCl_3$ at δ = 7.26 ppm). UV/Vis spectra were obtained with a JASCO V-670 spectrophotometer. FT-IR spectra were measured as neat samples

using a JASCO FT/IR-6300 spectrometer equipped with an ATR accessory. Electrospray mass spectra were obtained as electrospray in positive-ion mode with the aid of an Advion Expression Compact Mass Spectrometer. Elemental Analysis was carried out by Atlantic Micro Labs in Norcross, GA. Electrochemical analysis was done on a CHI620A voltammetric analyzer with a glassy carbon working electrode (diameter = 2 mm), a Pt-wire auxiliary electrode, and a Ag/AgCl reference electrode. The analyte concentration is 1.0 mM in 4 mL dry acetonitrile with a 0.1 M Bu_4NPF_6 electrolyte concentration, unless otherwise stated.

2.5.3 Synthesis of [{Co(MPC)Cl}$_2$(μ-C$_4$)]Cl$_2$ [1]Cl$_2$

To a methanolic solution of Co(MPC)Cl_3 (1.00 g, 1.83 mmol) was added triethylamine (5.0 mL, 36 mmol), followed by a THF solution of bis(trimethylsilyl)butadiyne (0.188 g, 0.967 mmol). The solution was allowed to reflux for 24h as the color turned from green to orange to red. The solvent was removed via rotary evaporation and the residue was purified on silica gel with a gradient of CH_2Cl_2-MeOH. The collected red product was recrystallized from CH_2Cl_2-Et_2O. Yield: 0.435 g, (44% based on Co). ESI-MS (MeCN): 498 $[\{Co(MPC)Cl\}_2(\mu\text{-}C_4)]^{2+}$. Elem. Anal. for $C_{54}H_{80}N_8O_2Co_2Cl_8$ (**1**·$2H_2O$·$2CH_2Cl_2$): calcd. C 50.88, H 6.32, N 8.79; found C 50.54, H 6.64, N 8.91. ^{1}H NMR ($CDCl_3$, δ): 8.29 (br, 2 H, NH), 7.60-7.10 (m, 20 H, ArH), 6.12 (br, 2 H, NH), 5.57 (br, 2 H, NH), 4.44 (m, 2 H, CH), 4.23 (m, 4 H, CH_2), 3.74 (m, 2 H), 3.58 (br, 2 H, NH), 3.37 (m, 2 H), 3.11 (m, 6 H), 2.79 (m, 4 H), 2.27 (m, 6 H), 1.99 (dd, 2 H), 1.83 (m, 4 H), 1.48 (d, 6 H, CH_3) , 1.35 (d, 6 H, CH_3) ppm. UV-Vis spectra, λ_{max} (nm, ε (M^{-1} cm^{-1})): 207 (66,000), 233 (74,000), 350 (3,100), 520 (380).

2.5.4 Synthesis of [{Co(MPC)(C$_2$Ph)}$_2$(μ-C$_4$)]Cl$_2$ [2]Cl$_2$

A solution of **1** (83 mg, 0.078 mmol) in THF was combined with a solution of Li-phenylacetylide (prepared from 0.36 mmol phenylacetylene and 0.50 mmol LDA) in THF at -78° C. This was allowed to warm to room temperature and stir 12 h before quenching with air and removal of solvent via rotary evaporation. The residue was purified on silica gel with a 15:1 ratio of CH_2Cl_2:MeOH. The collected orange fraction was recrystallized from CH_2Cl_2-Et_2O, yielding 63 mg (68% based on Co). ESI-MS (MeCN): 564 $[\{Co(MPC)(C_2Ph\}_2(\mu\text{-}C_4)]^{2+}$. Elem. Anal. for $C_{71.5}H_{89}N_8Co_2Cl_9$ (**2**·$3.5CH_2Cl_2$): calcd. C 57.35, H 5.99, N 7.48; found C 57.17, H 5.99, N 7.48.

^{1}H NMR ($CDCl_3$, δ): 8.29 (br, 2 H, NH), 7.65-7.05 (m, 30 H, ArH), 5.49 (br, 2 H, NH), 4.91 (br, 2 H, NH), 4.22 (m, 4 H), 4.00 (t, 2 H), 3.62 (br, 2 H, NH), 3.41 (m, 4 H), 3.02 (m, 6 H), 2.86 (m, 2 H), 2.65-2.05 (m, 8 H), 1.94 (dd, 2 H), 1.72 (m, 4 H), 1.42 (d, 6 H, CH_3) , 1.37 (d, 6 H, CH_3) ppm. UV-Vis spectra, λ_{max} (nm, ε (M^{-1} cm^{-1})): 224 (92,000), 260 (74,000), 349 (2,700), 484 (340).

2.5.5 Synthesis of [{Co(MPC)(3,5-ClC_2Ph)}$_2$(μ-C_4)]Cl_2 [3]Cl_2

A solution of **1** (86 mg, 0.080 mmol) in THF was combined with a solution of Li-3,5-dichlorophenylacetylide (prepared from 0.36 mmol 3,5-dichlorophenylacetylene and 0.50 mmol LDA) in THF at -78° C. This was allowed to warm to room temperature and stir 12 h before quenching with air and removal of solvent via rotary evaporation. The residue was purified on silica gel with a 24:1 ratio of CH_2Cl_2-MeOH. The collected orange fraction was recrystallized from CH_2Cl_2:Et_2O, yielding 56 mg (52% based on Co). ESI-MS (MeCN): 633 [{Co(MPC)(3,5-ClC_2Ph)}$_2$(μ-C_4)]$^{2+}$. Elem. Anal. for $C_{69}H_{82}N_8O_1Co_2Cl_8$ (**3**·H_2O·CH_2Cl_2): calcd. C 57.52, H 5.74, N 7.77; found C 57.34, H 5.89, N 7.51. ^{1}H NMR ($CDCl_3$, δ): 7.99 (br, 2 H, NH), 7.80-7.00 (m, 26 H, ArH), 5.57 (br, 2 H, NH), 4.84 (br, 2 H, NH), 4.22 (t, 2 H), 4.09 (m, 2 H), 3.85 (t, 2 H), 3.70-3.20 (m, 6 H), 3.15-2.85 (m, 6 H), 2.68-2.28 (m, 6 H), 2.17 (m, 4 H), 1.94 (dd, 2 H), 1.74 (m, 4 H), 1.40 (m, 12 H, CH_3) ppm. UV-Vis spectra, λ_{max} (nm, ε (M^{-1} cm^{-1})): 226 (100,000), 279 (62,000), 349 (2,500), 479 (320).

2.5.6 Synthesis of [Co(MPC)(3,5-ClC_2Ph)Cl]Cl [4]Cl

To a methanolic solution of [Co(MPC)Cl_2]Cl (0.500 g, 0.916 mmol) was added triethylamine (3 mL), followed by 3,5-dichlorophenylacetylene (0.783 g, 4.58 mmol), which was refluxed for 16 hours. The solvent was removed via rotary evaporation and the residue was purified on silica gel with a gradient of CH_2Cl_2-MeOH. The collected red-orange product was recrystallized in CH_2Cl_2-Et2O. Yield: 0.307 g, (49% based on Co). UV−vis spectra, λ_{max} (nm, ε ($M^{-1}cm^{-1}$)): 265 (34,000), 273 (33,000) 395 (290, sh), 495 (180). IR (cm^{-1}): C≡C: 2104(w).

2.5.7 Synthesis of [Co(MPC)(3,5-ClC$_2$Ph)(C2H)]Cl [5]Cl

[Co(MPC)(3,5-ClC$_2$Ph)Cl]Cl (0.200 g, 0.294 mmol) was dried under vacuum before being suspended in dry THF. NaC$_2$H (0.1 mL, was added at -78°C and allowed to warm to room temperature. The solvent was removed via rotary evaporation and the residue was purified on silica gel with a gradient of CH$_2$Cl$_2$-MeOH to remove symmetric bis-acetylide byproducts. The collected brown product was recrystallized in CH$_2$Cl$_2$-Et2O. Yield: 0.069 g, (35% based on Co). ^{1}H NMR (CDCl$_3$, δ): 7.64 (dd, 2 H, C$_6$H$_3$), 7.37 (m, 10 H, ArH), 7.25 (m, 1 H, C$_6$H$_3$) 5.03 (br, 1 H, NH), 4.84 (br, 1 H, NH), 4.4-3.9 (m, 5 H), 3.42 (m, 2 H), 2.86 (m, 2 H), 2.75-2.25 (m, 4 H), 2.2-1.7 (m, 6 H), 1.37 (m, 6 H) ppm. UV−vis spectra, λ_{max} (nm, ε ($M^{-1}cm^{-1}$)): 275 (28,000), 457 (120). IR (cm^{-1}): C≡C: 2085(m), C≡C: 2112(w, sh).

2.5.8 Computational Details

The geometries of [**1**-2Cl]$^{2+}$, [**2**-2Cl]$^{2+}$, and [**3**-2Cl]$^{2+}$ in the ground states were fully optimized using the crystal structure of **1**, reported in this work, as a starting point (with appropriate modifications). [**2**-2Cl]$^{2+}$ and [**3**-2Cl]$^{2+}$ had the additional ligands edited in manually without changing the rest of the structure. The density functional method B3LYP (Beck's three-parameter hybrid functional using the Lee−Yang−Parr correlation functional)[36] was used for calculations with the def2-TZVP basis set used for cobalt and the def2-SVP basis sets used for all other atoms.[37] The calculation was accomplished by using the Gaussian16 program package.[38]

2.5.9 X-ray Crystallographic Analysis

Single crystal X-ray data was collected on a Bruker AXS D8 Quest CMOS diffractometer using MoKα (λ = 0.71073 Å) radiation with Apex3 software.[39] Data was reduced using SAINT[39] and structures were solved with SHELXTL.[40] Refinement was performed with SHELXL.[41] ORTEP plots were produced using SHELXTL.[40]

2.6 Acknowledgements

I thank the National Science Foundation for generously supporting this work (CHE 1764347 for research and CHE 1625543 for X-ray diffractometers).

2.7 Appendix B: Chapter 2

The experimental crystallographic details, and supramolecular structure plots for 1; DPV plot for 1; DPV peak deconvolution for 2 and 3; orbital splitting diagram from DFT calculations for 3; bond lengths and angles from DFT calculations for all presented complexes; NMR, UV-vis, and IR for all complexes presented are provided in Appendix B: Chapter 2.

2.8 References

[1] R. Nast, *Zeitschrift fur Naturforsch. - Sect. B J. Chem. Sci.* **1953**, *8*, 381-382b.

[2] R. Nast, *Coord. Chem. Rev.* **1982**, *47*, 89–124.

[3] N. Hagihara, K. Sonogashira, S. Takaheashi, *Adv. Polym. Sci.* **1981**, *40*, 149–179.

[4] N. Le Narvor, C. Lapinte, *J. Chem. Soc., Chem. Commun.* **1993**, *8*, 357–359.

[5] F. Paul, C. Lapinte, *Coord. Chem. Rev.* **1998**, *178–180*, 431–509.

[6] Y. Zhou, J. W. Seyler, W. Weng, A. M. Arif, J. A. Gladysz, *J. Am. Chem. Soc.* **1993**, *115*, 8509–8510.

[7] R. Dembinski, T. Bartik, B. Bartik, M. Jaeger, J. A. Gladysz, *J. Am. Chem. Soc.* **2000**, *122*, 810–822.

[8] F. J. Fernández, K. Venkatesan, O. Blacque, M. Alfonso, H. W. Schmalle, H. Berke, *Chem. - A Eur. J.* **2003**, *9*, 6192–6206.

[9] J.-F. F. Halet, M. I. Bruce, G. A. Heath, K. Costuas, S. P. Best, P. J. Low, K. Costuas, J.-F. F. Halet, S. P. Best, G. A. Heath, *J. Am. Chem. Soc.* **2000**, *122*, 1949–1962.

[10] T. Ren, G. Zou, J. C. Alvarez, *Chem. Commun.* **2000**, *2*, 1197–1198.

[11] S. N. Semenov, O. Blacque, T. Fox, K. Venkatesan, H. Berke, *J. Am. Chem. Soc.* **2010**, *132*, 3115–3127.

[12] M. A. Reed, T. Lee, *Molecular Nanoelectronics*, American Scientific Publishers, Stevenson Ranch, CA, **2003**.

[13] A. R. Chakravarty, F. A. Cotton, *Inorganica Chim. Acta* **1986**, *113*, 19–26.

[14] Y. Li, B. Han, K. M. Kadish, J. L. Bear, *Inorg. Chem.* **1993**, *32*, 4175–4176.

[15] J. L. Bear, B. Han, S. Huang, K. M. Kadish, *Inorg. Chem.* **1996**, *35*, 3012–3021.

[16] R. J. Crutchley, T. Ren, G. Zou, Y.-H. H. Ni, G.-L. L. Xu, M. C. DeRosa, G. Zou, Y.-H. H. Ni, M. C. DeRosa, R. J. Crutchley, et al., *J. Am. Chem. Soc.* **2003**, *125*, 10057–10065.

[17] G.-L. Xu, C. G. Jablonski, T. Ren, *J. Organomet. Chem.* **2003**, *683*, 388–397.

[18] G.-L. L. Xu, M. C. DeRosa, R. J. Crutchley, T. Ren, *J. Am. Chem. Soc.* **2004**, *126*, 3728–3729.

[19] H. Zhu, S. J. Pookpanratana, J. E. Bonevich, S. N. Natoli, C. A. Hacker, T. Ren, J. S. Suehle, C. A. Richter, Q. Li, *ACS Appl. Mater. Interfaces* **2015**, *7*, 27306–27313.

[20] S. Pookpanratana, H. Zhu, E. G. Bittle, S. N. Natoli, T. Ren, C. A. Richter, Q. Li, C. A. Hacker, *J. Phys. Condens. Matter* **2016**, *28*, 094009.

[21] S. Pookpanratana, I. Savchenko, S. N. Natoli, S. P. Cummings, L. J. Richter, J. W. F. Robertson, C. A. Richter, T. Ren, C. A. Hacker, *Langmuir* **2014**, *30*, 10280–10289.

[22] T. Ren, *Chem. Commun.* **2016**, *52*, 3271–3279.

[23] W. A. Hoffert, M. K. Kabir, E. A. Hill, S. M. Mueller, M. P. Shores, *Inorganica Chim. Acta* **2012**, *380*, 174–180.

[24] J. Nishijo, M. Enomoto, *Inorg. Chem.* **2013**, *52*, 13263–13268.

[25] L. E. Eddy, P. U. Thakker, C. D. McMillen, J. A. Pienkos, J. J. Cordoba, C. E. Edmunds, P. S. Wagenknecht, *Inorganica Chim. Acta* **2019**, *486*, 141–149.

[26] T. D. Cook, S. N. Natoli, P. E. Fanwick, T. Ren, *Organometallics* **2016**, *35*, 1329–1338.

[27] T. D. Cook, S. N. Natoli, P. E. Fanwick, T. Ren, *Organometallics* **2015**, *34*, 686–689.

[28] T. D. Cook, P. E. Fanwick, T. Ren, *Organometallics* **2014**, *33*, 4621–4624.

[29] S. N. Natoli, M. Zeller, T. Ren, *Inorg. Chem.* **2017**, *56*, 10021–10031.

[30] C. Sun, P. U. Thakker, L. Khulordava, D. J. Tobben, S. M. Greenstein, D. L. Grisenti, A. G. Kantor, P. S. Wagenknecht, *Inorg. Chem.* **2012**, *51*, 10477–10479.

[31] P. U. Thakker, R. G. Aru, C. Sun, W. T. Pennington, A. M. Siegfried, E. C. Marder, P. S. Wagenknecht, *Inorganica Chim. Acta* **2014**, *411*, 158–164.

[32] B. L. Mash, T. Ren, *J. Organomet. Chem.* **2018**, *880*, 143–149.

[33] F. Barrière, W. E. Geiger, *J. Am. Chem. Soc.* **2006**, *128*, 3980–3989.

[34] A. Hildebrandt, D. Miesel, Q. Yuan, J. Freytag, J. Mahrholdt, H. Lang, *Dalt. Trans.* **2019**, *48*, 13162–13168.

[35] D. L. Musso, M. J. Clarke, J. L. Kelley, G. Evan Boswell, G. Chen, *Org. Biomol. Chem.* **2003**, *1*, 498–506.

[36] R. G. Parr, W. B. Yang, *Density Functional Theory of Atoms and Molecules*, Oxford University Press, New York, **1989**.

[37] F. Weigend, R. Ahlrichs, *Phys. Chem. Chem. Phys.* **2005**, *7*, 3297–3305.

[38] M. J. Frisch, G. W. Trucks, H. B. Schlegel, G. E. Scuseria, M. A. Robb, J. R. Cheeseman, G. Scalmani, V. Barone, G. A. Petersson, H. Nakatsuji, et al., **2016**.

[39] S. V. 37. Apex3 v2016.9-0, Saint V8.34A, **2016**.

[40] 2000− 2003. SHELXTL, version 6.14; Bruker AXS Inc.: Madison, WI, **n.d.**

[41] 2016. Sheldrick, G. M. SHELXL 2016; University of Göttingen, Göttingen, Germany, **n.d.**

CHAPTER 3. FURTHER INVESTIGATION INTO BEHAVIOR OF CYCLAM DERIVATIZED COBALT ALKYNYL AS A MOLECULAR WIRE: ETHYNYLFERROCENE HOLE DELOCALIZATION THROUGH COBALT

3.1 Abstract

Reported herein are the syntheses and characterization of Co^{III}(MPC) ethynylferrocene complexes *trans*-$[Co(MPC)(C_2Fc)_2]^+$ ([**1**]Cl), *trans*-$[Co(MPC)(C_2Fc)Cl]^+$ ([**2**]Cl), and *trans*-$[Co(MPC)(C_2Fc)(C_2H)]^+$ ([**3**]Cl), (MPC = 5,12-dimethyl-9,14-diphenyl-1,4,8,11-tetraazacyclotetradecane; Fc = ferrocene). Each complex was characterized by UV-Vis, FT-IR, voltammetric techniques, and single crystal X-ray diffraction ([**1**]Cl only). The core complex of this work, [**1**]Cl, shows a 110 mV separation of ferrocene oxidations when characterized by cyclic voltammetry and differential pulse voltammetry. Upon further analysis using spectroelectrochemical methods, the oxidized states for both complexes [**1**]Cl and [**3**]Cl show a heterometallic charge transfer band from cobalt to ferrocenium. In $[\mathbf{1}]^+$, this heterometallic charge transfer band is absent when oxidized to $[\mathbf{1}]^{2+}$, indicating the electron hole is delocalized across the bridge rather than localized to a ferrocene unit. Both of these results support the functionality of Co^{III}(MPC) complexes as molecular wires and the possible application of cobalt tetraazamacrocyclic complexes in molecular electronics.

3.2 Introduction

For the past decade, 3*d* transition metal alkynyl complexes based on the cyclam ligand framework have been investigated as an alternative to 4*d* and 5*d* transition metals in molecular wire and device applications.[1] Their pseudo-octahedral geometry with readily substituted trans-alkynyl sites enables the facile synthesis of complexes with robust properties, making them strong candidates for the potential incorporation into electronic systems. Initially, the only alkynyl complexes based on cyclam were Cr(cyclam) bis-alkynyls published by Wagenknecht,[2] Nishi,[3] and Berben.[4] Since then, our group[1] along with the groups of Wagenknecht,[5,6] Shores,[7,8] and Nishijo[9] have expanded this to encompass a wider array of complexes including Cr, Fe, Co, and Ni. Of particular interest for molecular wire type devices has been cobalt due to the available synthetic paths[7,10] and the redox potentials falling within reasonable windows.[11]

In 2014, our group produced a series of di-Co(cyclam) complexes bridged by butadiyndiyl (Figure 3.1).[11] These complexes displayed ideal customizability of the axial sites and observable reduction potentials, however they were unstable upon reduction and application towards devices was not possible. Subsequent work using the MPC (MPC = 5,12-dimethyl-9,14-diphenyl-1,4,8,11-tetraazacyclotetradecane) macrocyclic ligand showed quasi-reversible reduction of a bis-phenylacetylide complex[12] (Figure 3.1), in contrast to the irreversibility of the cyclam analogue.[7] Following this result, we produced butadiyndiyl linked di-Co(MPC) complexes (Figure 3.1) which showed reversible single electron reductions.[13] The ability for two identical cobalt centers to exhibit distinct, single electron reductions hints at the possibility of the complex to function as a wire, allowing an electron to shuttle between the metals and stabilizing the singly reduced state.

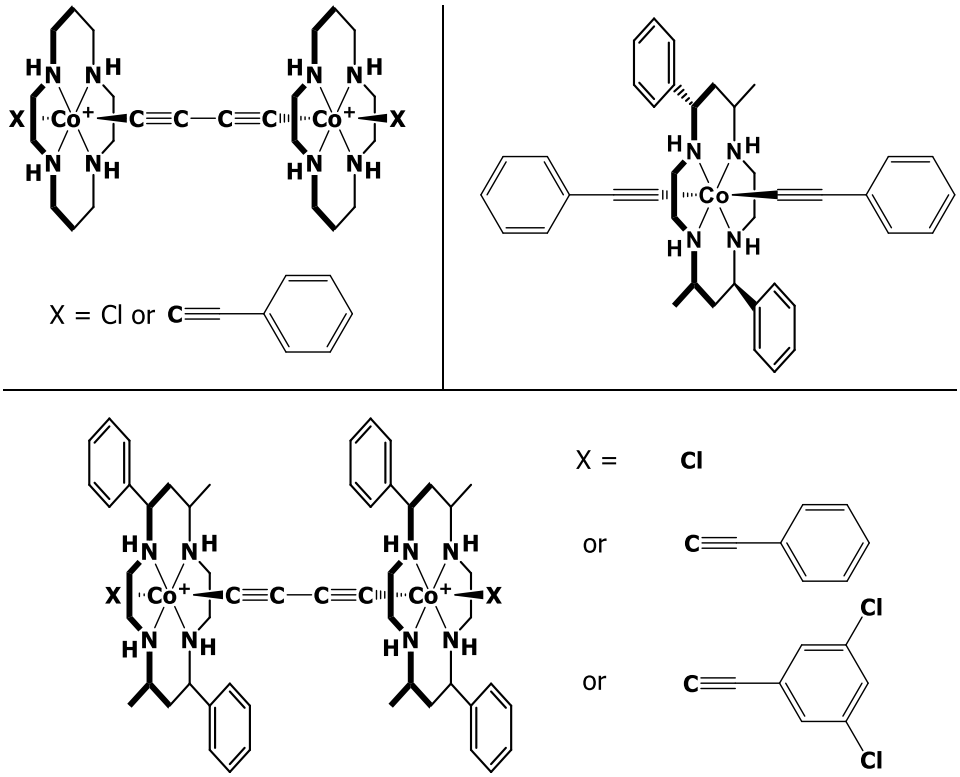

Figure 3.1. Schematic diagrams of representative complexes from our group's 2014 (top left),[11] 2019 (top right),[12] and 2020 (bottom) works.[13]

It is the goal of the current work to further investigate the promising electronic properties of the Co^{III}(MPC) framework. In our previous report on the bridged species, we probed the ability for electronic communication between cobalt centers upon reduction.[13] In this work, we examine

the ability for electron / hole delocalization across cobalt between ferrocene units. For this purpose, we have developed a series of complexes. *Trans*-[Co(MPC)($C_2Fc)_2$]Cl ([**1**]Cl) was prepared to directly investigate the communication between ferrocenes through cobalt, while t*rans*-[Co(MPC)(C_2Fc)Cl]Cl ([**2**]Cl) was made as a precursor to *trans*-[Co(MPC)(C_2Fc)(C_2H)]Cl ([**3**]Cl) to isolate ferrocene's interaction with cobalt in the absence of a third metal center. In this work we show that $[\mathbf{1}]^+$ displays delocalization between the iron metal centers of the ethynylferrocene ligands, as confirmed by cyclic voltammetry. Heterometallic charge transfer bands from cobalt to iron are present in the absorption spectra for $[\mathbf{1}]^{3+}$ and $[\mathbf{3}]^{2+}$. It is notable that this charge transfer band is absent in the singly oxidized $[\mathbf{1}]^{2+}$ species, indicating the oxidized hole is delocalized and an isolated ferrocenium moiety is absent.

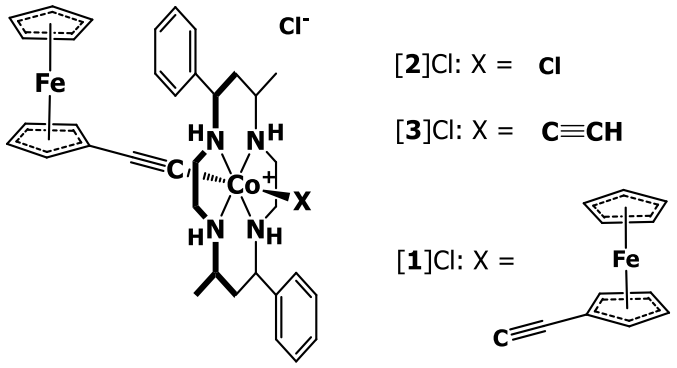

Figure 3.2. Structures of Complexes [**1**]Cl-[**3**]Cl.

3.3 Results and Discussion

3.3.1 Synthesis

[**1**]Cl was generated through standard lithiation procedure, by adding LiC_2Fc to *trans*-[Co(MPC)Cl_2]Cl in an inert atmosphere. After stirring for 1 hour, the orange product was isolated by filtration through silica with a gradient of CH_2Cl_2 and MeOH then recrystallized from a solution of CH_2Cl_2 with ether for a yield of 52% based on cobalt. [**2**]Cl was prepared by refluxing *trans*-[Co(MPC)Cl_2]Cl with ethynylferrocene and triethylamine for 24 h. The brick red product was isolated from the crude reaction mixture by purification on silica using a gradient of CH_2Cl_2 and MeOH and recrystallized using CH_2Cl_2 and ether for a yield of 26% based on cobalt. The diminished yields compared to other similar syntheses is a result of electronic donation from the

ethynylferrocene unit destabilizing the product. [**3**]Cl was prepared by addition of excess sodium acetylide to a solution of [**2**]Cl in dry THF. The dark orange product was filtered through celite and recrystallized from CH_2Cl_2 and ether for a yield of 80%.

As expected for strong field Co^{III} species, all compounds are diamagnetic and exhibit well behaved ^1H NMR spectra (Figures C.5-C.7). The UV-Vis spectra (Figure C.1) feature the iron based *d-d* bands at 441 nm for [**1**]Cl, 455 nm for [**2**]Cl, and a shoulder around 450 nm for [**3**]Cl. The cobalt based *d-d* bands all exist as shoulders, redshifted and masked by the aforementioned iron bands. Also present are intense $\pi-\pi^*$ bands in the UV region for all complexes (Figure C.2). In the infrared spectra (Figure C.3), the C≡C stretches are located at 2106 cm^{-1} for [**1**]Cl, 2134 cm^{-1} for [**2**]Cl, and 2106 cm^{-1} for [**3**]Cl and all bands are weak in intensity.

3.3.2 Molecular Structures

A suitable crystal for X-ray diffraction was grown by slow diffusion of hexanes into a CH_2Cl_2 solution of [**1**]Cl. The ORTEP plot is given in Figure 3.3, while relevant bond lengths are provided in Table 3.1. There is a crystallographic inversion center at Co1, which relates half of the complex ion to the other half. For reference, bond lengths of *trans*-$[Co(MPC)(C_2Ph)_2]^+$ are also given in Table 3.1.[12] Compound $[\mathbf{1}]^+$ retains the pseudo-octahedral *trans*-III geometry common to all Co^{III}(MPC) complexes to date.

It is immediately apparent that all bonds to the cobalt in [**1**]Cl are weakened in comparison to *trans*-$[Cr(MPC)(C_2Ph)_2]^+$. This is due to the σ-donating effect of the ethynylferrocene ligand, compounded with the σ-donation of the amine macrocycle, creating an electron rich Co center. This effect should stabilize the oxidized state, although it weakens the stability of the reduced complex, as discussed in the electrochemistry section below. Even with the increased σ-donation from the ethynylferrocene ligand, the Co-N bond lengths are longer than those of Co^{III}(cyclam) complexes with highly electron withdrawing ligands[10] and the Co-C bonds remain shorter than other less donating complexes.[7] Interestingly, even though the Co-C1 bond is weaker than *trans*-$[Co(MPC)(C_2Ph)_2]^+$, there is a hint of increased delocalization along the alkyne, with increased C1-C2 bond length and decreased C2-C3 bond length.

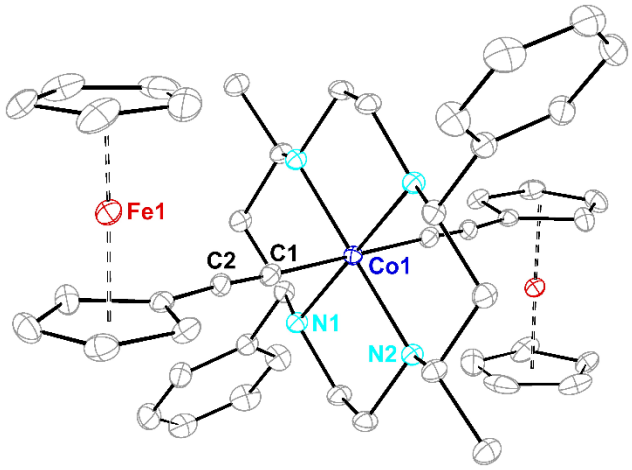

Figure 3.3. Molecular structure of [**1**]$^+$ at 30% probability level. Hydrogen atoms, solvate molecules and chloride anion have been removed for clarity.

Table 3.1. Comparison of Bond Lengths for [**1**]$^+$ and *trans*-[Co(MPC)(C_2Ph)$_2$]$^+$.

	[**1**]Cl	[Co(MPC)(C_2Ph)$_2$]$^+$
Co-N1	2.002(2)	2.019(2)
Co-N2	2.015(2)	1.990(2)
Co-C1	1.946(3)	1.924(3)
C1-C2	1.209(4)	1.201(4)
C2-C3	1.436(4)	1.440(4)

3.3.3 Voltammetric Studies

The electrochemical characterization of [**1**]Cl is the core of this work. The $Co^{III/II}$ couple is located at -1.839 V vs Fc. As with previous Co^{III}(MPC) complexes, a slight oxidation is seen on return from reduction of the cobalt with an $i_{p,a}/i_{p,c}$ of 0.31. The strong electron donation of the ethynylferrocene ligand results in destabilization of the reduced state and hence the irreversibility. More interestingly, two oxidations occur on the ferrocene units. Being symmetric, this is indicative of delocalization of the first oxidized hole between the two ferrocenes and distributed throughout the complex. After deconvolution (Figure C.4), the oxidations are separated by 110 mV with two reversible peaks at -30 and 80 mV. Naturally, both [**2**]Cl and [**3**]Cl show a single ferrocene oxidation. For [**2**]Cl, the irreversible $Co^{III/II}$ and $Co^{II/I}$ reductions are present at -1.40 V and -1.79 V with the $Fe^{II/III}$ couple found at -0.06 V. For [**3**]Cl, the $Co^{III/II}$ couple is located -1.74 V while the $Fe^{II/III}$ couple is observed at -0.04 V. The $Co^{III/IV}$ oxidation is not observable in any of the complexes, likely due to the oxidation of Fe.

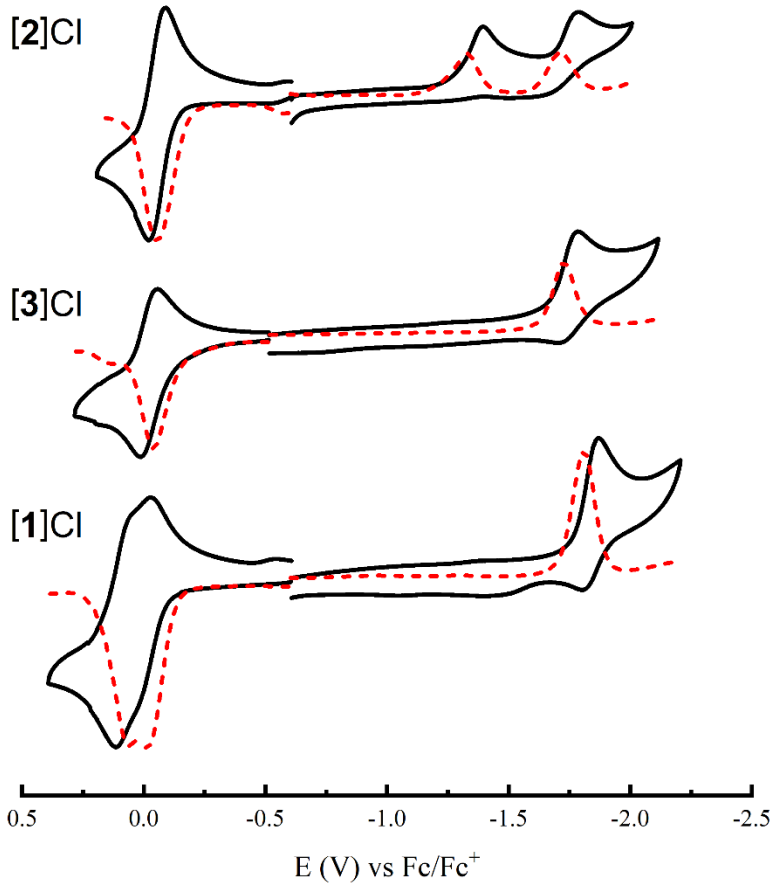

Figure 3.4. CVs (black, solid) and DPVs (red, dashed) of 1.0 mM [**1**]Cl, [**2**]Cl, and [**3**]Cl recorded in 0.1 M Bu_4NBArF CH_2Cl_2 solution at a scan rate of 0.10 V/s.

3.3.4 Spectroelectrochemistry

Spectroelectrochemistry was employed to further characterize the extent of delocalization of the hole in the ethynylferrocene complexes. As shown in Figure 3.5, complex $[\mathbf{1}]^+$ shows a standard *d-d* transition localized to the iron at 438 nm. An additional peak is present as a shoulder around 355 nm. Upon one electron oxidation to $[\mathbf{1}]^{2+}$, this 355 nm peak increases in intensity with no other changes. Once the potential increases to oxidize both ferrocene units, several changes occur. A new peak rises at 412 nm with a maximum extinction coefficient 500 $M^{-1}cm^{-1}$, along with a faint peak at 586 nm and another at 825 nm.

The absorption at 825 nm can be the attributed to one of the three things: (1) excitation localized at a single ferrocenium (2) heterometallic charge transfer between cobalt and ferrocenium or (3) full delocalization between ferrocene and ferrocenium. Scenario (1) can be immediately ruled out since ferrocenium is well-documented to absorb at higher energies. In order

to differentiate between conclusions (2) and (3), compound [**3**]Cl was prepared with one ethynylferrocene ligand replaced by acetylide. Spectroelectrochemical UV-vis-NIR data presented in Figure 3.5 clearly shows a similar charge transfer band located at 850 nm. Therefore, the identity of this peak is attributed to heterometallic charge transfer from cobalt to ferrocenium. This conclusion is further supported by literature, in which FcC_2Au, FcC_2Pt, and FcC_2Ar displayed nearly identical absorption bands assigned as metal or aryl to Fc charge transfer.[14,15] The existence of this peak confirms significant communication between Co(MPC) and ferrocene units. The absence of a ferrocene to ferrocenium IVCT band within the spectral range of our instruments, however, does not confirm or exclude the extent of delocalization observed in the voltammetry of [**1**]Cl.

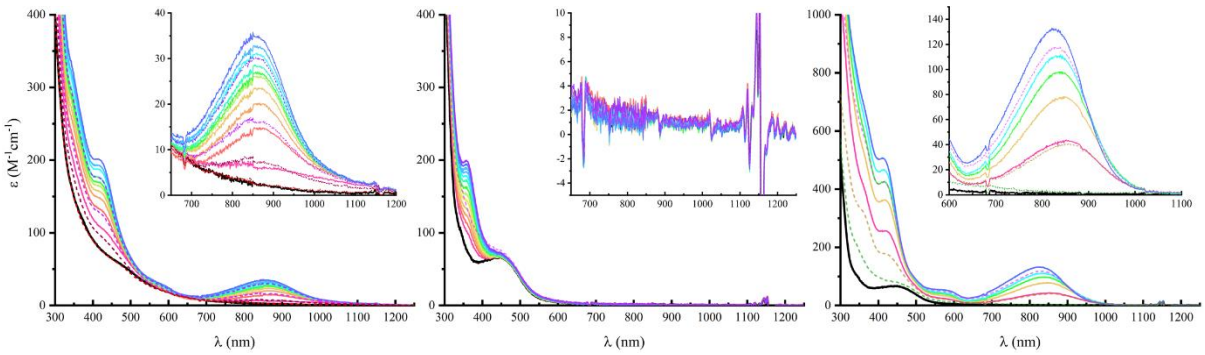

Figure 3.5. UV-vis OTTLE spectra of $[\mathbf{3}]^{+/2+}$ (left), $[\mathbf{1}]^{+/2+}$ (middle) and $[\mathbf{1}]^{+/3+}$ (right). The unbiased spectra are given in black and returns to 0 V are dashed. Insets show the region of heterometallic charge transfer bands.

The presence of a single ferrocenium unit should give rise to the heterometallic charge transfer band in $[\mathbf{1}]^{2+}$, however this band is absent in the spectra. We tentatively attribute this result to the extent of delocalization throughout the complex which removes the existence of a single localized ferrocenium unit and instead distributes the charge through the bridge until the second oxidation occurs.

3.4 Electronic Structures via DFT

To better understand the source of the absorption band located around 825 nm, density functional theory (DFT) calculations were performed. Due to the complexity of a three metal system, reliable calculations of the oxidized states could not be obtained. Instead, calculations were

performed for [**1**]$^+$ and [**3**]$^+$. The relevant frontier orbitals and energy levels are displayed in Figure 3.6. Relevant bond lengths are provided in Table C.2. For both complexes, the LUMO and LUMO+1 consist of the cobalt d_{x2-y2} and d_{z2} orbitals, respectively. Normally, the HOMO would consist of the cobalt d_{xz} or d_{yz} orbital, however, in the presence of the ethynylferrocene ligand, the highest occupied orbitals consist of the iron d_{x2-y2} and d_{xy} orbitals. Interestingly, there is minor cobalt d_{xz} orbital presence elevated in energy with the ferrocene orbitals in the HOMO which leads to significant orbital overlap from one Fe to the other in complex [**1**]$^+$. The cobalt d_{xz} orbital for [**1**]$^+$ and [**3**]$^+$ lies at the HOMO-4 and HOMO-2, respectively, and lies in plane with the z-axis of the iron. The cobalt d_{yz} orbitals, perpendicular to the z-axis of the iron, are located in the HOMO-10 and HOMO-5 for [**1**]$^+$ and [**3**]$^+$, respectively. These orbitals lie 1.568 eV (791 nm) and 1.603 eV (774 nm) away from the iron based HOMO and are the likely source of the heterometallic charge transfer band seen in the oxidized states; however, it is likely energies of the orbitals would change with oxidation.

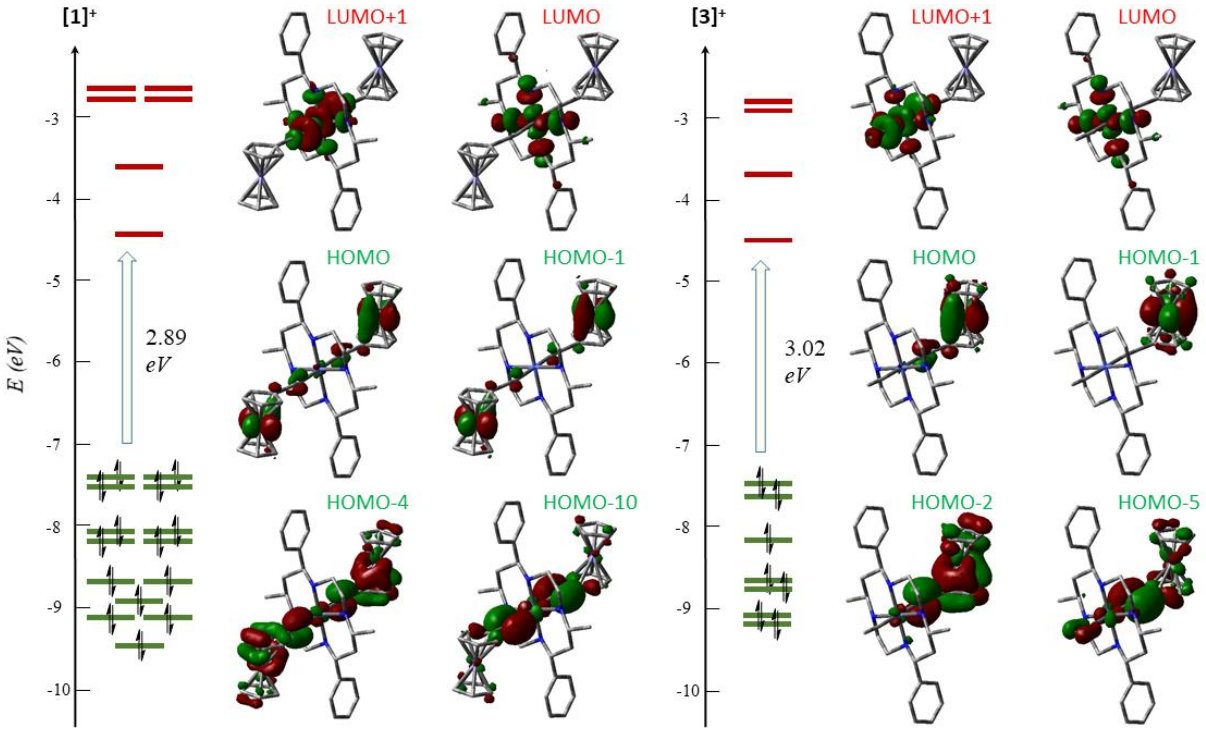

Figure 3.6. Molecular orbital diagrams for [**1**]$^+$ and [**3**]$^+$ from DFT calculations. The isovalue of the contour plots was set at 0.03.

3.5 Conclusions

A series of complexes were prepared to characterize the ability for Co^{III}(MPC) complexes to support electron / hole delocalization across the cobalt. By attaching ethynylferrocene ligands axially, this goal was accomplished in complex [**1**]Cl, which displays significant electronic delocalization between ferrocene units. The oxidations of Fc centers are separated by 110 mV by deconvolution of the DPV spectra. A heterometallic charge transfer band is present in both $[\mathbf{1}]^{3+}$ (825 nm) and $[\mathbf{3}]^{2+}$ (850 nm), confirming substantial electronic delocalization between cobalt and ferrocene. The absence of this peak in $[\mathbf{1}]^{2+}$ supports evidence for the delocalization between ferrocene centers observed in the voltammetric studies. These results further support the potential application of cobalt tetraazamacrocyclic complexes to molecular electronic devices. However, as evident by the lower yields and stability of the reduced complex, improvements can still be made to the macrocyclic framework.

3.6 Experimental

3.6.1 Materials

The synthesis of *trans*-[Co(MPC)Cl_2]Cl has been previously reported.[12] Ethynylferrocene was prepared according to literature procedures.[16] Bis(trimethylsilyl)butadiyne was purchased from GFS Chemicals. *n*-BuLi was purchased from Aldrich. All reagents were used as received. Tetrahydrofuran was freshly distilled over sodium/benzophenone. All lithiation reactions were carried out under N_2 using standard Schlenk techniques.

3.6.2 Physical Measurements

^{1}H NMR spectra were obtained with a Varian Mercury300 NMR instrument, with chemical shifts (δ) referenced to the residual solvent signal ($CHCl_3$ at δ = 7.26 ppm). UV/vis spectra were obtained with a JASCO V-670 spectrophotometer. FT-IR spectra were measured as neat samples using a JASCO FT/IR-6300 spectrometer equipped with an ATR accessory. Electrospray mass spectra (ESI-MS) were obtained as electrospray in positive ion mode with the aid of an Advion Expression Compact Mass Spectrometer. Elemental analysis was carried out by Atlantic Micro Laboratories in Norcross, GA. Electrochemical analysis was done on a CHI620A voltammetric analyzer with a glassy carbon working electrode (diameter = 2 mm), a Pt-wire auxiliary electrode,

and a Ag/AgCl reference electrode. The analyte concentration is 1.0 mM in 4 mL of dry CH_2Cl_2 with a 0.1 M *n*-Bu_4NBArF electrolyte concentration. Spectroelectrochemical analysis was performed using an OTTLE[17] liquid-sample cell with a 0.2 mm optical path length, 0.3 mL sample volume, and a CaF_2 window procured from F. Hartl (Reading, U.K.). The cell was equipped with a mesh Pt working electrode, a mesh Pt auxiliary electrode, and a Ag reference electrode. The analyte concentration was 1.0 mM in 5 mL of dry CH_2Cl_2 at a 0.1 M *n*-Bu_4NBArF electrolyte concentration.

3.6.3 Synthesis of *trans*-[Co(MPC)(C_2Fc)$_2$]Cl ([1]Cl)

A suspension of *trans*-[Co(MPC)Cl_2]Cl (200 mg, 0.366 mmol) in THF was combined with a solution of LiC_2Fc (prepared from 1.1 mmol ethynylferrocene and 1.5 mmol n-BuLi) in THF and allowed to stir 1 hour. The flask was opened to air and solvent was removed via rotary evaporation. The residue was purified on silica gel with a CH_2Cl_2-MeOH gradient. The solvent was removed and the remaining orange residue was recrystallized with CH_2Cl_2-Et_2O. Yield: 0.170 g (52% based on Co). ESI-MS (MeCN): 857 [**1**]$^+$. Elem. Anal. for $C_{48}H_{58}N_4OCoFe_2Cl$ ([**1**]Cl·H_2O): calcd C 63.14, H 6.40, N 6.13. Found C 63.41, H 6.13, N 6.14. ^{1}H NMR ($CDCl_3$, δ): 7.38 (m, 10 H, ArH), 4.63 (d, 4 H, C_5H_4), 4.53-4.32 (m, 4 H), 4.29 (s, 10 H, C_5H_5), 4.23 (t, 4 H, C_5H_4), 4.15 (t, 2 H), 3.49 (m, 2 H), 2.93 (d, 2 H), 2.61 (t, 2 H), 2.43 (t, 2 H) 2.18 (d, 2 H), 2.02 (q, 2 H), 1.84 (d, 2 H), 1.39 (d, 6 H, CH_3) ppm. UV−vis spectra, λ_{max} (nm, ε ($M^{-1}cm^{-1}$)): 212 (78,000), 222 (79,000), 272 (27,000, sh), 303 (8,000, sh), 343 (2,000, sh) 441 (1150), 500 (sh). IR (cm^{-1}): C≡C: 2106(w).

3.6.4 Synthesis of *trans*-[Co(MPC)(C_2Fc)Cl]Cl ([2]Cl)

To a methanolic solution of *trans*-[Co(MPC)Cl_2]Cl (0.300 g, 0.55 mmol) was added triethylamine (0.5 mL, 3.6 mmol), followed by ethynylferrocene (0.346 mL, 1.65 mmol). The solution was allowed to reflux under N_2 for 24 hours. The solvent was removed via rotary evaporation and the residue was purified on silica gel with a gradient of CH_2Cl_2-MeOH. The collected red product was recrystallized in CH_2Cl_2-Et_2O. Yield: 0.101 g, (26% based on Co). ESI-MS (MeCN): 683 [**2**]$^+$. Elem. Anal. for $C_{36}H_{51}N_4O_{2.5}CoFeCl_2$ ([**2**]Cl·2.5H_2O): calcd C 56.49, H 6.71, N 7.32. Found C 56.50, H 6.60, N 7.22. ^{1}H NMR ($CDCl_3$, δ): 7.65 (br, 1 H, NH), 7.41 (m,

10 H, ArH), 6.15 (br, 1 H, NH), 4.92 (br, 1 H, NH), 4.75 (d, 2 H, C_5H_4), 4.44 (m, 2 H), 4.31 (s, 5 H, C_5H_5), 4.20 (t, 2 H, C_5H_4), 4.13 (m, 4 H), 3.46 (br, 2 H), 3.10 (m, 1 H), 2.84 (m, 2 H), 2.57 (m, 2 H), 2.30 (m, 4 H), 1.44 (d, 6 H) ppm. UV−vis spectra, λ_{max} (nm, ε ($M^{-1}cm^{-1}$)): 205 (55000), 225 (41,000), 270 (17,000, sh), 340 (1300, sh), 455 (470), 520 (300, sh). IR (cm^{-1}): C≡C: 2134(w).

3.6.5 Synthesis of *trans*-[Co(MPC)(C_2Fc)(C_2H)]Cl ([3]Cl)

[**2**]Cl (0.071 g, 0.099 mmol) was dissolved in dry THF under N_2. NaC_2H (0.1 mL, 18% wt.) was added at -78 °C and the mixture allowed to warm to room temperature. After two hours, the mixture was filtered through celite, the solvent removed via rotary evaporation, and the product recrystallized from CH_2Cl_2/hexanes. Yield: 0.056 g (80% based on Co). ESI-MS (MeCN): 673 [**3**]$^+$. ^{1}H NMR ($CDCl_3$, δ): 7.32 (m, 10 H, ArH), 4.53 (m, 4 H), 4.44 (m, 2 H), 4.26 (s, 5 H, C_5H_5), 4.23 (m, 4 H), 4.21 (t, 2 H, C_5H_4), 3.45 (m, 2 H), 2.53 (m, 7 H), 2.15 (m, 2 H), 1.74 (m, 2 H), 1.22 (d, 6 H) ppm. UV−vis spectra, λ_{max} (nm, ε ($M^{-1}cm^{-1}$)): 205 (52,000), 220 (40,000), 270 (14,000, sh), 370 (2,400, sh), 478 (1200, sh). IR (cm^{-1}): C≡C: 2106(w).

3.6.6 Computational Details

The geometries of [**1**]$^+$ and [**3**]$^+$ in the ground state were fully optimized based on the crystal structure of [**1**]Cl reported in this work using the density functional method B3LYP (Beck's three-parameter hybrid functional using the Lee−Yang−Parr correlation functional)[18] and employing the def2-TZVP basis set for cobalt and the def2-SVP basis set for all other atoms.[19] The calculations were accomplished by using the Gaussian16 program package.[20]

3.6.7 X-ray Crystallographic Analysis

Single crystal X-ray data was collected on a Bruker AXS D8 Quest CMOS diffractometer using CuKα (λ = 1.54178 Å) radiation with Apex3 software.[21] Data was reduced using SAINT[21] and structures were solved with SHELXTL.[22] Refinement was performed with SHELXL.[23] ORTEP plots were produced through SHELXTL.[22]

3.7 Acknowledgements

I thank the National Science Foundation for generously supporting this work (CHE 1764347 for research and CHE 1625543 for X-ray diffractometers).

3.8 Appendix C: Chapter 3

The experimental crystallographic details for [**1**]Cl, UV-vis and IR plots for [**1**]Cl-[**3**]Cl, deconvolution of DPV spectra for [**1**]$^+$, table of calculated geometric parameters for [**1**]$^+$ and [**3**]$^+$, and NMR spectra for [**1**]Cl-[**3**]Cl can be found in Appendix C: Chapter 3.

3.9 References

[1] T. Ren, *Chem. Commun.* **2016**, *52*, 3271–3279.

[2] D. L. Grisenti, W. W. Thomas, C. R. Turlington, M. D. Newsom, C. J. Priedemann, D. G. VanDerveer, P. S. Wagenknecht, *Inorg. Chem.* **2008**, *47*, 11452–11454.

[3] J. Nishijo, K. Judai, S. Numao, N. Nishi, *Inorg. Chem.* **2009**, *48*, 9402–9408.

[4] L. A. Berben, **2005**.

[5] P. U. Thakker, R. G. Aru, C. Sun, W. T. Pennington, A. M. Siegfried, E. C. Marder, P. S. Wagenknecht, *Inorganica Chim. Acta* **2014**, *411*, 158–164.

[6] P. U. Thakker, C. Sun, L. Khulordava, C. D. McMillen, P. S. Wagenknecht, *J. Organomet. Chem.* **2014**, *772*, 107–112.

[7] W. A. Hoffert, M. K. Kabir, E. A. Hill, S. M. Mueller, M. P. Shores, *Inorganica Chim. Acta* **2012**, *380*, 174–180.

[8] W. A. Hoffert, M. P. Shores, *Acta Crystallogr. Sect. E Struct. Reports Online* **2011**, *67*, DOI 10.1107/S1600536811019969.

[9] J. Nishijo, M. Enomoto, *Inorganica Chim. Acta* **2015**, *437*, 59–63.

[10] S. N. Natoli, M. Zeller, T. Ren, *Inorg. Chem.* **2017**, *56*, 10021–10031.

[11] T. D. Cook, P. E. Fanwick, T. Ren, *Organometallics* **2014**, *33*, 4621–4624.

[12] B. L. Mash, T. Ren, *J. Organomet. Chem.* **2018**, *880*, 143–149.

[13] B. L. Mash, Y. Yang, T. Ren, *Organometallics* **2020**, *39*, 2019–2025.

[14] A. Jakob, P. Ecorchard, M. Linseis, R. F. Winter, H. Lang, *J. Organomet. Chem.* **2009**, *694*, 655–666.

[15] L. Cuffe, R. D. A. Hudson, J. F. Gallagher, S. Jennings, C. J. McAdam, R. B. T. Connelly, A. R. Manning, B. H. Robinson, J. Simpson, *Organometallics* **2005**, *24*, 2051–2060.

[16] G. Doisneau, G. Balavoine, T. Fillebeen-Khan, *J. Organomet. Chem.* **1992**, *425*, 113–117.

[17] M. Krejčik, M. Daněk, F. Hartl, *J. Electroanal. Chem. Interfacial Electrochem.* **1991**, *317*, 179–187.

[18] R. G. Parr, W. B. Yang, *Density Functional Theory of Atoms and Molecules*, Oxford University Press, New York, **1989**.

[19] F. Weigend, R. Ahlrichs, *Phys. Chem. Chem. Phys.* **2005**, *7*, 3297–3305.

[20] M. J. Frisch, G. W. Trucks, H. B. Schlegel, G. E. Scuseria, M. A. Robb, J. R. Cheeseman, G. Scalmani, V. Barone, G. A. Petersson, H. Nakatsuji, et al., **2016**.

[21] S. V. 37. Apex3 v2016.9-0, Saint V8.34A, **2016**.

[22] 2000− 2003. SHELXTL, version 6.14; Bruker AXS Inc.: Madison, WI, **n.d.**

[23] 2016. Sheldrick, G. M. SHELXL 2016; University of Göttingen, Göttingen, Germany, **n.d.**

CHAPTER 4. NICKEL(II) COMPLEXES OF C-SUBSTITUTED CYCLAM AS EFFICIENT CATALYSTS FOR REDUCTION OF CARBON DIOXIDE

"Reprinted with permission from: B. L. Mash, A. Raghavan, T. Ren, Eur. J. Inorg. Chem. ***2019****, 2019, 2065–2070. Copyright 2019 WILEY-VCH Verlag GmbH & Co. KGaA, Weinheim"*

4.1 Abstract

Two new nickel(II) complexes of cyclams bearing *C*-alkyl groups, Ni(MEC)OTf_2 (**1**, MEC = 5,12-diethyl-7,14-dimethyl-1,4,8,11-tetraazacyclotetradecane) and Ni(CTMC)OTf_2 (**2**, CTMC = 5,7,12,14-tetramethyl-1,4,8,11-tetraazacyclotetradecane), were prepared, and their similarity to Ni^{II}(MPC) (MPC = 5,12-dimethyl-7,14-diphenyl-1,4,8,11-tetraazacyclotetradecane) in ring conformation was revealed through single crystal X-ray diffraction studies. Solution electronic absorption spectroscopy indicates the retention of octahedral coordination mode for both **1** and **2** in 20% aqueous acetonitrile. Cyclic voltammetry studies of **1** and **2** under CO_2 in 20% aqueous acetonitrile revealed significantly increased catalytic currents compared to previously studied Ni^{II}(cyclam) and Ni^{II}(MPC). Controlled potential electrolysis studies of **2** revealed a 250% increase in CO turn over frequency from that of Ni(cyclam)OTf_2 and a 40% increase from that of Ni(MPC)OTf_2. Such improvements establish the benefit of electronically donating substituents that minimize steric interference around the axial catalytic sites.

4.2 Introduction

Conversion of CO_2 to carbon fuel sources using solar energy is one of the grand challenges in renewable sciences and technology.[1–4] In addition to generating the reducing equivalent (electrons) through water oxidation, efficient and robust catalysts for CO_2 reduction has been a bottleneck.[3] Efficacy in promoting CO_2 reduction to CO and formate has been demonstrated for many transition-metal complexes. Heavy / precious metal active sites are often involved, such as Re,[5–7] Ru,[8,9] Ir,[10] or Pd,[11,12] and these catalysts often exhibit low tolerance to aqueous conditions, preferentially producing H_2 in these cases. Hence, CO_2 reduction/activation by 3*d* metal-based catalysts has received intense interest. Among noteworthy examples of homogeneous catalysts are Fe-tetraphenylporphyrin and derivatives by Savéant and coworkers,[13–15] selective

reduction of CO_2 to formate using $[Fe_4N(CO)_{12}]^-$ by Berben and co-workers,[16–18] and reduction of CO_2 to methanol by borane with Ni and Fe pincer complexes by Guan and co-workers.[19,20] Li and co-workers reported photo-reduction of CO_2 to CO catalyzed by molecular Co complexes immobilized on solid support.[21,22] Lu and coworkers reported several examples of Cu complexes as photoelectron-catalysts for CO_2 reduction in aqueous solution.[23,24]

Among the earth-abundant transition-metal catalysts, Ni^{II}(cyclam) (cyclam = 1,4,8,11-tetraazacyclotetradecane) is one of the most active in producing CO from CO_2 and compares favorably even with its 4th- and 5th-row organometallic competitors.[4] Furthermore, Ni^{II}(cyclam) and many of its derivatives display selective production of CO over H_2 even under purely aqueous conditions, with the bulk of studies performed with a Hg working electrode.[25,26] Nevertheless, early observations by Fujihira and coworkers that a catalytic wave can indeed be observed at a glassy carbon electrode[27] reveals the promise of carbon electrode as an environmentally benign surrogate. Through controlled-potential electrolysis, Kubiak and co-workers recently verified that CO is the major electrolysis product in Ni^{II}(cyclam) catalyzed CO_2 reaction.[28] Seeking more robust and efficient catalysts, our laboratory recently reported the preparation of three new nickel(II) complexes of cyclams bearing *C*-aryl substituents, and demonstrated that of the new complexes, Ni^{II}(MPC) is significantly more efficient than Ni^{II}(cyclam) in reducing CO_2 to CO under the same conditions.[29] We postulate that the improved catalytic ability results from the increased electron-donor ability of the aryl functionalized cyclam ring, and that it can be further improved through reduction of the steric interference of the substituents with the active catalytic site. To test this hypothesis, we set out to develop catalysts with similar electron-donating *C*-substituents while minimizing their size. Reported in this contribution is our effort in synthesizing two nickel(II) complexes of cyclams bearing *C*-alkyl substituents, namely Ni^{II}(MEC) and Ni^{II}(CTMC), and studying their proficiency in reducing CO_2 through both cyclic voltammetry and controlled potential electrolysis (CPE).

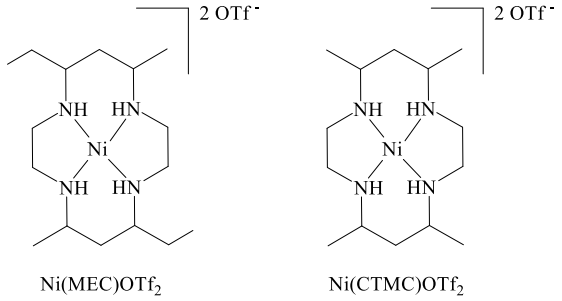

Scheme 4.1. Structures of $Ni(MEC)OTf_2$ (1) and $Ni(CTMC)OTf_2$ (2). Axial coordination is solvent dependent and discussed later.

4.3 Results and Discussion

4.3.1 Synthesis

As shown in Scheme 4.2, the preparation of the precursor MED (5,12-diethyl-7,14-dimethyl-1,4,8,11-tetraazacyclotetradeca-4,11-diene) follows that reported by Hay and coworkers:[30] a proton-templated condensation between ethylenediamine and 4-hexen-3-one (1:1) in the presence of one equiv of $HClO_4$ resulted in $[H_2MED](ClO_4)_2$ as a white microcrystalline material (66%). $[H_2MED](ClO_4)_2$ was reduced by $NaBH_4$ to yield MEC (>90%). The reaction between free base MEC and $NiCl_2$ resulted in $[Ni(MEC)]Cl_2$ as a light pink crystalline solid in 71% yield, and $[Ni(MEC)]Cl_2$ was converted to $[Ni(MEC)](OTf)_2$ (**1**) quantitatively upon reaction with triflic acid. The preparation of $[H_2CTMD](ClO_4)_2$, CTMC (97% yield), $Ni(CTMC)Cl_2$ (75%), and $[Ni(CTMC)]OTf_2$ (**2**, 66%) follow an identical protocol.

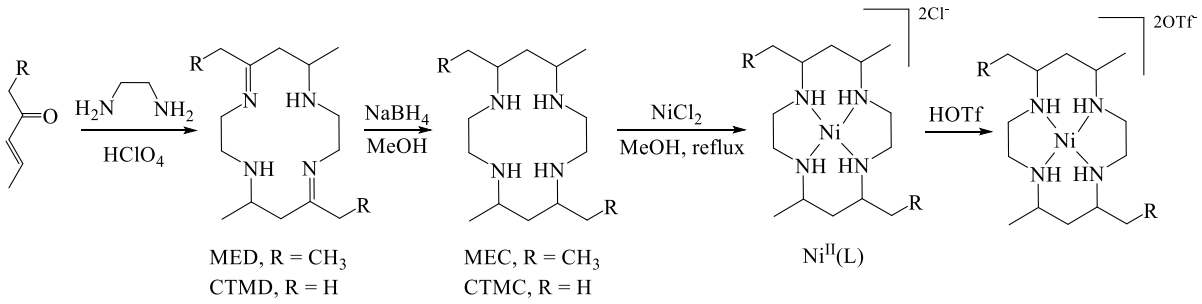

Scheme 4.2. Preparation of L (L = MEC or CTMC), $[Ni^{II}(L)]Cl_2$ and $Ni^{II}(L)(OTf)_2$. Axial coordination is solvent dependent.

4.3.2 Molecular Structures

X-ray quality single crystals of $Ni(MEC)(OTf)_2$ (**1**) and $[Ni(CTMC)(H_2O)_2](OTf)_2$ were grown via slow diffusion of Et_2O into a H_2O-MeCN (v/v, 1/4) solution of **1** and MeOH solution of **2**, respectively. Molecular structures of **1** and $[\mathbf{2}]^{2+}$ along with some selected bond lengths are provided in Figures 4.1a and 4.2, respectively. Interestingly, the cyclam frameworks of Ni^{II}(MEC) and Ni^{II}(CTMC) overlap perfectly with that of Ni^{II}(MPC) as shown in Figure 4.1b, indicating identical ring conformations. This is an important feature, as the ring conformation is a key parameter in the efficacy of carbon dioxide reduction.[31] Previous results indicate that *cis*-coordination geometry or boat-shaped ring conformation reduces the catalytic capacity of the complexes. In addition to the identity in ring conformation, the Ni-N bond lengths in both complexes **1** and $[\mathbf{2}]^{2+}$ are about the same as those of Ni^{II}(MPC) (Ni-N1, 2.093(2) Å; Ni-N2, 2.080(2) Å), despite the change in the donor strength of macrocycles that stems from the replacement of aryls in MPC with alkyls in MEC and CTMC.

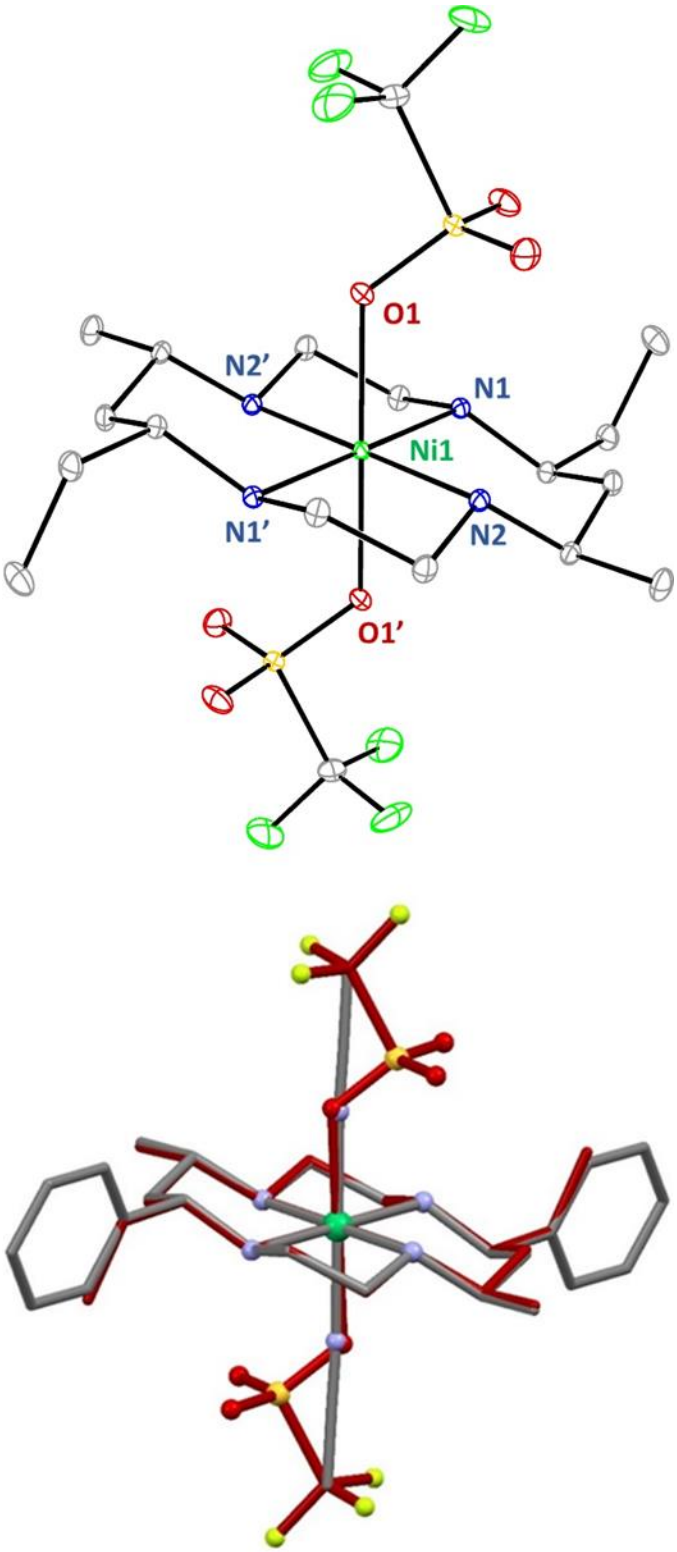

Figure 4.1. (a, top) Molecular structure of **1** at 30% probability level. Hydrogen atoms have been removed for clarity. Selected bond lengths (Å): Ni1–N1, 2.0880(7); Ni1–N2, 2.0802(7); Ni1–O1, 2.1742(7). (b, bottom) Overlay of cyclam rings of **1** (red) and $[Ni(MPC)(MeCN)_2]^{2+}$ (grey).

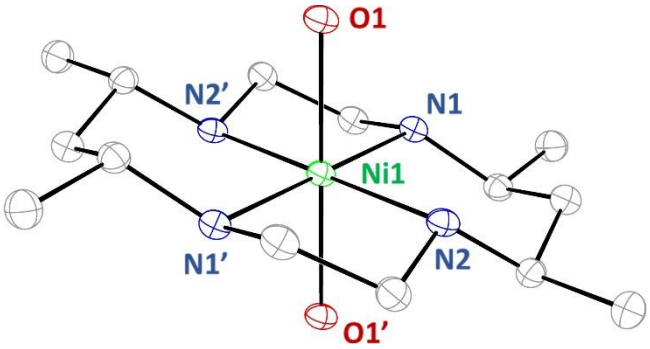

Figure 4.2. Molecular structure of $[\mathbf{2}]^{2+}$ at 30% probability level. Hydrogen atoms and the two triflate counterions have been removed for clarity. Selected bond lengths (Å): Ni1–N1, 2.088(2); Ni1–N2, 2.095(2); Ni1–O1, 2.149(2).

4.3.3 Electronic Absorption Spectra

Having established the pseudo-octahedral coordination geometry for both **1** and $[\mathbf{2}]^{2+}$ in solid state, we endeavored to study the solution geometry of these complexes based on visible-light absorption spectroscopy. In solution, Ni^{II}(tetraamine) species may exist in a spin-state equilibrium between the diamagnetic square-planar geometry and the octahedral paramagnetic geometry, with the population of each state being affected by factors such as solvent and counterion.[32] UV-vis absorption spectra were collected for complexes **1** and **2** in a 20% aqueous MeCN solution (Figure 4.3), the same solvent conditions as those used in subsequent voltammetric studies. As expected from their appearance as purple solids, complexes **1** and **2** display nearly identical absorption spectra in 20% aqueous acetonitrile. Similar to the case of Ni^{II}(MPC), the feature of the visible region is dominated by a weak *d-d* band around 330 nm, and a slightly weaker *d-d* band around 500 nm, both of which are indicative of an octahedral, high-spin species. An even weaker unassigned band is present around 690 nm. Similar absorption spectra were obtained in dichloromethane and neat acetonitrile for both complexes, revealing the retention of octahedral geometry. Curiously, while the spectrum of **1** in methanol retains octahedral characteristics, the methanolic solution of **2** is red, and displays a sharp *d-d* transition at 466 nm, while the above-mentioned *d-d* bands fade (Figure 4.3), thus indicating the dominance of the square planar form.

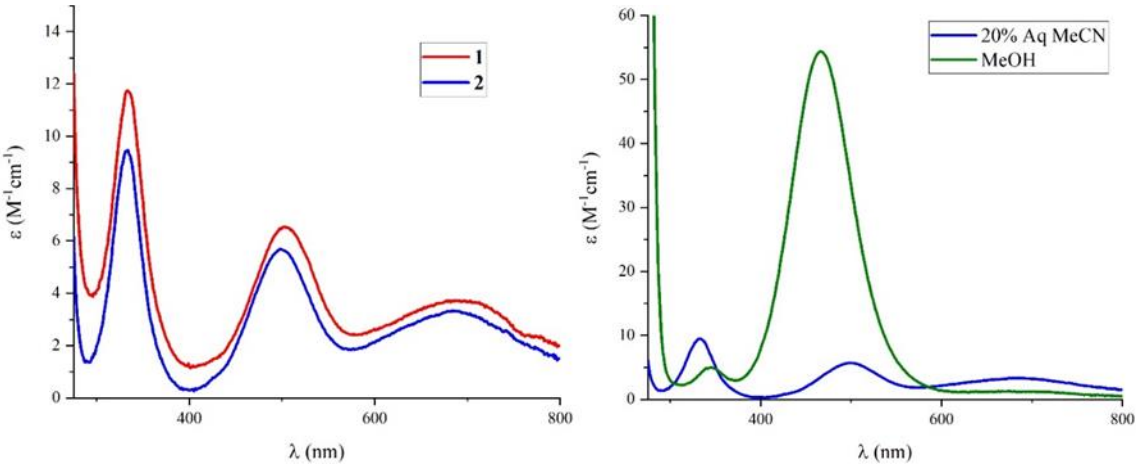

Figure 4.3. (left) UV-vis absorption spectra of **1** (red) and **2** (blue) in 20% aqueous MeCN. (right) UV-vis absorption spectra of **2** in 20% Aq. MeCN (blue) and MeOH (green).

4.3.4 Solution Voltammetry

As shown in Figure 4.4a, the cyclic voltammograms of **1**, **2** and Ni^{II}(MPC) recorded in aqueous acetonitrile are nearly identical under Ar. Each complex displays a reversible one-electron reduction as well as a reversible one electron oxidation (See supporting information for anodic CVs), which are assigned as the Ni(+1/+2) and Ni(+3/+2) couples, respectively. The Ni(+1/+2) couples for **1** (-1.81 V vs Fc) and **2** (-1.80 V vs Fc) are slightly cathodically shifted from Ni^{II}(MPC) (-1.78 V vs Fc), presumably due to the less electron-donating substituents in the latter.

While the cyclic voltammograms of **1**, **2** and Ni^{II}(MPC) under Ar are nearly identical, the CVs recorded under CO_2 are quite different (Figure 4.4b). They all share the common features of the loss of reversibility for the Ni(+1/+2) couple, significant increase in current and the growth of an additional reduction peak at more negative potentials. These features are indicative of catalytic reduction of CO_2.[29] Furthermore, while the catalytic currents at -1.76 V are about the same for **1** (56 μA) and Ni^{II}(MPC) (49 μA), it is nearly doubled for **2** (96 μA). Clearly, the decrease in the steric bulk of *C*-substituents results in a noticeable increase in catalytic efficiency.

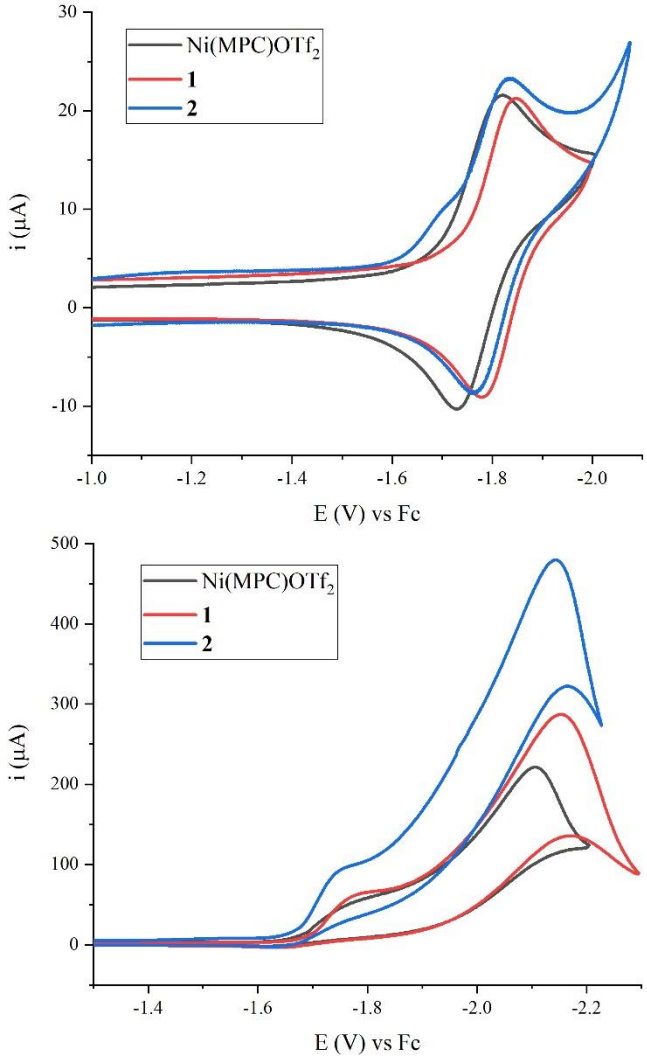

Figure 4.4. (a, top) Cyclic voltammograms of 1.0 mM solutions of **1** (red), **2** (blue), and Ni(MPC)$(OTf)_2$ (black) recorded in a 0.08 M solution of Bu_4NPF_6 in 20% aqueous MeCN on glassy carbon working electrode, purged with Ar; (b) Cyclic voltammograms of **1** (red), **2** (blue), and Ni(MPC)$(OTf)_2$ (black) purged with CO_2.

4.3.5 Controlled Potential Electrolysis

The improved catalytic currents of **1** and **2** compared to Ni^{II}(MPC) prompted further examination of their catalytic proficiency through controlled potential electrolysis (CPE) experiments, which allow for the establishment of the composition of reduction products through headspace analysis and ensuing estimation of Faradaic efficiency and catalytic turnover. The conditions of CPE experiments were identical to those described in our previous report,[29] except for a AgCl coated silver wire being used as the reference electrode in place of a Ag wire pseudoreference electrode. The potential for each experiment was held at a constant -1.76 V vs

Fc/Fc^+, which is slightly more positive than Ni(+1/+2) couples for each complex under CO_2. Each experiment was performed with 0.5 mM catalyst in 20 mL of solution. Similar to our previous work, the headspace was sampled after 30 minutes of electrolysis and injected into a gas chromatograph with a thermal conductivity detector (GC-TCD) to quantify the gaseous products. The gaseous products for **1**, **2**, Ni(MPC)OTf_2 and Ni(cyclam)OTf_2 as well as their catalytic efficiencies are reported in Table 4.1.

The selected electrolysis potential resulted in lower FE but higher TOF for Ni^{II}(MPC) and Ni^{II}(cyclam) compared to our previous report.[29] While each experiment showed significant and highly variable H_2 production, a catalyst-free CPE experiment revealed that the H_2 production is mostly due to the background current instead of the catalysts. In accordance with cyclic voltammetry studies, compound **2** showed both the highest TOF (15.2 h^{-1}) and FE (66%) for the production of CO. Compound **2** is closely followed by **1** in each category (TOF: 14.5 h^{-1}, FE: 57%), while Ni(MPC)OTf_2 held a lower TOF (TOF: 11.0 h^{-1}, FE: 52%). In agreement with our previous work, all catalysts outperformed Ni^{II}(cyclam) substantially (TOF: 4.4 h^{-1}, FE: 35%) under the same conditions. These results follow a clear trend of increasing catalytic ability with reduction in steric bulk of the electronically donating carbon substituents. With identical conformations and axial ligand behavior in solution, the importance of easily accessible axial catalytic sites is highlighted.

Table 4.1. CPE data for **1**, **2**, Ni^{II}(MPC), Ni^{II}(cyclam), and catalyst-free experiments.

	Q (C)	TON, CO	TON, H_2	TOF (h^{-1}), CO	TOF (h^{-1}), H_2	FE, CO (%)	FE, H_2 (%)	μmol CO	μmol H_2
1	24.2	7.3±0.4	2.1±0.9	14.5	4.2	57±2	16±7	72	21
2	22.3	7.7±0.3	1.7±0.7	15.2	3.4	66±1	15±6	77	17
$Ni(MPC)^{2+}$	20.6	5.5	1.0	11.0	2.0	52	10	55	10
$Ni(cyclam)^{2+}$	12.2	2.2	2.4	4.4	4.7	35	38	22	24
blank	7.5	-	-	-	-	3	60	1	23

[a] Performed in CO_2-saturated solutions of 20% aqueous MeCN with 0.08 M NBu_4PF_6; data for **1** and **2** reported as the averages of 2 trials; all other data reported from a single trial; solutions were electrolyzed for 30 min and headspace gases were analyzed via GC–TCD. Q = total charge passed, faradaic efficiency (FE) = $\frac{charge\ to\ form\ product}{total\ charge\ passed}$, turnover number (TON) = $\frac{mol\ product}{mol\ catalyst}$; turnover frequency (TOF) = $\frac{TON}{time}$.

4.4 Conclusions

Both Ni(MEC)OTF_2 (**1**) and Ni(CTMC)OTf_2 (**2**) show significantly improved catalytic current for CO_2 reduction as opposed to Ni^{II}(cyclam) and **2** displayed double the current of our previously reported Ni(MPC)OTf_2. Controlled potential electrolysis revealed CO turnover frequencies of 14.5 and 15.2 h^{-1} for **1** and **2**, respectively. This significant increase from Ni(MPC)OTf_2 (11.0 h^{-1}) and Ni(cyclam)OTf_2 (4.4 h^{-1}) is attributed to the use of electronically donating alkyl substituents without the steric interference around the axial catalytic sites of the phenyl groups present in Ni(MPC)OTf_2. The necessity of the *trans*-III conformation of the cyclam framework is highlighted by comparison of the molecular structures of **1** and **2** with that of Ni(MPC)OTf_2. The results of this work may allow for further development of cyclam-like ligands to improve catalytic activity for the conversion of CO_2 to CO.

4.5 Experimental

4.5.1 Materials

The ketone precursor for $[H_2MED](ClO_4)_2$ was purchased from Sigma-Aldrich and the precursor for $[H_2CTMD](ClO_4)_2$ was purchased from Arctom Chemicals. 5,12-diethyl-7,14-dimethyl-1,4,8,11-tetraazacyclotetradeca-4,11-diene and 5,7,12,14-tetramethyl-1,4,8,11-tetraazacyclotetradeca-4,11-diene dihydroperchlorate were prepared according to literature procedures.[30,33] All reagents were used as received.

4.5.2 Physical Measurements

^{1}H NMR spectra were obtained with a Varian Mercury300 NMR instrument, with chemical shifts (δ) referenced to the residual solvent signal ($CHCl_3$ at 7.26 ppm). UV-Vis spectra were obtained with a JASCO V-670 spectrophotometer. Gas chromatography data were collected on an Agilent 7890A instrument with a thermal conductivity detector (TCD) and an HP-Molsieve column (length = 30 m, diameter = 0.320 mm, film = 12.0 μm). Electrospray mass spectra were obtained as electrospray in positive-ion mode with the aid of an Advion Expression Compact Mass Spectrometer. Cyclic voltammograms were recorded at a scan rate of 100 mVs^{-1} on a CHI620A voltammetric analyzer with a glassy carbon working electrode (diameter = 2 mm, area = 0.0314 cm^2), a Pt-wire auxiliary electrode and a Ag/AgCl wire reference electrode. Potentials were

referenced to a ferrocene internal standard added to the solution. Controlled-potential electrolyses were performed with a CHI620A voltammetric analyzer with a Duocel reticulated vitreous carbon disc (porosity = 100 ppi, diameter = 200 mm, thickness = 5 mm) as the working electrode, a graphite rod auxillary electrode, and an Ag/AgCl reference electrode. The concentration of analyte is always 1.0 mM for cyclic voltammetry experiments and 0.5 mM for bulk electrolysis experiments.

4.5.3 5,12-diethyl-7,14-dimethyl-1,4,8,11-tetraazacyclotetradecane (MEC)

5,12-diethyl-7,14-dimethyl-1,4,8,11-tetraazacyclotetradeca-4,11-diene diperchlorate (1.00 g, 2.07 mmol) was suspended in 50 mL of MeOH. $NaBH_4$ (0.400 g, 10.6 mol) was added in small portions and stirred for 3 h at 45° C, causing the solid to dissolve slowly in the effervescent solution. The solvent was removed under reduced pressure and an aqueous solution of 2M KOH was added. The product was extracted with CH_2Cl_2, dried over Na_2SO_4 and filtered. Solvent was removed under reduced pressure leaving white crystalline solid. Yield: 0.544 g, 92%. ESI-MS (CH_2Cl_2): 285.4 – $[MEC+H^+]^+$. ^1H NMR ($CDCl_3$, δ): 3.04-2.21 (m, 16H, CH, CH_2), 1.60-1.17 (m, 8H, NH, CH_2), 1.01 (d, 6H, CH_3), 0.80 (m, 6H, CH_3).

4.5.4 5,7,12,14-tetramethyl-1,4,8,11-tetraazacyclotetradecane (CTMC)

5,7,12,14-tetramethyl-1,4,8,11-tetraazacyclotetradeca-4,11-diene diperchlorate (2.00 g, 4.41 mmol) was suspended in 50 mL of MeOH. $NaBH_4$ (0.835 g, 22.1 mol) was added in small portions and stirred for 3 h at 45° C, causing the solid to dissolve slowly in the effervescent solution. The solvent was removed under reduced pressure and an aqueous solution of 2 M KOH was added. The product was extracted with CH_2Cl_2, dried over Na_2SO_4 and filtered. Solvent was removed under reduced pressure leaving white crystalline solid. Yield: 1.10 g, 97%. ESI-MS (CH_2Cl_2): 257.4 – $[CTMC+H^+]^+$. ^1H NMR ($CDCl_3$, δ): 3.00 (m, 2H, CH_2), 2.76 (m, 8H, CH, CH_2), 2.31 (m, 6H, NH, CH_2), 1.49 (m, 2H, CH_2), 1.29 (m, 2H, CH_2), 1.02 (m, 12H, CH_3).

4.5.5 Ni(MEC)Cl_2

MEC (0.300 g, 1.06 mmol) was dissolved in 20 mL of MeOH. A methanolic solution of $NiCl_2 \cdot 6H_2O$ (0.261 g, 1.11 mmol) was added and the solution immediately turned purple. The

solution was heated for 30 minutes before adding ether to produce purple solid. The solid was collected, washed with ether, and dried under vacuum. Yield: 0.308 g, 71% based on MEC.

4.5.6 Ni(MEC)(OTf)$_2$ (1)

Ni(MEC)Cl_2 (0.308 g, 0.897 mmol) was dissolved in ~5 mL triflic acid, producing an purple solution. This was allowed to stir 12 hours with a stream of N_2 bubbling through the solution into an aqueous KOH trap. Et_2O was then added producing a purple solid, which was collected by filtration, washed with ether, and dried under vacuum. Yield: 0.397 g, 97%. ESI-MS (CH_2Cl_2): 532.5 – [Ni(MEC)(OTf)]$^+$; 341.4 – [Ni(MEC)-H$^+$]$^+$. Anal. for—$C_{18}H_{36}F_6N_4NiO_6S_2$ {[Ni(MEC)]OTf_2}: calcd. C 33.71, H 5.66, N 8.74; found C 33.71, H 5.84, N 8.74.

4.5.7 Ni(CTMC)Cl_2

CTMC (0.500 g, 1.95 mmol) was dissolved in 20 mL of MeOH. A methanolic solution of $NiCl_2 \cdot 6H_2O$ (0.463 g, 1.95 mmol) was added and the solution turned cloudy with a red/green hue. The solution was allowed to stir overnight, over which time purple crystals formed. This was filtered and collected. The solvent was removed from the red filtrate under reduced pressure leaving red/yellow residue. Upon addition of CH_2Cl_2, the solid turned purple and a light purple solution formed. This was sonicated and filtered. This process was repeated and all collected solid was combined. Yield: 0.638 g, 75%.

4.5.8 Ni(CTMC)(OTf)$_2$ (2)

Ni(CTMC)Cl_2 (0.380 g, 0.984 mmol) was dissolved in ~7 mL triflic acid, producing an orange solution. The solution was stirred for 12 h with a stream of N_2 bubbling through the solution into an aqueous KOH trap. Addition of Et_2O to the solution produced a purple solid, which was collected and washed with ether. Yield: 0.397 g, 66%. ESI-MS (CH_2Cl_2): 463.4 – [Ni(CTMC)(OTf)]$^+$; 313.3 – [Ni(MEC)-H$^+$]$^+$. Anal. for $C_{16}H_{32}F_6N_4NiO_6S_2$ {[Ni(TMC)]OTf_2} (613.26): calcd. C 31.34, H 5.26, N 9.14; found C 31.33, H 5.14, N 9.08.

4.5.9 X-ray Crystallographic Analysis

Single crystal X-ray diffraction data for **1** were collected on a Bruker AXS D8 Quest CMOS diffractometer using Mo-K_α (λ = 0.71073 Å) radiation with Apex3 software.[34] Single crystal X-ray diffraction data for **2** were collected on a Bruker AXS D8 Quest CMOS diffractometer using Cu-K_α radiation (λ = 1.54178 Å) radiation with Apex3 software.[34] Data set was reduced using SAINT[34] and structures were solved with SHELXTL.[35] Refinement was performed with SHELXL.[36] ORTEP plots were produced using SHELXTL.[35]

4.6 Acknowledgements

This work was supported by the National Science Foundation (CHE 1609151 for research and CHE 1625543 for X-ray diffractometers). I thank Prof. Dennis Peters for the loan of electrolysis cell and Prof. Dennis Evans for helpful discussion.

4.7 Appendix D: Chapter 4

Crystal data for **1** and **2**; NMR spectra for MEC and CTMC; GC calibration plots; anodic cyclic voltammograms for **1**, **2**, and Ni(MPC)OTf_2 can be found in Appendix D: Chapter 4.
CCDC 1870623 (**1**) and 1870624 (**2**) contain the supplementary crystallographic data for this paper. These data can be obtained free of charge from The Cambridge Crystallographic Data Centre.

4.8 References

[1] A. J. Morris, G. J. Meyer, E. Fujita, *Acc. Chem. Res.* **2009**, *42*, 1983–1994.

[2] H. Takeda, C. Cometto, O. Ishitani, M. Robert, *ACS Catal.* **2017**, *7*, 70–88.

[3] A. M. Appel, J. E. Bercaw, A. B. Bocarsly, H. Dobbek, D. L. Dubois, M. Dupuis, J. G. Ferry, E. Fujita, R. Hille, P. J. A. Kenis, et al., *Chem. Rev.* **2013**, *113*, 6621–6658.

[4] E. E. Benson, C. P. Kubiak, A. J. Sathrum, J. M. Smieja, *Chem. Soc. Rev.* **2009**, *38*, 89–99.

[5] J. Hawecker, J.-M. Lehn, R. Ziessel, *J. Chem. Soc., Chem. Commun.* **1984**, *3*, 328–330.

[6] E. E. Benson, K. A. Grice, J. M. Smieja, C. P. Kubiak, *Polyhedron* **2013**, *58*, 229–234.

[7] E. E. Benson, C. P. Kubiak, *Chem. Commun.* **2012**, *48*, 7374.

[8] H. Ishida, K. Tanaka, T. Tanaka, *Organometallics* **1987**, *6*, 181–186.

[9] H. Ishida, H. Tanaka, K. Tanaka, T. Tanaka, *J. Chem. Soc., Chem. Commun.* **1987**, *7*, 131–132.

[10] S. Sato, T. Morikawa, T. Kajino, O. Ishitani, *Angew. Chemie Int. Ed.* **2013**, *52*, 988–992.

[11] D. L. Dubois, *Comments Inorg. Chem.* **1997**, *19*, 307–325.

[12] D. L. DuBois, A. Miedaner, R. C. Haltiwanger, *J. Am. Chem. Soc.* **1991**, *113*, 8753–8764.

[13] C. Costentin, S. Drouet, M. Robert, J.-M. Savéant, *Science (80-.).* **2012**, *338*, 90–94.

[14] C. Costentin, M. Robert, J.-M. Savéant, *Chem. Soc. Rev.* **2013**, *42*, 2423–2436.

[15] C. Costentin, M. Robert, J.-M. Savéant, A. Tatin, *Proc. Natl. Acad. Sci.* **2015**, *112*, 6882–6886.

[16] M. D. Rail, L. A. Berben, *J. Am. Chem. Soc.* **2011**, *133*, 18577–18579.

[17] A. Taheri, L. A. Berben, *Inorg. Chem.* **2016**, *55*, 378–385.

[18] N. D. Loewen, E. J. Thompson, M. Kagan, C. L. Banales, T. W. Myers, J. C. Fettinger, L. A. Berben, *Chem. Sci.* **2016**, *7*, 2728–2735.

[19] S. Chakraborty, P. Bhattacharya, H. Dai, H. Guan, *Acc. Chem. Res.* **2015**, *48*, 1995–2003.

[20] S. Chakraborty, J. Zhang, J. A. Krause, H. Guan, *J. Am. Chem. Soc.* **2010**, *132*, 8872–8873.

[21] T. Jin, C. Liu, G. Li, *Chem. Commun.* **2014**, *50*, 6221–6224.

[22] D. He, T. Jin, W. Li, S. Pantovich, D. Wang, G. Li, *Chem. - A Eur. J.* **2016**, *22*, 13064–13067.

[23] W. Liu, H. Huang, T. Ouyang, L. Jiang, D. Zhong, W. Zhang, T. Lu, *Chem. – A Eur. J.* **2018**, *24*, 4503–4508.

[24] T. Ouyang, C. Hou, J.-W. Wang, W.-J. Liu, D.-C. Zhong, Z.-F. Ke, T.-B. Lu, *Inorg. Chem.* **2017**, *56*, 7307–7311.

[25] G. B. Balazs, F. C. Anson, *J. Electroanal. Chem.* **1993**, *361*, 149–157.

[26] J. Schneider, H. Jia, K. Kobiro, D. E. Cabelli, J. T. Muckerman, E. Fujita, *Energy Environ. Sci.* **2012**, *5*, 9502.

[27] M. Fujihira, Y. Hirata, K. Suga, *J. Electroanal. Chem. Interfacial Electrochem.* **1990**, *292*, 199–215.

[28] J. D. Froehlich, C. P. Kubiak, *Inorg. Chem.* **2012**, *51*, 3932–3934.

[29] T. D. Cook, S. F. Tyler, C. M. McGuire, M. Zeller, P. E. Fanwick, D. H. Evans, D. G. Peters, T. Ren, *ACS Omega* **2017**, *2*, 3966–3976.

[30] R. W. Hay, I. Fraser, N. C. Owen, **1998**, *17*, 1611–1615.

[31] J. Schneider, H. Jia, J. T. Muckerman, E. Fujita, *Chem. Soc. Rev.* **2012**, *41*, 2036–2051.

[32] M. Boiocchi, L. Fabbrizzi, F. Foti, M. Vázquez, *Dalt. Trans.* **2004**, 2616–2620.

[33] R. A. Kolinski, B. Korybut-Daszkiewicz, *Inorganica Chim. Acta* **1975**, *14*, 237–245.

[34] S. V. 37. Apex3 v2016.9-0, Saint V8.34A, **2016**.

[35] 2000− 2003. SHELXTL, version 6.14; Bruker AXS Inc.: Madison, WI, **n.d.**

[36] 2016. Sheldrick, G. M. SHELXL 2016; University of Göttingen, Göttingen, Germany, **n.d.**

APPENDIX A. CHAPTER 1

Table A.1. Crystal data for **2a**, **2b**, **3a**, and **3b**

	2a	2b	3a	3b
Chemical formula	$C_{32}H_{37}ClCoN_4$	$C_{32}H_{41}ClCoN_4 \cdot C_2H_3N \cdot Cl \cdot 2(H_2O)$	$C_{40}H_{42}CoN_4 \cdot 3(CH_4O) \cdot Cl$	$C_{40}H_{46}CoN_4 \cdot Cl$
Formal Weight	572.03	688.6	769.28	677.19
space group	*P*-1	$P2_12_12_1$	$P2_1/n$	$P2_1/n$
a (Å)	9.1530(6)	9.2299 (3)	12.6437 (9)	9.6152(5)
b (Å)	14.3513(9)	14.1575 (6)	10.4743 (7)	9.5135(5)
c(Å)	14.6173(10)	25.9569 (12)	14.6061 (10)	19.6006(10)
α (°)	114.622(4)	90	90	90
β (°)	98.255(5)	90	100.376 (3)	97.475 (2)
γ (°)	105.601(4)	90	90	90
V (Å^3)	1607.96(19)	3391.8 (2)	1902.7 (2)	1777.71 (16)
Z	2	4	2	2
Density	1.181	1.231	1.237	1.313
T (K)	150	150	150	150
Final R indices	R1 = 0.0688	R1 = 0.0285	R1 = 0.0400	R1 = 0.0510
$(I > 2\sigma(I))$	wR2 = 0.1937	wR2 = 0.0748	wR2 = 0.1067	wR2 = 0.1286
GooF	1.070	1.063	1.034	1.073

Table A.2. Relevant bond lengths and angles for **[1b]**, **[1c]**, **[2b]**, and **[2c]** from density functional theory calculations.

	[1b]	[2b]	[1c]	[2c]
Co—C	1.9036	1.9087	1.9780	1.9491
Co—Cl	2.3857	2.3747	-	-
Co—N1	2.0161	2.0003	2.0180	2.0030
Co—N2	2.0344	1.9712	2.0327	1.9802
Co—N3	2.0242	2.0003	-	-
Co—N4	2.0250	1.9712	-	-
C1—C2	1.2391	1.2384	1.2069	1.2410
C—Co—C(Cl)	178.727	179.996	180.000	179.992

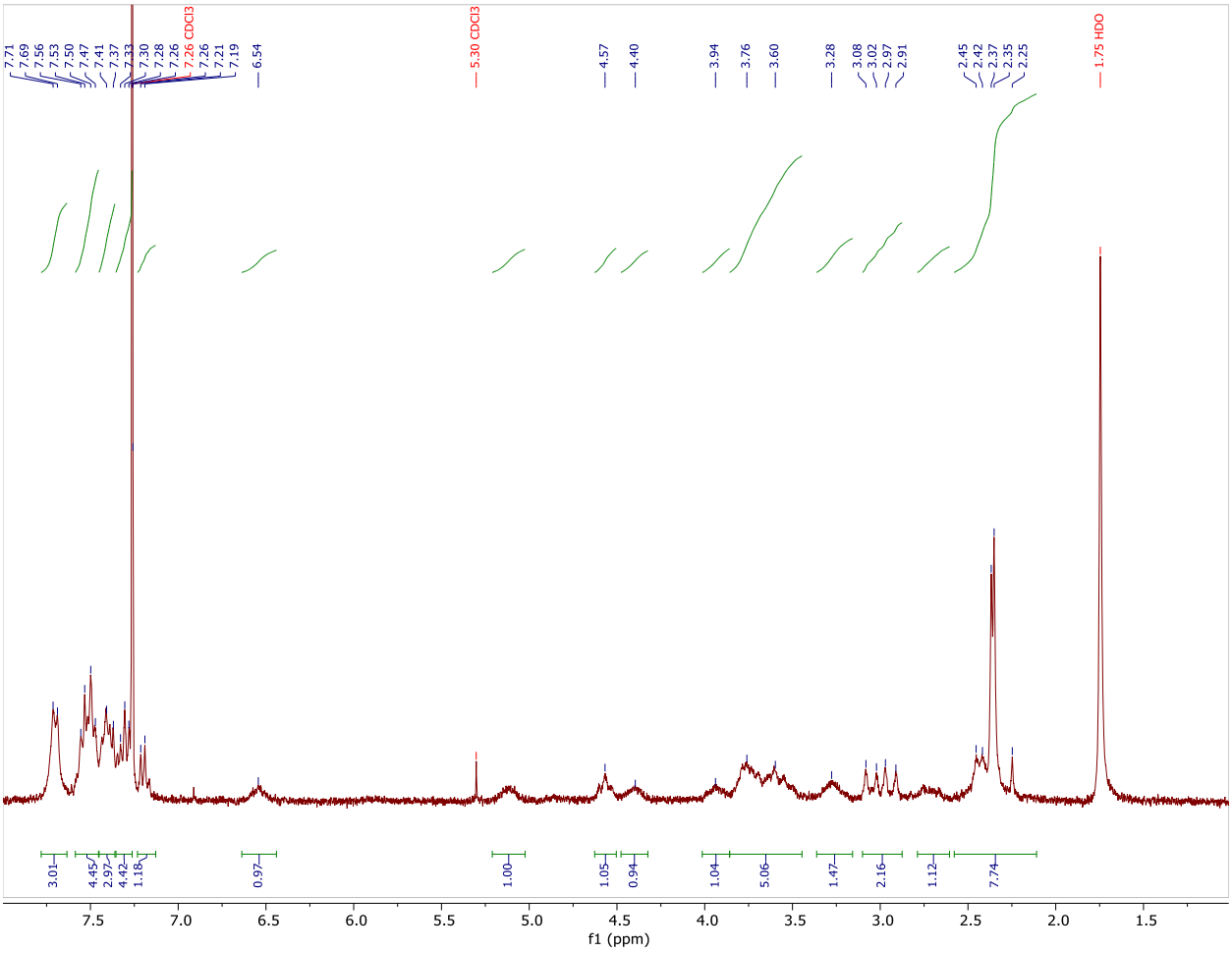

Figure A.1. ^{1}HNMR spectra for **2a**. Peak at 5.30 ppm is CH_2Cl_2. $CHCl_3$ overlaps with aryl region.

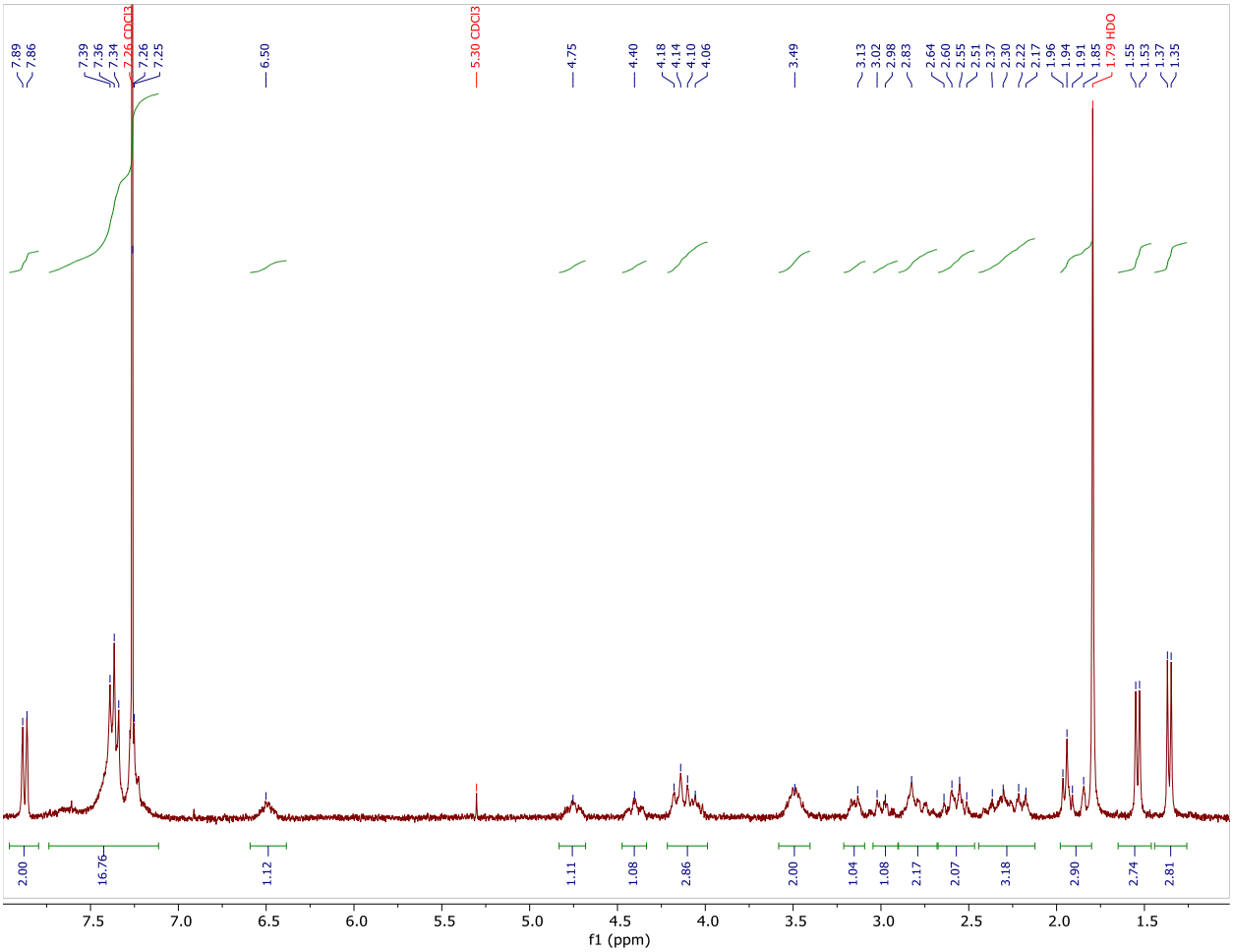

Figure A.2. ^{1}HNMR spectra for **2b**. Peak at 5.30 ppm is CH_2Cl_2. $CHCl_3$ overlaps with aryl region.

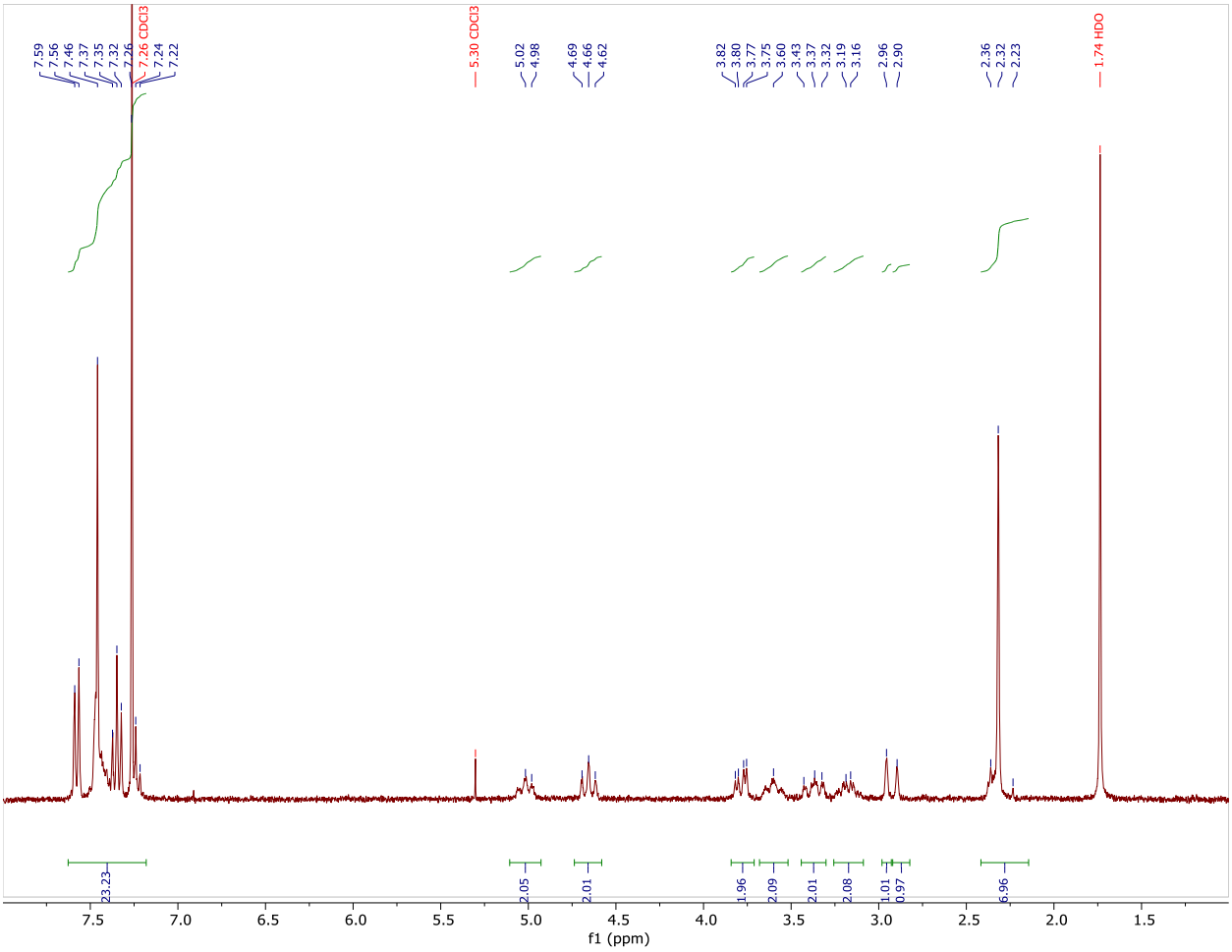

Figure A.3. ^{1}HNMR spectra for **3a**. Peak at 5.30 ppm is CH_2Cl_2. $CHCl_3$ overlaps with aryl region.

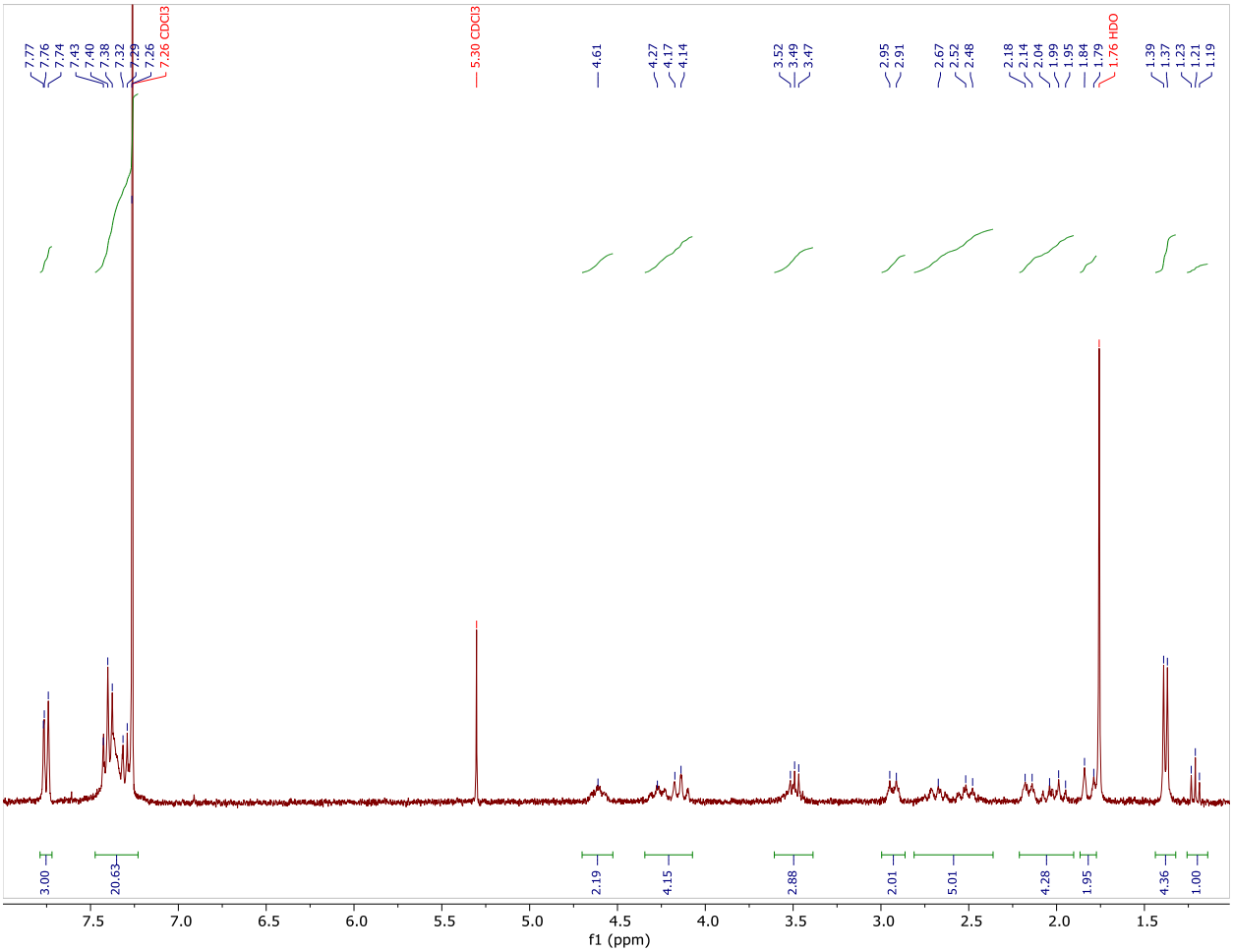

Figure A.4. ^{1}HNMR spectra for **3b**. Peak at 5.30 ppm is CH_2Cl_2. $CHCl_3$ overlaps with aryl region.

APPENDIX B. CHAPTER 2

Table B.1. Experimental details for compound [**1**]$(BPh_4)_2$. The structure contains 4 independent solvent accessible voids of 1776 Ang3 combined. The residual electron density peaks are not arranged in an interpretable pattern. The structure factors were instead augmented via reverse Fourier transform methods using the SQUEEZE routine (P. van der Sluis & A.L. Spek (1990). Acta Cryst. A46, 194-201) as implemented in the program Platon. The resultant FAB file containing the structure factor contribution from the electron content of the void space was used in together with the original hkl file in the further refinement. (The FAB file with details of the Squeeze results is appended to this cif file). The Squeeze procedure corrected for 264 electrons within the solvent accessible voids.

	BLM0028_0m
Crystal data	
Chemical formula	$C_{52}H_{72}Cl_2Co_2N_8 \cdot 2(C_{24}H_{20}B)$[+solvent]
M_r	1636.35
Crystal system, space group	Triclinic, $P\bar{1}$
Temperature (K)	150
a, *b*, *c* (Å)	14.2358 (8), 16.8867 (7), 23.2628 (14)
α, β, γ (°)	80.4695 (14), 81.1332 (14), 79.2906 (19)
V (Å^3)	5374.9 (5)
Z	2
Radiation type	Mo *K*α
μ (mm^{-1})	0.40
Crystal size (mm)	0.42 × 0.34 × 0.17
Data collection	
Diffractometer	Bruker AXS D8 Quest CMOS diffractometer
Absorption correction	Multi-scan *SADABS* 2016/2: Krause, L., Herbst-Irmer, R., Sheldrick G.M. & Stalke D., J. Appl. Cryst. 48 (2015) 3-10
T_{min}, T_{max}	0.697, 0.746
No. of measured, independent and observed [$I > 2\sigma(I)$] reflections	270036, 25738, 20708
R_{int}	0.045
$(\sin \theta/\lambda)_{max}$ (Å^{-1})	0.659

Refinement	
$R[F^2 > 2\sigma(F^2)]$, $wR(F^2)$, S	0.046, 0.132, 1.04
No. of reflections	25738
No. of parameters	1032
H-atom treatment	H-atom parameters constrained
$\Delta\rangle_{max}$, $\Delta\rangle_{min}$ (e Å^{-3})	0.63, -0.70

Computer programs: Apex3 v2018.1-0 (Bruker, 2018), *SAINT* V8.38A (Bruker, 2016), *SHELXS97* (Sheldrick, 2008), *SHELXL2018*/3 (Sheldrick, 2015, 2018), SHELXLE Rev937 (Hübschle *et al.*, 2011).

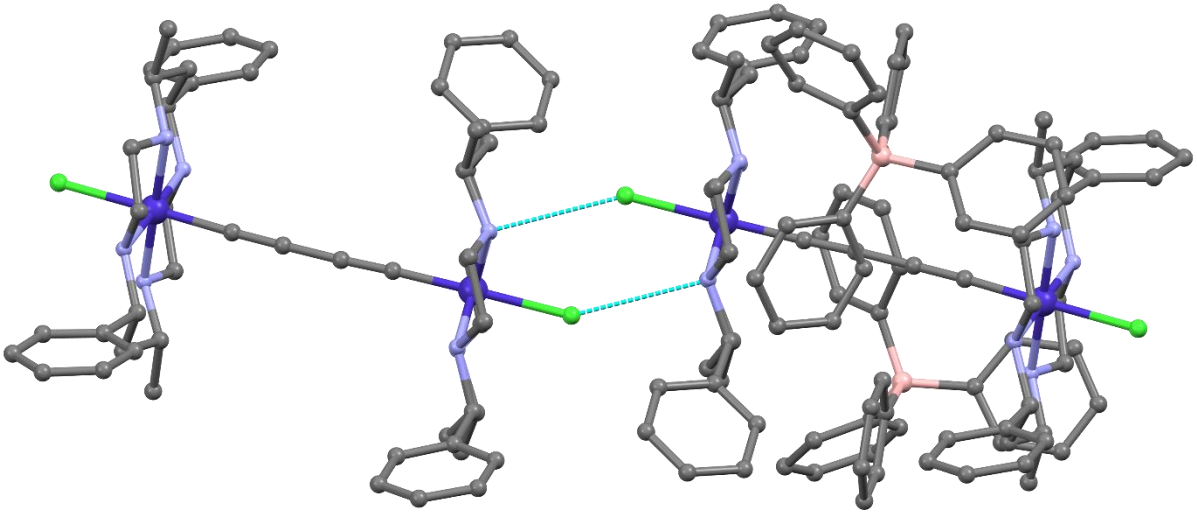

Figure B.1. A ball and stick structural plot of [**1**](BPh$_4$)$_2$ is shown. Hydrogen atoms are omitted for clarity. Both cationic structures are symmetrically equivalent. The hydrogen bonding along the ends of each molecule as well as the positioning of the tetraphenylborate anion allow a stable packing structure. The longer alkynyl capping ligands for [**2**]$^{2+}$ and [**3**]$^{2+}$ prevent the possibility of hydrogen bonding, making crystallization difficult.

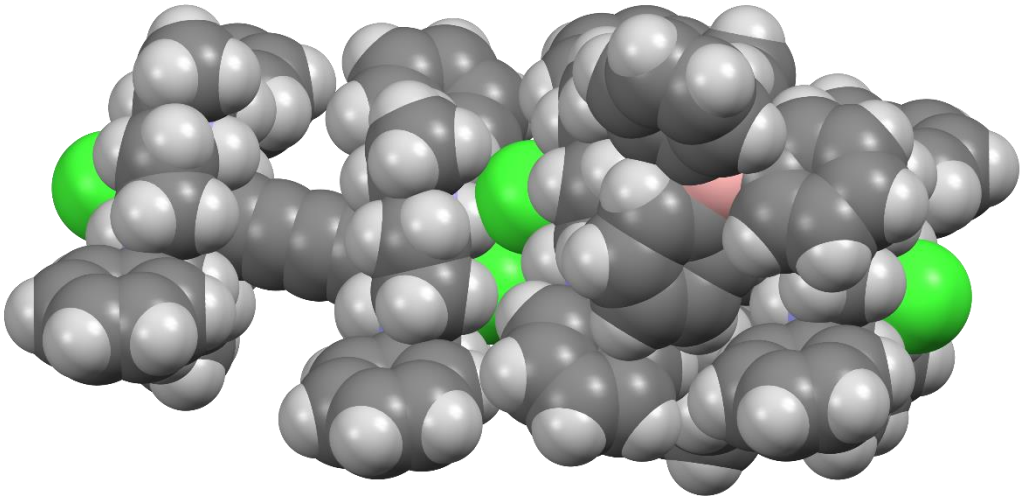

Figure B.2. A spacefill model of [**1**]$(BPh_4)_2$ with the same view as in the previous figure is shown. The space around the alkynyl bridge does not allow for most solvent molecules to fill.

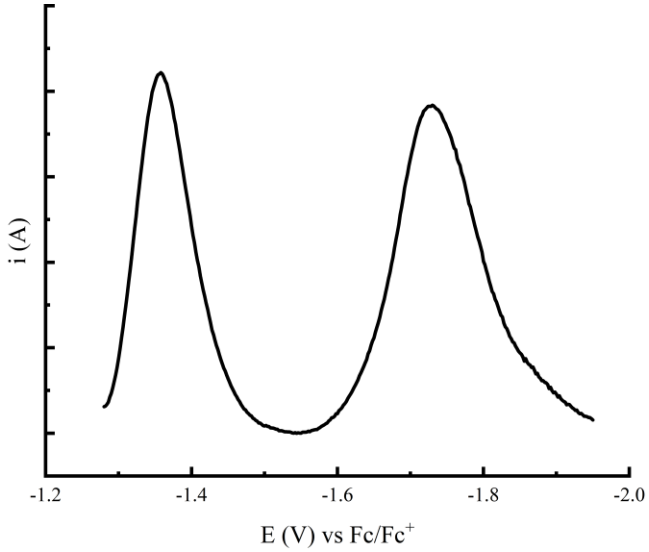

Figure B.3. A DPV plot for [**1**]Cl_2 is shown.

Peak Analysis

Data Set:[AC2Phsplittin]Sheet1!B Date:11/12/2019

BaseLine:Spline

Chi^2=1.05469E-015 Adj. R-Square=9.99338E-001 # of Data Points=400

SS=4.15548E-013 Degrees of Freedom=394

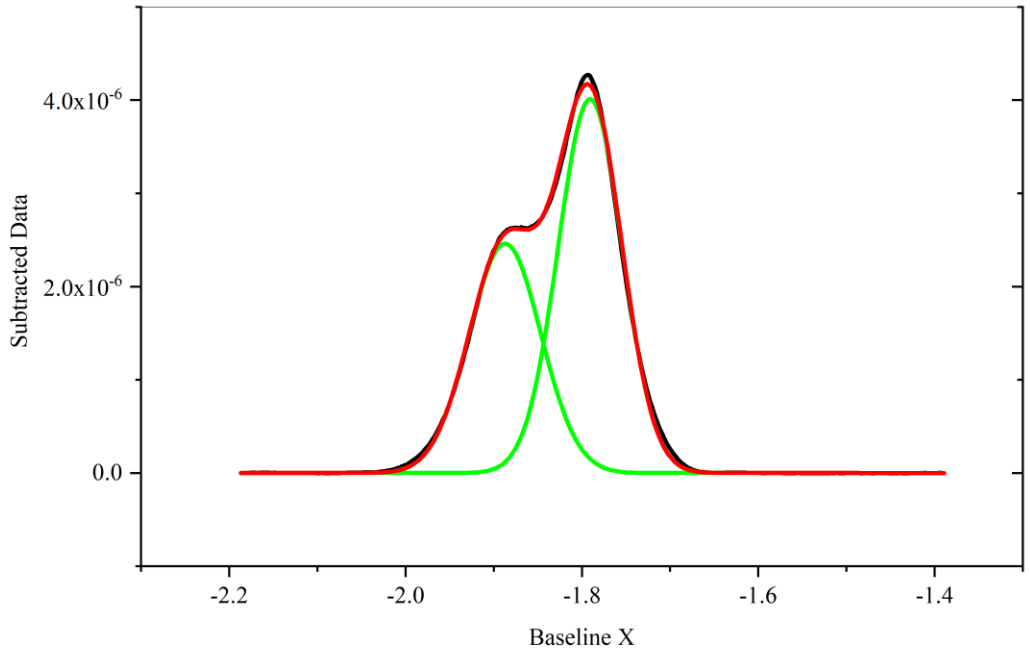

Fitting Results

Peak Index	Peak Type	Area Intg	FWHM	Max Height	Center Grvty	Area IntgP
1	Gaussian	3.64353E-7	0.08533	4.01149E-6	-1.79079	59.15396
2	Gaussian	2.51587E-7	0.09607	2.46015E-6	-1.88729	40.84604

Figure B.4. Peak analysis for differential pulse voltammogram of [**2**]Cl_2. Data was collected using 1.0 mM [**2**]Cl_2 in a 0.1 M Bu_4NPF_6 MeCN solution. Data was collected following the parameters described by Richardson and Taube (*Inorg. Chem.* **1981**, *20* (4), 1278–1285.).

Peak Analysis

Data Set:[Book1]Sheet1!B Date:11/12/2019

BaseLine:Spline

Chi^2=5.31894E-016 Adj. R-Square=9.99744E-001 # of Data Points=450

SS=2.36161E-013 Degrees of Freedom=444

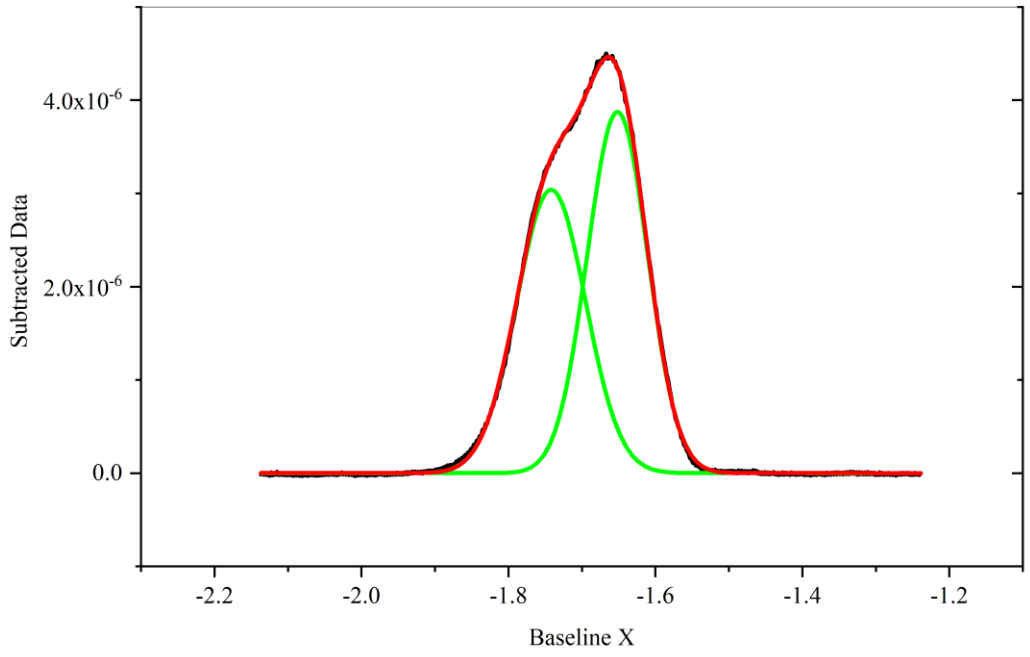

Fitting Results

Peak Index	Peak Type	Area Intg	FWHM	Max Height	Center Grvty	Area IntgP
1	Gaussian	3.9812E-7	0.09652	3.87477E-6	-1.65173	52.68225
2	Gaussian	3.5758E-7	0.1105	3.04003E-6	-1.74202	47.31775

Figure B.5. Peak analysis for differential pulse voltammogram of [**2**]Cl_2. Data was collected using 1.0 mM [**2**]Cl_2 in a 0.1 M Bu_4NPF_6 MeCN solution. Data was collected following the parameters described by Richardson and Taube (*Inorg. Chem.* **1981**, *20* (4), 1278–1285.).

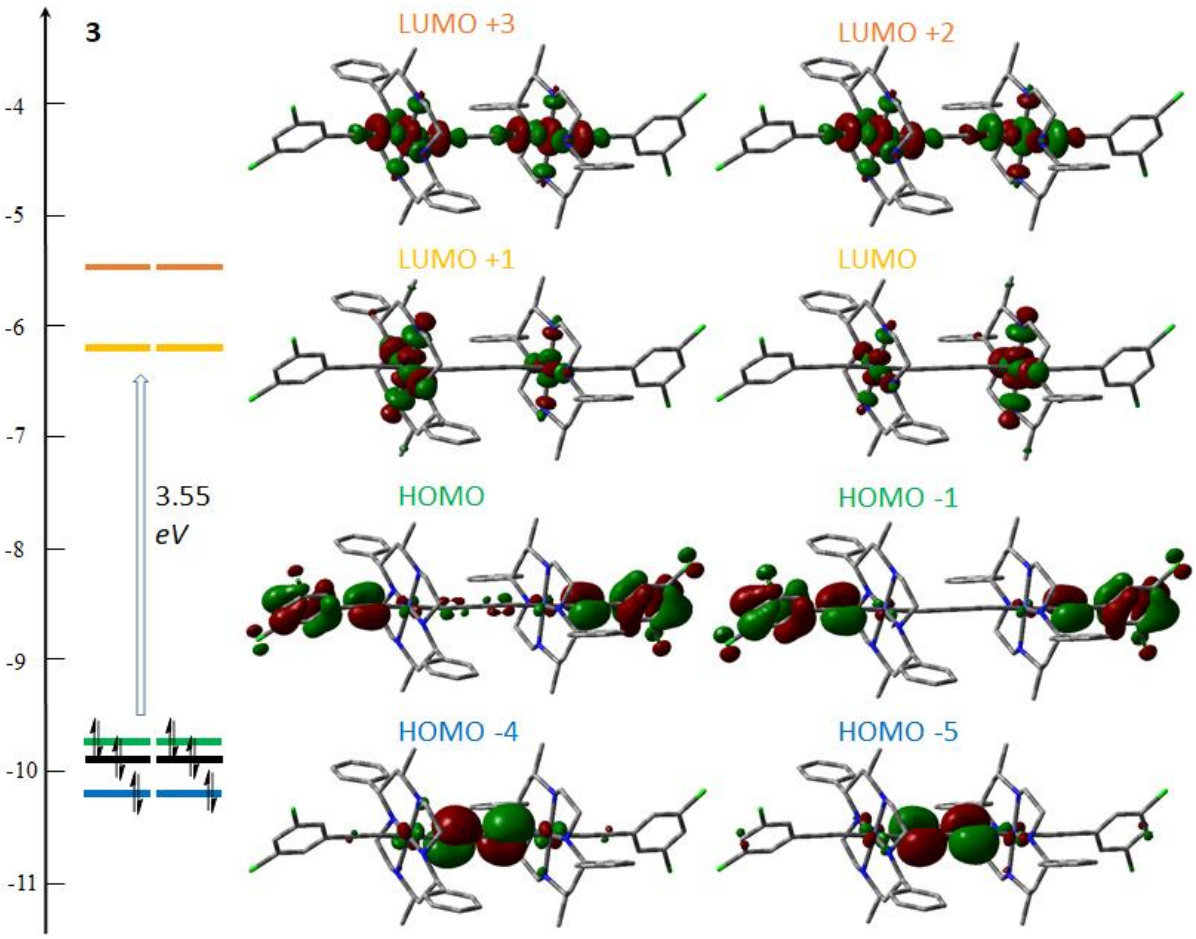

Figure B.6. Molecular orbital diagram for [**3**]$^{2+}$ from DFT calculations. The isovalue of the contour plots was set at 0.03.

Table B.2. Relevant bond lengths (Å) and angles (°) for $[\mathbf{1}]^{2+}$, $[\mathbf{2}]^{2+}$, and $[\mathbf{3}]^{2+}$ from DFT calculations. Axial1 and Axial2 refer to the atom coordinated to cobalt opposite the bridging ligand.

	$[\mathbf{1}]^{2+}$	$[\mathbf{2}]^{2+}$	$[\mathbf{3}]^{2+}$
Co1-N1	2.064	2.024	2.025
Co1-N2	2.024	2.036	2.036
Co1-N3	2.016	2.026	2.026
Co1-N4	2.037	2.033	2.034
Co2-N5	2.015	2.026	2.026
Co2-N6	2.037	2.033	2.033
Co2-N7	2.026	2.024	2.025
Co2-N8	2.024	2.037	2.036
Co1-Axial1	2.318	1.942	1.943
Co2-Axial2	2.319	1.942	1.943
Co1-C1	1.914	1.963	1.961
Co2-C4	1.914	1.963	1.961
C1-C2	1.236	1.238	1.238
C2-C3	1.379	1.380	1.380
C3-C4	1.236	1.238	1.238
Axial1-Co1-C1	179.26	179.93	179.97
Axial2-Co2-C4	179.17	179.93	179.95
Co1-C1-C2	175.82	175.06	175.09
Co2-C4-C3	176.09	175.06	175.02

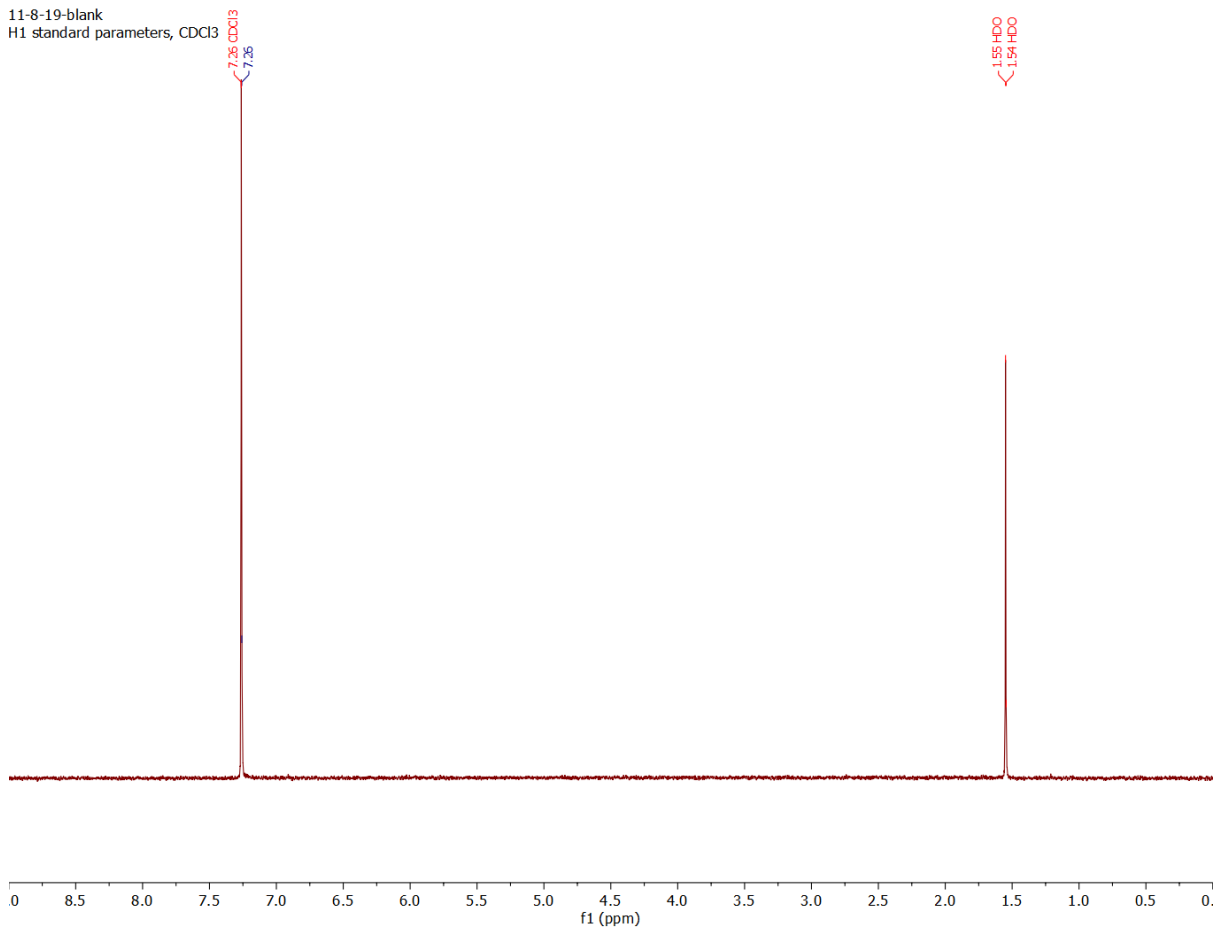

Figure B.7. Blank ^{1}HNMR spectrum of $CDCl_3$ collected at the same time as compounds [**1**]Cl_2-[**3**]Cl_2. H_2O is present in the solvent.

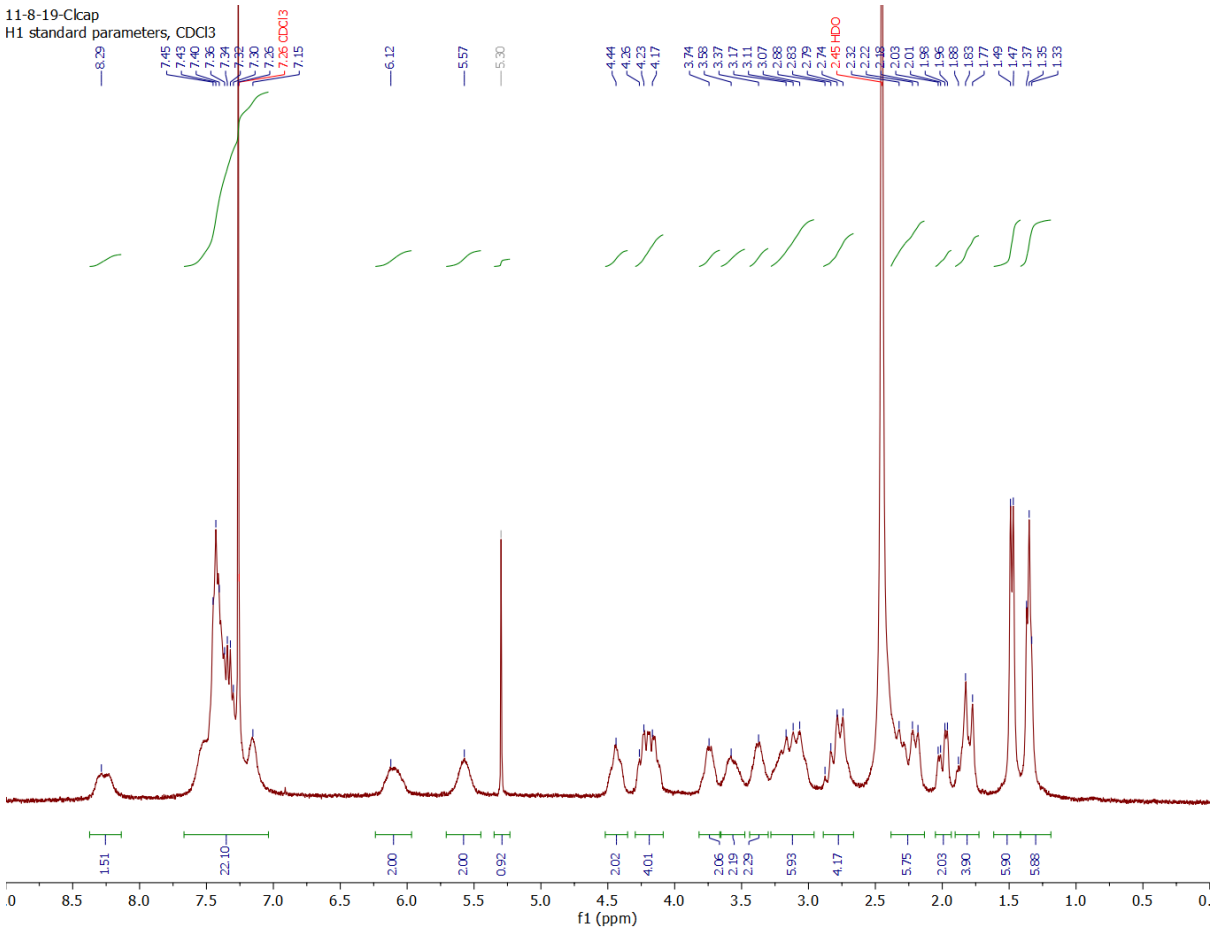

Figure B.8. ^{1}HNMR spectrum of [**1**]Cl_2 in $CDCl_3$. H_2O has shifted from the blank and CH_2Cl_2 (5.30 ppm) is present after vacuum drying the compound.

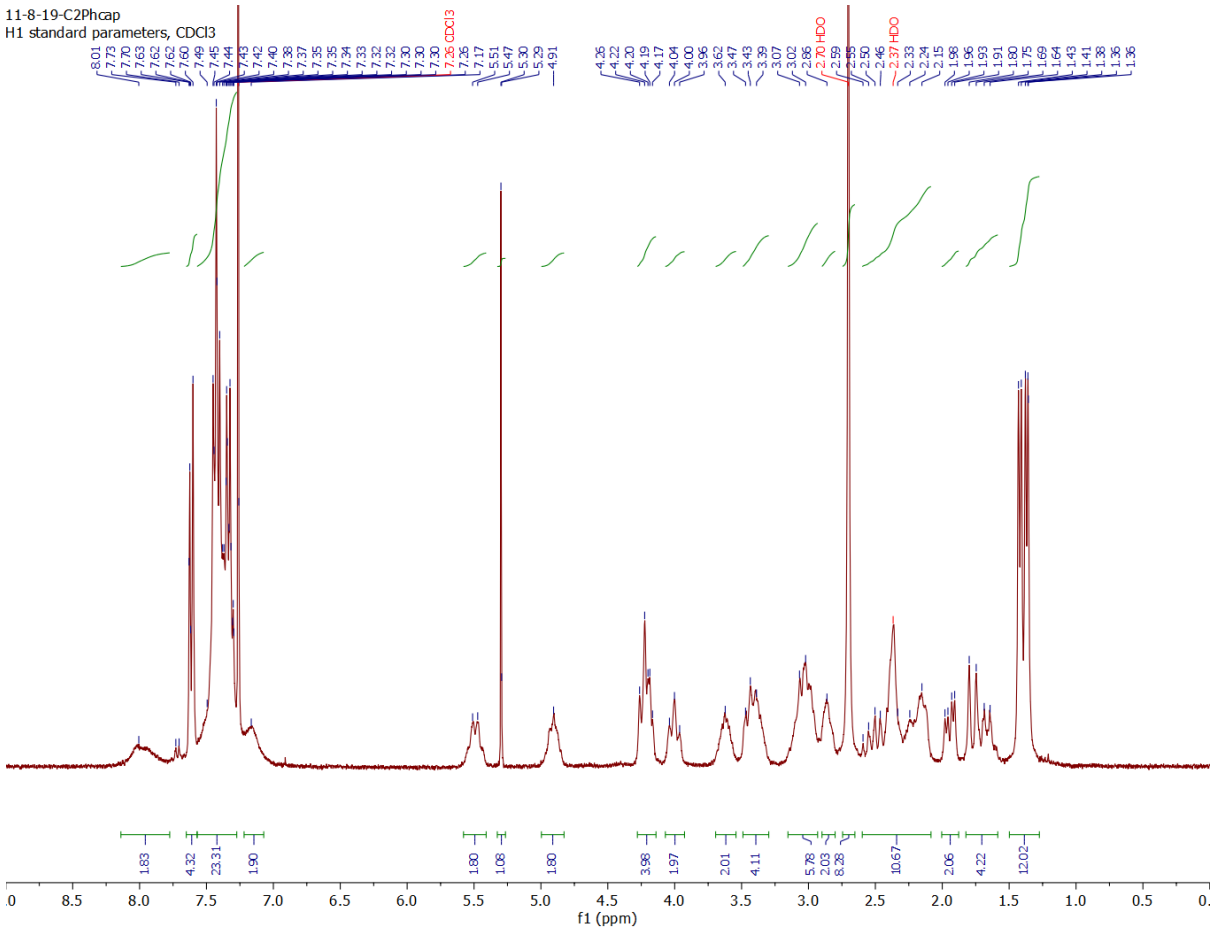

Figure B.9. ^{1}HNMR spectrum of [**2**]Cl_2 in $CDCl_3$. H_2O has shifted from the blank and CH_2Cl_2 (5.30 ppm) is present after vacuum drying the compound.

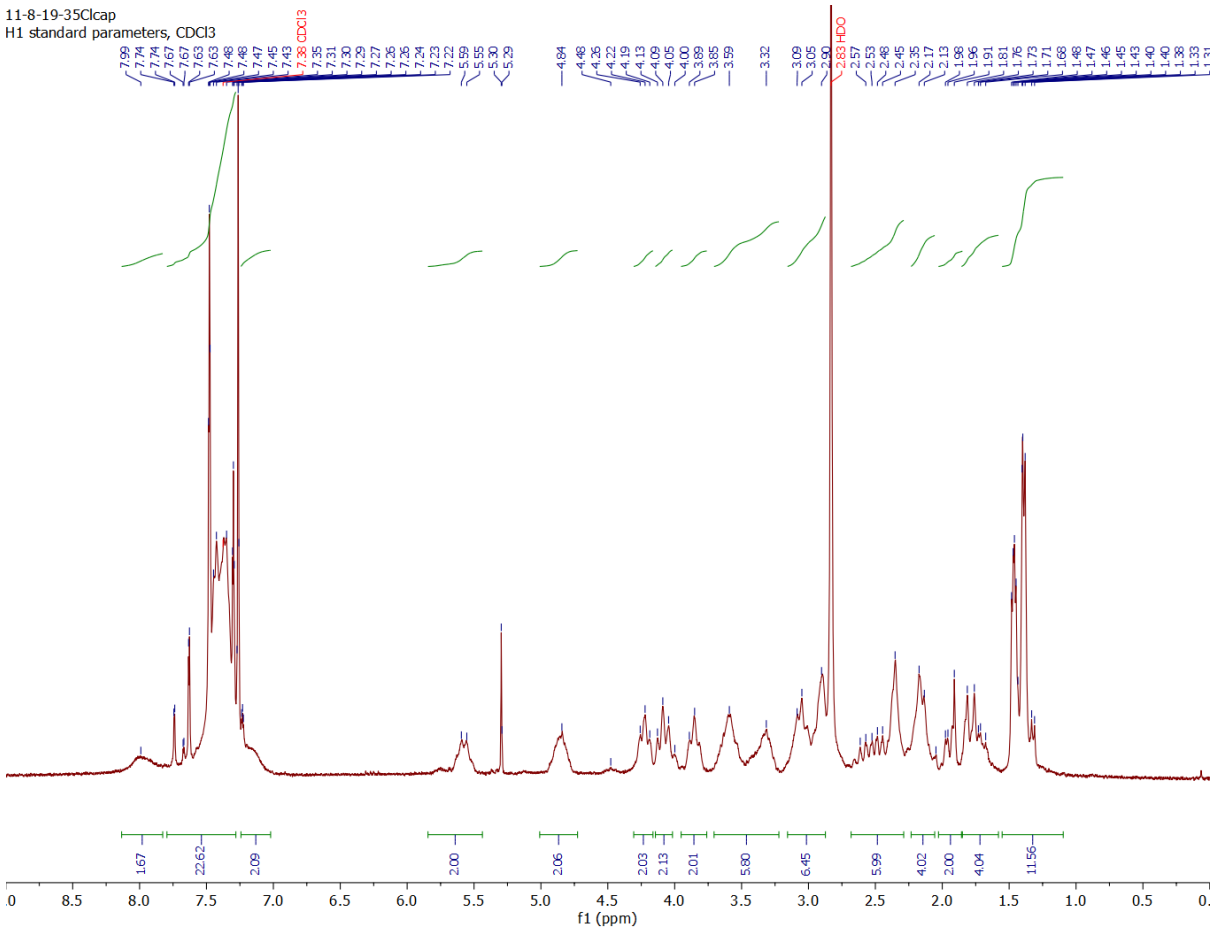

Figure B.10. ^{1}HNMR spectrum of [**3**]Cl_2 in $CDCl_3$. H_2O has shifted from the blank and CH_2Cl_2 (5.30 ppm) is present after vacuum drying the compound.

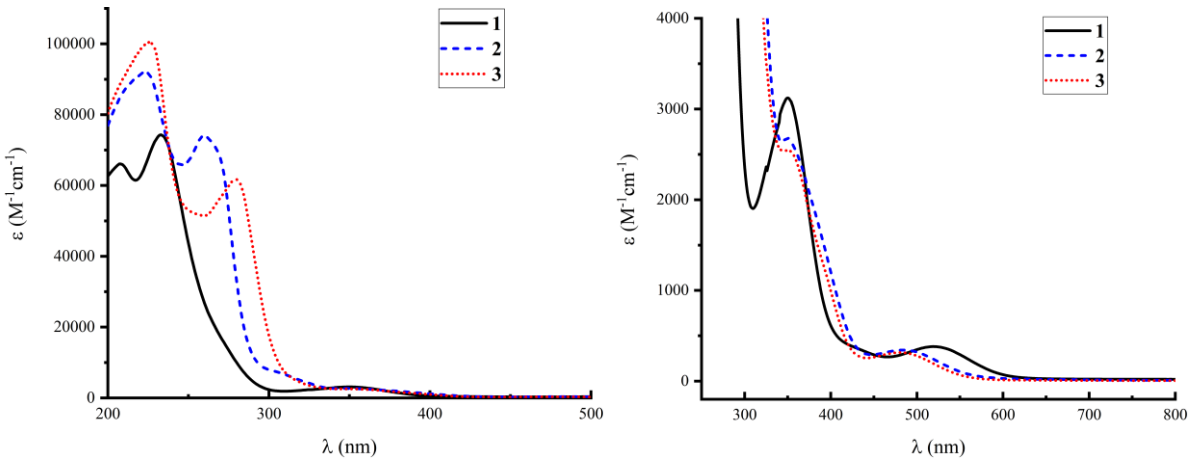

Figure B.11. Electronic absorption spectra for [**1**]Cl_2, [**2**]Cl_2, and [**3**]Cl_2 in neat MeCN solutions. The stronger UV absorptions are shown on the left while the weak metal-based absorptions are shown on the right.

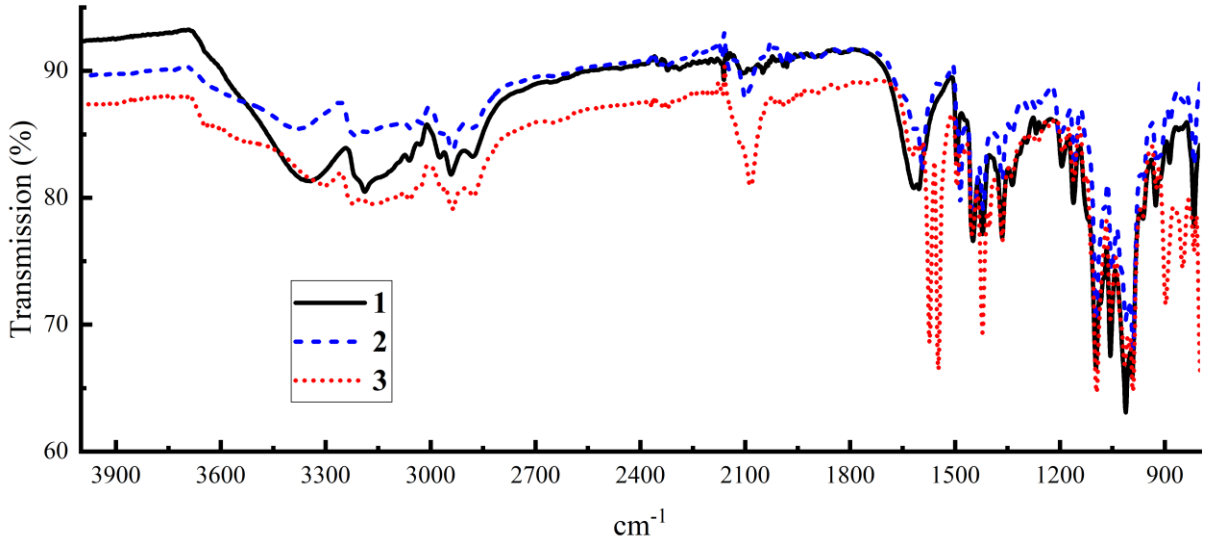

Figure B.12. IR spectra for [**1**]Cl_2, [**2**]Cl_2, and [**3**]Cl_2.

APPENDIX C. CHAPTER 3

Table C.1. Experimental crystallographic details for compound [**1**]Cl.

	BLM0023_0m
Crystal data	
Chemical formula	$C_{48}H_{54}CoFe_2N_4 \cdot CH_2Cl_2 \cdot Cl \cdot 3(H_2O)$
M_r	1032.00
Crystal system, space group	Triclinic, $P\bar{1}$
Temperature (K)	150
a, *b*, *c* (Å)	7.6705 (4), 11.0266 (6), 14.4607 (8)
α, β, γ (°)	92.871 (3), 94.173 (4), 109.217 (4)
V (Å^3)	1148.30 (11)
Z	1
Radiation type	Cu *K*α
μ (mm^{-1})	9.77
Crystal size (mm)	0.25 × 0.15 × 0.06
Data collection	
Diffractometer	Bruker AXS D8 Quest CMOS diffractometer
Absorption correction	Multi-scan *SADABS* 2016/2: Krause, L., Herbst-Irmer, R., Sheldrick G.M. & Stalke D., J. Appl. Cryst. 48 (2015) 3-10
T_{min}, T_{max}	0.411, 0.754
No. of measured, independent and observed [$I > 2\sigma(I)$] reflections	22755, 4952, 4303
R_{int}	0.056
$(\sin \theta/\lambda)_{max}$ (Å^{-1})	0.641
Refinement	
$R[F^2 > 2\sigma(F^2)]$, $wR(F^2)$, *S*	0.044, 0.128, 1.15
No. of reflections	4952
No. of parameters	317
No. of restraints	23
H-atom treatment	H atoms treated by a mixture of independent and constrained refinement

$\Delta\rangle_{max}$, $\Delta\rangle_{min}$ (e Å^{-3})	0.54, −0.49

Computer programs: Apex3 v2018.1-0 (Bruker, 2018), *SAINT* V8.38A (Bruker, 2016), *SHELXS97* (Sheldrick, 2008), *SHELXL2018*/3 (Sheldrick, 2015, 2018), SHELXLE Rev937 (Hübschle *et al.*, 2011).

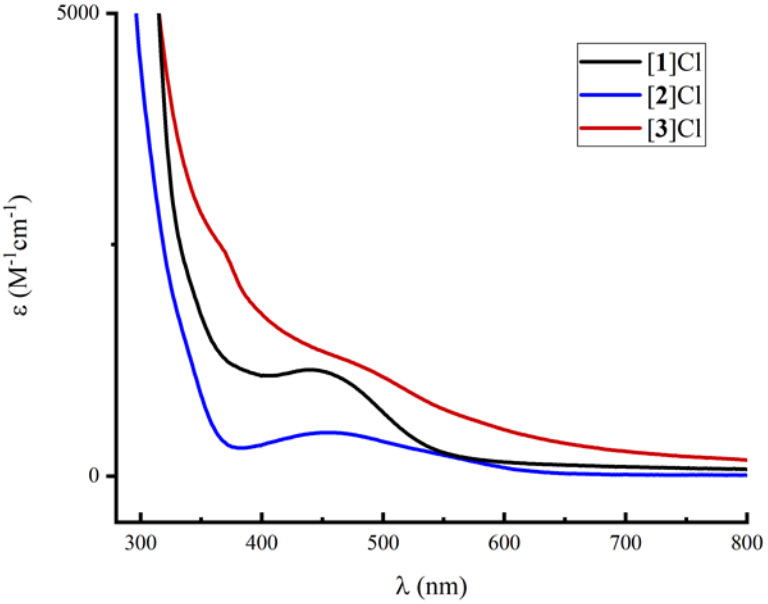

Figure C.1. Electronic absorption spectra for [**1**]Cl, [**2**]Cl, and [**3**]Cl.

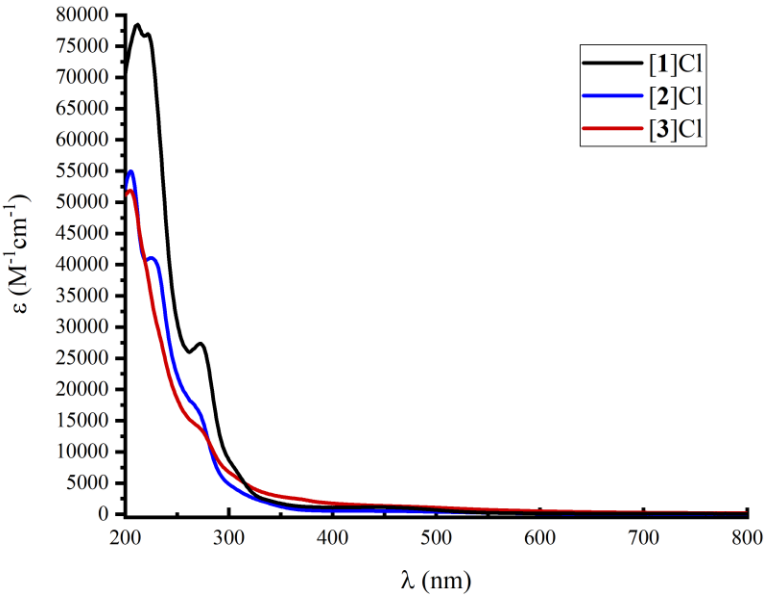

Figure C.2. Full electronic absorption spectra for [**1**]Cl, [**2**]Cl, and [**3**]Cl.

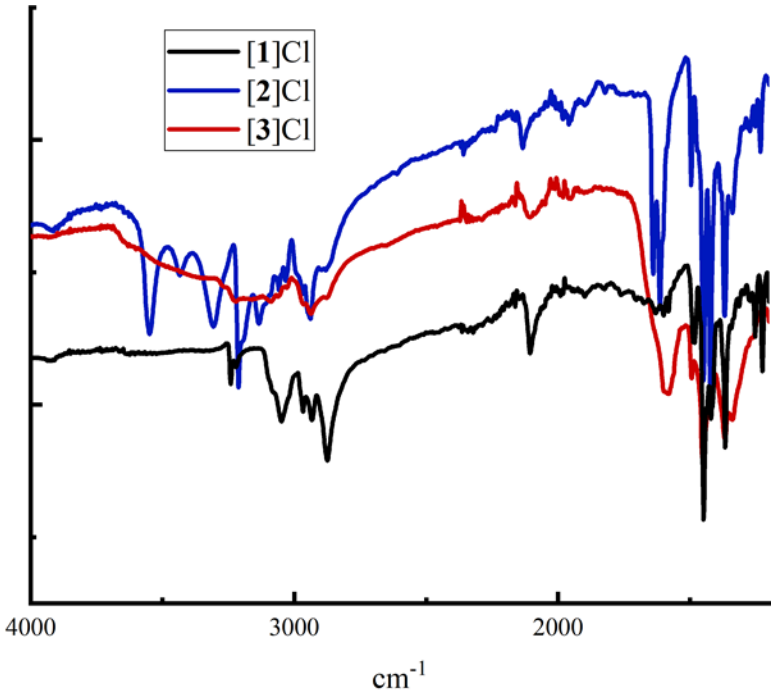

Figure C.3. Infrared spectra for [**1**]Cl, [**2**]Cl, and [**3**]Cl.

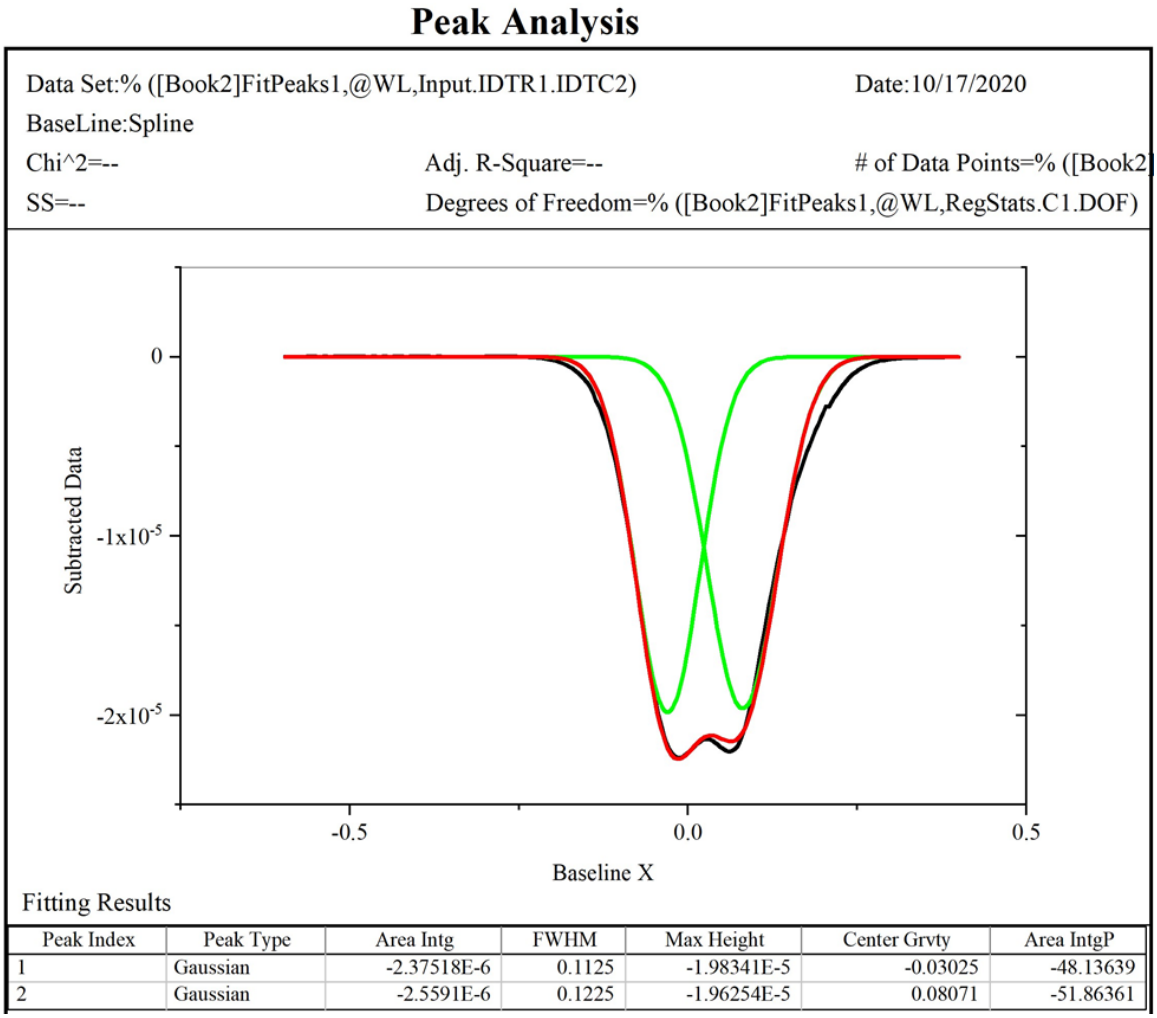

Peak Index	Peak Type	Area Intg	FWHM	Max Height	Center Grvty	Area IntgP
1	Gaussian	-2.37518E-6	0.1125	-1.98341E-5	-0.03025	-48.13639
2	Gaussian	-2.5591E-6	0.1225	-1.96254E-5	0.08071	-51.86361

Figure C.4. Deconvolution of DPV spectra for $[1]^+$.

Table C.2. Relevant bond lengths (Å) and angles (°) for $[\mathbf{1}]^+$ and $[\mathbf{3}]^+$ from DFT calculations.

	$[\mathbf{1}]^+$	$[\mathbf{3}]^+$
Co1-N1	2.025	2.027
Co1-N2	2.034	2.035
Co1-N3	-	2.026
Co1-N4	-	2.037
Co1-C1	1.951	1.953
C1-C2	1.231	1.242
C2-C3	1.430	1.431
Co1-C13	-	1.949
C13-C14	-	1.239
C1-Co1-C13	180	179.82

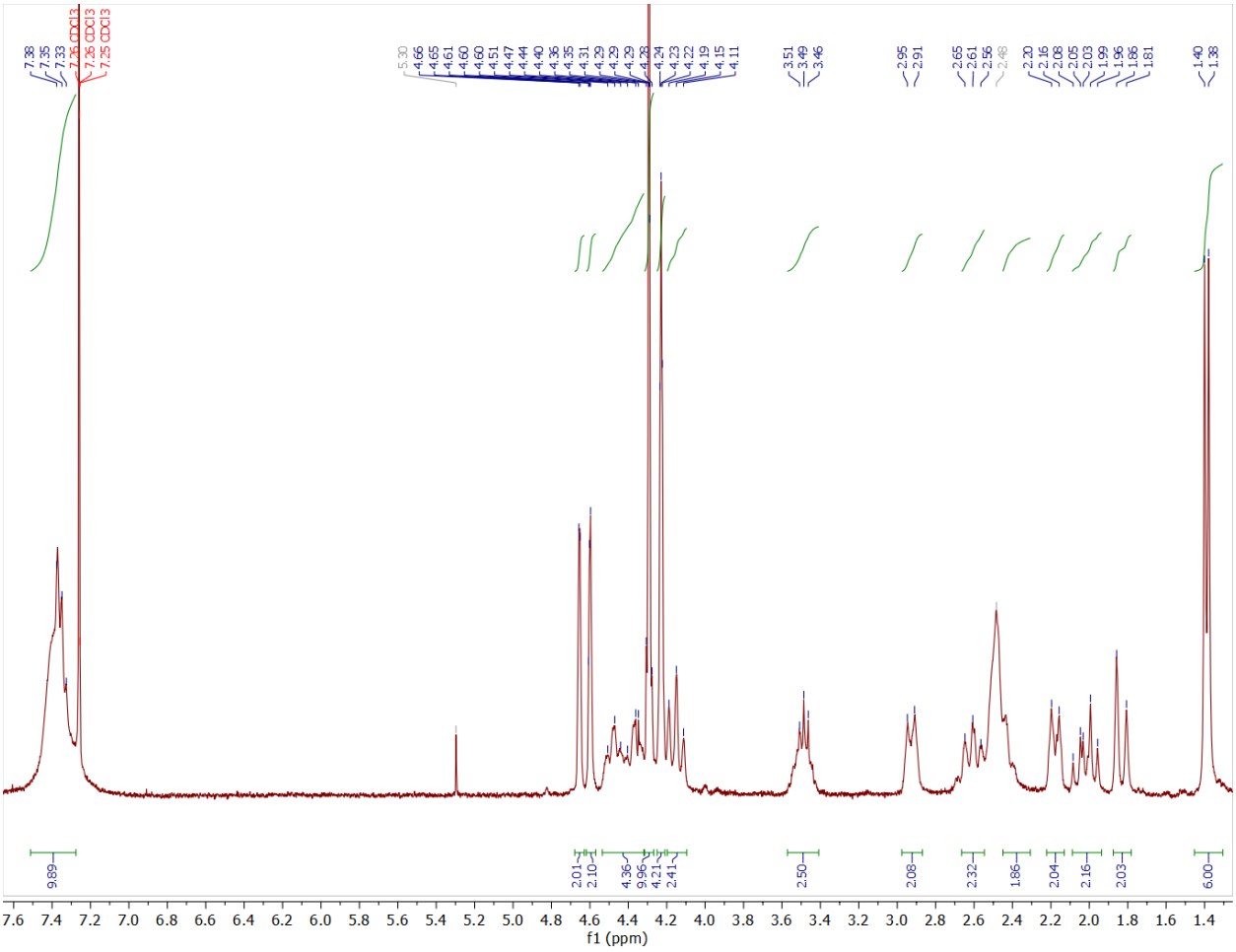

Figure C.5. NMR spectra for [**1**]Cl in $CDCl_3$.

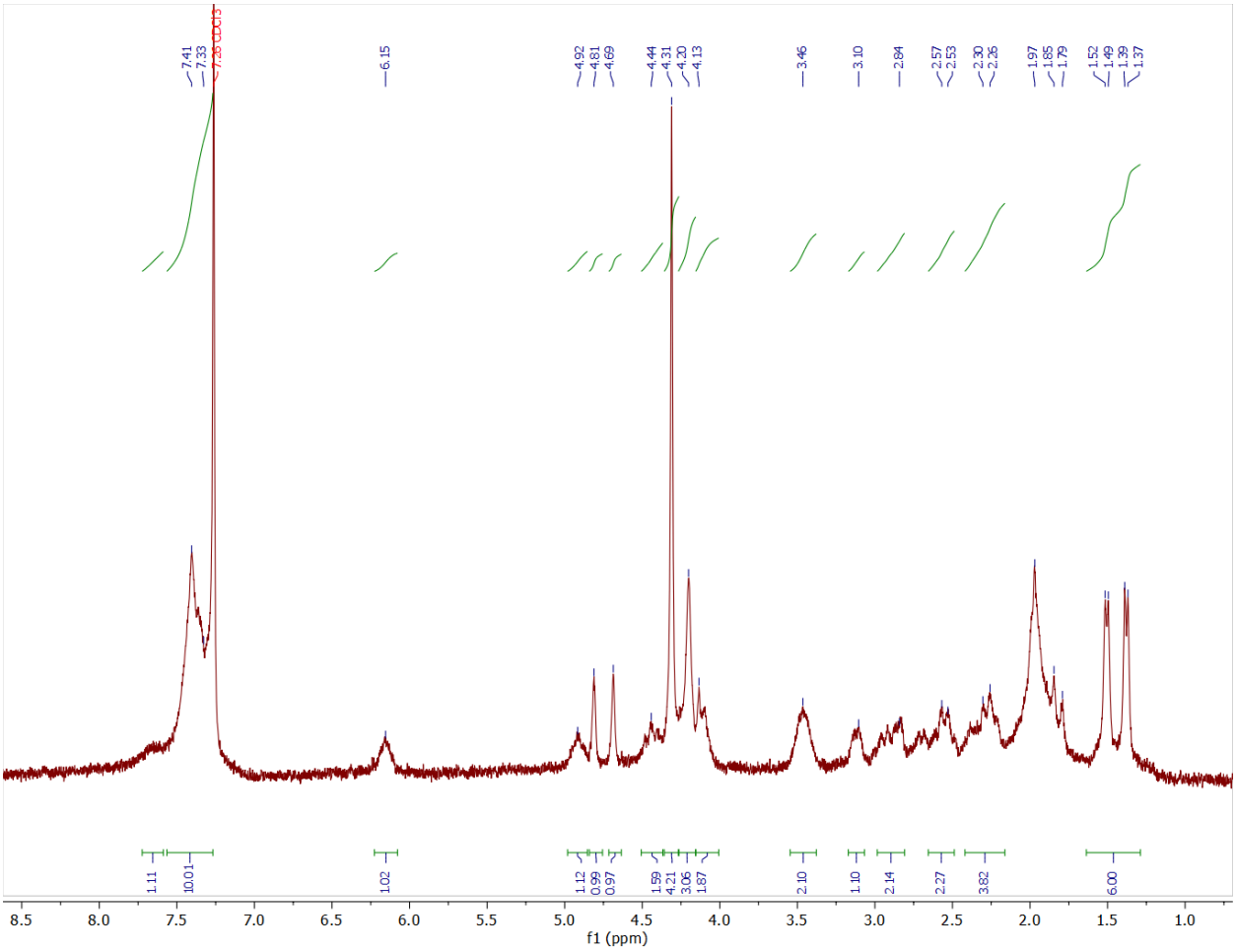

Figure C.6. NMR spectra for [**2**]Cl in $CDCl_3$.

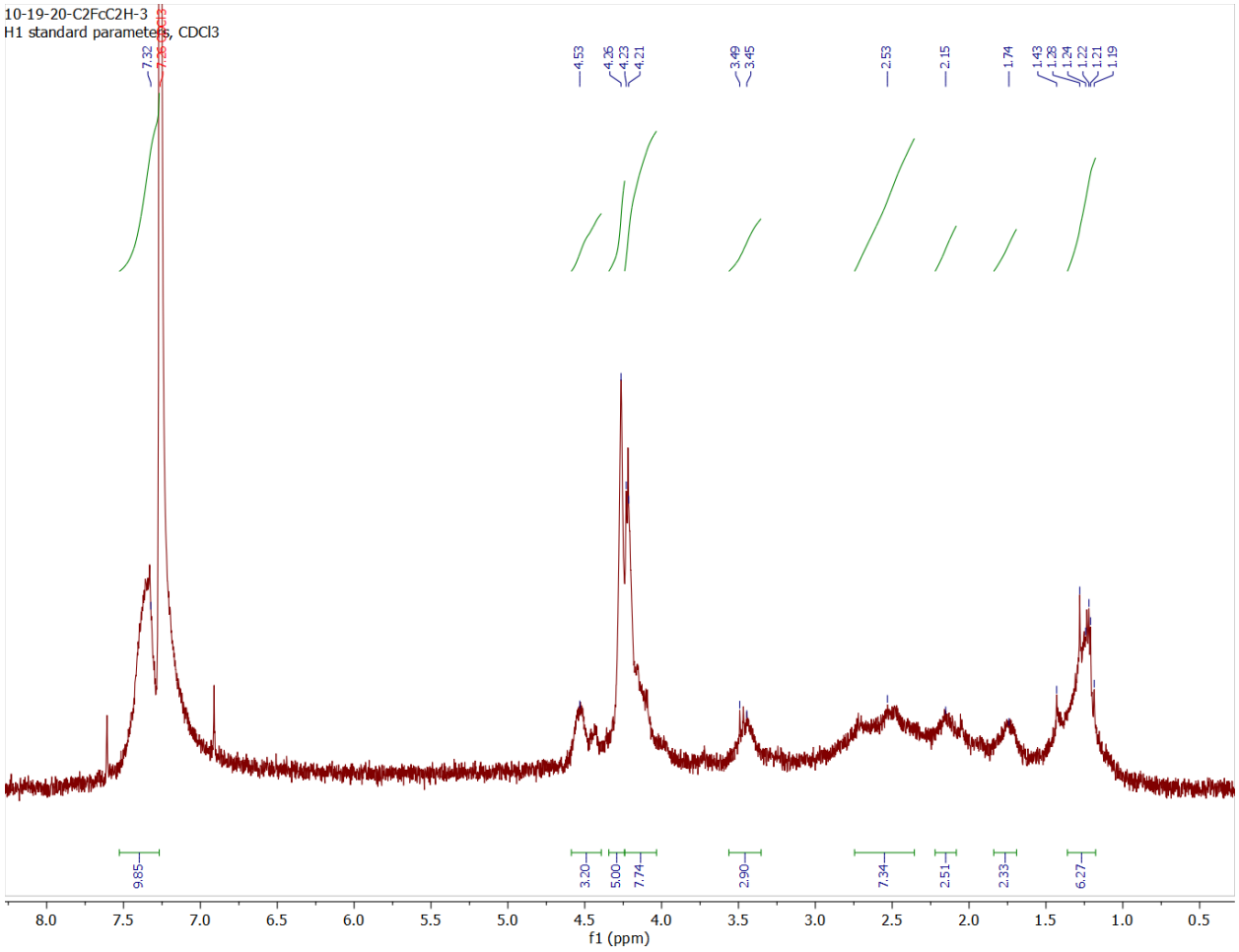

Figure C.7. NMR spectra for [**3**]Cl in $CDCl_3$.

APPENDIX D. CHAPTER 4

Table D.1. Crystal data for **1** and **2**.

	1	**2**
Chemical formula	$C_{18}H_{36}N_4NiF_6O_6S_2$	$C_{14}H_{36}N_4NiO_2$•2(CF_3SO_3)
Formal Weight	641.32	649.32
space group	$P2_1/n$	P -1
a (Å)	8.8591 (4)	8.3003 (3)
b (Å)	9.4230 (4)	11.6462 (5)
c(Å)	16.1149 (8)	15.5321 (6)
α (°)	90	75.1211 (13)
β (°)	102.819 (2)	80.7867 (13)
γ (°)	90	70.7630 (13)
V (Å^3)	1311.73 (10)	1365.38(9)
Z	2	2
Density	1.624	1.579
T (K)	150	150
Final R indices	R1 = 0.0242	R1 = 0.0466
(I > 2σ(I))	wR2 = 0.0627	wR2 = 0.1403
GooF	1.084	1.165

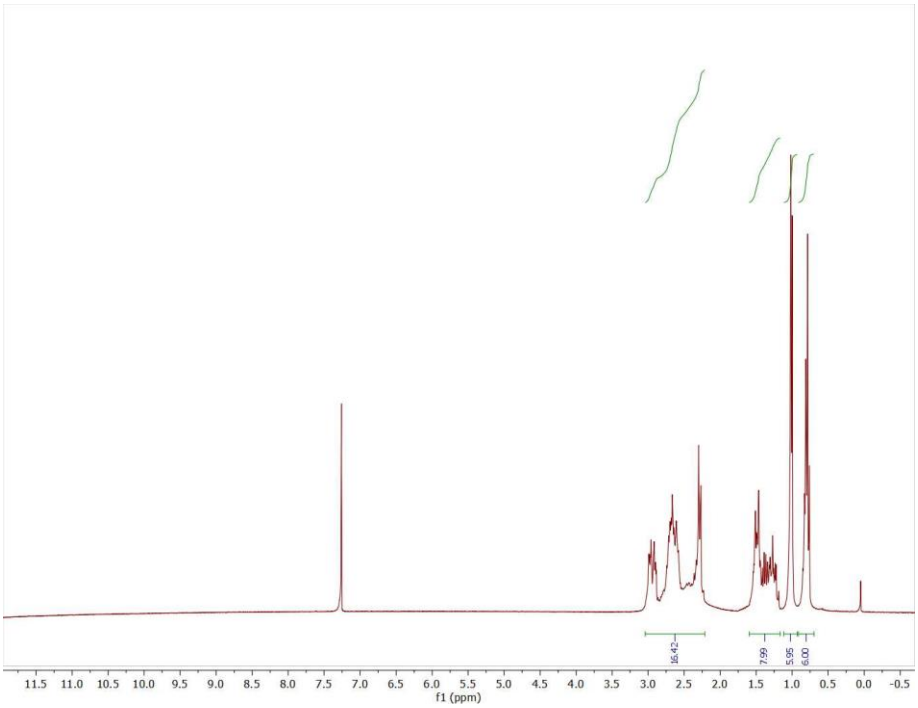

Figure D.1. Full NMR spectrum of MEC in $CDCl_3$.

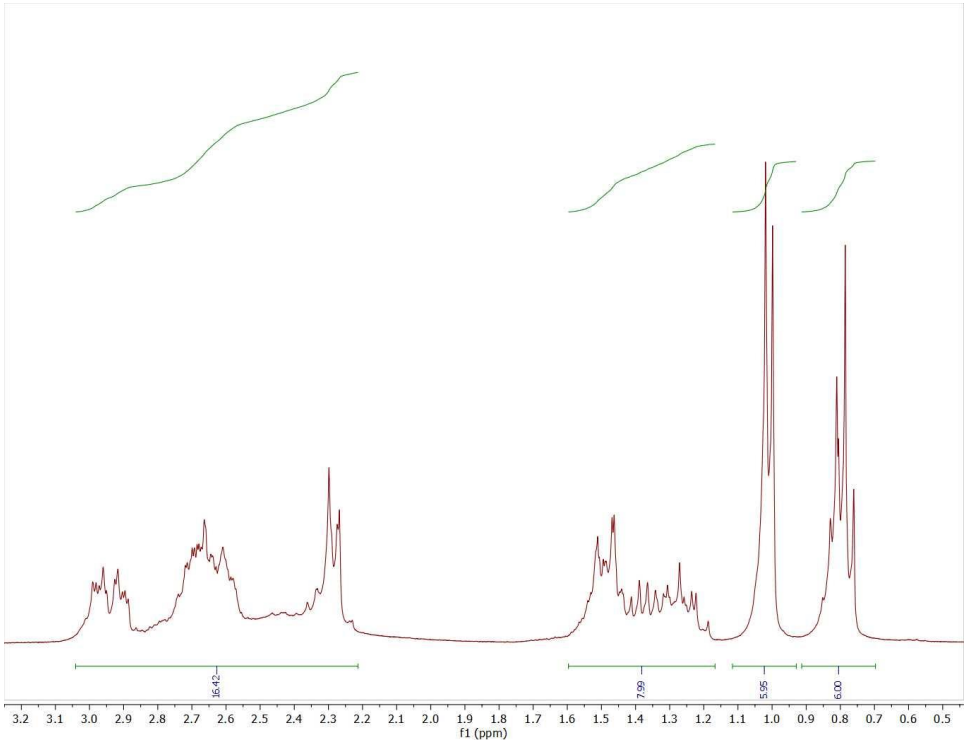

Figure D.2. Expanded NMR spectrum of MEC in $CDCl_3$.

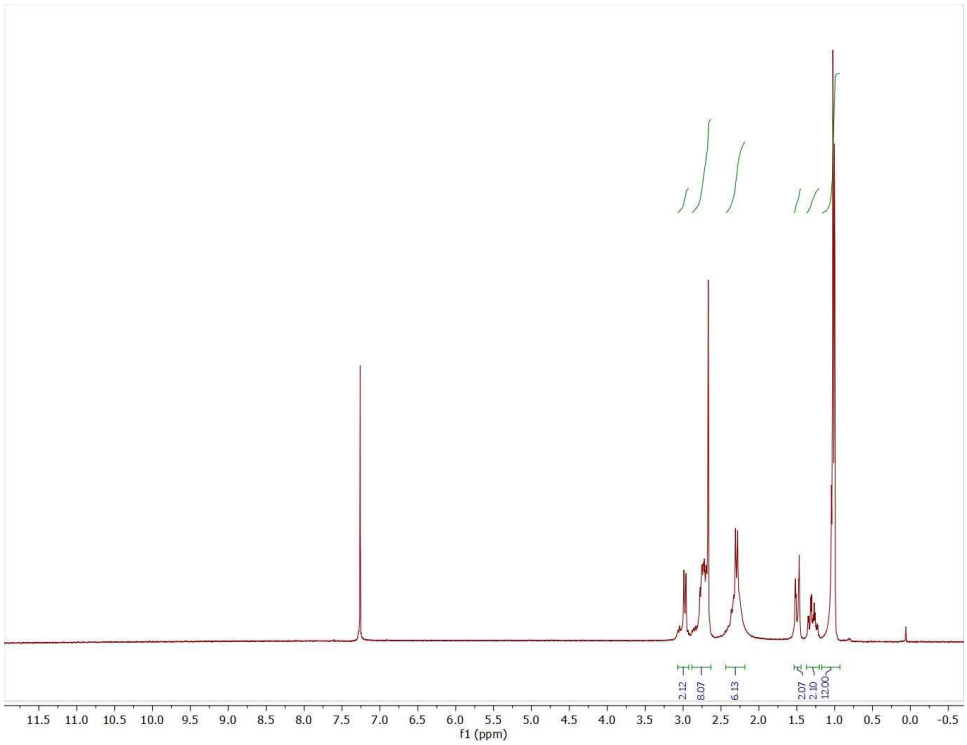

Figure D.3. Full NMR spectrum of CTMC in $CDCl_3$.

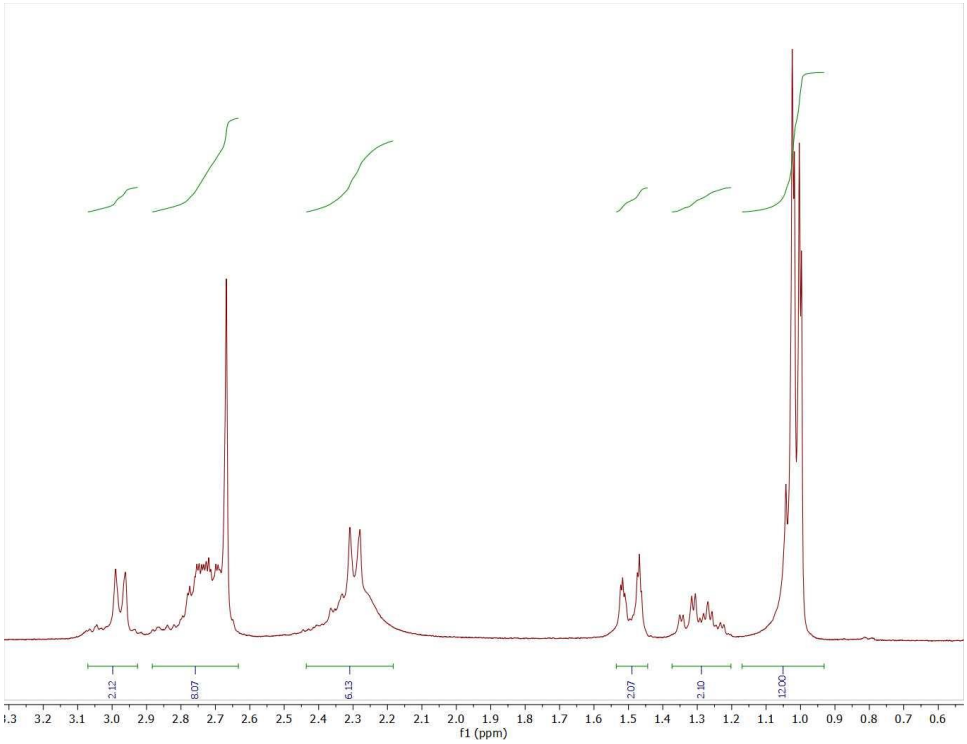

Figure D.4. Expanded NMR spectrum of CTMC in $CDCl_3$.

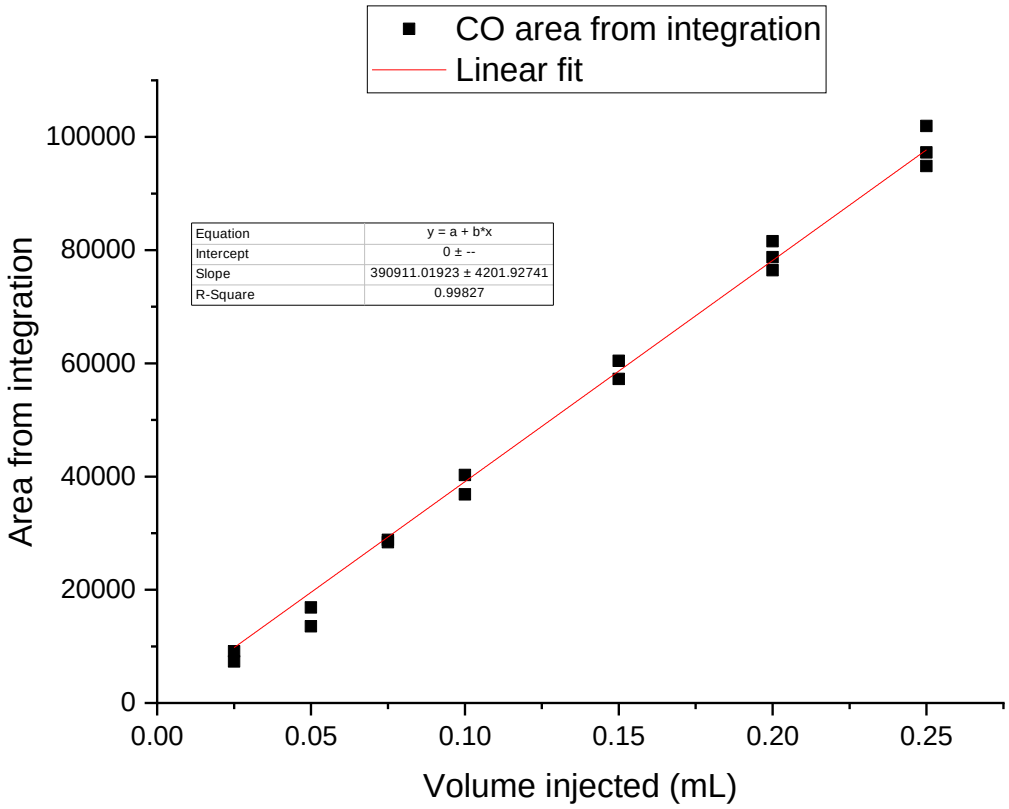

Figure D.5. GC calibration curve for CO.

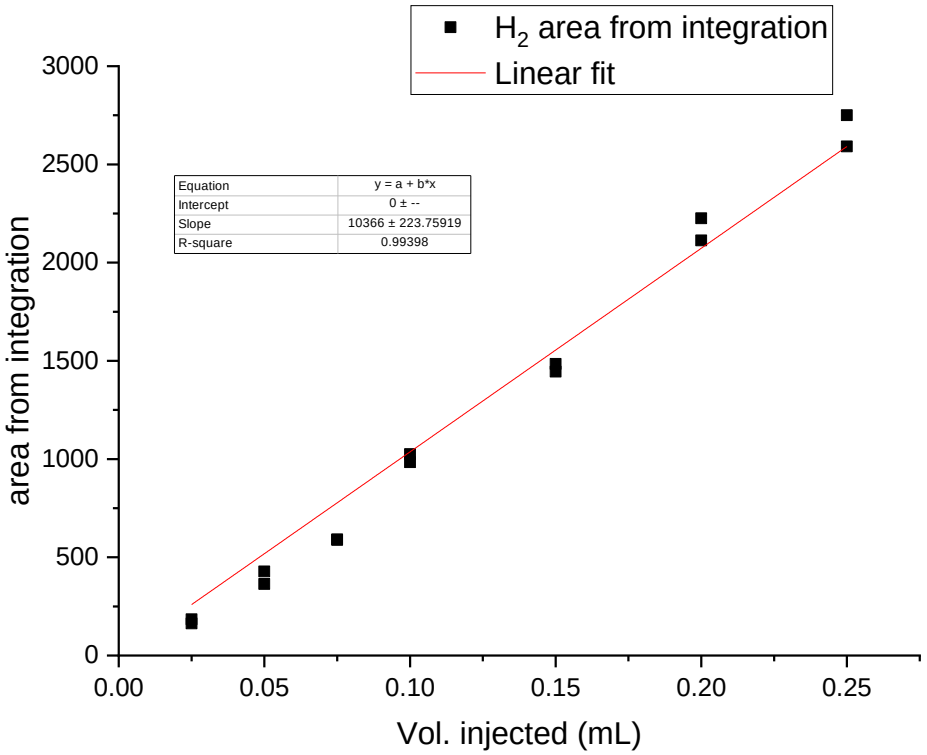

Figure D.6. GC calibration curve for H_2.

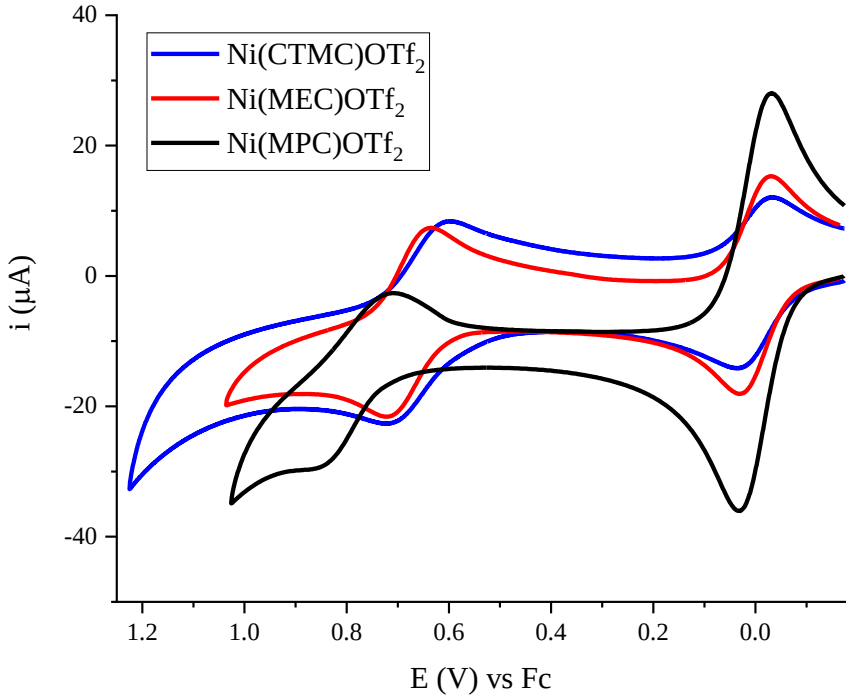

Figure D.7. Cyclic voltammograms of 1.0 mM solutions of **1** (red), **2** (blue), and Ni(MPC)$(OTf)_2$ (black) recorded in a 0.08 M solution of Bu_4NPF_6 in 20% aqueous MeCN on glassy carbon working electrode, purged with Ar, with internal ferrocene reference.

VITA

Brandon Mash was born in Scituate, Massachusetts on June 7, 1994, however grew up mostly in Katy, Texas until the age of 13. Upon moving back to Scituate, he attended South Shore Vocational Technical High School and worked as a welder. Deciding late to attend college, he was provisionally accepted to Bridgewater State University. After a rocky start to university he realized in junior year potential to excel academically which led him to pursue research with Dr. Steve Haefner. It was this experience that opened his passion for chemistry and research which drove him to continue to graduate studies. With the desire to contribute to the development of electronics, he joined Dr. Ren's group at Purdue University as a zero-year student in order to work on the molecular electronics the group is known for. While there, he also discovered his passion for crystallography through working with Matthias Zeller in the X-ray crystallography facility. With a constant desire to continue research and improve technologies through multidisciplinary thinking and applying the various skills learned through life, Brandon is expanding the range of topics he wishes to pursue outside of molecular electronics. He is following interests in carbon dioxide catalysis at national laboratories.

PUBLICATIONS

Journal of Organometallic Chemistry 880 (2019) 143–149

Contents lists available at ScienceDirect

Journal of Organometallic Chemistry

journal homepage: www.elsevier.com/locate/jorganchem

Co(III) phenylacetylide complexes supported by tetraazamacrocyclic ligands: Syntheses and characterizations

Brandon L. Mash, Tong Ren*

Department of Chemistry, Purdue University, West Lafayette, IN, 47907, USA

ARTICLE INFO

Article history:
Received 9 October 2018
Received in revised form
1 November 2018
Accepted 3 November 2018
Available online 5 November 2018

Dedicated to Professor Richard J. Puddephatt on the occasion of his 75th birthday.

Keywords:
Cobalt
MPC
MPD
Phenylacetylene

ABSTRACT

Reported herein are the syntheses and characterization of mono- and bis- Co(III) phenylacetylide complexes *trans*-$[Co(L)(C_2Ph)Cl]^+$ (**2a/b**) and *trans*-$[Co(L)(C_2Ph)_2]^+$ (**3a/b**), where L is MPD (**a**) or MPC (**b**) (MPD = 5,12-dimethyl-7,14-diphenyl-1,4,8,11-tetraazacyclotetradeca-4,11-diene, MPC = 5,12-dimethyl-9,14-diphenyl-1,4,8,11-tetraazacyclotetradecane). All the new complexes were characterized by UV–Vis, FT-IR spectroscopic and voltammetric techniques. Single crystal X-ray diffraction studies revealed that the MPD ligand is a stronger donor to the Co(III) center than the MPC ligand, and the enhanced Co–N interactions manifest some subtle contrast in terms of spectroscopic and voltammetric properties between Co(MPD) and Co(MPC) complexes. These experimental observations were further corroborated by DFT calculations.

© 2018 Elsevier B.V. All rights reserved.

1. Introduction

The chemistry of metal alkynyl compounds has been studied for decades since the pioneering work of Nast [1–4], and both the structural rigidity and conjugated M–$(C\equiv C)_n$R backbone render these compounds ideal candidates for molecular wires [5–10]. Earlier successful examples include the work of Lapinte with C_4-bridged diiron compounds [11] and that of Gladysz with C_4-bridged dirhenium compounds [12]. Similar compounds developed in the following years include Mn [13], Ru [14], Pt [15] and Au [16]. The potential of diruthenium/triruthenium termini bridged by oligoyndiyls as prototypical molecular wires were explored by our group [17–19], the laboratories of Lehn [20] and Peng [21–23], where both wire characteristics [24,25] and functional devices [26,27] have been demonstrated. Besides wire-like motifs, rings, double-rings and [2]-catenane supramolecules have been realized based on Au(I) acetylide building blocks [28–31].

With the exception of Fe [11] and Mn [13], the majority of the aforementioned examples are based on 4*d* and 5*d* metals. Our group is interested in expanding this class of compounds to include 3*d* metal based systems supported by tetra-azamacrocyclic ligands [32–38]. In addition to our efforts, alkynyl complexes supported by cyclam (1,4,8,11-tetraazacyclotetradecane) have been explored by other laboratories including Wagenknecht [39–42], Shores [43,44] and Nishijo [45–49], and provide a promising framework for low cost replacement for precious metal based materials. Although metal complexes of *C*– and *N*-substituted tetra-azamacrocyclic ligands have received significant attention as catalysts for oxygen activation and carbon dioxide reduction [50,51], the exploration of alkynyl complexes remains limited [36,52–55].

While the synthesis of M(cyclam) is fairly expedient with M as 3*d* metals, the cyclam ligand is costly to procure and nontrivial to synthesize. With *C*-substituted cyclam derivatives prepared from a simple route [56], the cost is significantly reduced. The synthesis of these ligands and their complexes have been discussed in depth by the laboratories of Curtis [56–58], Lloyd [59–61], and Hay [62,63]. Notable among these are MPD (MPD = 5,12-dimethyl-7,14-diphenyl-1,4,8,11-tetraazacyclotetradeca-4,11-diene) and MPC (MPC = 5,12-dimethyl-9,14-diphenyl-1,4,8,11-tetraazacyclotetradecane) [57,60,63,64]. While most of the macrocycles in diene form were produced via Schiff base condensation reaction of a singly protonated ethylenediamine and a vinyl ketone [56], MPD can be formed simply by mixing ethylenediamine and benzylideneacetone in ether over several days. Subsequent reduction of MPD using sodium borohydride yields MPC. Due to the wide

* Corresponding author.
E-mail address: tren@purdue.edu (T. Ren).

https://doi.org/10.1016/j.jorganchem.2018.11.008
0022-328X/© 2018 Elsevier B.V. All rights reserved.

availability of the reagents, both MPD and MPC can be produced on any desired scale at low cost. Herein, we report the first examples of alkynyl complexes based on the tetraazacyclotetradeca-4,11-diene framework, complexes **2a** and **3a** (Scheme 1), and provide additional examples of alkynyl complexes of C-substituted cyclam with complexes **2b** and **3b**.

2. Results and discussion

2.1. Synthesis

The complexes $[Co(MPD)Cl_2]Cl$ (**1a**) and $[Co(MPC)Cl_2]Cl$ (**1b**) were synthesized using a procedure modified from the preparation of $[Co(cyclam)Cl_2]Cl$ [65]. Specifically, a methanolic solution of the desired macrocyclic ligand with $CoCl_2{\bullet}6H_2O$ was sparged with oxygen followed by the addition of HCl to yield the desired cobalt(III) complex. Complex **1b** is insoluble in water, allowing for the removal of residual cobalt chloride with a water rinse to provide **1b** in 89% yield. Due to its solubility in water, complex **1a** was extracted using dichloromethane from the crude reaction mixture, and then recrystallized with ether for a yield of *ca.* 70%.

From complexes **1a** and **1b** were prepared the monophenylacetylide complexes, *trans*-$[Co(MPD)(C_2Ph)Cl]Cl$ (**2a**) and *trans*-$[Co(MPC)(C_2Ph)Cl]Cl$ (**2b**) under weak base conditions in ambient atmosphere, similar to the method developed by Shores [43,44]. Specifically, complex **1a** was reacted with excess phenylacetylene in the presence of triethylamine under reflux for 24 h. The crude reaction mixture was purified on silica to afford **2a** in a yield of *ca.* 20%. Complex **2b** was similarly prepared from **1b** and purified in a yield of 54%. The low yield of **2a** is likely due to the hydrolysis of the imino bonds of MPD under basic conditions [66], as well as the lability of the chloro ligand. It was noted in the synthesis of **2b** that the use of 5 equiv or more of phenylacetylene led to the formation of the bis-phenylacetylide complex as a minor product, and the yield of the *bis*-byproduct increases with equivalency of phenylacetylide. The bis-phenylacetylide complexes, $[Co(MPD)(C_2Ph)_2]Cl$ (**3a**) and $[Co(MPC)(C_2Ph)_2]Cl$ (**3b**), were prepared from the reaction between a large excess of LiC_2Ph and complexes **1a** or **1b**, and purified over silica with a gradient of dichloromethane and methanol in yields of 64% and 56%, respectively. All complexes are diamagnetic, which is consistent with a low spin Co(III) center.

2.2. Molecular structures

Single crystals of X-ray quality were grown by slow diffusion of diethyl ether into either a 1:1 mixture of acetonitrile and water (**2a**, **2b**) or methanol (**3a**, **3b**). The ORTEP plots for the complex cations are shown in Figs. 1–4, and the selected geometric parameters are

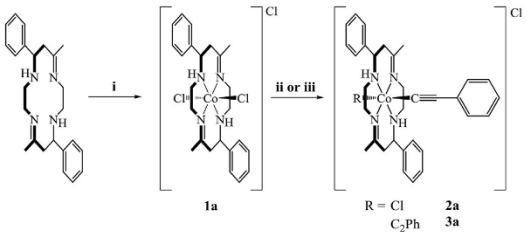

Scheme 1. Synthesis of Co(MPD) complexes **1a-3a**. (i) 1 equiv $CoCl_2{\bullet}6H_2O$, MeOH, O_2, excess HCl; (ii) 7 equiv. HC_2Ph, Et_3N, MeOH, reflux, 24 h; (iii) excess LiC_2Ph, dry THF, 24 h. Co(MPC)-based complexes **1b-3b** were similarly prepared.

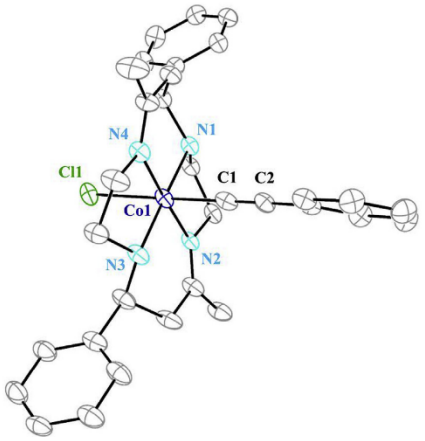

Fig. 1. ORTEP plot of $[\mathbf{2a}]^+$ at the 30% probability level. Hydrogen atoms, solvent molecules, and Cl^- counter ion were omitted for clarity.

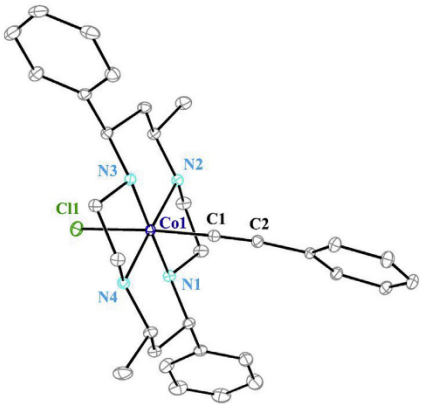

Fig. 2. ORTEP plot of $[\mathbf{2b}]^+$ at the 30% probability level. Hydrogen atoms, solvent molecules, and Cl^- counter ion were omitted for clarity.

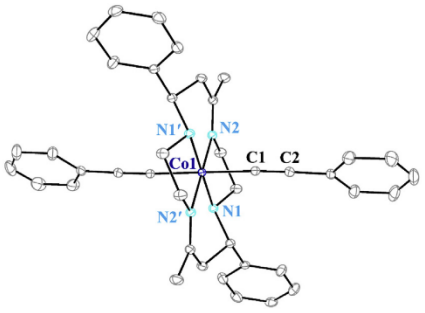

Fig. 3. ORTEP plot of $[\mathbf{3a}]^+$ at the 30% probability level. Hydrogen atoms, solvent molecules, and Cl^- counter ion were omitted for clarity.

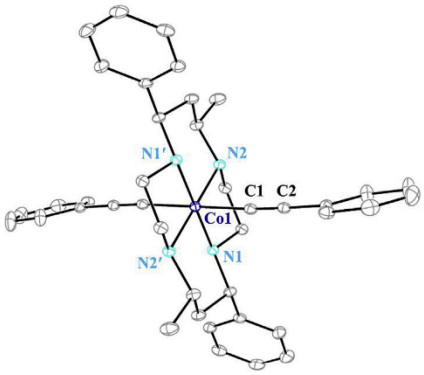

Fig. 4. ORTEP plot of $[\mathbf{3b}]^+$ at the 30% probability level. Hydrogen atoms, solvent molecules, and Cl^- counter ion were omitted for clarity.

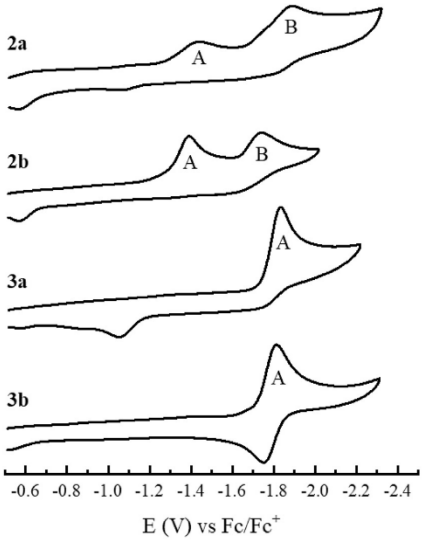

Fig. 5. Cyclic voltammograms of 1.0 mM **2a**, **2b**, **3a**, and **3b** recorded in 0.1 M Bu_4NPF_6 MeCN solution at a scan rate of 0.10 V/s.

listed in Table 1. Each unit cell contains one crystallographically independent formula unit. All cations display a nearly linear Cl–Co–C or C–Co–C linkage, which lies normal to the plane of the coordinated nitrogen atoms, conforming to a pseudo-octahedral geometry. The bis-alkynyl cations, $[\mathbf{3a}]^+$ and $[\mathbf{3b}]^+$, are centro-symmetric at the cobalt center, while the mono-alkynyl cations, $[\mathbf{2a}]^+$ and $[\mathbf{2b}]^+$, possess no crystallographic symmetry. Both cyclam based complexes, **2b** and **3b**, hold the trans-III conformation that is ubiquitous in this class of compounds with no chiral variation at the methyl or phenyl sites (Figs. 2 and 4) [65]. Depending on the orientation of phenyl groups, the M(MPD) complex may exist as one of three possible stereo-isomers, namely (*R,R*), (*S,S*) and (*R,S*) forms, as shown in Scheme 2. The ring conformation differs among stereo-isomers, with both (*R,R*) and (*S,S*) adopting a boat conformation (Fig. 1) and (*R,S*) a chair conformation (Fig. 3). It is possible

Table 1
Selected bond lengths and angles for $[\mathbf{2a}]^+$, $[\mathbf{2b}]^+$, $[\mathbf{3a}]^+$ and $[\mathbf{3b}]^+$.

	$[2a]^+$	$[2b]^+$	$[3a]^+$	$[3b]^+$
Co–N1	1.978(4)	2.005(2)	1.980(1)	2.019(2)
Co–N2	1.945(3)	2.012(2)	1.947(1)	1.990(2)
Co–N3	1.971(4)	2.007(2)	–	–
Co–N4	1.932(3)	2.002(2)	–	–
Co–Cl	2.329(1)	2.3115(6)	–	–
Co–C	1.876(5)	1.870(2)	1.943(1)	1.924(3)
C1–C2	1.202(7)	1.200(4)	1.212(2)	1.201(4)
Cl–Co–C1	177.3(1)	175.19(7)	–	–
Co–C1–C2	172.5(4)	171.8(2)	176.6(1)	172.0(2)
C1–C2–C3	176.7(5)	174.6(3)	178.6(1)	178.8(3)

that the (*R,R*), (*S,S*) isomers were lost in the purification of the reduced form, MPC, hence those isomers are not seen in the Co(III)(MPC) complexes. A further source of isomerism is introduced in mono-acetylide complexes, depending on which chloride is displaced. Since the stereo-isomerism has minimal impact on the electronic structures of the resultant Co complexes, isolation of each of possible isomers was not pursued in this work.

X-ray structures of both the mono- and bis-phenyacetylide complexes of Co(III)(cyclam), $[Co(cyclam)(C_2Ph)Cl]^{+}$ and $[Co(cyclam)(C_2Ph)_2]^{+}$, were reported by Shores [43]. Compared with these structures, the addition of methyl and phenyl groups in compound **2b** causes an increase in Co–N bond length to 2.006 [2] Å from the 1.975 [2] Å in $[Co(cyclam)(C_2Ph)Cl]^+$ [43]. Intuitively, the σ-donation of the nitrogen atoms should be increased with the addition of electron rich substituents. Clearly, the lengthening of the Co–N bonds in **2b** is attributed to the steric effects of the added *C*-substitutents. The Co–C bond (1.870 (2) Å) is shortened while the Co–Cl bond (2.3115 (6) Å) is lengthened compared to those of Co(III)(cyclam) (Co–C 1.898 [2] Å, Co–Cl 23089 [5] Å). Similar lengthening of Co–N (2.004 [2] Å) and shortening of Co–C (1.924(3) Å) bond are observed for **3b** from $[Co(cyclam)(C_2Ph)_2]^{+}$ (Co–N 1.983 [2] Å, Co–C 2.001 [3] Å) [43]. The strengthening of Co–C bond has a pronounced effect on the electrochemical properties as discussed later. Structures of the diene-based complexes, namely **2a** and **3a**, display substantial differences in bond lengths from those of cyclam-based complexes, **2b** and **3b**. As shown in Table 1, the π-accepting capability and structurally smaller ring of MPD shortens the Co–N bonds significantly, which also results in the lengthening of the Co–C and Co–Cl bonds. The C1–C2 alkynyl bond lengths exhibit little variation among the complexes studied, ranging from 1.200 (4) Å for **2b** to 1.212 (2) Å for **3a**. These bonds are longer than those reported for the unsubstituted cyclam variant [43], however they are consistent with other Co(III)(cyclam) complexes reported from our laboratory [34,35,67,68].

2.3. Voltammetric studies

Cyclic voltammograms of complexes **2a**, **2b**, **3a** and **3b** are shown in Fig. 5, and the electrode potentials are listed in Table 2. The overall characteristics are similar to those observed for related Co(III)(cyclam) based complexes [43,69]. Irreversible $Co^{3-/2+}$ (**A**) and $Co^{2+/1+}$ (**B**) couples were observed for both mono complexes. The cathodic shifts in potential from Co(III)(MPC) to Co(III)(MPD) complexes are likely due to a stronger σ-donation from MPD, consistent with the trend noted from structural studies. The presence of a second phenylacetylide in the bis complexes further shifts the reductions cathodically, so that only the $Co^{3-/2+}$ couple can be observed within the solvent window. An irreversible reduction for **3a** is present at −1.83 V, as noted previously for $[Co(cyclam)(C_2Ph)_2]^{+}$ [43]. Interestingly, **3b** undergoes a quasi-reversible reduction at −1.81 V ($\Delta E_p = 63$ mV, $i_{p,a}/i_{p,c} = 0.70$).

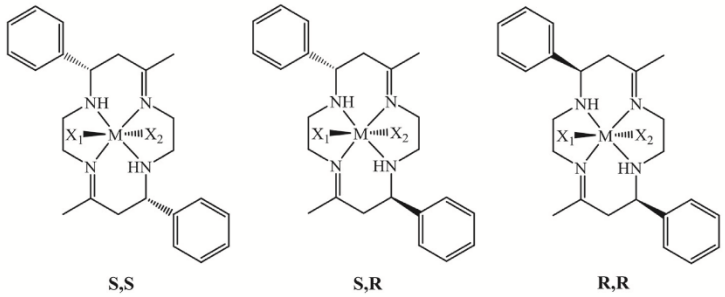

Scheme 2. Stereo-isomers of M(MPD). X_1, X_2 = axial ligands. ⟨*R*,*S*⟩ and ⟨*S*,*R*⟩ are meso when $X_1 = X_2$.

Table 2
Reduction potentials for **2a**, **2b**, **3a**, and **3b**.

	2a	2b	3a	3b
E_{pc} $Co^{3+/2+}$	−1.44	−1.39	−1.83	−1.81
E_{pc} $Co^{2+/1+}$	−1.89	−1.74	–	–

Though not observed in the cyclam analogue reported by Shores [43], a reversible couple was detected for Co(III)(cyclam) bearing both trifluoropropynyl [40] and pentafluorophenylacetylide ligands [35]. The irreversibility in Co(III)(cyclam) complexes is generally associated with the dissociation of labile axial ligands from the reduced Co(II) center [35,40,69]. Sun and coworkers attributed the reversibility of complexes with electron withdrawing ligands to the π-accepting nature of the alkyne rather than the electron density on the metal. These results indicate it is in fact the electron density on the metal, or at least a combination of the two factors, which leads to the reversible couple. Notably, the Co–C bond length of **3b** is comparable to the aforementioned complexes ($[Co(cyclam)(C_2C_6F_5)_2]^+$ (1.926(3) Å) [35]; $[Co(cyclam)(C_2CF_3)_2]^+$ (1.917(4) Å) [40]) without the use of electron withdrawing alkynyls. It is apparent that the reduced σ-donation from the macrocycle to the metal allows for a stronger axial ligand bond in both the Co(III) and Co(II) states. This improved stability is promising for the possible future application of Co(III)(MPC) to molecular wire type devices and opens the possibility of stable Co(II) complexes with sufficiently electron withdrawing cyclam derivatives.

2.4. Electronic absorption spectra

Studies of electronic absorption spectra corroborate the findings in previous sections. As shown in Fig. 6, the tighter binding of MPD results in a greater HOMO-LUMO energy gap and a hypsochromic shift in the absorption spectra. Consequently, the DMSO-d_6 transition located at 463 nm for **2a** is shifted to 499 nm for **2b**. For comparison, the DMSO-d_6 transition for $[Co(cyclam)(C_2Ph)Cl]^+$ lies between these compounds with its absorption band located at 486 nm (in THF) [43]. The bis-phenylacetylide complexes show similar results with a bathochromic shift from MPD to cyclam and then MPC (453 nm in **3a**, 475 nm in **3b** and 463 nm in $[Co(cyclam)(C_2Ph)_2]^+$; spectra in Fig. S1).

2.5. Electronic structures via DFT

In order to understand the electronic structures of Co(III)(MPD) alkynyl species and rationalize the geometric differences between Co(III)(MPD) and Co(III)(MPC) species, density functional theory (DFT) calculations were performed at the B3LYP/LANL2DZ level using the Gaussian16 suite [70]. Calculated bond lengths and angles are in agreement with the crystallographically determined parameters (Table S2). The computed contour plots and energy levels for the frontier molecular orbitals are given in Fig. 7. Expanded plots are given in Figs. S2-S5.

In complexes **2a** and **3a**, the X and Y axes approximately coincide with the Co–N bonds. In such a setting, interactions between the d_{xz} orbitals and the π orbitals of the imino groups are clearly displayed (Figs. S2, S4). For **2a** the d_{yz}, d_{z2}, and d_{xy} orbitals reside in the HOMO, LUMO, and LUMO+1, respectively (Fig. S2). For **3a** the d_{z2} lies in the LUMO+3, while the d_{yz} and d_{xy} lie in the HOMO and LUMO, respectively (Fig. S4). Both complexes **2b** and **3b** have the d_{yz}, d_{x2-y2}, and d_{z2} orbitals as the HOMO, LUMO, and LUMO+1, respectively (Figs. S3, S5). It can be seen that the d_{xz} and d_{yz} orbitals form planes bisecting Co–N bonds, which conforms to the computational analysis in previous studies of related Co(III)(cyclam) species [33–35,67–69]. The axial phenylacetylide groups are major contributors to the frontier molecular orbitals, with antibonding interactions to the d_{yz} orbital in the HOMO of each compound (Figs. S2-S5). The calculated HOMO-LUMO gaps for MPD based complexes **2a** and **3a** are slightly larger than the corresponding MPC complexes **2b** and **3b**, corroborating the hypsochromic shift from MPD to MPC observed in the visible absorption spectra (Fig. 6). The orbitals for the MPD compounds are also higher in energy than MPC, as noted in voltammetric studies.

3. Conclusion

Cobalt(III) complexes supported by a diene-macrocycle (MPD, **1a-3a**) and its cyclam derivative (MPC, **1b-3b**) have been prepared in yields ranging from 20 to 90%. Complexes **2a** and **3a** are the first examples of metal acetylide complexes based on a 1,4,7,11-tetraazacyclotetradeca-4,11-diene type ligand. In comparison with cobalt(III) cyclam complexes, complexes **2a** and **3a** display enhanced Co(III)–N bonding, which increases the HOMO-LUMO energy gap and decreases axial ligand bond strength. On the other hand, complexes **2b** and **3b** exhibit weaker Co–N bonding, resulting in enhanced axial ligand strength. With stronger axial ligand binding, pseudo-reversibility of the $Co^{3+/2+}$ couple was observed for **3b**. The pseudo-reversible reduction observed in **3b** and Co(III)(cyclam) complexes bearing electron-deficient axial ligands highlights the profound effect of changes in the macrocycle on axial ligation. The ability of the *C*-substituted macrocycles to support Co-acetylide complexes encourages further exploration of similar chemistry based on other 3*d* metals, such as Cr, Fe and Ni, an ongoing effort in our laboratory.

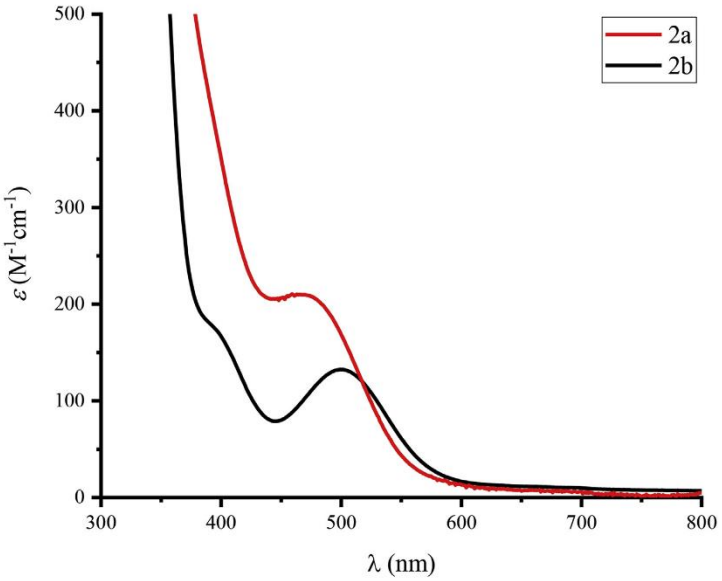

Fig. 6. UV–vis spectra for **2a** (red) and **2b** (black) in MeCN. (For interpretation of the references to colour in this figure legend, the reader is referred to the Web version of this article.)

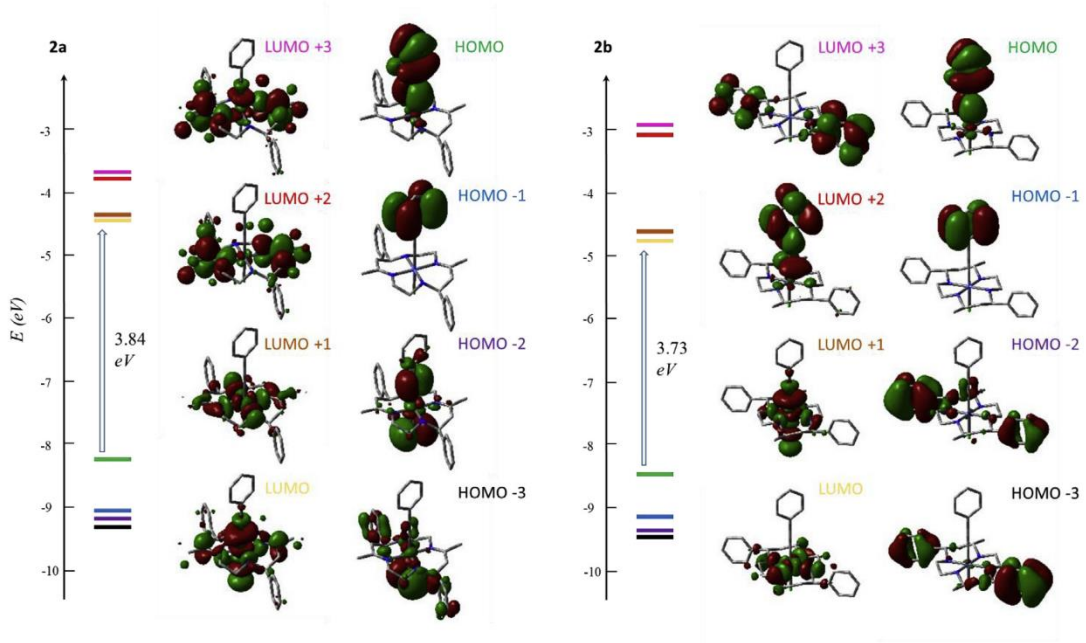

Fig. 7. Molecular orbital diagrams and energy levels for **2a** and **2b.** Diagrams for **3a** and **3b** are given in SI.

4. Experimental

4.1. Materials

Phenylacetylene was purchased from GFS chemicals. $CoCl_2{\cdot}6H_2O$ and *n*-BuLi were purchased from Aldrich. MPD [58] and MPC [60] were prepared according to literature procedures. Tetrahydrofuran was freshly distilled over sodium/benzophenone. All lithiation reactions were carried out under N_2 using standard Schlenk techniques.

4.2. Physical measurements

UV–vis spectra were obtained with a JASCO V-670 spectrophotometer. FT-IR spectra were measured as neat samples using a JASCO FT/IR-6300 spectrometer equipped with an ATR accessory. ESI-MS were analyzed on an Advion Expression Compact Mass Spectrometer. Elemental Analysis was carried out by Atlantic Micro Labs in Norcross, GA. Electrochemical analysis was done on a CHI620A voltammetric analyzer with a glassy carbon working electrode (diameter = 2 mm), a Pt-wire auxiliary electrode, and a Ag/AgCl reference electrode. The analyte concentration is 1.0 mM in 4 mL dry acetonitrile with a 0.1 M Bu_4NPF_6 electrolyte concentration.

4.3. Synthesis of [Co(MPD)Cl_2]Cl **1a**

A methanolic solution of $CoCl_2{\cdot}6H_2O$ (2.20 g, 9.24 mmol) with MPD (3.00 g, 7.97 mmol) was sparged with O_2 for 1h before addition of 7 mL of 12 M HCl. Upon addition of HCl, the solution changed from brown to green. The solution was allowed to sparge for 1 h before being transferred to a petri dish and heated at 45 °C until dry. The residue was taken up in CH_2Cl_2 and filtered to give an emerald green solution, which was recrystallized with ether. Yield: 3.03 g (70%, based on MPD).

4.4. Synthesis of [Co(MPC)Cl_2]Cl **1b**

A methanolic solution of $CoCl_2{\cdot}6H_2O$ (0.640 g, 2.69 mmol) with MPC (1.00 g, 2.63 mmol) was sparged with O_2 for 1 h before addition of 4 mL of 12 M HCl. Upon addition of HCl, the solution changed from red to green with precipitate forming. The solution was allowed to sparge for 1h before the solvent was removed *in vacuo*. The crude solid was sonicated in H_2O before being filtered and washed with H_2O, THF, and ether. The collected green powder was dried under vacuum for 1.00 g. The combined filtrate was boiled down and allowed to cool producing an additional 0.28 g green crystals. Yield: 1.28 g (89% based on MPC).

4.5. Synthesis of [Co(MPD)(C_2Ph)Cl]Cl **2a**

To a methanolic solution of **1a** (0.500 g, 0.923 mmol) was added triethylamine (2.0 mL, 14 mmol), followed by phenylacetylene (1.01 mL, 9.23 mmol). The solution was allowed to reflux 24h. The solvent was removed via rotary evaporation and the residue was purified on silica gel with a gradient of CH_2Cl_2–MeOH. The collected orange product was recrystallized in CH_2Cl_2–Et_2O. Yield: 0.107 g, (20% based on Co). Data for **2a**: ESI-MS (MeCN) 571-[Co(MPD)(C_2Ph)Cl]$^+$. Elem. Anal. Found (Calcd) for $C_{32.5}H_{40}N_4CoCl_3O_1$ ([**2a**]·H_2O·0.5CH_2Cl_2) C, 58.47 (58.44); H, 6.05 (6.04); N, 8.58 (8.39). IR (cm $^{-1}$) 2124 (C≡C). UV–vis absorption spectrum (MeCN) λ_{max} nm (ε_{max}, L mol $^{-1}$ cm $^{-1}$): 257 (38100), 463 (210).

4.6. Synthesis of [Co(MPC)(C_2Ph)Cl]Cl **2b**

To a methanolic solution of **1b** (0.200 g, 0.366 mmol) was added triethylamine (1.5 mL, 11 mmol), followed by phenylacetylene (0.20 mL, 1.8 mmol). The solution was allowed to reflux 4 h. The solvent was removed via rotary evaporation and the residue was purified on silica gel with a gradient of CH_2Cl_2–MeOH. The collected red product was recrystallized in CH_2Cl_2–Et_2O. Yield: 0.120 g, (54% based on Co). Data for **2b**: ESI-MS (MeCN) 575-[Co(MPC)(C_2Ph)Cl]$^+$. Elem. Anal. Found (Calcd) for $C_{33}H_{46}N_4CoCl_4O_{1.5}$ ([**2b**]·1.5H_2O·CH_2Cl_2) C, 54.62 (54.79); H, 6.37 (6.41); N, 7.85 (7.74). IR (cm $^{-1}$) 2124 (C≡C). UV–vis absorption spectrum (MeCN) λ_{max} nm (ε_{max}, L mol $^{-1}$ cm $^{-1}$): 256 (32900), 499 (132).

4.7. Synthesis of [Co(MPD)(C_2Ph)$_2$]Cl **3a**

A suspension of **1a** (0.250 g, 0.461 mmol) in THF was combined with a solution of LiC_2Ph (prepared from 4.6 mmol PhC_2H and 4.8 mmol *n*-BuLi) in THF and allowed to stir 24 h. The flask was opened to air and solvent was removed via rotary evaporation. The residue was purified on silica gel with a CH_2Cl_2–MeOH gradient. The solvent was removed and the remaining orange residue was recrystallized with CH_2Cl_2–Et_2O. Yield: 0.200 g (64% based on Co). Data for **3a**: ESI-MS (MeCN) 637-[Co(MPD)(C_2Ph)$_2$]$^+$. Elem. Anal. Found (Calcd) for $C_{41}H_{48}N_4CoCl_3O_2$ ([**3a**]·2H_2O·CH_2Cl_2) C, 61.83 (62.01); H, 6.19 (6.09); N, 7.31 (7.06). IR (cm $^{-1}$) 2100 (C≡C). UV–vis absorption spectrum (MeCN) λ_{max} nm (ε_{max}, L mol $^{-1}$ cm $^{-1}$): 263 (39700), 453 (191).

4.8. Synthesis of [Co(MPC)(C_2Ph)$_2$]Cl **3b**

A suspension of **1b** (130 mg, 0.238 mmol) in THF was combined with a solution of LiC_2Ph (prepared from 4.6 mmol PhC_2H and 4.8 mmol *n*-BuLi) in THF and allowed to stir 24h. The flask was opened to air and solvent was removed via rotary evaporation. The residue was purified on silica gel with a CH_2Cl_2–MeOH gradient. The solvent was removed and the remaining orange residue was recrystallized with CH_2Cl_2–Et_2O. Yield: 0.090 g (56% based on Co). Data for **3b**: ESI-MS (MeCN) 641-[Co(MPC)(C_2Ph)$_2$]$^+$. Elem. Anal. Found (Calcd) for $C_{40.5}H_{48}N_4CoCl_2O_{0.5}$ ([**3b**]·0.5H_2O·0.5CH_2Cl_2) C, 66.24 (66.76); H, 6.70 (6.64); N, 7.74 (7.69). IR (cm $^{-1}$) 2111 (C≡C). UV–vis absorption spectrum (MeCN) λ_{max} nm (ε_{max}, L mol $^{-1}$ cm $^{-1}$): 269 (50500), 475 (148).

4.9. Computational details

The geometries of **2a**, **2b**, **3a**, and **3b** in the ground state were fully optimized from the crystal structures reported in this work using the density functional method B3LYP (Beck's three-parameter hybrid functional using the Lee–Yang–Parr correlation functional) and employing the LanL2DZ basis sets. The calculation was accomplished by using the Gaussian03 program package {Frisch, 2016 #189}.

4.10. X-ray crystallographic analysis

Single crystal X-ray data was collected on a Bruker AXS D8 Quest CMOS diffractometer using MoKα (λ = 0.71073 Å) radiation with Apex3 software. Data was reduced using SAINT and structures were solved with SHELXTL [71]. Refinement was performed with SHELXL. ORTEP plots were produced using SHELXTL [71].

Notes

The authors declare no competing financial interest.

Acknowledgement

We thank the National Science Foundation for generously supporting this work (CHE 1764347 for research and CHE 1625543 for X-ray diffractometers).

Appendix A. Supplementary data

Supplementary data to this article can be found online at https://doi.org/10.1016/j.jorganchem.2018.11.008.

References

[1] R. Nast, Z. Naturforsch, Teil B 8 (1953) 381.
[2] R. Nast, Coord. Chem. Rev. 47 (1982) 89.
[3] J. Manna, K.D. John, M.D. Hopkins, Adv. Organomet. Chem. 38 (1995) 79.
[4] M.I. Bruce, Coord. Chem. Rev. 166 (1997) 91.
[5] F. Paul, C. Lapinte, Coord. Chem. Rev. 178–180 (Part 1) (1998) 431.
[6] T. Ren, Organometallics 24 (2005) 4854.
[7] K. Costuas, S. Rigaut, Dalton Trans. 40 (2011) 5643.
[8] X.-Y. Zhang, Q.Q. Zheng, Q. Chen-Xi, J.-L. Zuo, Chin. J. Inorg. Chem. 27 (2011) 1451.
[9] D. Xiang, X. Wang, C. Jia, T. Lee, X. Guo, Chem. Rev. 116 (2016) 4318.
[10] A. Haque, R.A. Al-Balushi, I.J. Al-Busaidi, Muhammad S. Khan, P.R. Raithby, Chem. Rev. 118 (2018) 8474.
[11] N. Le Narvor, C. Lapinte, J. Chem. Soc., Chem. Commun. (1993) 357.
[12] Y.L. Zhou, J.W. Seyler, W. Weng, A.M. Arif, J.A. Gladysz, J. Am. Chem. Soc. 115 (1993) 8509.
[13] S. Kheradmandan, K. Heinze, H.W. Schmalle, H. Berke, Angew. Chem. Int. Ed. 38 (1999) 2270.
[14] M.I. Bruce, P.J. Low, K. Costuas, J.F. Halet, S.P. Best, G.A. Heath, J. Am. Chem. Soc. 122 (2000) 1949.
[15] Q. Zheng, J.A. Gladysz, J. Am. Chem. Soc. 127 (2005) 10508.
[16] C.M. Che, H.Y. Chao, V.M. Miskowski, Y.Q. Li, K.K. Cheung, J. Am. Chem. Soc. 123 (2001) 4985.
[17] T. Ren, G. Zou, J.C. Alvarez, Chem. Commun. (2000) 1197.
[18] G.L. Xu, G. Zou, Y.H. Ni, M.C. DeRosa, R.J. Crutchley, T. Ren, J. Am. Chem. Soc. 125 (2003) 10057.
[19] Z. Cao, B. Xi, D.S. Jodoin, L. Zhang, S.P. Cummings, Y. Gao, S.F. Tyler, P.E. Fanwick, R.J. Crutchley, T. Ren, J. Am. Chem. Soc. 136 (2014) 12174.
[20] K.-T. Wong, J.-M. Lehn, S.-M. Peng, G.-H. Lee, Chem. Commun. (2000) 2259.
[21] C. Kuo, J. Chang, C. Yeh, G. Lee, C. Wang, S. Peng, Dalton Trans. (2005) 3696.
[22] C.K. Kuo, I.P.C. Liu, C.Y. Yeh, C.H. Chou, T.B. Tsao, G.H. Lee, S.M. Peng, Chem. Eur J. 13 (2007) 1442.
[23] M.-C. Cheng, S.-A. Hua, Q. Lv, M. Sigrist, G.-H. Lee, Y.-C. Liu, M.-H. Chiang, S.-M. Peng, Dalton Trans. 47 (2018) 1422.
[24] A.S. Blum, T. Ren, D.A. Parish, S.A. Trammell, M.H. Moore, J.G. Kushmerick, G.L. Xu, J.R. Deschamps, S.K. Pollack, R. Shashidhar, J. Am. Chem. Soc. 127 (2005) 10010.
[25] A.K. Mahapatro, J.W. Ying, T. Ren, D.B. Janes, Nano Lett. 8 (2008) 2131.
[26] S. Pookpanratana, H. Zhu, E.G. Bittle, S.N. Natoli, T. Ren, C.A. Richter, Q. Li, C.A. Hacker, J. Phys. Condens. Matter 28 (2016). Art. 094009.
[27] H. Zhu, S.J. Pookpanratana, J.Y. Bonevich, S.N. Natoli, C.A. Hacker, T. Ren, J.S. Suehle, C.A. Richter, Q.L. Li, ACS Appl. Mater. Interfaces 7 (2015) 27306.
[28] F. Mohr, M.C. Jennings, R.J. Puddephatt, Eur. J. Inorg. Chem. (2003) 217.
[29] F. Mohr, D.J. Eisler, C.P. McArdle, K. Atieh, M.C. Jennings, R.J. Puddephatt, J. Organomet. Chem. 670 (2003) 27.
[30] N.C. Habermehl, M.C. Jennings, C.P. McArdle, F. Mohr, R.J. Puddephatt, Organometallics 24 (2005) 5004.
[31] N.C. Habermehl, D.J. Eisler, C.W. Kirby, N.L.-S. Yue, R.J. Puddephatt, Organometallics 25 (2006) 2921.
[32] T. Ren, Chem. Commun. 52 (2016) 3271.
[33] S.N. Natoli, T.J. Azbell, P.E. Fanwick, M. Zeller, T. Ren, Organometallics 35 (2016) 3594.
[34] S.N. Natoli, M. Zeller, T. Ren, Inorg. Chem. 55 (2016) 5756.
[35] S.N. Natoli, M. Zeller, T. Ren, Inorg. Chem. 56 (2017) 10021.
[36] E.C. Judkins, M. Zeller, T. Ren, Inorg. Chem. 57 (2018) 2249.
[37] W.P. Forrest, Z. Cao, R. Hambrick, B.M. Prentice, P.E. Fanwick, P.S. Wagenknecht, T. Ren, Eur. J. Inorg. Chem. (2012) 5616.
[38] S.D. Banziger, T.D. Cook, S.N. Natoli, P.E. Fanwick, T. Ren, J. Organomet. Chem. 799–800 (2015) 1.
[39] C. Sun, C.R. Turlington, W.W. Thomas, J.H. Wade, W.M. Stout, D.L. Grisenti, W.P. Forrest, D.G. VanDerveer, P.S. Wagenknecht, Inorg. Chem. 50 (2011) 9354.
[40] C. Sun, P.U. Thakker, L. Khulordava, D.J. Tobben, S.M. Greenstein, D.L. Grisenti, A.G. Kantor, P.S. Wagenknecht, Inorg. Chem. 51 (2012) 10477.
[41] P.U. Thakker, R.G. Aru, C. Sun, W.T. Pennington, A.M. Siegfried, E.C. Marder, P.S. Wagenknecht, Inorg. Chim. Acta. 411 (2014) 158.
[42] P.U. Thakker, C. Sun, L. Khulordava, C.D. McMillen, P.S. Wagenknecht, J. Organomet. Chem. 772 (2014) 107.
[43] W.A. Hoffert, M.K. Kabir, E.A. Hill, S.M. Mueller, M.P. Shores, Inorg. Chim. Acta. 380 (2012) 174.
[44] W.A. Hoffert, M.P. Shores, Acta Crystallogr. 67 (2011) m853.
[45] J. Nishijo, K. Judai, S. Numao, N. Nishi, Inorg. Chem. 48 (2009) 9402.
[46] J. Nishijo, K. Judai, N. Nishi, Inorg. Chem. 50 (2011) 3464.
[47] J. Nishijo, M. Enomoto, Inorg. Chem. 52 (2013) 13263.
[48] J. Nishijo, Y. Shima, M. Enomoto, Polyhedron 136 (2017) 35.
[49] J. Nishijo, M. Enomoto, Inorg. Chim. Acta. 437 (2015) 59.
[50] W. Nam, Y.-M. Lee, S. Fukuzumi, Acc. Chem. Res. 47 (2014) 1146.
[51] J. Schneider, H. Jia, J.T. Muckerman, E. Fujita, Chem. Soc. Rev. 41 (2012) 2036.
[52] S.F. Tyler, S.N. Natoli, B. Vlaisavljevich, P.E. Fanwick, T. Ren, Inorg. Chem. 54 (2015) 10058.
[53] S.F. Tyler, E. Judkins, Y. Song, F. Cao, D.R. McMillin, P.E. Fanwick, T. Ren, Inorg. Chem. 55 (2016) 8736.
[54] E.C. Judkins, S.F. Tyler, M. Zeller, P.E. Fanwick, T. Ren, Eur. J. Inorg. Chem. (2017) 4068, 2017.
[55] B.M. Oxley, B. Mash, M. Zeller, S. Banziger, T. Ren, Acta Crystallogr. E. 74 (2018) 522.
[56] N.F. Curtis, R.W. Hay, Chem. Commun. (1966) 524.
[57] D.F. Cook, N.F. Curtis, R.W. Hay, J. Chem. Soc., Dalton Trans. (1973) 1160.
[58] N.F. Curtis, Inorg. Chim. Acta. 317 (2001) 27.
[59] K. Hideg, D. Lloyd, J. Chem. Soc., Chem. Commun. (1970) 929.
[60] K. Hideg, D. Lloyd, J. Chem. Soc. C (1971) 3441.
[61] Oh Hankovsz, K. Hideg, D. Lloyd, H. McNab, J. Chem. Soc., Chem. Commun. (1974) 378.
[62] R.W. Hay, G.A. Lawrence, J. Chem. Soc., Dalton Trans. (1975) 1466.
[63] R.W. Hay, P.M. Gidney, J. Chem. Soc., Dalton Trans. (1976) 974.
[64] N.F. Curtis, J. Chem. Soc., Dalton Trans. (1973) 1212.
[65] B. Bosnich, C.K. Poon, M.L. Tobe, Inorg. Chem. 4 (1965) 1102.
[66] R.W. Hay, G.A. Lawrance, J. Chem. Soc., Dalton Trans. (1975) 1556.
[67] T.D. Cook, S.N. Natoli, P.E. Fanwick, T. Ren, Organometallics 35 (2016) 1329.
[68] S.N. Natoli, T.D. Cook, T.R. Abraham, J.J. Kiernicki, P.E. Fanwick, T. Ren, Organometallics 34 (2015) 5207.
[69] T.D. Cook, S.N. Natoli, P.E. Fanwick, T. Ren, Organometallics 34 (2015) 686.
[70] Gaussian 03, Revision D.02, Gaussian, Inc, 2003.
[71] G. Sheldrick, Acta Crystallogr. A 64 (2008) 112.

ORGANOMETALLICS

pubs.acs.org/Organometallics Article

Improving Redox Reversibility and Intermetallic Coupling of Co(III) Alkynyls through Tuning of Frontier Orbitals

Brandon L. Mash, Yiwei Yang, and Tong Ren*

Cite This: *Organometallics* 2020, 39, 2019−2025 Read Online

ACCESS | Metrics & More | Article Recommendations | Supporting Information

ABSTRACT: Reported herein are the syntheses and characterizations for a series of butadiyndiyl-bridged Co^{III}(MPC) (MPC = 5,12-dimethyl-7,14-diphenyl-1,4,8,11-tetraazacyclotetradecane) complexes, capped with chloride ($[\mathbf{1}]^{2+}$), phenylacetylide ($[\mathbf{2}]^{2+}$), or 3,5-dichlorophenylacetylide ($[\mathbf{3}]^{2+}$). The MPC ligand was chosen to weaken the ligand field around the equatorial plane, allowing stronger axial coordination. Cyclic voltammetry measurement revealed the first unambiguous examples of stepwise one-electron reductions in bridged Co(cyclam′) complexes (cyclam′ = any ligand bearing the 1,4,8,11-tetraazacyclotetradecane framework). Further voltammetric analysis using NBu_4BArF (NBu_4BArF = tetrabutylammonium tetrakis[3,5-bis(trifluoromethyl)phenyl]borate) as electrolyte resulted in well-separated reversible reduction waves with up to 160 mV separation for $[\mathbf{2}]^{2+}$. These features hint at the possibility of application of earth-abundant metal complexes to function as molecular wires. These complexes were also characterized with infrared and UV−vis spectroscopy, density functional theory calculations, and single-crystal X-ray diffraction ($[\mathbf{1}](BPh_4)_2$ only).

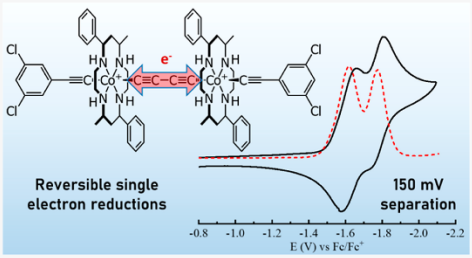

Downloaded via PURDUE UNIV on May 27, 2020 at 15:00:46 (UTC).
See https://pubs.acs.org/sharingguidelines for options on how to legitimately share published articles.

INTRODUCTION

Following the seminal work on organometallic σ-alkynyl complexes by Nast and co-workers,[1,2] considerable attention has been given to the application of these compounds as electronic and optoelectronic materials due to their structural rigidity and high degree of conjugation.[3−6] In particular, the use of metal alkynyls as the prototypical molecular wires has been investigated by the laboratories of Launay,[7,8] Gladysz,[9,10] Halet,[11,12] Rigaut,[13] and Akita.[14] Compounds exhibiting extraordinary degrees of electron delocalization include those of Fe,[15] Mn,[16] Ru,[17] Ru_2,[18−20] and Re.[21,22] Though rare, single-molecule conductance has been measured for alkynyl compounds of Pt,[23,24] Ru,[25−27] and Ru_2,[28,29] and functional devices have been fabricated as well.[30−33]

With the desire to use more earth-abundant elements and cost-efficient resources, our recent efforts have focused on cyclam complexes of 3d transition metals (cyclam = 1,4,8,11-tetraazacyclotetradecane). Our work,[34,35] along with those from the laboratories of Shores,[36,37] Nishijo,[38−42] and Wagenknecht,[43−48] has significantly expanded the scope of this previously underexplored field. While previous work on dicobalt species bridged by oligoynes revealed the structural features similar to highly delocalized Ru_2 compounds, their voltammetric responses were not ideal. The dicobalt species typically displays irreversible two-electron reductions, indicating localized charges on each cobalt center and chemical instability upon reduction,[49−51] the latter of which is associated with the lability of the axial chloro-/alkynyl ligands upon the reduction of Co^{III} center.

Reversible reduction of Co^{III}(cyclam) complexes has been achieved thus far only through the use of significantly electron-withdrawing axial ligands, which are less labile on the reduced Co^{II} center.[43,46,48,52] Recently, we reported that a Co^{III} complex of a C-substituted cylam, $[Co(MPC)(C_2Ph)_2]^+$ (MPC = 5,12-dimethyl-7,14-diphenyl-1,4,8,11-tetraazacyclotetradecane), displays a quasi-reversible reduction,[53] in stark contrast to the irreversible reduction displayed by $[Co(cyclam)(C_2Ph)_2]^+$.[36] Similar in effect to the use of electron-withdrawing ligands, this change in voltammetric behavior is achieved through the strengthening of the axial bonds, which is the result of a weakened equatorial ligand field. Addition of bulky phenyl groups to the cyclam skeleton appears to stiffen the macrocyle, which results in significantly weakened Co−N bonds and a net increase in positive charge density on the metal, thereby allowing stronger Co−σ-alkynyl bonds.

It is the goal of the present work to determine if the increased electrochemical stability and axial ligand bond

Received: March 17, 2020
Published: April 28, 2020

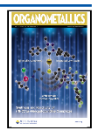

ACS Publications © 2020 American Chemical Society

https://dx.doi.org/10.1021/acs.organomet.0c00183
Organometallics 2020, 39, 2019−2025

strength of Co^{III}(MPC) complexes translate into discernible electronic coupling between two cobalt centers bridged by an oligoyne. To this end, a series of butadiyndiyl-bridged complexes, $[\{Co(MPC)Cl\}_2(\mu\text{-}C_4)]Cl_2$ ($[\mathbf{1}]Cl_2$), $[\{Co(MPC)(C_2Ph)\}_2(\mu\text{-}C_4)]Cl_2$ ($[\mathbf{2}]Cl_2$), and $[\{Co(MPC)(C_2\text{-}3,5\text{-}Cl\text{-}C_6H_3)\}_2(\mu\text{-}C_4)]Cl_2$ ($[\mathbf{3}]Cl_2$), have been prepared (Chart 1). The syntheses and characterizations of $[\mathbf{1}]^{2-}$–$[\mathbf{3}]^{2+}$ will be discussed henceforth.

Chart 1. Structures of Complexes $[\mathbf{1}]Cl_2$–$[\mathbf{3}]Cl_2$

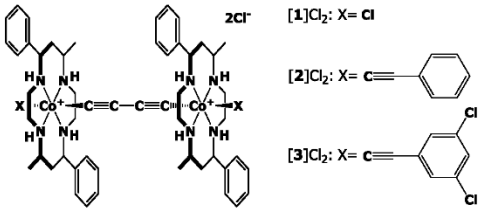

RESULTS AND DISCUSSION

Synthesis. $[Co(MPC)Cl_2]Cl$ and 0.5 equiv of 1,4-bis-(trimethylsilyl)butadiyne were refluxed in MeOH and Et_3N for 24 h under N_2, and the crude product from the reaction was purified on silica gel and recrystallized to afford $[\{Co(MPC)Cl\}_2(\mu\text{-}C_4)]Cl_2$ ($[\mathbf{1}]Cl_2$) in 44% yield with $[Co(MPC)Cl_2]Cl$ and $[Co(MPC)(C_4H)Cl]Cl$ as the major byproducts. Increased reaction time did not significantly increase the ratio of product to starting material. The reactions between $[\{Co(MPC)Cl\}_2(\mu\text{-}C_4)]Cl_2$ and excess LiC_2Ar (prepared from lithium diisopropylamide) at −78 °C, using standard Schlenk techniques under nitrogen atmosphere, resulted in near quantitative conversion to $[\{Co(MPC)(C_2Ar)\}_2(\mu\text{-}C_4)]Cl_2$ with minimal scrambling of acetylides or undesired products (Scheme 1). When alkynylation of $[\mathbf{1}]Cl_2$ is performed at room temperature, various mononuclear and dinuclear alkynyl products of various combinations form, as determined by mass spectrometry, and were not isolated or further characterized. Compounds $[\mathbf{2}]Cl_2$ and $[\mathbf{3}]Cl_2$ were isolated in 68 and 52% yields (based on $[\mathbf{1}]Cl_2$), respectively.

Typical for strong-field Co(III) species, complexes $[\mathbf{1}]Cl_2$, $[\mathbf{2}]Cl_2$, and $[\mathbf{3}]Cl_2$ are diamagnetic and exhibit well behaved ^1H NMR spectra (Figures S6–S8). The UV–vis spectra featured the d–d bands at 520 nm for $[\mathbf{1}]Cl_2$, 484 nm for $[\mathbf{2}]Cl_2$, and 479 nm for $[\mathbf{3}]Cl_2$, and intense LMCT ($[\mathbf{1}]Cl_2$–$[\mathbf{3}]Cl_2$) and π–π^* ($[\mathbf{2}]Cl_2$ and $[\mathbf{3}]Cl_2$) bands in the UV region (Figure S10). In spite of the Co–Co coupling detected in the voltammetric study (see below), there is no significant feature associated with intermetallic coupling in the absorption spectra. The IR peaks between 2000–2100 cm^{-1}, the window for $\nu(C{\equiv}C)$, were barely discernible for $[\mathbf{1}]Cl_2$ because of the centro-symmetric nature of the butydiynyl bridge, but fairly intense for $[\mathbf{2}]Cl_2$ and $[\mathbf{3}]Cl_2$ because of the contribution from the capping aryl acetylides (Figure S11).

Molecular Structures. While X-ray quality single crystals of $[\mathbf{1}]Cl_2$ could not be obtained, single crystals of $[\mathbf{1}](BPh_4)_2$ were successfully grown. Suitable crystals for $[\mathbf{2}]^{2+}$ and $[\mathbf{3}]^{2+}$ could not be obtained despite many attempts with different counterions and solvent combinations. The ORTEP plot for $[\mathbf{1}](BPh_4)_2$ is given in Figure 1, while additional experimental

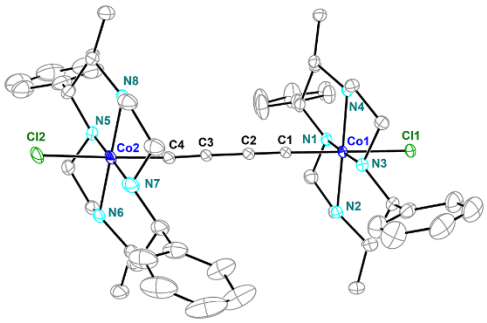

Figure 1. Molecular structure of $[\mathbf{1}]^{2+}$ at 30% probability level. Hydrogen atoms and tetraphenylborate anions have been removed for clarity.

and refinement details are given in Table S1. As with previous Co^{III}(MPC) compounds, $[\mathbf{1}]^{2+}$ maintains the *trans*-III conformation of the macrocyclic ring with equatorial methyl and phenyl substituents. The Co centers exhibit pseudo-octahedral geometries with the four nitrogen members of the macrocyclic ring forming the equatorial plane and alkynyl/chloro ligands in the axial sites.

It was postulated in previous work that the long Co–N bonds and shorter Co axial bonds were the result of replacing cyclam with the MPC ligand.[53] As shown in Table 1, this structural feature remains true for $[\mathbf{1}]^{2+}$, with the elongation of

Scheme 1. Synthetic Route to Prepare $[\mathbf{1}]Cl_2$, $[\mathbf{2}]Cl_2$, and $[\mathbf{3}]Cl_2$[a]

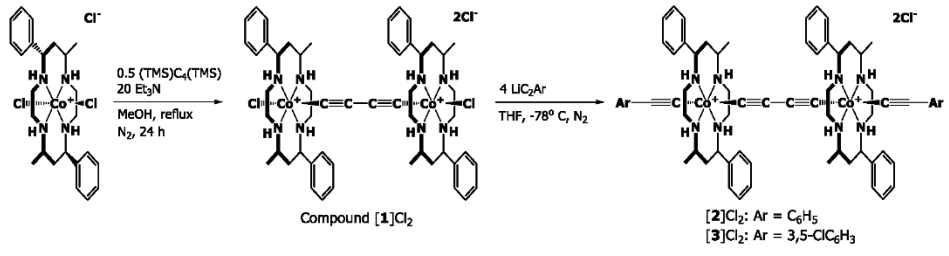

[a]Ar = C_6H_5 or 3,5-Cl–C_6H_3.

https://dx.doi.org/10.1021/acs.organomet.0c00183
Organometallics 2020, 39, 2019–2025

Table 1. Comparison of Bond Lengths and Angles for $[1]^{2+}$ and $[\{Co(cyclam)Cl\}_2(\mu\text{-}C_4)]^{2+}$ (cyclam)

	$[1]^{2+}$	cyclam[a]
Co−N_{avg}	1.996[1]	1.977[3]
Co−Cl_{avg}	2.2978[5]	2.3137[11]
Co1−C1	1.874(2)	1.878(4)
Co2−C4	1.875(2)	1.890(5)
C1−C2	1.211(2)	1.208(6)
C2−C3	1.376(2)	1.388(5)
C3−C4	1.209(2)	1.201(5)
Cl1−Co1−C1	178.92(5)	177.25(13)
Cl2−Co2−C4	177.57(6)	177.49(12)
Co1−C1−C2	177.48(2)	170.1(4)
Co2−C4−C3	174.27(2)	169.3(4)

[a]Taken from ref 49.

Co−N bonds and shortening of Co axial bonds relative to those of $[\{Co(cyclam)Cl\}_2(\mu\text{-}C_4)]^{2+}$. Consequently, the alkynyl C≡C bonds are lengthened, and the C−C single bond is shortened, indicating a small but discernible contribution of the cumulenic resonance structure.

Voltammetric Studies. The $Co^{III/II}$ couple of previously studied $[Co(MPC)(C_2Ph)_2]^+$ is quasi-reversible[53] whereas that of $[Co(cyclam)(C_2Ph)_2]^+$ is irreversible.[36] The concurrent weakening of MPC coordination and strengthening of axial bonds have a clear impact on the electronics of the dicobalt species, as shown by the cyclic voltammograms (CV) and differential pulse voltammograms (DPV) of complexes $[1]^{2+}$–$[3]^{2+}$ in Figure 2. In Co^{III}(cyclam)-based complexes, the

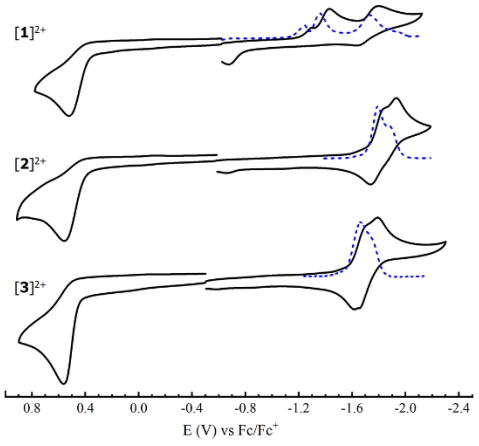

Figure 2. CVs (black, solid) and DPVs (blue, dashed) of 1.0 mM $[1]^{2+}$, $[2]^{2+}$, and $[3]^{2+}$ recorded in 0.1 M Bu_4NPF_6 MeCN solution at a scan rate of 0.10 V/s.

chloro ligand tends to dissociate upon reduction, resulting in irreversibility of the $Co^{III/II}$ redox couple.[52] The CV of $[1]^{2+}$ shares this feature with two irreversible reductions at −1.39 V ($Co^{III/II}$) and −1.76 V ($Co^{II/I}$) and an irreversible oxidation at 0.52 V ($Co^{IV/III}$) (Table 2). The CV and DPV of $[2]^{2+}$ are substantially different from those of $[\{Co(cyclam)(C_2Ph)\}_2(\mu\text{-}C_4)]^{2+}$.[51] The $Co^{III/II}$ couples are the only observable reduction events within the cathodic end of the solvent window, and are

Table 2. Reduction Potentials (V vs $Fc^{+/0}$) for $[1]^{2+}$, $[2]^{2+}$, and $[3]^{2+}$

E	$[1]^{2+}$	$[2]^{2+}$	$[3]^{2+}$
E_{pa} 4+/2+	0.52	0.56	0.64
E_{pc} 2+/1+	−1.39[a]	−1.79[b]	−1.65[b]
E_{pc} 1+/0		−1.89[b]	−1.74[b]
E_{pc} 0/2−	−1.76		
E(2+/1+) ($BArF_{24}$)[c]		−1.75	−1.66
E(1+/0) ($BArF_{24}$)[c]		−1.91	−1.81

[a]Potential for a 2-electron 2+/0 process. [b]Determined from deconvoluted DPV. [c]Determined using NBu_4BArF electrolyte

both quasi-reversible and clearly two separated one electron processes. The second reduction has a lower peak current than the first, indicating a partial chemical degradation after the first reduction. The oxidation ($Co^{IV/III}$) appears as a two-electron process at 0.56 V.

Compound $[3]Cl_2$ was prepared with the goal of increasing the stability of the reduced state by combining the effects seen from electron-withdrawing ligands with the effect of the MPC ligand. In this regard, $[3]^{2-}$ is more electrochemically stable than $[2]^{2+}$, with a larger return wave and absence of the degradation peak around −0.55 V seen in the other two compounds (Figure 2). The reduction peaks were found to be separated by 0.09 V, located at −1.65 and −1.74 V, with the second reduction being 90% the size of the first reduction (Figure S4). The increased electron-withdrawing effect of the 3,5-dichloro substituents shifts the reduction of $[3]^{2+}$ to a more anodic value than that of $[2]^{2+}$, indicating the increased electron deficiency at the Co centers. While the enhanced coordination of the 3,5-dichlorophenylacetylide ligand improves stability of the reduced state, it also decreases the peak separation of each reduction when compared to $[2]^{2+}$ (0.10 V for $[2]^{2+}$, 0.09 V for $[3]^{2+}$), as was hypothesized in previous works.[49]

The use of anions with low affinities for ion pairing as the electrolyte has been proven to improve separation of single-electron reductions in mixed valence compounds by thermodynamically stabilizing the singly reduced state.[54,55] In order to improve the separation of the stepwise reduction processes in $[2]^{2+}$ and $[3]^{2+}$, NBu_4BArF (NBu_4BArF = tetrabutylammonium tetrakis[3,5-bis(trifluoromethyl)phenyl]-borate) was employed as the electrolyte in place of NBu_4PF_6, using dichloromethane as a noncoordinating solvent. As shown in Figure 3, the electrochemical stability of the singly reduced states of both $[2]^{2+}$ and $[3]^{2+}$ in the cathodic window improved significantly. For $[2]^{2+}$, the first and second redox waves are well-defined at −1.69 and −1.85 V, respectively, and the stability is much improved, judging from the equal currents of each reduction in the DPV. For $[3]^{2+}$, the reduction couples are more reversible than those of $[2]^{2+}$ with the first and second couples at −1.62 and −1.77 V, respectively. Finally, the well-resolved DPV waves allow for an unambiguous determination of the separation between the two stepwise one-electron reductions as 160 mV for $[2]^{2+}$ and 150 mV $[3]^{2+}$.

Density Functional Theory (DFT) Calculations. To gain further insight into the electronic structures, DFT calculations/analysis were performed for complexes $[1]^{2+}$, $[2]^{2+}$, and $[3]^{2+}$. In the absence of suitable crystal structures for $[2]^{2+}$ and $[3]^{2+}$, all DFT calculations were based on the molecular structure of $[1]^{2+}$ with appropriate modifications whenever necessary. The frontier orbitals and energy levels for $[1]^{2+}$ and $[2]^{2+}$ are

https://dx.doi.org/10.1021/acs.organomet.0c00183
Organometallics 2020, 39, 2019−2025

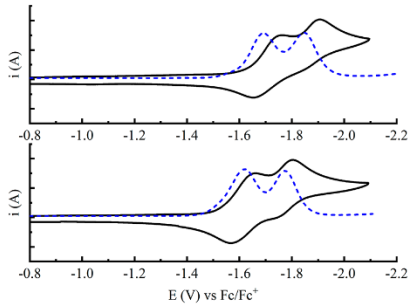

Figure 3. CVs (black, solid) and DPVs (blue, dashed) for 1 mM $[2]^{2+}$ (top) or $[3]^{2+}$(bottom) recorded in 0.1 M Bu_4BArF CH_2Cl_2 solutions.

displayed in Figure 4. Those of $[3]^{2-}$ are given in Figure S5, and relevant bonds lengths are given in Table S2.

Complexes $[1]^{2+}$, $[2]^{2+}$, and $[3]^{2+}$ share the same feature in their LUMO−LUMO+3, with the LUMO and LUMO+1 consisting of the $d_{x^2-y^2}$ orbitals and LUMO+2 and LUMO+3 consisting of the d_{z^2} orbitals. This feature is consistent with the e_g set of orbitals for a low-spin, pseudo-octahedral, d^6 Co^{III} center. The stabilization of $d_{x^2-y^2}$ orbitals over the d_{z^2} orbitals is clearly a manifestation of weaker ligand field in the *xy* plane exerted by the MPC ligand. In contrast, the d_{z^2} orbitals dominate the LUMO and LUMO+1 of $[\{Co(cyclam)Cl\}_2(\mu\text{-}C_4)]^{2+}$, which are σ^*(Co axial ligand) in nature.[49] Hence, while the reduction of $[\{Co(cyclam)Cl\}_2(\mu\text{-}C_4)]^{2+}$ is followed by the dissociation of one of the axial ligands (likely Cl^-), the reduction of $[\{Co(MPC)(C_2Ar)\}_2(\mu\text{-}C_4)]^{2+}$ populates the $d_{x^2-y^2}$ orbitals, which does not lead to the dissociation of arylacetylide and thus enhances electrochemical reversibility. However, the highest occupied orbitals in the MPC-based complexes are similar to those of $[\{Co(cyclam)Cl\}_2(\mu\text{-}C_4)]^{2+}$.[49] For $[1]^{2+}$, the HOMO and HOMO−1 are the mixtures of the d_{xz} and d_{yz} orbitals with the π(C≡C) orbitals of the butadiyndiyl bridge. For $[2]^{2+}$ and $[3]^{2+}$, the mixtures of the d_{xz} and d_{yz} orbitals with the π(C≡C) orbitals of capping arylacetylide ligands dominate the HOMO and HOMO−1, while the mixtures of the d_{xz} and d_{yz} orbitals with the π(bridge) orbitals result in the orbitals HOMO−2 and HOMO−3. Although LUMO/LUMO+1 in $[2]^{2+}$ and $[3]^{2+}$ are the localized $d_{x^2-y^2}$ orbitals with no obvious Co−Co interaction, two Co^{III} centers can still engage in significant electronic coupling manifested by the HOMO−2 and HOMO−3 via a hole-transfer formalism outlined by Launay.[7,8]

■ CONCLUSION

A series of Co^{III}(MPC) alkynyl complexes have been prepared in modest to high yields. The alkynyl-capped compounds $[2]^{2+}$ and $[3]^{2+}$ are the first examples of cyclam-based complexes which display unambiguous intermetallic coupling across an oligoyne bridge. Furthermore, $[2]^{2+}$ is the first such cobalt cyclam-derived complex to have a quasi-stable reduced state without the use of electron-withdrawing axial ligands. These properties are the result of weaker coordination of the MPC ligand when compared to those of cyclam, which allows for enhanced axial ligand binding. The combined effects of electron-withdrawing arylacetylides and the weakened equatorial ligand field by the MPC ligand resulted in two reversible one electron reductions in $[3]^{2+}$, a rarity in Co^{III} redox chemistry. Compounds bearing more electron-deficient macrocyclic ligands that retain the steric bulk of MPC are being developed in our laboratory to fully elaborate the effect of LUMO engineering through the tuning of equatorial ligand field strength.

■ EXPERIMENTAL SECTION

Materials. The synthesis for $[Co(MPC)Cl_2]Cl$ was described previously.[53] 3,5-Dichlorophenylacetylene was prepared according to a literature procedure.[56] Bis(trimethylsilyl)butadiyne was purchased from GFS Chemicals. *n*-BuLi was purchased from Aldrich. Lithium diisopropylamide was prepared in situ by addition of *n*-BuLi to

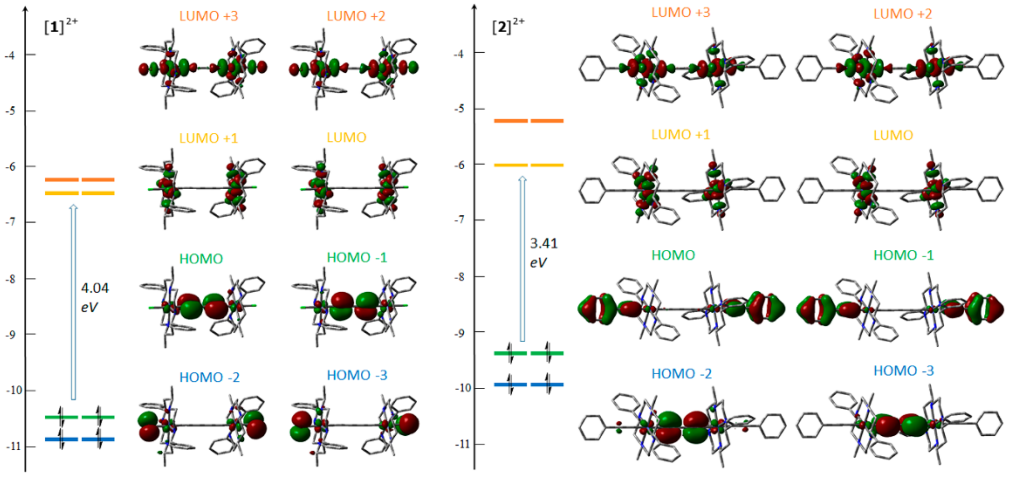

Figure 4. Molecular orbital diagrams for $[1]^{2+}$ and $[2]^{2+}$ from DFT calculations. The isovalue of the contour plots was set at 0.03.

https://dx.doi.org/10.1021/acs.organomet.0c00183
Organometallics 2020, 39, 2019−2025

distilled diisopropylamine. All reagents were used as received. Tetrahydrofuran was freshly distilled over sodium/benzophenone. All lithiation reactions were carried out under N_2 using standard Schlenk techniques.

Physical Measurements. ^{1}H NMR spectra were obtained with a Varian Mercury300 NMR instrument, with chemical shifts (δ) referenced to the residual solvent signal ($CHCl_3$ at δ = 7.26 ppm). UV/vis spectra were obtained with a JASCO V-670 spectrophotometer. FT-IR spectra were measured as neat samples using a JASCO FT/IR-6300 spectrometer equipped with an ATR accessory. Electrospray mass spectra were obtained as electrospray in positive-ion mode with the aid of an Advion Expression Compact Mass Spectrometer. Elemental analysis was carried out by Atlantic Micro Laboratories in Norcross, GA. Electrochemical analysis was done on a CHI620A voltammetric analyzer with a glassy carbon working electrode (diameter = 2 mm), a Pt-wire auxiliary electrode, and a Ag/AgCl reference electrode. The analyte concentration is 1.0 mM in 4 mL of dry acetonitrile with a 0.1 M Bu_4NPF_6 electrolyte concentration, unless otherwise stated.

Synthesis of [{Co(MPC)Cl}$_2$(μ-C$_4$)]Cl$_2$ ([1]Cl$_2$). To a methanolic solution of [Co(MPC)Cl_2]Cl (1.00 g, 1.83 mmol) was added triethylamine (5.0 mL, 36 mmol), followed by a THF solution of bis(trimethylsilyl)butadiyne (0.188 g, 0.967 mmol). The solution was allowed to reflux for 24 h as the color turned from green to orange to red. The solvent was removed via rotary evaporation, and the residue was purified on silica gel with a gradient of CH_2Cl_2-MeOH, gradually proceeding from pure CH_2Cl_2 to a 9:1 ratio of CH_2Cl_2 to MeOH. The collected red product was recrystallized from CH_2Cl_2-Et_2O. Yield: 0.435 g, (44% based on Co). ESI-MS (MeCN): 498 [{Co(MPC)Cl}$_2$(μ-C_4)]$^{2+}$. Elem. Anal. for $C_{54}H_{80}N_8O_2Co_2Cl_8$ ([1]Cl_2·2H_2O·2CH_2Cl_2): calcd C 50.88, H 6.32, N 8.79. Found C 50.54, H 6.64, N 8.91. ^{1}H NMR ($CDCl_3$, δ): 8.29 (br, 2 H, NH), 7.60−7.10 (m, 20 H, ArH), 6.12 (br, 2 H, NH), 5.57 (br, 2 H, NH), 4.44 (m, 2 H, CH), 4.23 (m, 4 H, CH_2), 3.74 (m, 2 H), 3.58 (br, 2 H, NH), 3.37 (m, 2 H), 3.11 (m, 6 H), 2.79 (m, 4 H), 2.27 (m, 6 H), 1.99 (dd, 2 H), 1.83 (m, 4 H), 1.48 (d, 6 H, CH_3), 1.35 (d, 6 H, CH_3) ppm. UV−vis spectra, λ_{max} (nm, ε (M^{-1} cm^{-1})): 207 (66 000), 233 (74 000), 350 (3100), 520 (380).

Synthesis of [{Co(MPC)(C$_2$Ph)}$_2$(μ-C$_4$)]Cl$_2$ ([2]Cl$_2$). A solution of [1]Cl_2 (83 mg, 0.078 mmol) in THF was combined with a solution of Li-phenylacetylide (prepared from 0.36 mmol phenylacetylene and 0.50 mmol LDA) in THF at −78 °C. This was allowed to warm to room temperature and stirred 12 h before quenching with air and removal of solvent via rotary evaporation. The residue was purified on silica gel with a 15:1 ratio of CH_2Cl_2:MeOH. The collected orange fraction was recrystallized from CH_2Cl_2-Et_2O, yielding 63 mg (68% based on Co). ESI-MS (MeCN): 564 [{Co(MPC)(C_2Ph)}$_2$(μ-C_4)]$^{2+}$. Elem. Anal. for $C_{71.5}H_{89}N_8Co_2Cl_2$ ([2]Cl_2·3.5CH_2Cl_2): calcd C 57.35, H 5.99, N 7.48. Found C 57.17, H 5.99, N 7.48. ^{1}H NMR ($CDCl_3$, δ): 8.29 (br, 2 H, NH), 7.65−7.05 (m, 30 H, ArH), 5.49 (br, 2 H, NH), 4.91 (br, 2 H, NH), 4.22 (m, 4 H), 4.00 (t, 2 H), 3.62 (br, 2 H, NH), 3.41 (m, 4 H), 3.02 (m, 6 H), 2.86 (m, 2 H), 2.65−2.05 (m, 8 H), 1.94 (dd, 2 H), 1.72 (m, 4 H), 1.42 (d, 6 H, CH_3), 1.37 (d, 6 H, CH_3) ppm. UV−vis spectra, λ_{max} (nm, ε (M^{-1} cm^{-1})): 224 (92 000), 260 (74 000), 349 (2,700), 484 (340).

Synthesis of [{Co(MPC)(3,5-ClC$_2$Ph)}$_2$(μ-C$_4$)]Cl$_2$ ([3]Cl$_2$). A solution of [1]Cl_2 (86 mg, 0.080 mmol) in THF was combined with a solution of Li-3,5-dichlorophenylacetylide (prepared from 0.36 mmol of 3,5-dichlorophenylacetylene and 0.50 mmol of LDA) in THF at −78 °C. This was allowed to warm to room temperature and stirred for 12 h before quenching with air and removal of solvent via rotary evaporation. The residue was purified on silica gel with a 24:1 ratio of CH_2Cl_2−MeOH. The collected orange fraction was recrystallized from CH_2Cl_2/Et_2O, yielding 56 mg (52% based on Co). ESI-MS (MeCN): 633 [{Co(MPC)(3,5-ClC_2Ph)}$_2$(μ-C_4)]$^{2+}$. Elem. Anal. for $C_{69}H_{82}N_8O_1Co_2Cl_8$ ([3]Cl_2·H_2O·CH_2Cl_2): calcd C 57.52, H 5.74, N 7.77. Found C 57.34, H 5.89, N 7.51. ^{1}H NMR ($CDCl_3$, δ): 7.99 (br, 2 H, NH), 7.80−7.00 (m, 26 H, ArH), 5.57 (br, 2 H, NH), 4.84 (br, 2 H, NH), 4.22 (t, 2 H), 4.09 (m, 2 H), 3.85 (t, 2 H), 3.70−3.20 (m, 6 H), 3.15−2.85 (m, 6 H), 2.68−2.28 (m, 6 H), 2.17 (m, 4 H), 1.94 (dd, 2 H), 1.74 (m, 4 H), 1.40 (m, 12 H, CH_3) ppm. UV−vis spectra, λ_{max} (nm, ε (M^{-1} cm^{-1})): 226 (100 000), 279 (62 000), 349 (2500), 479 (320).

Computational Details. The geometries of $[1]^{2+}$, $[2]^{2+}$, and $[3]^{2+}$ in the ground states were fully optimized based on the crystal structure of [1]$(BPh_4)_2$. Both $[2]^{2+}$ and $[3]^{2+}$ had the additional ligands manually edited without changing the rest of the structure. The density functional method B3LYP (Beck's three-parameter hybrid functional using the Lee−Yang−Parr correlation functional)[57] was used for calculations with the def2-TZVP basis set used for cobalt, and the def2-SVP basis set was used for all other atoms.[58] The calculation was accomplished by using the Gaussian16 program package.[59]

X-ray Crystallographic Analysis. Single-crystal X-ray data was collected on a Bruker AXS D8 Quest CMOS diffractometer using Mo Kα (λ = 0.71073 Å) radiation with Apex3 software.[60] Data was reduced using SAINT[60] and structures were solved with SHELXTL.[61] Refinement was performed with SHELXL.[62] ORTEP plots were produced using SHELXTL.[61]

■ ASSOCIATED CONTENT

Supporting Information

The Supporting Information is available free of charge at https://pubs.acs.org/doi/10.1021/acs.organomet.0c00183.

Experimental crystallographic details, and supramolecular structure plots for 1; DPV plot for $[1]^{2+}$; DPV peak deconvolution for $[2]^{2+}$ and $[3]^{2+}$; orbital splitting diagram from DFT calculations for $[3]^{2+}$; bond lengths and angles from DFT calculations for all presented complexes; NMR, UV−vis, and IR for all complexes (PDF)

Accession Codes

CCDC 1991075 contains the supplementary crystallographic data for this paper. These data can be obtained free of charge via www.ccdc.cam.ac.uk/data_request/cif, or by emailing data_request@ccdc.cam.ac.uk, or by contacting The Cambridge Crystallographic Data Centre, 12 Union Road, Cambridge CB2 1EZ, UK; fax: +44 1223 336033.

■ AUTHOR INFORMATION

Corresponding Author

Tong Ren − *Department of Chemistry, Purdue University, West Lafayette, Indiana 47907, United States;* orcid.org/0000-0002-1148-0746; Email: tren@purdue.edu

Authors

Brandon L. Mash − *Department of Chemistry, Purdue University, West Lafayette, Indiana 47907, United States*

Yiwei Yang − *Department of Chemistry, Purdue University, West Lafayette, Indiana 47907, United States*

Complete contact information is available at: https://pubs.acs.org/10.1021/acs.organomet.0c00183

Notes

The authors declare no competing financial interest.

■ ACKNOWLEDGMENTS

We thank the National Science Foundation for generously supporting this work (CHE 1764347 for research and CHE 1625543 for X-ray diffractometers), and Mr. R. A. Clendening and Mr. A. Raghavan for experimental assistance.

REFERENCES

(1) Nast, R. Zur Existenz Metallorganischer Verbindungen Von Ubergangsmetallen. *Z. Naturforsch., B: J. Chem. Sci.* **1953**, *8*, 381.
(2) Nast, R. Coordination Chemistry of Metal Alkynyl Compounds. *Coord. Chem. Rev.* **1982**, *47*, 89−124.
(3) Haque, A.; Al-Balushi, R. A.; Al-Busaidi, I. J.; Khan, M. S.; Raithby, P. R. Rise of Conjugated Poly-ynes and Poly(Metalla-ynes): From Design Through Synthesis to Structure−Property Relationships and Applications. *Chem. Rev.* **2018**, *118*, 8474−8597.
(4) Wong, W.-Y.; Ho, C.-L. Organometallic Photovoltaics: A New and Versatile Approach for Harvesting Solar Energy Using Conjugated Polymetallaynes. *Acc. Chem. Res.* **2010**, *43*, 1246−1256.
(5) Ho, C.-L.; Yu, Z.-Q.; Wong, W.-Y. Multifunctional polymetallaynes: properties, functions and applications. *Chem. Soc. Rev.* **2016**, *45*, 5264−5295.
(6) Haque, A.; Xu, L. L.; Al-Balushi, R. A.; Al-Suti, M. K.; Ilmi, R.; Guo, Z. L.; Khan, M. S.; Wong, W. Y.; Raithby, P. R. Cyclometallated tridentate platinum(II) arylacetylide complexes: old wine in new bottles. *Chem. Soc. Rev.* **2019**, *48*, 5547−5563.
(7) Launay, J.-P. Long-distance intervalence electron transfer. *Chem. Soc. Rev.* **2001**, *30*, 386−397.
(8) Launay, J. P. Mixed-Valent Compounds and their Properties - Recent Developments. *Eur. J. Inorg. Chem.* **2020**, *2020*, 329−341.
(9) Szafert, S.; Gladysz, J. A. Carbon in One Dimension: Structural Analysis of the Higher Conjugated Polyynes. *Chem. Rev.* **2003**, *103*, 4175−4206.
(10) Szafert, S.; Gladysz, J. A. Update 1 of: Carbon in One Dimension: Structural Analysis of the Higher Conjugated Polyynes. *Chem. Rev.* **2006**, *106*, PR1−PR33.
(11) Halet, J. F.; Lapinte, C. Charge delocalization vs localization in carbon-rich iron mixed-valence complexes: A subtle interplay between the carbon spacer and the (dppe)Cp*Fe organometallic electrophore. *Coord. Chem. Rev.* **2013**, *257*, 1584−1613.
(12) Gendron, F.; Groizard, T.; Le Guennic, B.; Halet, J. F. Electronic Properties of Poly-Yne Carbon Chains and Derivatives with Transition Metal End-Groups. *Eur. J. Inorg. Chem.* **2020**, *2020*, 667−681.
(13) Costuas, K.; Rigaut, S. Polynuclear carbon-rich organometallic complexes: clarification of the role of the bridging ligand in the redox properties. *Dalton Trans.* **2011**, *40*, 5643−5658.
(14) Tanaka, Y.; Akita, M. Organometallic radicals of iron and ruthenium: Similarities and dissimilarities of radical reactivity and charge delocalization. *Coord. Chem. Rev.* **2019**, *388*, 334−342.
(15) Le Narvor, N.; Lapinte, C. First C_4 Bridged Mixed-valence Iron(II)-Iron(III) Complex Delocalized on the Infrared Timescale. *J. Chem. Soc., Chem. Commun.* **1993**, *0*, 357−359.
(16) Fernández, F. J.; Venkatesan, K.; Blacque, O.; Alfonso, M.; Schmalle, H. W.; Berke, H. Generation and Coupling of [Mn(dmpe)-2(CCR)(CC)]. Radicals Producing Redox-Active C4-Bridged Rigid-Rod Complexes. *Chem. - Eur. J.* **2003**, *9*, 6192−6206.
(17) Bruce, M. I.; Low, P. J.; Costuas, K.; Halet, J.-F.; Best, S. P.; Heath, G. A. Oxidation Chemistry of Metal-Bonded C4 Chains: A Combined Chemical, Spectroelectrochemical, and Computational Study. *J. Am. Chem. Soc.* **2000**, *122*, 1949−1962.
(18) Ren, T.; Zou, G.; Alvarez, J. C. Facile Electronic Communication between Bimetallic Termini Bridged by Elemental Carbon Chains. *Chem. Commun.* **2000**, 1197−1198.
(19) Wong, K.-T.; Lehn, J.-M.; Peng, S.-M.; Lee, G.-H. Nanoscale molecular organometallo-wires containing diruthenium cores. *Chem. Commun.* **2000**, 2259−2260.
(20) Ren, T. Diruthenium σ-Alkynyl Compounds: A New Class of Conjugated Organometallics. *Organometallics* **2005**, *24*, 4854−4870.
(21) Zhou, Y. L.; Seyler, J. W.; Weng, W.; Arif, A. M.; Gladysz, J. A. New Families of Coordinated Carbon: Oxidative Coupling of an Ethynyl Complex to Isolable and Crystallographically Characterized MC = CC = CM amd + MC = CC = CM+ Assemblies. *J. Am. Chem. Soc.* **1993**, *115*, 8509−8510.
(22) Dembinski, R.; Bartik, T.; Bartik, B.; Jaeger, M.; Gladysz, J. A. Toward Metal-Capped One-Dimensional Carbon Allotropes: Wire-like C6-C20 Polyynediyl Chains That Span Two Redox-Active ([Image]5-C5Me5)Re(NO)(PPh3) Endgroups. *J. Am. Chem. Soc.* **2000**, *122*, 810−822.
(23) Schull, T. L.; Kushmerick, J. G.; Patterson, C. H.; George, C.; Moore, M. H.; Pollack, S. K.; Shashidhar, R. Ligand Effects on Charge Transport in Platinum(II) Acetylides. *J. Am. Chem. Soc.* **2003**, *125*, 3202−3203.
(24) Ballmann, S.; Hieringer, W.; Secker, D.; Zheng, Q.; Gladysz, J. A.; Görling, A.; Weber, H. B. Molecular Wires in Single-Molecule Junctions: Charge Transport and Vibrational Excitations. *ChemPhysChem* **2010**, *11*, 2256−2260.
(25) Tanaka, Y.; Kato, Y.; Tada, T.; Fujii, S.; Kiguchi, M.; Akita, M. "Doping" of Polyyne with an Organometallic Fragment Leads to Highly Conductive Metallapolyyne Molecular Wire. *J. Am. Chem. Soc.* **2018**, *140*, 10080−10084.
(26) Kim, B.; Beebe, J. M.; Olivier, C.; Rigaut, S.; Touchard, D.; Kushmerick, J. G.; Zhu, X.-Y.; Frisbie, C. D. Temperature and Length Dependence of Charge Transport in Redox-Active Molecular Wires Incorporating Ruthenium(II) Bis(-arylacetylide) Complexes. *J. Phys. Chem. C* **2007**, *111*, 7521−7526.
(27) Ezquerra, R.; Eaves, S. G.; Bock, S.; Skelton, B. W.; Perez-Murano, F.; Cea, P.; Martin, S.; Low, P. J. New routes to organometallic molecular junctions via a simple thermal processing protocol. *J. Mater. Chem. C* **2019**, *7*, 6630−6640.
(28) Blum, A. S.; Ren, T.; Parish, D. A.; Trammell, S. A.; Moore, M. H.; Kushmerick, J. G.; Xu, G.-L.; Deschamps, J. R.; Pollack, S. K.; Shashidhar, R. $Ru_2(ap)_4$(σ-oligo(phenyleneethynyl)) Molecular Wires: Synthesis and Electronic Characterization. *J. Am. Chem. Soc.* **2005**, *127*, 10010−10011.
(29) Mahapatro, A. K.; Ying, J.; Ren, T.; Janes, D. B. Electronic Transport through Ruthenium Based Redox-Active Molecules in Metal-Molecule-Metal Nanogap Junctions. *Nano Lett.* **2008**, *8*, 2131−2136.
(30) Zhu, H.; Pookpanratana, S. J.; Bonevich, J. E.; Natoli, S. N.; Hacker, C. A.; Ren, T.; Suehle, J. S.; Richter, C. A.; Li, Q. Redox-Active Molecular Nanowire Flash Memory for High-Endurance and High-Density Non-Volatile Memory Applications. *ACS Appl. Mater. Interfaces* **2015**, *7*, 27306−27313.
(31) Jiang, K.; Pookpanratana, S. J.; Natoli, S. N.; Ren, T.; Sperling, B. A.; Robertson, J.; Richter, C. A.; Yu, S.; Li, Q. Nonvolatile memory based on redox-active Ruthenium molecular monolayers. *Appl. Phys. Lett.* **2019**, *115*, No. 162102.
(32) Meng, F. B.; Hervault, Y. M.; Norel, L.; Costuas, K.; Van Dyck, C.; Geskin, V.; Cornil, J.; Hng, H. H.; Rigaut, S.; Chen, X. D. Photomodulable molecular transport junctions based on organometallic molecular wires. *Chem. Sci.* **2012**, *3*, 3113−3118.
(33) Meng, F. B.; Hervault, Y. M.; Shao, Q.; Hu, B. H.; Norel, L.; Rigaut, S.; Chen, X. D. Orthogonally modulated molecular transport junctions for resettable electronic logic gates. *Nat. Commun.* **2014**, *5*, No. 3023.
(34) Ren, T. Sustainable metal alkynyl chemistry: 3d metals and polyaza macrocyclic ligands. *Chem. Commun.* **2016**, *52*, 3271−3279.
(35) Banziger, S. D.; Ren, T. Syntheses, Structures and Bonding of 3d Metal Alkynyl Complexes of Cyclam and Its Derivatives. *J. Organomet. Chem.* **2019**, *885*, 39−48.
(36) Hoffert, W. A.; Kabir, M. K.; Hill, E. A.; Mueller, S. M.; Shores, M. P. Stepwise acetylide ligand substitution for the assembly of ethynylbenzene-linked Co(III) complexes. *Inorg. Chim. Acta* **2012**, *380*, 174−180.
(37) Hoffert, W. A.; Shores, M. P. Crystallographic coincidence of two bridging species in a dinuclear CoIII ethynylbenzene complex. *Acta Crystallogr., Sect. E: Struct. Rep. Online* **2011**, *67*, m853−m854.
(38) Nishijo, J.; Judai, K.; Numao, S.; Nishi, N. Chromium Acetylide Complex Based Ferrimagnet and Weak Ferromagnet. *Inorg. Chem.* **2009**, *48*, 9402−9408.
(39) Nishijo, J. Chromium-ethynyltetrathiafulvalene complex based magnetic materials. *Polyhedron* **2013**, *66*, 43−47.
(40) Nishijo, J.; Judai, K.; Nishi, N. Weak Ferromagnetism and Strong Spin-Spin Interaction Mediated by the Mixed-Valence

https://dx.doi.org/10.1021/acs.organomet.0c00183
Organometallics 2020, 39, 2019−2025

Ethynyltetrathiafulvalene-Type Ligand. *Inorg. Chem.* **2011**, *50*, 3464−3470.
(41) Nishijo, J.; Enomoto, M. A Series of Weak Ferromagnets Based on a Chromium-Acetylide-TTF Type Complex: Correlation of the Structures and Magnetic Properties and Origin of the Weak Ferromagnetism. *Inorg. Chem.* **2013**, *52*, 13263−13268.
(42) Nishijo, J.; Enomoto, M. Synthesis, structure and magnetic properties of [CrCyclam(C C-6-methoxynaphthalene) 2](TCNQ) n (1,2-dichloroethane) (n = 1, 2). *Inorg. Chim. Acta* **2015**, *437*, 59−63.
(43) Eddy, L. E.; Thakker, P. U.; McMillen, C. D.; Pienkos, J. A.; Cordoba, J. J.; Edmunds, C. E.; Wagenknecht, P. S. A comparison of the metal-ligand interactions of the pentafluorophenylethynyl and trifluoropropynyl ligands in transition metal cyclam complexes. *Inorg. Chim. Acta* **2019**, *486*, 141−149.
(44) Grisenti, D. L.; Thomas, W. W.; Turlington, C. R.; Newsom, M. D.; Priedemann, C. J.; VanDerveer, D. G.; Wagenknecht, P. S. Emissive Chromium(III) Complexes with Substituted Arylethynyl Ligands. *Inorg. Chem.* **2008**, *47*, 11452−11454.
(45) Sun, C.; Turlington, C. R.; Thomas, W. W.; Wade, J. H.; Stout, W. M.; Grisenti, D. L.; Forrest, W. P.; VanDerveer, D. G.; Wagenknecht, P. S. Synthesis of cis and trans Bis-alkynyl Complexes of Cr(III) and Rh(III) Supported by a Tetradentate Macrocyclic Amine: A Spectroscopic Investigation of the M(III)â€"Alkynyl Interaction. *Inorg. Chem.* **2011**, *50*, 9354−9364.
(46) Sun, C.; Thakker, P. U.; Khulordava, L.; Tobben, D. J.; Greenstein, S. M.; Grisenti, D. L.; Kantor, A. G.; Wagenknecht, P. S. Trifluoropropynyl as a Surrogate for the Cyano Ligand and Intense, Room-Temperature, Metal-Centered Emission from Its Rh(III) Complex. *Inorg. Chem.* **2012**, *51*, 10477−10479.
(47) Thakker, P. U.; Sun, C.; Khulordava, L.; McMillen, C. D.; Wagenknecht, P. S. Synthetic control of the cis/trans geometry of [M(cyclam)(CCR)2]OTf complexes and photophysics of cis-[Cr(cyclam)(CCCF3)2]OTf and cis-[Rh(cyclam)(CCCF3)2]OTf. *J. Organomet. Chem.* **2014**, *772*−*773*, 107−112.
(48) Thakker, P. U.; Aru, R. G.; Sun, C.; Pennington, W. T.; Siegfried, A. M.; Marder, E. C.; Wagenknecht, P. S. Synthesis of trans bis-alkynyl complexes of Co(III) supported by a tetradentate macrocyclic amine: A spectroscopic, structural, and electrochemical analysis of Ï€-interactions and electronic communication in the CCMCC structural unit. *Inorg. Chim. Acta* **2014**, *411*, 158−164.
(49) Cook, T. D.; Natoli, S. N.; Fanwick, P. E.; Ren, T. CoIII(cyclam) Oligoynyls: Monomeric Oligoynyl Complexes and Dimeric Complexes with an Oligoyn-diyl Bridge. *Organometallics* **2016**, *35*, 1329−1338.
(50) Cook, T. D.; Natoli, S. N.; Fanwick, P. E.; Ren, T. Dimeric Complexes of CoIII(cyclam) with a Polyynediyl Bridge. *Organometallics* **2015**, *34*, 686−689.
(51) Cook, T. D.; Fanwick, P. E.; Ren, T. Unsymmetric Mononuclear and Bridged Dinuclear CoIII(cyclam) Acetylides. *Organometallics* **2014**, *33*, 4621−4624.
(52) Natoli, S. N.; Zeller, M.; Ren, T. An Aerobic Synthetic Approach toward Bis-Alkynyl Cobalt(III) Compounds. *Inorg. Chem.* **2017**, *56*, 10021−10031.
(53) Mash, B. L.; Ren, T. Co(III) phenylacetylide complexes supported by tetraazamacrocyclic ligands: Syntheses and characterizations. *J. Organomet. Chem.* **2019**, *880*, 143−149.
(54) Barriere, F.; Geiger, W. E. Use of weakly coordinating anions to develop an integrated approach to the tuning of Delta E-1/2 values by medium effects. *J. Am. Chem. Soc.* **2006**, *128*, 3980−3989.
(55) Geiger, W. E.; Barriere, F. Organometallic Electrochemistry Based on Electrolytes Containing Weakly-Coordinating Fluoroarylborate Anions. *Acc. Chem. Res.* **2010**, *43*, 1030−1039.
(56) Musso, D. L.; Clarke, M. J.; Kelley, J. L.; Evan Boswell, G.; Chen, G. Novel 3-phenylprop-2-ynylamines as inhibitors of mammalian squalene epoxidase. *Org. Biomol. Chem.* **2003**, *1*, 498−506.
(57) Parr, R. G.; Yang, W. B. *Density Functional Theory of Atoms and Molecules*; Oxford University Press: New York, 1989.
(58) Weigend, F.; Ahlrichs, R. Balanced basis sets of split valence, triple zeta valence and quadruple zeta valence quality for H to Rn: Design and assessment of accuracy. *Phys. Chem. Chem. Phys.* **2005**, *7*, 3297−3305.
(59) Frisch, M. J.; Trucks, G. W.; Schlegel, H. B.; Scuseria, G. E.; Robb, M. A.; Cheeseman, J. R.; Scalmani, G.; Barone, V.; Petersson, G. A.; Nakatsuji, H.; Li, X.; Caricato, M.; Marenich, A. V.; Bloino, J.; Janesko, B. G.; Gomperts, R.; Mennucci, B.; Hratchian, H. P.; Ortiz, J. V.; Izmaylov, A. F.; Sonnenberg, J. L.; Williams-Young, D.; Ding, F.; Lipparini, F.; Egidi, F.; Goings, J.; Peng, B.; Petrone, A.; Henderson, T.; Ranasinghe, D.; Zakrzewski, V. G.; Gao, J.; Rega, N.; Zheng, G.; Liang, W.; Hada, M.; Ehara, M.; Toyota, K.; Fukuda, R.; Hasegawa, J.; Ishida, M.; Nakajima, T.; Honda, Y.; Kitao, O.; Nakai, H.; Vreven, T.; Throssell, K.; Montgomery, J. A., Jr.; Peralta, J. E.; Ogliaro, F.; Bearpark, M.; Heyd, J. J.; Brothers, E. N.; Kudin, K. N.; Staroverov, V. N.; Kobayashi, R.; Normand, J.; Raghavachari, K.; Rendell, A.; Burant, J. C.; Iyengar, S. S.; Tomasi, J.; Cossi, M.; Millam, J. M.; Klene, M.; Adamo, C.; Cammi, R.; Ochterski, J. W.; Martin, R. L.; Morokuma, K.; Farkas, O.; Foresman, J. B.; Fox, D. J. *Gaussian 16*, revision C.01; Gaussian, Inc.: Wallingford CT, 2016.
(60) (a) *Apex3* v2016.9−0; Bruker AXS Inc.: Madison, WI, 2016. (b) *Saint* V8.34A, V8.37A; Bruker AXS Inc.: Madison, WI, 2016.
(61) *SHELXTL*, version 6.14; Bruker AXS Inc.: Madison, WI, 2000-2003.
(62) Sheldrick, G. M. *SHELXL 2016*; University of Göttingen: Göttingen, Germany, 2016.

https://dx.doi.org/10.1021/acs.organomet.0c00183
Organometallics 2020, 39, 2019−2025

ChemPubSoc Europe

DOI: 10.1002/ejic.201801198

EurJIC European Journal of Inorganic Chemistry

Full Paper

Check for updates

Carbon Dioxide Reduction | *Very Important Paper* |

SPECIAL ISSUE

VIP

Ni^{II} Complexes of *C*-Substituted Cyclam as Efficient Catalysts for Reduction of CO_2 to CO

Brandon L. Mash,[a] Adharsh Raghavan,[a] and Tong Ren*[a]

Abstract: Two new nickel(II) complexes of cyclams bearing *C*-alkyl groups, Ni(MEC)OTf_2 (**1**, MEC = 5,12-diethyl-7,14-dimethyl-1,4,8,11-tetraazacyclotetradecane) and Ni(CTMC)OTf_2 (**2**, CTMC = 5,7,12,14-tetramethyl-1,4,8,11-tetraazacyclotetradecane), were prepared, and their similarity to Ni^{II}(MPC) (MPC = 5,12-dimethyl-7,14-diphenyl-1,4,8,11-tetraazacyclotetradecane) in ring conformation was revealed through single-crystal X-ray diffraction studies. Solution electronic absorption spectroscopy indicates the retention of octahedral coordination mode for both **1** and **2** in 20 % aqueous acetonitrile. Cyclic voltammetry studies of **1** and **2** under CO_2 in 20 % aqueous acetonitrile revealed significantly increased catalytic currents compared to previously studied Ni^{II}(cyclam) and Ni^{II}(MPC). Controlled potential electrolysis studies of **2** revealed a 250 % increase in CO turn over frequency from that of Ni(cyclam)OTf_2 and a 40 % increase from that of Ni(MPC)OTf_2. Such improvements establish the benefit of electronically donating substituents that minimize steric interference around the axial catalytic sites.

Introduction

Conversion of CO_2 to carbon fuel sources using solar energy is one of the grand challenges in renewable sciences and technology.[1–3] In addition to generating the reducing equivalent (electrons) through water oxidation, efficient and robust catalysts for CO_2 reduction has been a bottleneck.[2] Efficacy in promoting CO_2 reduction to CO and formate has been demonstrated for many transition-metal complexes. Heavy/precious metal active sites are often involved, such as Re,[4] Ru,[5] Ir,[6] or Pd,[7] and these catalysts often exhibit low tolerance to aqueous conditions, preferentially producing H_2 in these cases. Hence, CO_2 reduction/activation by 3*d* metal-based catalysts has received intense interest. Among noteworthy examples of homogeneous catalysts are Fe-tetraphenylporphyrin and derivatives by Savéant and co-workers,[8] selective reduction of CO_2 to formate using $[Fe_4N(CO)_{12}]^-$ by Berben and co-workers,[9] and reduction of CO_2 to methanol by borane with Ni and Fe pincer complexes by Guan and co-workers.[10] Li and co-workers reported photoreduction of CO_2 to CO catalyzed by molecular Co complexes immobilized on solid support.[11] Lu and co-workers reported several examples of Cu complexes as photoelectron-catalysts for CO_2 reduction in aqueous solution.[12]

Among the earth-abundant transition-metal catalysts, Ni^{II}(cyclam) (cyclam = 1,4,8,11-tetraazacyclotetradecane) is one of the most active in producing CO from CO_2 and compares favorably even with its 4th- and 5th-row organometallic competitors.[3] Furthermore, Ni^{II}(cyclam) and many of its derivatives display selective production of CO over H_2 even under purely aqueous conditions, with the bulk of studies performed with a Hg working electrode.[13] Nevertheless, early observations by Fujihira and co-workers that a catalytic wave can indeed be observed at a glassy carbon electrode[14] reveals the promise of carbon electrode as an environmentally benign surrogate. Through controlled-potential electrolysis, Kubiak and co-workers recently verified that CO is the major electrolysis product in Ni^{II}(cyclam) catalyzed CO_2 reaction.[15] Seeking more robust and efficient catalysts, our laboratory recently reported the preparation of three new nickel(II) complexes of cyclams bearing *C*-aryl substituents, and demonstrated that of the new complexes, Ni^{II}(MPC) is significantly more efficient than Ni^{II}(cyclam) in reducing CO_2 to CO under the same conditions.[16] We postulate that the improved catalytic ability results from the increased electron-donor ability of the aryl functionalized cyclam ring, and that it can be further improved through reduction of the steric interference of the substituents with the active catalytic site. To test this hypothesis, we set out to develop catalysts with similar electron-donating *C*-substituents while minimizing their size. Reported in this contribution is our effort in synthesizing

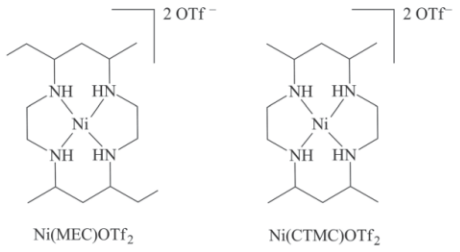

Ni(MEC)OTf_2 Ni(CTMC)OTf_2

Figure 1. Structures of Ni(MEC)OTf_2 (**1**) and Ni(CTMC)OTf_2 (**2**). See discussion below regarding axial coordination.

[a] *Department of Chemistry, Purdue University, 560 Oval Drive, West Lafayette, IN 47906, USA*
E-mail: tren@purdue.edu
www.chem.purdue.edu/tren/

Supporting information and ORCID(s) from the author(s) for this article are available on the WWW under https://doi.org/10.1002/ejic.201801198.

© 2019 Wiley-VCH Verlag GmbH & Co. KGaA, Weinheim

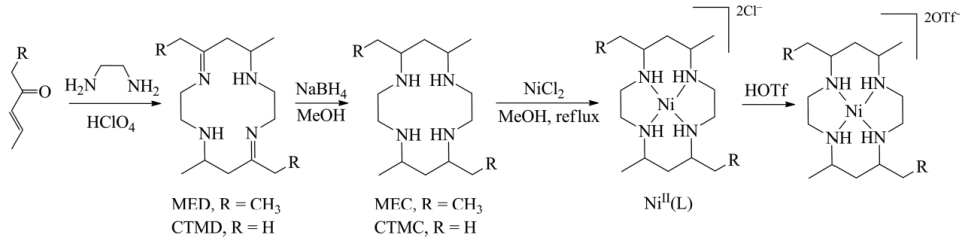

Scheme 1. Preparation of L (L = MEC or CTMC), $[Ni^{II}(L)]Cl_2$ and $Ni^{II}(L)(OTf)_2$. Axial coordination is solvent dependent.

two nickel(II) complexes of cyclams bearing *C*-alkyl substituents, namely Ni^{II}(MEC) and Ni^{II}(CTMC) (Figure 1), and studying their proficiency in reducing CO_2 through both cyclic voltammetry and controlled potential electrolysis (CPE).

Results and Discussion

Synthesis

As shown in Scheme 1, the preparation of the precursor MED (5,12-diethyl-7,14-dimethyl-1,4,8,11-tetraazacyclotetradeca-4,11-diene) follows that reported by Hay and co-workers:[17] a proton-templated condensation between ethylenediamine and 4-hexen-3-one (1:1) in the presence of one equiv. of $HClO_4$ resulted in $[H_2MED](ClO_4)_2$ as a white microcrystalline material (66 %). $[H_2MED](ClO_4)_2$ was reduced by $NaBH_4$ to yield MEC (> 90 %). The reaction between free base MEC and $NiCl_2$ resulted in $[Ni(MEC)]Cl_2$ as a light pink crystalline solid in 71 % yield, and $[Ni(MEC)]Cl_2$ was converted to $[Ni(MEC)](OTf)_2$ (**1**) quantitatively upon reaction with triflic acid. The preparation of $[H_2CTMD](ClO_4)_2$, CTMC (97 % yield), $Ni(CTMC)Cl_2$ (75 %), and $[Ni(CTMC)]OTf_2$ (**2**, 66 %) follow an identical protocol.

Molecular Structures

X-ray quality single crystals of $Ni(MEC)(OTf)_2$ (**1**) and $[Ni(CTMC)(H_2O)_2](OTf)_2$ were grown via slow diffusion of Et_2O into a H_2O-MeCN (v/v, 1:4) solution of **1** and MeOH solution of **2**, respectively. Molecular structures of **1** and $[\mathbf{2}]^{2+}$ along with some selected bond lengths are provided in Figure 2a and Figure 3, respectively. Interestingly, the cyclam frameworks of Ni^{II}(MEC) and Ni^{II}(CTMC) overlap perfectly with that of Ni^{II}(MPC) as shown in Figure 2b, indicating identical ring conformations. This is an important feature, as the ring conformation is a key parameter in the efficacy of carbon dioxide reduction.[18] Previous results indicate that *cis*-coordination geometry or boat-shaped ring conformation reduces the catalytic capacity of the complexes. In addition to the identity in ring conformation, the Ni–N bond lengths in both complexes **1** and $[\mathbf{2}]^{2+}$ are about the same as those of Ni^{II}(MPC) [Ni–N1, 2.093(2) Å; Ni–N2, 2.080(2) Å], despite the change in the donor strength of macrocycles that stems from the replacement of aryls in MPC with alkyls in MEC and CTMC.

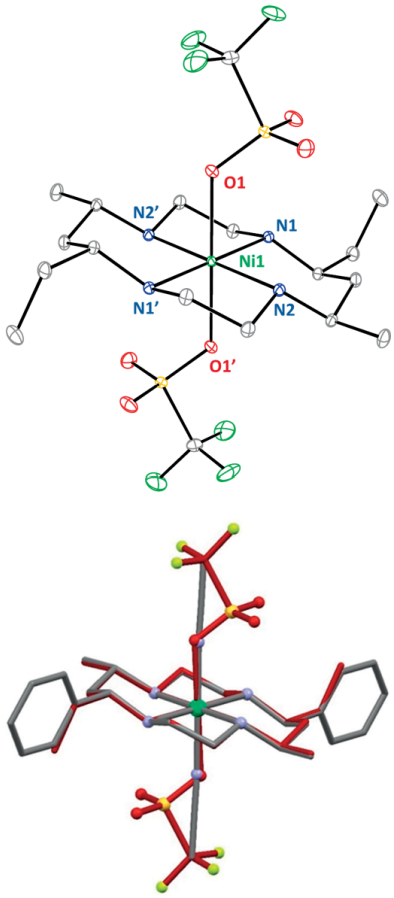

Figure 2. (a, top) Molecular structure of **1** at 30 % probability level. Hydrogen atoms have been removed for clarity. Selected bond lengths [Å]: Ni1–N1, 2.0880(7); Ni1–N2, 2.0802(7); Ni1–O1, 2.1742(7). (b, bottom) Overlay of cyclam rings of **1** (red) and $[Ni(MPC)(MeCN)_2]^{2+}$ (grey).

UV/Vis Spectroscopic Analysis

Having established the pseudo-octahedral coordination geometry for both **1** and $[\mathbf{2}]^{2+}$ in solid state, we endeavored to study

© 2019 Wiley-VCH Verlag GmbH & Co. KGaA, Weinheim

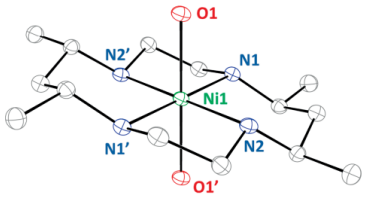

Figure 3. Molecular structure of $[2]^{2+}$ at 30 % probability level. Hydrogen atoms and the two triflate counterions have been removed for clarity. Selected bond lengths [Å]: Ni1–N1, 2.088(2); Ni1–N2, 2.095(2); Ni1–O1, 2.149(2).

the solution geometry of these complexes based on visible-light absorption spectroscopy. In solution, Ni^{II}(tetraamine) species may exist in a spin-state equilibrium between the diamagnetic square-planar geometry and the octahedral paramagnetic geometry, with the population of each state being affected by factors such as solvent and counterion.[19] UV/Vis absorption spectra were collected for complexes **1** and **2** in a 20 % aqueous MeCN solution (Figure 4), the same solvent conditions as those used in subsequent voltammetric studies. As expected from their appearance as purple solids, complexes **1** and **2** display nearly identical absorption spectra in 20 % aqueous acetonitrile. Similar to the case of Ni^{II}(MPC), the feature of the visible region is dominated by a weak *d-d* band around 330 nm, and a slightly weaker *d-d* band around 500 nm, both of which are indicative of an octahedral, high-spin species. An even weaker unassigned band is present around 690 nm. Similar absorption spectra were obtained in dichloromethane and neat acetonitrile for both complexes, revealing the retention of octahedral geometry. Curiously, while the spectrum of **1** in methanol retains octahedral characteristics, the methanolic solution of **2** is red, and displays a sharp *d-d* transition at 466 nm, while the above-mentioned *d-d* bands fade (Figure 5), thus indicating the dominance of the square planar form.

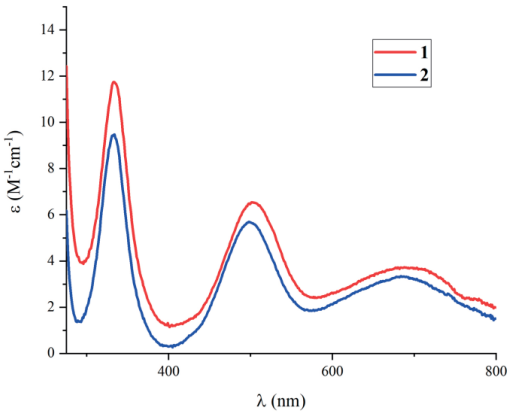

Figure 4. UV/Vis absorption spectra of **1** (red) and **2** (blue) in 20 % aqueous MeCN.

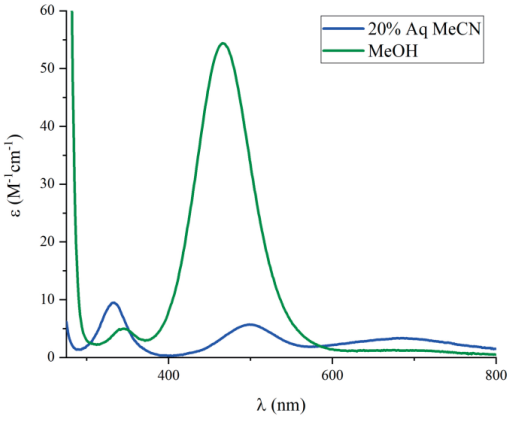

Figure 5. UV/Vis absorption spectra of **2** in 20 % Aq. MeCN (blue) and MeOH (green).

Solution Voltammetry

As shown in Figure 6a, the cyclic voltammograms of **1**, **2** and Ni^{II}(MPC) recorded in aqueous acetonitrile are nearly identical under Ar. Each complex displays a reversible one-electron reduction as well as a reversible one electron oxidation (See supporting information for anodic CVs), which are assigned as the Ni(+1/+2) and Ni(+3/+2) couples, respectively. The Ni(+1/+2) couples for **1** (–1.81 V vs. Fc) and **2** (–1.80 V vs. Fc) are slightly cathodically shifted from Ni^{II}(MPC) (–1.78 V vs. Fc), presumably due to the less electron-donating substituents in the latter.

While the cyclic voltammograms of **1**, **2** and Ni^{II}(MPC) under Ar are nearly identical, the CVs. recorded under CO_2 are quite different (Figure 6b). They all share the common features of the loss of reversibility for the Ni(+1/+2) couple, significant increase in current and the growth of an additional reduction peak at more negative potentials. These features are indicative of catalytic reduction of CO_2.[16] Furthermore, while the catalytic currents at –1.76 V are about the same for **1** (56 μA) and Ni^{II}(MPC) (49 μA), it is nearly doubled for **2** (96 μA). Clearly, the decrease in the steric bulk of *C*-substituents results in a noticeable increase in catalytic efficiency.

Controlled Potential Electrolysis

The improved catalytic currents of **1** and **2** compared to Ni^{II}(MPC) prompted further examination of their catalytic proficiency through controlled potential electrolysis (CPE) experiments, which allow for the establishment of the composition of reduction products through headspace analysis and ensuing estimation of Faradaic efficiency and catalytic turnover. The conditions of CPE experiments were identical to those described in our previous report,[16] except for a AgCl coated silver wire being used as the reference electrode in place of a Ag wire pseudoreference electrode. The potential for each experiment was held at a constant –1.76 V vs. Fc/Fc^+, which is slightly more

© 2019 Wiley-VCH Verlag GmbH & Co. KGaA, Weinheim

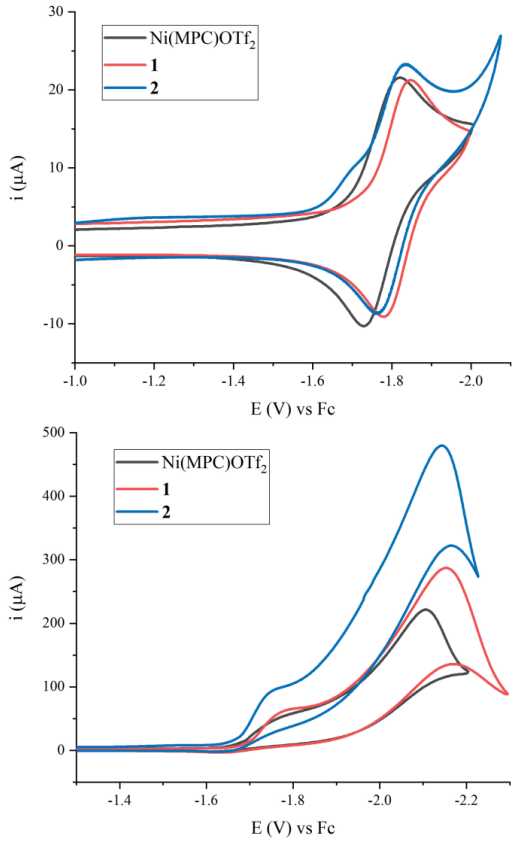

Figure 6. (a, top) Cyclic voltammograms of 1.0 mM solutions of **1** (red), **2** (blue), and Ni(MPC)$(OTf)_2$ (black) recorded in a 0.08 M solution of Bu_4NPF_6 in 20 % aqueous MeCN on glassy carbon working electrode, purged with Ar; (b) Cyclic voltammograms of **1** (red), **2** (blue), and Ni(MPC)$(OTf)_2$ (black) purged with CO_2.

positive than Ni(+1/+2) couples for each complex under CO_2. Each experiment was performed with 0.5 mM catalyst in 20 mL of solution. Similar to our previous work, the headspace was sampled after 30 minutes of electrolysis and injected into a gas chromatograph with a thermal conductivity detector (GC-TCD) to quantify the gaseous products. The gaseous products for **1**, **2**, Ni(MPC)OTf_2 and Ni(cyclam)OTf_2 as well as their catalytic efficiencies are reported in Table 1.

The selected electrolysis potential resulted in lower FE but higher TOF for Ni^{II}(MPC) and Ni^{II}(cyclam) compared to our previous report.[16] While each experiment showed significant and highly variable H_2 production, a catalyst-free CPE experiment revealed that the H_2 production is mostly due to the background current instead of the catalysts. In accordance with cyclic voltammetry studies, compound **2** showed both the highest TOF (15.2 h^{-1}) and FE (66 %) for the production of CO. Compound **2** is closely followed by **1** in each category (TOF: 14.5 h^{-1}, FE: 57 %), while Ni(MPC)OTf_2 held a lower TOF (TOF: 11.0 h^{-1}, FE: 52 %). In agreement with our previous work, all catalysts outperformed Ni^{II}(cyclam) substantially (TOF: 4.4 h^{-1}, FE: 35 %) under the same conditions. These results follow a clear trend of increasing catalytic ability with reduction in steric bulk of the electronically donating carbon substituents. With identical conformations and axial ligand behavior in solution, the importance of easily accessible axial catalytic sites is highlighted.

Conclusions

Both Ni(MEC)OTF_2 (**1**) and Ni(CTMC)OTf_2 (**2**) show significantly improved catalytic current for CO_2 reduction as opposed to Ni^{II}(cyclam) and **2** displayed double the current of our previously reported Ni(MPC)OTf_2. Controlled potential electrolysis revealed CO turnover frequencies of 14.5 and 15.2 h^{-1} for **1** and **2**, respectively. This significant increase from Ni(MPC)OTf_2 (11.0 h^{-1}) and Ni(cyclam)OTf_2 (4.4 h^{-1}) is attributed to the use of electronically donating alkyl substituents without the steric interference around the axial catalytic sites of the phenyl groups present in Ni(MPC)OTf_2. The necessity of the *trans*-III conformation of the cyclam framework is highlighted by comparison of the molecular structures of **1** and **2** with that of Ni(MPC)OTf_2. The results of this work may allow for further development of cyclam-like ligands to improve catalytic activity for the conversion of CO_2 to CO.

Experimental Section

Materials: The ketone precursor for $[H_2MED](ClO_4)_2$ was purchased from Sigma–Aldrich and the precursor for $[H_2CTMD](ClO_4)_2$ was purchased from Arctom Chemicals. 5,12-diethyl-7,14-dimethyl-1,4,8,11-tetraazacyclotetradeca-4,11-diene and 5,7,12,14-tetramethyl-1,4,8,11-tetraazacyclotetradeca-4,11-diene dihydroperchlorate were prepared according to literature procedures.[17,20] All reagents were used as received.

Physical Measurements: ^1H NMR spectra were obtained with a Varian Mercury300 NMR instrument, with chemical shifts (δ) referenced to the residual solvent signal ($CHCl_3$ at δ = 7.26 ppm). UV/Vis spectra were obtained with a JASCO V-670 spectrophotometer. Gas chromatography data were collected on an Agilent 7890A instrument with a thermal conductivity detector (TCD) and an HP-Molsieves column (length = 30 m, diameter = 0.320 mm, film = 12.0 μm). Electrospray mass spectra were obtained as electrospray in positive-ion mode with the aid of an Advion Expression Compact Mass Spectrometer. Cyclic voltammograms were recorded at a scan rate of 100 mV s^{-1} on a CHI620A voltammetric analyzer with a glassy carbon working electrode (diameter = 2 mm, area = 0.0314 cm^2), a Pt-wire auxiliary electrode and a Ag/AgCl wire reference electrode. Potentials were referenced to a ferrocene internal standard added to the solution. Controlled-potential electrolyses were performed with a CHI620A voltammetric analyzer with a Duocel reticulated vitreous carbon disc (porosity = 100 ppi, diameter = 200 mm, thickness = 5 mm) as the working electrode, a graphite rod auxillary electrode, and an Ag/AgCl reference electrode. The concentration of analyte is always 1.0 mM for cyclic voltammetry experiments and 0.5 mM for bulk electrolysis experiments.

© 2019 Wiley-VCH Verlag GmbH & Co. KGaA, Weinheim

Table 1. CPE data for **1**, **2**, Ni^{II}(MPC), Ni^{II}(cyclam), and catalyst-free experiments.[a]

	Q (C)	TON, CO	TON, H_2	TOF [h^{-1}], CO	TOF [h^{-1}], H_2	FE, CO [%]	FE, H_2 [%]	µmol CO	µmol H_2
1	24.2	7.3 ± 0.4	2.1 ± 0.9	14.5	4.2	57 ± 2	16 ± 7	72	21
2	22.3	7.7 ± 0.3	1.7 ± 0.7	15.2	3.4	66 ± 1	15 ± 6	77	17
$Ni(MPC)^{2+}$	20.6	5.5	1.0	11.0	2.0	52	10	55	10
$Ni(cyclam)^{2+}$	12.2	2.2	2.4	4.4	4.7	35	38	22	24
blank	7.5	–	–	–	–	3	60	1	23

[a] Performed in CO_2-saturated solutions of 20 % aqueous MeCN with 0.08 M NBu_4PF_6; data for **1** and **2** reported as the averages of 2 trials; all other data reported from a single trial; solutions were electrolyzed for 30 min and headspace gases were analyzed via GC–TCD. Q = total charge passed, faradaic efficiency (FE) = $\frac{\text{charge to form product}}{\text{total charge passed}}$, turnover number (TON) = $\frac{\text{mol product}}{\text{mol catalyst}}$; turnover frequency (TOF) = $\frac{\text{TON}}{\text{time}}$.

5,12-Diethyl-7,14-dimethyl-1,4,8,11-tetraazacyclotetradecane (MEC): 5,12-Diethyl-7,14-dimethyl-1,4,8,11-tetraazacyclotetradeca-4,11-diene diperchlorate (1.00 g, 2.07 mmol) was suspended in 50 mL of MeOH. $NaBH_4$ (0.400 g, 10.6 mol) was added in small portions and stirred for 3 h at 45 °C, causing the solid to dissolve slowly in the effervescent solution. The solvent was removed under reduced pressure and an aqueous solution of 2 M KOH was added. The product was extracted with CH_2Cl_2, dried with Na_2SO_4 and filtered. Solvent was removed under reduced pressure leaving white crystalline solid. Yield: 0.544 g, 92 %. ESI-MS (CH_2Cl_2): 285.4 [MEC + H^+]$^+$. ^{1}H NMR ($CDCl_3$, δ): 3.04–2.21 (m, 16 H, CH, CH_2), 1.60–1.17 (m, 8 H, NH, CH_2), 1.01 (d, 6 H, CH_3), 0.80 (m, 6 H, CH_3) ppm.

5,7,12,14-Tetramethyl-1,4,8,11-tetraazacyclotetradecane (CTMC): 5,7,12,14-Tetramethyl-1,4,8,11-tetraazacyclotetradeca-4,11-diene diperchlorate (2.00 g, 4.41 mmol) was suspended in 50 mL of MeOH. $NaBH_4$ (0.835 g, 22.1 mol) was added in small portions and stirred for 3 h at 45 °C, causing the solid to dissolve slowly in the effervescent solution. The solvent was removed under reduced pressure and an aqueous solution of 2 M KOH was added. The product was extracted with CH_2Cl_2, dried with Na_2SO_4 and filtered. Solvent was removed under reduced pressure leaving white crystalline solid. Yield: 1.10 g, 97 %. ESI-MS (CH_2Cl_2): 257.4 [CTMC + H^+]$^+$. ^{1}H NMR ($CDCl_3$, δ): 3.00 (m, 2 H, CH_2), 2.76 (m, 8 H, CH, CH_2), 2.31 (m, 6 H, NH, CH_2), 1.49 (m, 2 H, CH_2), 1.29 (m, 2 H, CH_2), 1.02 (m, 12 H, CH_3) ppm.

Ni(MEC)Cl_2: MEC (0.300 g, 1.06 mmol) was dissolved in 20 mL of MeOH. A methanolic solution of $NiCl_2{\cdot}6H_2O$ (0.261 g, 1.11 mmol) was added and the solution immediately turned purple. The solution was heated for 30 min before adding ether to produce purple solid. The solid was collected, washed with diethyl ether, and dried under vacuum. Yield: 0.308 g, 71 % based on MEC.

Ni(MEC)(OTf)$_2$ (1): Ni(MEC)Cl_2 (0.308 g, 0.897 mmol) was dissolved in ≈ 5 mL of triflic acid, producing an purple solution. This was allowed to stir 12 hours with a stream of N_2 bubbling through the solution into an aqueous KOH trap. Et_2O was then added producing a purple solid, which was collected by filtration, washed with diethyl ether, and dried under vacuum. Yield: 0.397 g, 97 %. ESI-MS (CH_2Cl_2): 532.5 [Ni(MEC)(OTf)]$^+$; 341.4 [Ni(MEC) – H^+]$^+$. Anal. for $C_{18}H_{36}F_6N_4NiO_6S_2$ {[Ni(MEC)]OTf_2}: calcd. C 33.71, H 5.66, N 8.74; found C 33.71, H 5.84, N 8.74.

Ni(CTMC)Cl_2: CTMC (0.500 g, 1.95 mmol) was dissolved in 20 mL of MeOH. A methanolic solution of $NiCl_2{\cdot}6H_2O$ (0.463 g, 1.95 mmol) was added and the solution turned cloudy with a red/green hue. The solution was allowed to stir overnight, over which time purple crystals formed. This was filtered and collected. The solvent was removed from the red filtrate under reduced pressure leaving red/yellow residue. Upon addition of CH_2Cl_2, the solid turned purple and a light purple solution formed. This was sonicated and filtered. This process was repeated and all collected solid was combined. Yield: 0.638 g, 75 %.

Ni(CTMC)(OTf)$_2$ (2): Ni(CTMC)Cl_2 (0.380 g, 0.984 mmol) was dissolved in ≈ 7 mL of triflic acid, producing an orange solution. The solution was stirred for 12 h with a stream of N_2 bubbling through the solution into an aqueous KOH trap. Addition of Et_2O to the solution produced a purple solid, which was collected and washed with diethyl ether. Yield: 0.397 g, 66 %. ESI-MS (CH_2Cl_2): 463.4 [Ni(CTMC)(OTf)]$^+$; 313.3 [Ni(MEC) H^+]$^+$. Anal. for $C_{16}H_{32}F_6N_4NiO_6S_2$ {[Ni(TMC)]OTf_2} (613.26): calcd. C 31.34, H 5.26, N 9.14; found C 31.33, H 5.14, N 9.08.

X-ray Crystallographic Analysis: Single crystal X-ray diffraction data for **1** were collected on a Bruker AXS D8 Quest CMOS diffractometer using Mo-K_α (λ = 0.71073 Å) radiation with Apex3 software. Single crystal X-ray diffraction data for **2** were collected on a Bruker AXS D8 Quest CMOS diffractometer using Cu-K_α radiation (λ = 1.54178 Å) radiation with Apex3 software. Data set was reduced using SAINT and structures were solved with SHELXTL. Refinement was performed with SHELXL. ORTEP plots were produced using SHELXTL.[21]

CCDC 1870623 (for **1**), and 1870624 (for [**2**]OTf_2) contain the supplementary crystallographic data for this paper. These data can be obtained free of charge from The Cambridge Crystallographic Data Centre.

Acknowledgments

This work was supported by the National Science Foundation (CHE 1609151 for research and CHE 1625543 for X-ray diffractometers). BLM thanks the Purdue University for an Andrew Fellowship. We thank Prof. Dennis Peters for the loan of electrolysis cell and Prof. Dennis Evans for helpful discussion.

Keywords: Nickel · MEC · CTMC · Carbon dioxide reduction

[1] A. J. Morris, G. J. Meyer, E. Fujita, *Acc. Chem. Res.* **2009**, *42*, 1983–1994; H. Takeda, C. Cometto, O. Ishitani, M. Robert, *ACS Catal.* **2017**, *7*, 70–88.
[2] A. M. Appel, et al., *Chem. Rev.* **2013**, *113*, 6621–6658.
[3] E. E. Benson, C. P. Kubiak, A. J. Sathrum, J. M. Smieja, *Chem. Soc. Rev.* **2009**, *38*, 89–99.
[4] J. Hawecker, J. M. Lehn, R. Ziessel, *J. Chem. Soc., Chem. Commun.* **1984**, 328–330; E. E. Benson, K. A. Grice, J. M. Smieja, C. P. Kubiak, *Polyhedron* **2013**, *58*, 229–234; E. E. Benson, C. P. Kubiak, *Chem. Commun.* **2012**, *48*, 7374–7376.
[5] H. Ishida, H. Tanaka, K. Tanaka, T. Tanaka, *J. Chem. Soc., Chem. Commun.* **1987**, 131–132; H. Ishida, K. Tanaka, T. Tanaka, *Organometallics* **1987**, *6*, 181–186.

© 2019 Wiley-VCH Verlag GmbH & Co. KGaA, Weinheim

[6] S. Sato, T. Morikawa, T. Kajino, O. Ishitani, *Angew. Chem. Int. Ed.* **2013**, *52*, 988–992; *Angew. Chem.* **2013**, *125*, 1022.
[7] D. L. Dubois, *Commun. Inorg. Chem.* **1997**, *19*, 307–325; D. L. Dubois, A. Miedaner, R. C. Haltiwanger, *J. Am. Chem. Soc.* **1991**, *113*, 8753–8764.
[8] C. Costentin, S. Drouet, M. Robert, J. M. Saveant, *Science* **2012**, *338*, 90–94; C. Costentin, M. Robert, J. M. Saveant, *Chem. Soc. Rev.* **2013**, *42*, 2423–2436; C. Costentin, M. Robert, J. M. Saveant, A. Tatin, *Proc. Natl. Acad. Sci. USA* **2015**, *112*, 6882–6886.
[9] M. D. Rail, L. A. Berben, *J. Am. Chem. Soc.* **2011**, *133*, 18577–18579; A. Taheri, L. A. Berben, *Inorg. Chem.* **2016**, *55*, 378–385; N. D. Loewen, E. J. Thompson, M. Kagan, C. L. Banales, T. W. Myers, J. C. Fettinger, L. A. Berben, *Chem. Sci.* **2016**, *7*, 2728–2735.
[10] S. Chakraborty, J. Zhang, J. A. Krause, H. Guan, *J. Am. Chem. Soc.* **2010**, *132*, 8872–8873; S. Chakraborty, P. Bhattacharya, H. G. Dai, H. R. Guan, *Acc. Chem. Res.* **2015**, *48*, 1995–2003.
[11] T. Jin, C. Liu, G. H. Li, *Chem. Commun.* **2014**, *50*, 6221–6224; D. He, T. Jin, W. Li, S. Pantovich, D. W. Wang, G. H. Li, *Chem. Eur. J.* **2016**, *22*, 13064–13067.
[12] W. J. Liu, H. H. Huang, T. Ouyang, L. Jiang, D. C. Zhong, W. Zhang, T. B. Lu, *Chem. Eur. J.* **2018**, *24*, 4503–4508; T. Ouyang, C. Hou, J.-W. Wang, W.-J. Liu, D.-C. Zhong, Z.-F. Ke, T.-B. Lu, *Inorg. Chem.* **2017**, *56*, 7307–7311.
[13] G. B. Balazs, F. C. Anson, *J. Electroanal. Chem.* **1993**, *361*, 149–157; J. Schneider, H. F. Jia, K. Kobiro, D. E. Cabelli, J. T. Muckerman, E. Fujita, *Energy Environ. Sci.* **2012**, *5*, 9502–9510.
[14] M. Fujihira, Y. Hirata, K. Suga, *J. Electroanal. Chem.* **1990**, *292*, 199–215.
[15] J. D. Froehlich, C. P. Kubiak, *Inorg. Chem.* **2012**, *51*, 3932–3934.
[16] T. D. Cook, S. F. Tyler, C. M. McGuire, M. Zeller, P. E. Fanwick, D. H. Evans, D. G. Peters, T. Ren, *ACS Omega* **2017**, *2*, 3966–3976.
[17] R. W. Hay, I. Fraser, N. C. Owen, *Polyhedron* **1998**, *17*, 1611–1615.
[18] J. Schneider, H. Jia, J. T. Muckerman, E. Fujita, *Chem. Soc. Rev.* **2012**, *41*, 2036–2051.
[19] M. Boiocchi, L. Fabbrizzi, F. Foti, M. Vazquez, *Dalton Trans.* **2004**, 2616–2620.
[20] R. A. Kolinski, B. Korybut-Daszkiewicz, *Inorg. Chim. Acta* **1975**, *14*, 237–245.
[21] G. M. Sheldrick, *Acta Crystallogr., Sect. A* **2008**, *64*, 112–122.

Received: October 1, 2018

© 2019 Wiley-VCH Verlag GmbH & Co. KGaA, Weinheim